# THE COMPATIBILITY RELATIONSHIPS OF PERICLASE IN BASIC REFRACTORIES AT HIGH TEMPERATURES WITH SPECIAL REFERENCE TO THE EFFECTS OF THE SOLID SOLUBILITY OF $Al_2O_3$, $Cr_2O_3$ AND IRON OXIDES IN MAGNESIA

A thesis presented for the degree of

Doctor of Philosophy

by

Geraldo Eduardo Gonçalves

Department of Ceramics,
Faculty of Materials Technology,
University of Sheffield.

September 1973

# DAMAGED TEXT IN ORIGINAL

This thesis is dedicated to my friends Dr. Cláudio Jorge Gomes e Souza and his wife who have given me help and encouragement throughout my professional career.

## ACKNOWLEDGEMENTS

The author has pleasure in expressing his thanks to his supervisor, Professor James White, for his guidance, advice and many helpful discussions during the course of this work.

He is grateful to Magnesita S.A., Belo Horizonte, Brazil, for financial support during this investigation and to Dr. Paulo R.H. Bittencourt and Dr. Ivan de Menezes from Magnesita S.A. for their encouragement and help in the course of the work.

The writer also acknowledges the staff of the Department of Research of Magnesita S.A. for chemical and X-ray analysis of the materials used in this investigation.

Thanks are also expressed to Mrs. P.M. Latimer for the typing of this thesis and to Mrs. C.M. Blagburn for her assistance with the diagrams.

Finally, he thanks his wife for her encouragement and help and the members of the staff of the Department of Ceramics of the University of Sheffield, and his colleagues there, for making his stay such a happy one.

## SUMMARY

The objective of the investigation was to establish melting relationships in certain phase diagrams of importance to the technology of basic refractories, with special reference to the effects of the solid solubility of $Al_2O_3$, $Cr_2O_3$ and iron oxide in magnesia at high temperatures. Because of this solubility, the freezing paths of mixtures lying in the primary phase volumes of periclase in the systems $CaO-MgO-Al_2O_3-SiO_2$, $CaO-MgO-Fe_2O_3-SiO_2$ and $CaO-MgO-Cr_2O_3-SiO_2$ do not radiate from the MgO corner of the composition tetrahedron. Hence projections of the boundary surface of the primary phase volume of periclase, through the MgO corner onto the opposite face of the tetrahedron, do not describe the freezing behaviour of such mixtures accurately.

The first investigation was of the phase changes occurring in mixtures containing 80 Wt.% MgO in the system $CaO-MgO-Al_2O_3-SiO_2$. Conventional techniques involving firing and microscopic examination, after water quenching were used to establish the identity and crystallization temperatures of the secondary phases and the results were plotted on a composition triangle in terms of the CaO, $Al_2O_3$ and $SiO_2$ contents of the mixtures recalculated to 100 wt.%. Comparison of this diagram with the published diagram of the boundary surface shows

that displacement of the boundary lines due to solid solution of $Al_2O_3$ becomes appreciable at temperatures over 1500°C, where the solid solubility of this oxide becomes appreciable.

Comparison with similar diagrams established in the Department for the systems $CaO-MgO-Fe_2O_3-SiO_2$ and $CaO-MgO-Cr_2O_3-SiO_2$ has further shown that, at comparable MgO contents the range of $R_2O_3/(CaO + SiO_2)$ ratios over which spinel is the secondary phase decreases in the order

$$Al_2O_3 > Cr_2O_3 >> Fe_2O_3$$

which is the order of increasing solid solubility of the sesquioxide in periclase at high temperatures. An explanation for this effect has been advanced and a graphical method of predicting the displacement of the spinel-silicate boundary with varying MgO content has been described.

Other phase diagrams investigated were those of the systems $MgO-Cr_2O_3-C_2S$, $MgO-Al_2O_3-CS$, $MgO-Al_2O_3-C_3S_2$ and $MgO-Fe_2O_3-C_3S_2$ and, from the boundaries of the periclase fields in these systems the boundary surfaces of the phase volumes of periclase in the quaternary systems $CaO-MgO-Cr_2O_3-SiO_2$, $CaO-MgO-Al_2O_3-SiO_2$ and $CaO-MgO-Fe_2O_3-SiO_2$ have been located, where these surfaces are intersected by the planes of these systems.

Finally the investigation of the system $MgAl_2O_4-MgCr_2O_4-C_3MS_2$, which had been partially investigated in the Department previously, was completed and a phase diagram constructed.

# TABLE OF CONTENTS

# 1. INTRODUCTION

The objective of the present investigation was to establish melting relationships in certain combinations of phases, which earlier work had shown to occur in basic refractories but which had not so far been investigated.

If both ferrous and ferric ions are included, basic refractories can be regarded as belonging to the seven-component system MgO, CaO, $SiO_2$, FeO, $Fe_2O_3$, $Al_2O_3$, $Cr_2O_3$. Because of the complexity of the complete system, in the programme of work at Sheffield, which has been aimed at establishing the significance of the minor individual components on melting behaviour, phase equilibrium relationships in selected three-phase and four-phase combinations known to be compatible with each other in the solid state, have been studied[1,2,3].

Broadly, the object of this approach has been to enable the refractory manufacturer to minimise the effects of impurities by controlling the composition to avoid low-melting eutectics and to ensure minimum solubility of the refractory phases in the liquid phase at high temperatures.

A complementary approach is aimed at minimising the harmful effect of the liquid phase formed in service by controlling its distribution so that it does not penetrate between the crystal grains of the refractory phases.

This work has shown that in refractories consisting of periclase and a liquid phase at the operating temperature, penetration of the liquid phase between the periclase grains decreases with increasing $Cr_2O_3$ content and $CaO/SiO_2$ ratio and increases with increasing $Al_2O_3$ and $Fe_2O_3$ content. It has also been found that the ability of the liquid phase to penetrate between periclase grains is markedly depressed when certain second solid phases, e.g. spinel, forsterite, dicalcium silicate, are present at the operating temperature[4,5].

## 2. REVIEW OF RELEVANT LITERATURE

### 2.1. Solid Phase Relationships in Basic Refractories

White[6,7] and Rait[8] were probably the first investigators to deduce a system of phase assemblages, which explained the reactions taking place in basic refractories. Their assemblage defines the combination of phases coexisting with periclase (MgO) in the solid state in the seven-component system $CaO-MgO-FeO-Fe_2O_3-Al_2O_3-Cr_2O_3-SiO_2$. They used a process which in principle involved writing down the possible combinations of phases which could occur, the maximum number of phases in any combination being restricted by the phase rule and eliminating those which contained incompatible pairs of phases, i.e. phases which it was known could not coexist at equilibrium.

Fortunately, the relationships were found to be fairly simple owing to the prevalence of solid solution and the principal features can be understood from the solid phase relationships in the corresponding part of the system $CaO-MgO-Fe_2O_3-SiO_2$ which are shown in Figure 1. This shows the various phase combinations or assemblages which can occur in the presence of free MgO (periclase). Each assemblage consists of four phases whose compositions lie at the corners of a tetrahedron within the composition tetrahedron of the complete system. These smaller tetrahedra also define the composition limits within which the various phase assemblages exist.

These limits can be defined in terms of the $CaO/SiO_2$ ratio. When it is 2/1 molecularly the composition lies on the plane $MgO-2CaO.SiO_2-MgO.Fe_2O_3$; when it is greater than 2/1, all or part of the $Fe_2O_3$ occurs in combination with CaO as low melting dicalcium ferrite and when it is less than 2/1, all the $Fe_2O_3$ occurs in combination with MgO as spinel.

If $Fe_2O_3$ is replaced by FeO, $Al_2O_3$ and $Cr_2O_3$ similar relationships hold. This is illustrated in Table 1 which omits certain complications that arise at $CaO/SiO_2$ molecular ratios greater than 2.0 (when CaO occurs in combination with $Fe_2O_3$, $Al_2O_3$ and $Cr_2O_3$). Up to a ratio of 2.0, i.e. so long as the CaO occurs entirely in the silicates, the phase combination is determined uniquely by the value of the ratio. With ratios greater than 2.0, this is no longer rigorously true, although if the sesquioxide content is kept constant, the tendency is still to move toward the right-hand side of the table as the ratio increases. When FeO is present, it occurs mainly in the solid solution in the periclase phase, forming magnesiowustite and as a partial replacement for MgO in the spinel phase.

It is important to note that, up to a ratio of 2.0, each of the three phase combinations occurring contains four phases: magnesiowustite, a spinel solid solution phase containing MgO, FeO, $Fe_2O_3$, $Al_2O_3$ and $Cr_2O_3$, and two silicates. At the critical values of the ratio that

define the limits between which each combination occurs, only one silicate will occur. These are forsterite ($Mg_2SiO_4$) when no CaO is present, monticellite ($CaMgSiO_4$) at a ratio of 1.0, merwinite at 1.5 and dicalcium silicate ($Ca_2SiO_4$) at 2.0.

The phase assemblages have been found to account for the phases found both in unused fired bricks and in used bricks after CaO and iron oxides have been picked up in service. Thus the constitution of dead-burned dolomite is represented by assemblage (6) and that of dolomite stabilised against hydration by addition of serpentine by assemblage (5), while the constitution of magnesites usually corresponds to assemblages (2) or (3), or if the $CaO/SiO_2$ ratio is low enough to assemblage (1).

The constitution of fired chrome-magnesite and magnesite-chrome bricks, which normally have $CaO/SiO_2$ ratios less than 1.0, usually corresponds to phase assemblage (1) and all the CaO is present as monticellite, which melts incongruently at 1502°C. It is for this reason that a high CaO content has usually been considered undesirable in chrome-magnesite refractories. In addition in basic open hearth furnaces CaO is picked up by the bricks during service. Monticellite then forms at the expense of forsterite and the liquid migrates back into the bricks. Consequently, in used bricks, the $CaO/SiO_2$ ratio usually increases behind the hot face,

and phase combinations corresponding to (2) and (3) may occur. In some cases ratios greater than 2.0 can be reached and dicalcium ferrite, dicalcium silicate and tri-calcium silicate have been reported.

While the phase assemblages have proved useful in predicting the solid phases to be expected in basic refractories, some latitude must be allowed in applying the $CaO/SiO_2$ ratios given in Table 1. The reason is that there is appreciable solubility between certain of the phases at high temperatures.

Hatfield and Richmond[9], Biggar and O'Hara[10], and Ricker and Osborn[11] pointed out that monticellite has appreciable solubility in forsterite.

Hatfield and Richmond[9], using the techniques of reflected-light microscopy on quenched specimens found the maximum solubility of CMS in $M_2S$ at 1500°C to be 9 wt.%, compared with 28 wt.% reported by Ricker and Osborn[11].

Ricker and Osborn[11] and Biggar and O'Hara[10] used an X-ray technique and the results reported by the latter two were mainly on a redetermination of the solvus curve and their conclusions were that the solubility of CMS in $M_2S$ is appreciably lower than that reported by Ricker and Osborn[11] and higher than that found by Hatfield and Richmond[9].

It is also now known that there is appreciable solid solubility of CaO in MgO at high temperatures. Doman

et al.[12] investigated the system CaO-MgO, and confirmed that lime and magnesia are appreciably soluble in each other at high temperatures, the solubility of CaO in MgO rising from approximately 0.9 wt.% at 1620°C to 7.8 wt.% at 2370°C and that of MgO in CaO from 2.5 wt.% at 1620°C to 17 wt.% at 2370°C.

According to Jones and Melford[13], who used an electron probe microanalyser to determine the CaO content of the periclase grains in their samples, magnesia in contact with $C_2S$ at 1750°C dissolves appreciable CaO and this finding was later confirmed by Henney and Jones[14] who used an X-ray technique. The latter were interested in the solubilities of CaO and $SiO_2$ in MgO and in the effects on the system CaO-MgO-$SiO_2$. They found that at 1750°C the CaO content of the MgO increased as the CaO content of silicate decreased.

Spencer et al.[15] have also studied the solubility of CaO in MgO and its effect on the CaO-MgO-$SiO_2$ system at 1800°C and found that at constant $SiO_2$ content the degree of solid solubility of CaO in the periclase phase generally rose as the CaO/$SiO_2$ ratio of the silicates increased.

Neither of the latter workers found any appreciable solid solubility of $SiO_2$ in MgO at 1750°C-1800°C although Schlaudt and Roy[16] had reported relatively high solubilities in the system MgO-$Mg_2SiO_4$ up to 10.5 mole % and 8 mole % $Mg_2SiO_4$ can be accommodated in the periclase structure

respectively at 1800°C and 1700°C.

Hatfield et al.[17] investigated the compatibility relationships between MgO-CaO solid solutions and the silicate phases at high temperatures in the system $CaO-MgO-SiO_2$. They found no indication of any appreciable solubility of $SiO_2$ in the periclase phase and their results are summarized in Figure 2 which shows that the effect of CaO solubility is small in mixtures containing 5 wt.%, but is considerable in mixtures containing 2 wt.% and 1 wt.%. Thus in a mixture having a $CaO/SiO_2$ ratio of 1.87 by weight (ratio molar 2.0) and a $SiO_2$ content of 2 wt.% cooling from above 1700°C would actually deposit a mixture of dicalcium silicate and merwinite, while a mixture having 1 wt.% $SiO_2$ and the same ratio would deposit merwinite and monticellite.

$Al_2O_3$, $Cr_2O_3$ and $Fe_2O_3$ are also partially soluble in MgO at high temperatures, the solubilities increasing in the order $Al_2O_3 < Cr_2O_3 <<$ iron oxides. The solubilities in the systems, $MgO-MgAl_2O_4$[18], $MgO-MgCr_2O_4$[19,20] and $MgO-MgFe_2O_4$[21,22] are shown in Figure 3. In the case of the iron oxide solubility, loss of oxygen occurs at high temperature and the extent of this loss is determined by oxygen pressure and temperature. The magnesiowustite phase will, therefore, contain both $Fe^{2+}$ and $Fe^{3+}$ ions. Determination of the curve shown was carried out in air.

Since all three solubilities increase with rising temperature and are very low below 1000°C, it follows that

when chrome-magnesite and magnesite-chrome refractories are heated to high temperatures, the periclase grains will dissolve $Al_2O_3$, $Cr_2O_3$, $Fe_2O_3$ and FeO from the grains of chrome spinel. On subsequent cooling the dissolved oxides precipitate as particles of a mixed spinel within the periclase grains. Since solution is selective, because of the different solubilities of the three sesquioxides, the composition of this spinel will differ from that of the original chrome spinel. Menezes and Stubican[23,24] investigated the chemical changes which occur during the heating in air of specimens an unused chemically bonded magnesia-chrome brick from 800°C to 1820°C, using the electron probe microanalyser. They pointed out that iron, chromic and aluminium ions diffuse out from the chromite spinel to periclase and also found that any temperature the order of decreasing diffusion is : Fe >> Cr > Al.

A final omission from the phase assemblage is an orthosilicate which occurs between dicalcium silicate and merwinite and has been called phase T.[25,26,27] ($Ca_{1.7}Mg_{0.3}SiO_4$.) Schlaudt and Roy[25] pointed out that this phase was stable between 979°Cand 1381°C and Gutt[27] found the T was stable between 0°C and 1460°C.

The existence of this silicate would mean that phase assemblage (3) in Table 1 should be subdivided into two phase assemblages containing $C_2S$ and T and T + merwinite. However T has been found to dissociate about 1400°C into merwinite and α-dicalcium silicate in the solid

state and seems to be formed with some difficulty so it has been ignored for the present purpose.

## 2.2. Iron Oxide Stability Relationships in Basic Refractories

At high temperatures, iron oxide in the phase assemblage in Table 1, will normally be present as both FeO and $Fe_2O_3$. Its state of oxidation will be determined by the furnace atmosphere and temperature and cannot be deduced from the phase assemblages but a partial replacement of $Mg^{2+}$ by $Fe^{2+}$ will occur in the magnesiowustite, spinel and silicate phases. It is not generally possible to predict how the FeO will be distributed between them but, since the FeO can be expressed as its molar equivalent of MgO in estimating the proportions of the phases present at equilibrium in a body of known composition, the predicted phase assemblages will not be invalidated. The relative proportions of each phase will, however, be dependent on the state of oxidation of the iron and this could affect the dimensional stability of the refractories during temperature and atmospheric changes.

The system MgO-FeO-$Fe_2O_3$ is important for an understanding of the stability relationship of iron oxides in basic refractories and many studies have been carried out on it[21,22,28,29]. Recently, Willshee and White[30], used a thermobalance to follow the changes in $Fe_2O_3$/FeO ratio at equilibrium in air, up to 1750°C, in pre-reacted mixtures

of MgO and $Fe_2O_3$. The result of the work is shown in Figure 4.

Isotherms were plotted in the composition triangle, so that composition/temperature relationships in the system could be indicated, and the phase field boundaries were deduced from changes in the direction of the isotherms. Compositions of the initial, fully oxidised, mixtures at room temperature would lie along the $Fe_2O_3$-MgO edge. When such mixtures are heated, however, they will lose oxygen and their compositions will move along reaction paths at a constant Mg/Fe ratio. Five reaction paths only are shown for clarity, the temperature variation along them being indicated by the intersection with the isotherms. The phases present in any composition on the isotherms are determined by the phase field within which that composition lies. The phase fields existing in this diagram are given in Table 2.

Figure 5 was obtained by plotting the temperatures along the various phase boundaries in Figure 4 against the initial compositions of the mixtures, the lettering corresponding to that in Figure 4. The boundary D-MgO in Figure 4 is the iron oxide solubility curve of Figure 3.

The changes taking place during heating and cooling (reduction and oxidation) in iron-containing magnesites can be understood in terms of Figures 3, 4 and 5.

## 2.3. Solid-Liquid Relationships in Basic Refractories

The phase assemblages indicate the solid phases to be expected in a refractory of given composition, and hence the conditions under which low melting phases such as monticellite and dicalcium ferrite will be formed, but give no indication of the extent to which the temperature of melting of the individual phases may be lowered by formation of eutectics.

Prince[31] investigated the system dicalcium silicate and the spinel($MgO.Al_2O_3$)and found the melting begun at 1418°C, which is considerably below the melting points of dicalcium silicate (2130°C) and spinel MA (2135°C).

The study of melting relationships in the relevant portion of the seven-component system would prove difficult but El-Shahat and White[1,2,3] adopted a simplified approach to establish trends in melting with compositions up to a $CaO/SiO_2$ ratio of 2.0.

Within each of the three phase assemblages existing within this range four solid phases coexist and, if the system contained only four components, melting would begin in each at a quaternary invariant point at which the four phases would coexist with a liquid phase. Figure 6 illustrates this feature. It shows diagrammatically the phase diagram of the quaternary system $MgO-MgAl_2O_4-Mg_2SiO_4-Ca_2SiO_4$ (part of the system $CaO-MgO-Al_2O_3-SiO_2$) redrawn by White[32] from the experimentally-established diagram of Solacolu[33]. It shows the composition tetrahedron

erected on the composition triangle $MgO$-$Mg_2SiO_4$-$Ca_2SiO_4$ and divided by two sub-liquidus planes of $CaO/SiO_2$ ratios 1.0 and 1.5 into three smaller tetrahedra corresponding, from left to right, to phase assemblages (1), (2) and (3) of Table 1. Melting relationships are indicated by twelve 3-phase (2 solids + 1 liquid) boundary surfaces intersecting three at a time along ten 4-phase (3 solids + 1 liquid) boundary lines, which intersect four at a time at three quaternary invariant points. The latter lie outside the composition tetrahedron and are therefore peritectic reaction points. They occur in Solacolu's diagram, at 1380°C, 1366°C and 1387°C, these being the temperatures of initial melting in phase assemblages (1), (2) and (3) in this system.

In the system $MgAl_2O_4$-$MgCr_2O_4$-$Ca_2SiO_4$ shown in Figure 7, which was established by El-Shahat and White[1], the temperature of the binary eutectic formed between the silicate and the continuous series of spinel solid solutions increases from 1418°C to 1700°C as the $Al_2O_3$ of the spinel is replaced by $Cr_2O_3$. The solubility of the spinel in the liquid silicate decreases as the $Cr_2O_3$ content increases and consequently, in mixtures of spinel with minor amounts of $Ca_2SiO_4$, the quantity of melt formed at a given temperature will decrease as the $Cr_2O_3/Al_2O_3$ ratio in the spinel increases. Similar relationships were found to exist in the system $MgFe_2O_4$-$MgCr_2O_4$-$Ca_2SiO_4$[1] investigated in air, the temperature of

the eutectic increasing from 1415°C to 1700°C as the iron oxide was replaced by $Cr_2O_3$ while the solubility of the spinel in the melt decreased. In the system $MgFe_2O_4$-$MgAl_2O_4$-$Ca_2SiO_4$[1], as shown in Figure 8, the temperature of the eutectic increased only slightly from 1415°C to 1418°C as $Fe_2O_3$ was replaced by $Al_2O_3$.

The solubility of the spinel in the melt, however, decreased appreciably so that the order of increasing solubility of the spinel sesquioxides in the melt is

$$Cr_2O_3 << Al_2O_3 < Fe_2O_3.$$

This series may be compared with that giving the order of increasing solubility of the spinel sesquioxides in magnesia mentioned previously, viz.

$$Al_2O_3 < Cr_2O_3 << Fe_2O_3$$

(in both cases $Fe_2O_3$ would contain some FeO).

A limited investigation of the quaternary system[3], as shown in Figure 9, confirmed the conclusion that $Cr_2O_3$ spinel is less soluble in the melt than $Al_2O_3$ and $Fe_2O_3$ spinels.

Figure 9 also shows that temperatures of initial and complete melting of the eutectic increase as the $Cr_2O_3$ content of the spinel increases, but was little affected by the $Al_2O_3/Fe_2O_3$ ratio.

In the corresponding systems containing monticellite and merwinite, the phase relationships are more complex owing to the fact that both these compounds melt incongruently with separation of MgO. Similar trends with spinel composition were observed but the influence of

$Cr_2O_3$ on the temperature of initial melting was considerably less due to the relatively low temperatures of peritectic melting of the silicates. Thus the effect of replacing all the $Al_2O_3$ in the $MgAl_2O_4$-CMS mixtures was to raise the temperature of initial melting by only 80°C, from 1410°C to 1490°C. These temperatures are in good agreement with an early observation by Berry et al.[34] who found that additions of $MgCr_2O_4$ to a mixture of MgO, forsterite and monticellite had a negligible effect on the temperature of complete melting, whereas the addition of $MgAl_2O_4$ lowered it to 1420°C. They also found, in agreement with the relative solubilities of the sesquioxides in the liquid silicates given above, that in zones adjacent to the hot face of used chrome magnesite roof blocks, the $Al_2O_3$ content of the spinel grains had decreased while that of the silica matrix had increased.

## 2.4. The Spatial Arrangement of the Phases in Basic Refractories

Phase equilibrium studies establish the nature of the reactions taking place in basic refractories in service, but considerable practical importance must be attached to controlling the spatial distribution of the phases. Thus a refractory in which the fusible components formed a continuous film surrounding the solid grains, would probably have inferior load-bearing properties at high temperatures to one in which these components formed discrete globules

in a continuous solid matrix. Indirect evidence for the presence of films of liquid bond between the solid grains in many refractories at high temperatures was provided by Houseman and White[35], who showed that during firing, the hot compressive strength measured at the firing temperature passed through a maximum and then fell as the temperature was increased. This was attributed to progressive fusion. As samples were cooled back from above the maximum, a rapid initial rise in strength occurred, which was attributed to freezing of the liquid film.

The importance of the distribution of low-melting phases in furnace refractories was discussed by Allison, Brock and White[36]. They pointed out that hot strength in bodies with a high degree of solid-solid bonding would not be greatly reduced by the formation of isolated globules of a liquid phase.

Chrome-magnesite bricks taken from a particularly long-lived roof were examined by Rigby and Richardson[37] who found that the silicates which tend to be associated with chrome grains in normally fired bricks had migrated away from the latter into the magnesite matrix. By use of the refractoriness-under-load test procedure they found that the changes in the structure of the brick had enabled it to withstand greater compressive stresses at steelmaking temperatures than the unused brick.

Laming[38] and Richardson[39] discovered that this type

of structure could be produced by firing in the region of 1800°C, when the silicates become mobile and tend to be displaced into interstices between chrome and magnesite grains, permitting the development of a direct bond between them.

Subsequently, Ford et al.[40] showed that the development of direct bonding was accompanied by an increase in the ability to withstand tensile loading at high temperatures.

A consequence of the solubility of spinel sesquioxides in liquid silicates is that, when chrome-magnesite refractories are fired at high temperatures and subsequently cooled, crystals of spinel separate from the melt between periclase grains, forming "bridges" between them. This effect has been used to produce what is sometimes referred to as "spinel bonding" in fired chrome-magnesite refractories[41,42].

Although much of the resultant direct bonding will disappear at service temperatures, it is suggested that the values of the "secondary" spinels is due to the high hot strength imparted to that part of the brick 2 to 3" behind the hot face, resulting in wear by solution or thin peeling as opposed to thick layers flaking off.

The factors determining the distribution of phases in equilibrium structures were first established by work on alloys. Smith[43] showed that the distribution of the minor phase in a two-phase alloy is governed by the

geometrical balance of the surface tension forces where phase boundaries and grain boundaries intersect. In particular the condition that a liquid phase should penetrate completely along the grain boundary between two solid grains is that the surface tension of the solid-solid boundary should be equal to or greater than twice that of the solid-liquid boundary, i.e. $\gamma_{ss} > 2\gamma_{SL}$. When $\gamma_{ss} < 2\gamma_{SL}$, complete penetration will not occur but a balance of forces will be reached when

$$\gamma_{ss} = 2\gamma_{SL} \cos \frac{\Phi}{2}.$$

Where $\Phi$ is the dihedral angle formed by the intersecting solid-liquid interfaces.

The first study of this kind on refractories was done by Van Vlack[44] who determined the values of the dihedral angle in fired mixtures of silica and iron oxides. Metallographic examination of quenched structures showed that in samples containing cristobalite, the dihedral angle was $55^{\circ}$ at $1500^{\circ}C$ and that is decreased only slowly with rising temperature so that direct contact between the cristobalite grains was maintained up to the temperature of complete melting. He suggested that this behaviour might explain the high refractoriness-under-load of silica bricks.

Subsequently the nature of the factors which control the distribution of the liquid phase in basic refractories at high temperatures was investigated by Jackson et al.[45].

The basis of their approach was the earlier work of Smith[43] and their mutual objective was to establish the type of distribution to be expected in bodies consisting of periclase with minor amounts of liquid silicate and then to examine the effects of other oxides occurring in basic refractories on the distribution. For this purpose a body consisting of 85 wt.% MgO and 15 wt.% CMS, which would consist of periclase and a liquid phase saturated with MgO at temperatures above 1502°C was selected and additions of $Cr_2O_3$ and $Fe_2O_3$ were made to it as replacements for equal weights of MgO so that the content of CMS remained constant. It was found that additions of $Cr_2O_3$ up to 10 wt.% increased the dihedral angle from 25° to 40° in bodies fired at 1550°C. Further additions did not affect the angle but $MgCr_2O_4$ was observed in the microstructure, often forming bridges between periclase grains. Additions of $Fe_2O_3$ even in small amounts decreased the dihedral angle and when both sesquioxides were added together, $Fe_2O_3$ was found to reduce the effective increase in angle produced by the $Cr_2O_3$ addition. It was also found that high values of the contact ratio and low grain sizes were associated with high values of the dihedral angle.

Subsequent investigations[46] at temperatures up to 1725°C have shown that additions of $Al_2O_3$ and $TiO_2$ also lower $\Phi$ and decrease the degree of contact, while increasing the $CaO/SiO_2$ in the silicate increases $\Phi$ and the degree

of contact, possibly because, as shown by the phase diagrams, the concentration of MgO in the saturated melt will decrease as the $CaO/SiO_2$ ratio increases.

Smith[43] found similarly with alloys that $\Phi$ increased as the concentration of the solid phase in the saturated liquid phase decreased. The practical implications of these findings are shown by the fact that both here and in the U.S., manufacturers of sea-water magnesites subsequently introduced a grade of higher $CaO/SiO_2$ ratios.

To establish the nature of the factors controlling the distribution of the liquid phase in dolomite and in chrome-magnesite (and magnesite-chrome) refractories, investigations have been carried out on mixtures consisting at the firing temperature of lime, periclase and a liquid phase and of periclase, chrome spinel and a liquid phase[47]. The most significant finding was that, in these systems, the ability of the liquid to penetrate between unlike grains was less than between like grains, so that the degree of solid-solid bonding was greater when two solid phases were present than when either coexisted with the liquid phase alone.

The dihedral angle between unlike grains was higher than between like grains, indicating that the energy of the interface between unlike grains is less than between like grains.

In chrome-magnesite and magnesite-chrome refractories improved hot strength is now being obtained by utilizing

the principle (see above) that solid-solid contact between periclase and spinel grains is greater than that between periclase and periclase. One way of producing the necessary structure, that makes use of the solubility of the spinel phase in the liquid silicate, is by firing at high temperatures followed by slow cooling, which causes small grains of spinel to crystallize between the periclase grains. A possible limitation of this method is that in service, in the vicinity of the hot face of the brick, these "bridging" spinel grains are likely to redissolve in the liquid phase, if the operating temperatures reaches or exceeds the firing temperature. This difficulty can be overcome by the addition of finely-ground spinel-containing material to the matrix fraction.

## 2.5. Representation of Melting Relationships in Quaternary Systems

In Figure 10 the invariant (peritectic) points at 1575°C, 1498°C and 1502°C at which (1) periclase, dicalcium silicate and merwinite, (2) periclase, merwinite and monticellite, and (3) periclase, monticellite and forsterite coexist with the liquid phase correspond to invariant points in the ternary system $CaO-MgO-SiO_2$.

In each of the quaternary systems formed by $CaO-MgO-SiO_2$ and $Al_2O_3$, $Fe_2O_3$ and $Cr_2O_3$ these points will give rise to three invariant points at which four solid phases will coexist with liquid, e.g. as shown by the work of Solacolu[33],

in the system $CaO-MgO-Al_2O_3-SiO_2$, invariant points occur at which (1) MgO, MA, $M_2S$, CMS, (2) MgO, MA, CMS, $C_3MS_2$ and (3) MgO, MA, $C_3MS_2$, $C_2S$ coexist with the liquid phase. Solacolu's[33] diagram, which is shown in Figure 6, as redrawn by White[32], shows these invariant points, and the four phase boundary lines radiating from them, three of which, in each case, lie in the boundary surface of the primary phase volume of periclase.

However it is difficult to show precisely temperatures and compositions in the boundary surface in such a diagram and an alternative method of representation is to project the boundary surface of the periclase phase volume through the MgO corner of the diagram on to the $CaO-Al_2O_3-SiO_2$ face of the composition tetrahedron. Such a projection, which is obtained simply by expressing compositions on the boundary surfaces in terms of their CaO, $Al_2O_3$ and $SiO_2$ contents recalculated to 100%, gives a triangular diagram with boundaries, which subdivide it into crystallization fields of the second phases to separate on cooling (periclase being the first). The temperatures of initial crystallization of these secondary phases (up to which they will exist on heating) are indicated by drawing isotherms in the surface.

This procedure was probably first used by McMurdie and Insley[48] and has been used by several other workers, including de Aza, Richmond and White[49], O'Hara and Biggar[50] Crookes[51] and recently Tarboton[52].

McMurdie and Insley[48] showed the temperature and compositions of three phase and four phase equilibria in that part of the system $CaO-MgO-2CaO.SiO_2-5CaO.3Al_2O_3$ in which periclase is the primary phase. For this purpose they projected phase boundaries and isotherms in the boundary surface of the primary volume of periclase through the MgO corner on to the $CaO-2CaO.SiO_2-5CaO.3Al_2O_3$ plane in the composition tetrahedron.

de Aza, Richmond and White[49], in their experimental investigation of phase relationships in the system $CaO-MgO-ZrO_2-SiO_2$produced a projection, through the MgO corner on to the $CaO-ZrO_2-SiO_2$ face of the composition tetrahedra, showing phase boundaries and isotherms on the boundary surface of the phase volume of periclase.

O'Hara and Biggar[50] published a similar projection of the boundary surface of the phase volume of periclase in the system $CaO-MgO-Al_2O_3-SiO_2$, which had been determined from a compilation of established data. Their diagram, shown in Figure 11, indicates the phase boundaries which separate the second phase fields and the isotherms, which mark the temperatures at which the second phases separate on cooling (periclase being the primary phase).

Such projections (of the boundary surface through the MgO corner) will however provide a true description of the freezing behaviour of mixtures lying in the primary phase volume of periclase only when solid solubility in the

latter is negligible, i.e. when the freezing paths of the mixtures to the boundary surface are straight lines radiating from the MgO corner. Where there is appreciable solid solubility in the periclase, the latter condition will not generally be fulfilled since solid solutions of ranging composition will separate during freezing.

This situation exists in the systems $CaO-MgO-Fe_2O_3-SiO_2$ and $CaO-MgO-Cr_2O_3-SiO_2$, which were investigated by Crookes[51] and Tarboton[52] respectively, since both iron oxide and $Cr_2O_3$ form entering solid solutions in MgO at high temperatures. In investigating the effects of composition on melting behaviour in these systems, these authors established the phase changes occurring in mixtures lying on a plane of constant MgO content (70 wt.% and 80 Wt.% MgO respectively) in the primary phase volume of periclase and the phase boundaries and initial crystallisation temperatures of the second phases to freeze on cooling were plotted in ternary diagrams in which the compositions of the mixtures were expressed in terms of their CaO, $R_2O_3$ and $SiO_2$ contents recalculated to 100 wt.%. Their diagrams are shown in Figures 12 and 13. They are not, however, "true" projections of the boundary surfaces of the periclase crystallization volumes but are distorted versions of these projections, which show the actual phases separating during freezing of compositions lying in the planes investigated.

## 2.6. The Polymorphism of Dicalcium Silicate

Dicalcium silicate melts congruently at 2130°C and undergoes a number of polymorphic transitions in cooling from this temperature. The hexagonal α-phase is stable between the melting point and 1450°C, below which it inverts to structurally similar α'-phase; α'-$Ca_2SiO_4$ inverts to γ-$Ca_2SiO_4$ at about 850°C but since this transition involves a reconstitution of the structure, the α'phase can occur metastably below the inversion temperature. It then inverts at 675°C to β-$Ca_2SiO_4$ which could theoretically convert to the stable γ-phase at any temperature. The free energy diagram of Figure 14 from Bredig[53] illustrates the above phase relationships. It shows the free energy increasing with increasing temperature, whereas it should decrease, but the diagram is valid if the ordinate is considered to represent vapour pressure instead of free energy.

Due to a decrease in density on the transition to the γ form, there is a volume increase which may result in the destructive expansion of a material in which $Ca_2SiO_4$ is present. This phenomenon is known as "dusting". Stabilization of $Ca_2SiO_4$ can be achieved by the addition of various inhibitors and $B_2O_3$, $Cr_2O_3$, $P_2O_5$, $As_2O_5$, $Mn_2O_3$ have been established[54] as effective chemical inhibitors of the transition to γ-$Ca_2SiO_4$. The suggested mechanism of this inhibition depends on the solid solution of these oxides in the higher temperature α'lattice, their insolubility

in the low temperature γ lattice, and their sluggish exsolution or precipitation from the α'-form. Solid solution itself is not a criterion for inhibition. $Fe_2O_3$ also forms solid solutions in α'-$C_2S$ but does not inhibit the α'-γ inversion except in $Fe_2O_3$-rich compositions.

The temperature at which phase changes occur is lowered by the presence of a soluble impurity. Newman and Wells[55], who studied the effect of additions on the inversion temperature, found that the α-α' inversion was lowered from 1450° to 1400°C by the addition of 2.5 wt.% $Cr_2O_3$ approximately. Since higher additions gave no further lowering they concluded that this figure represented the solubility limit of $Cr_2O_3$ in the α-form. The same method was used to obtain solubility limits for the other oxides added.

Schlaudt and Roy[25] found that the α-α' $Ca_2SiO_4$ inversion temperature was lowered from 1447°C to 1400°C by Mg substitution in the lattice. α'-$Ca_2SiO_4$ takes Mg into its lattice up to the composition $Ca_{1.94}Mg_{0.06}SiO_4$ at 1400°C and to $Ca_{1.96}Mg_{0.04}SiO_4$ at 900°C. Gutt[27] pointed out that the temperature of the α-α' $Ca_2SiO_4$ inversion is lowered from 1447°C to 1360°C.

Recently, Glasser[56] has also studied the polymorphism of $Ca_2SiO_4$ and its importance in cement chemistry.

## 3. PLAN OF INVESTIGATION

1. System $CaO-MgO-Al_2O_3-SiO_2$: An investigation of the compatibility relationships of periclase in the system $CaO-MgO-Al_2O_3-SiO_2$ was done to establish the influence of variation in the relative proportions of $CaO$, $Al_2O_3$ and $SiO_2$ on melt formation in magnesite refractories. As described in Section 2.5., O'Hara and Biggar[50] constructed Figure 11 from literature data and their diagram makes no allowance for the effect of the solid solubility of $Al_2O_3$ in periclase at high temperatures on the position of the projected boundaries. A study has therefore been made of the phase changes occurring in mixtures containing 80 wt.% MgO and a projection of the phase boundaries on the boundary surface of the primary phase volume of periclase constructed from the data. By comparison with the data of Crookes[51] and Tarboton[52], diagrams have also been constructed to show the influence of partial replacement of $Al_2O_3$ by $Fe_2O_3$ and $Cr_2O_3$.

2. System $MgO-MgCr_2O_4-Ca_2SiO_4$: This system is a section of the system $CaO-MgO-Cr_2O_3-SiO_2$ which was investigated by Tarboton[52]. The primary object of the investigation was to determine the limits of the primary phase volume of periclase in this section in the quaternary composition tetrahedron and to estabiish the composition of the eutectic point (piercing point) at which MgO, spinel, $Ca_2SiO_4$ and

liquid coexist.

3. System $MgO-Fe_2O_3-Ca_3MgSi_2O_8$: An investigation of solid-liquid relationships in the section $MgO-Fe_2O_3-Ca_3MgSi_2O_8$ of the system $CaO-MgO-Fe_2O_3-SiO_2$ at 1550°C was carried out to supplement the work of Crookes[51] on the compatibility relationships of periclase in this system and the triangles within which MW + MF; MW + $C_3MS_2$; MW + $C_3MS_2$ + $C_2S$; MW + $C_2S$ coexist with liquid phase were established.

The binary section $MF-C_3MS_2$ was also investigated. A significant finding was that specimens containing $C_3MS_2$ must be quenched in water prior to examination since this phase tends to crystallize from the melt during air-quenching.

4. The Pseudo-Ternary System $MgAl_2O_4-MgCr_2O_4-Ca_3MgSi_2O_8$: The Pseudo-Ternary system $MgAl_2O_4-MgCr_2O_4-Ca_3MgSi_2O_8$ was previously investigated by El-Shahat and White[3] who used air-quenching and was re-investigated using water-quenching following the discovery that air-quenching was unsatisfactory for mixtures containing appreciable $C_3MS_2$.

# 4. APPARATUS AND STARTING MATERIALS

## 4.1. The Molybdenum Furnace

The furnace used for firing sample was a small molybdenum-wound resistance furnace, of the type that has been used in the department for a number of years. It is capable of firing to temperatures of 1750°C, is economic and easy to build. The essential features of the furnace are shown in Figure 15 and the power supply and control circuit are shown in Figure 16.

The furnace consisted of two concentric, impervious, recrystallised alumina tubes, each 12" long, with a wall thickness of ⅛" and having an internal diameter of 1⅞" and 1" respectively. Around the central 7" of the narrower tube a length of molybdenum wire (0.028" diameter) was tightly wound, the windings being spaced at 1/10" intervals and held in place at each end by extra pieces of double, tightly wound molybdenum wire which were plaited with the ends of the winding to provide electrical leads made up of three wires. At each end of the winding these leads were fed through short lengths of ¼" thick alumina tubes which were strapped tightly to the alumina furnace tube with molybdenum wire.

The winding was covered with a layer of C.C.60 high alumina cement with 2" collars at each end for positioning it centrally in the wider tube. Both ends of the furnace were then sealed with a 1:1 mixture of C.C.60 and "Autostick" ceramic cement (product of Carlton Brown) and

at the same time Pyrex glass T-pieces were cemented to the small alumina tubes at both ends with the same mixture. The whole assemblage was further made gas-tight by cementing the lead wires into the Pyrex T-pieces, leaving the remaining arms open for gas entry and exit. Asbestos string was wound around the tube about 1½" from one end such that the furnace assemblage was supported vertically on the asbestos sheet within the Dexion frame of the furnace. A 4" diameter recrystallised alumina tube was placed round the furnace tubes and the gap filled with insulating alumina powder. Insulating bricks were cut to the required shapes to fill the gap between the outer alumina tube and the Dexion frame.

To prevent the molybdenum winding from oxidising above 250$^{o}$C, a mixture of 90% nitrogen/10% hydrogen gas (by volume) was passed into the furnace at one end via the top glass T-piece and out the other end via the bottom T-piece. The rate of gas flow was regulated by placing bubbles at the inlet and outlet to the furnace.

During the initial heat-up some water was liberated from the furnace and this was drained off from the bottom T-piece before sealing it.

A loose plug of insulating brick was positioned in the top and bottom of the furnace to minimise air currents affecting the temperature, the top plug being cut to allow a thermocouple entrance into the furnace. A Pt 5% Rh: Pt 20% Rh thermocouple with a solid 18" alumina sheath,

positioned with the hot junction in the centre of the hot zone (1½") of the furnace and connected to a portable potentiometer was used to measure the temperature.

A motor-driven "Variac" transformer was used to vary the current supplied to the furnace. The "Variac" motor could either be driven continuously or intermittently, or using a "Simmerstat" regulator, to control the heating or cooling rate at about 10°C per minute. The furnace was controlled at the required temperature using a "West Gardsman" controller.

## 4.2. Starting Materials

All the materials used after the treatments described below were ground in a mechanical agate mortar to pass a -300 mesh B.S. sieve and were stored in sealed bottles. The chemical analysis and X-ray results of all the materials used are shown in Tables 3, 4 and 5.

### 4.2.1. Magnesium Oxide (MgO)

The starting material for the production of MgO was 99.96% pure magnesium metal (see Table 3). A section of a magnesium ingot was degreased and cleaned with nitric acid. It was then milled dry with a new clean milling cutter. The millings were obtained in the finest possible form and any large pieces were rejected. About 100 gm. of turnings were placed in polypropylene beakers, moistened with distilled water and then steam-heated in a pressure-cooker at two atmospheres for at least 30 hrs. to produce

magnesium hydroxide. Unreacted magnesium particles greater than 104μ were sieved out through 150 mesh B.S. and the hydroxide was calcined for five hrs. at 1360°C in a covered platinum dish in a Carbolite furnace.

4.2.2. Calcium Carbonate ($CaCO_3$)

"Analar" grade calcium carbonate of 96.4% purity was used as a source of CaO.

4.2.3. Silica ($SiO_2$)

Washed Belgian glass sand of 99.6% purity was used.

4.2.4. Chromium Oxide ($Cr_2O_3$)

Chromium oxide was prepared from "Analar" chromium trioxide, $CrO_3$, of 99.99% purity by firing it at 1000°C for 3 hrs. Care had to be taken during the initial heating-up when the $CrO_3$ melted and emitted dense fumes. This was done in a fume cupboard. The material proved impossible to grind, due to its tendency to ball, and was rubbed through a 200 mesh B.S. screen with the fingers.

4.2.5. Alumina ($Al_2O_3$)

"Linde" calcined alumina (supplied by Union Carbide) of 0.3 micron particle size, and 99.8% purity was used after ignition to 1000°C.

4.2.6. Ferric Oxide ($Fe_2O_3$)

"Specpure" grade ferric oxide, supplied by Johnson Matthey, was ignited to 700°C before use.

4.2.7. Merwinite ($Ca_3MgSi_2O_8$)

Merwinite was prepared by intimately mixing the finely ground, high-purity Belgian sand, "Analar" $CaCO_3$ and MgO in the correct proportions. The mixture was then pressed (10 t.s.i.) into cylinders (25 mm. diameter and 10 mm. height) with a 5% starch solution as a binder and fired in a Carbolite furnace for 4 hrs. at 1400°C in a covered platinum dish. The product was then ground, repressed and refired for another 4 hrs. at 1400°C.

4.2.8. $MgAl_2O_4$-$MgCr_2O_4$ Solid Solutions

Spinel solid solutions were prepared by intimately mixing MgO, $Al_2O_3$ and $Cr_2O_3$ in the correct proportions to give spinel solid solutions having the molar compositions $MgAl_{0.8}Cr_{1.2}O_4$ and $MgAl_{1.5}Cr_{0.5}O_4$.

The mixtures were pressed into cylinders with a 5% starch solution as a binder and fired in a Carbolite furnace for 10 hrs. at 1400°C in a covered platinum dish. The product was then ground, repressed and refired for another 30 hrs. at 1400°C.

4.2.9. The Spinels $MgAl_2O_4$ and $MgCr_2O_4$

The same procedure was again used to prepare these spinels, the firing temperature being 1400°C.

4.2.10. The Spinel $MgFe_2O_4$

The appropriate amounts of MgO and $Fe_2O_3$ were weighed out, mixed and pressed as above and the pellet then fired for 6 hrs. at 1300°C in air. The pellet was then coarsely

crushed to ensure free access of air, replaced in the carbolite furnace at 1300°C and slowly cooled to 600°C to bring about complete reoxidation of any ferrous iron to the ferric state[30].

4.2.11. Chemical Analysis and X-rays of the Materials Used

It is important to observe the following points in Table 5:

(i) Belgian glass sand contains impurities that are partially removed after washing in distilled water.

(ii) Probably the time and temperature used in firing Merwinite and Spinel (MA) were insufficient because those compositions are not in equilibrium as shown by the X-ray results.

(iii) Comparison of the theoretical compositions of the synthetic spinels and merwinite with the chemical analysis after firing exhibit some deviations. The chemical analysis of the spinels MF, MK and MA suggest that some $Fe_2O_3$, $Cr_2O_3$ and $Al_2O_3$ were volatilized during firing.

## 5. EXPERIMENTAL METHODS AND TECHNIQUES

The techniques used in this investigation have been established in the Department over a number of years. A pellet of known composition is fired at a predetermined temperature, in the molybdenum furnace for a chosen period and then it is removed from the furnace and quenched. A section from the specimen is then prepared for examination under the optical microscope, using reflected light techniques.

Reflected light techniques have been used for the study of ore minerals since about 1917. However, it was not until 1951 that Schouten[57] indicated the extreme usefulness of these techniques as applied to the study of polished sections of refractory products.

Other early workers in this field were Snow[58] in America and Roberts[59] in this country. More recently, Treffner[60] has worked on the microstructure of raw chrome ores and the work of Van Vlack[44], previously mentioned, also indicated the usefulness of this approach.

### 5.1. Preparation of Specimens for Firing

In studying each system, required compositions were prepared by mixing appropriate weights of the above starting materials.

The relevant amounts were weighed into small glass vials (to $10^{-4}$ gm.) to give a total weight of 1.0000 gm.

after firing. They were then mixed together in a Glen Creston mixer for 30 minutes. After mixing, the sides of the container were carefully scraped with a spatula to remove any adhering mixture.

When the mixtures used contained calcium carbonate they were initially dry pressed into cylindrical pellets in a steel mould of 6 mm. diameter at a pressure of 15 - 20 t.s.i. The pellets were heated for one hour in a platinum wound tube furnace at 1000°C to decompose the calcium carbonate and then re-pressed in the steel mould at 35 - 40 t.s.i. to give a final pellet 4 - 5 mm. in height. Re-pressing was carried out before complete cooling had taken place in order to minimise hydration of the calcium oxide.

If the specimens were not pre-heated in this way, those containing appreciable amounts of $CaCO_3$ displayed a high porosity after firing resulting in non-uniform microstructures. Contamination from the mould was removed from the surface of the pellets after each pressing using a razor blade. It was not found necessary to use a binder for any of the mixture.

## 5.2. Firing of Pellets

Pellets were fired four at a time in the molybdenum furnace described in Section 4.1. To do this, containers for the pellets were made from platinum foil, shaped into small boxes just large enough to accept the pellet.

When the liquid content of the fired specimens was expected to be high, they were put in a double-walled platinum box or in small dense magnesia crucibles made by isostatic pressing and sintering, as described by Pressley[61].

These precautions were found to be very effective in preventing loss of liquid from the platinum box or crucibles, the walls of which tended to be drawn inwards by the melt at high temperatures, when only a single thickness of platinum foil was used. This deformation was apparently caused by the action of the surface tension of the liquid on the walls of the box.

The boxes were fastened concentrically around the end of the thermocouple with platinum wire (as shown in Figure 15) and were lowered slowly into the hot zone of the furnace. The temperature was then held constant for periods ranging from 1 hr. to 24 hrs. until equilibrium had been achieved.

If the samples had small amounts of a liquid phase and a secondary phase, a prolonged soaking time (24 hrs.) was used to produce larger grain-sizes in the specimens, for easier identification of the phases under the optical microscope.

At the end of the firing period the specimens were quenched by removing the thermocouple rapidly from the furnace and cooling it in a stream of cool air. This procedure was replaced in the course of the investigation

by quenching the samples in cold water since this also assisted in improving certain microstructural features.

## 5.3. Preparation of Specimens for Microscopic Examination

All the specimens were examined using standard reflected light microscopy techniques. After detaching adhering platinum from the quenched specimens they were set in epoxy resin using cylindrical moulds. Sections were then cut through them and polished for microscopic investigation. The resin used was a mixture of Araldite MY753 and Araldite Hardener HY951 in the ratio 6:1 by volume, the liquid mixture being poured over the pellet in a greased metal mould. The mould was then placed in a vacuum dessicator. This was evacuated and air then was admitted slowly allowing the pressure to force Araldite into the open pores of the pellet. The mount was allowed to harden either by leaving at room temperature overnight or by heating to 60$^{o}$C for about an hour.

During the present investigation, a new kind of epoxy resin, M.E.L. Transfast was also used, one scoop (0.45 gm.) or four scoops (1.80 gm.) of Benzoyl Peroxide Catalyst (purity 50%) was used per 25 ml. of resin, and the mixture poured into plastic moulds, without greasing and allowed to set for 60 minutes or 15 minutes respectively.

When it had set, the mount was released from the mould. To prepare a section for examination the specimen

was first ground on a wet diamond wheel to remove the surface layers. The cut face was then ground on progressively finer silicon carbide papers, starting on a 360 grit and finishing on a 600 grit paper, and using Microfin lapping fluid as a lubricant. The time of grinding on each successive paper was increased progressively being 20 seconds on the 360 grit and 2 minutes on the 600 grit paper.

Following this the samples were polished on a nylon cloth fixed to a brass lapping plate, starting with a cloth impregnated with 6μ diamond paste, then on to 3μ, 1μ and 0.1μ, in that order. "Microfin" lapping fluid was used as a lubricant for each stage and about two minutes was spent polishing on each paste. This method gave relief-free samples suitable for microscopic work and etching, but in some cases a final polish on 0.1μ γ-alumina powder was done, which gave the sample some relief and helped in the identification of certain phases.

## 5.4. Phase Identification Using Reflected Light Microscopy

The samples fired at low temperatures, generally contained high porosity and very poor crystallinity, and it was difficult to distinguish the liquid phase from the solid phase.

This problem was overcome leaving the samples for a longer soaking period in the furnace and in some cases the samples were heated to a higher temperature, then

cooled and soaked at the required temperature. This technique resulted in increased grain size of the primary phase which made examination of the interstitial phases easier.

During the present investigation four silicate phases (forsterite, monticellite, merwinite and dicalcium silicate) were found in the specimens studied.

A series of etching solutions was used which selectively etched the four silicate phases and helped considerably in distinguishing these phases. For this technique to be effective however the polished section had to be free from relief and previously unetched. The etchants used and the phases they affected were as follows:

| Etchant | Etching Time | Silicate Phase | | | |
|---|---|---|---|---|---|
| | | $C_2S$ | $C_3MS_2$ | CMS | $M_2S$ |
| 1% Borax solution | 10 mins. | ++ | - | - | - |
| 5%$NH_4Cl$ solution | 100 secs. | +++ | ++ | - | - |
| 10% HCl solution | 12 secs. | +++ | +++ | ++ | - |
| 5% HF solution | 3 secs. | +++ | +++ | +++ | - |

+++ strongly etched
++ moderately etched
- unetched

Thus by starting with the 1% Borax solution, etching and inspecting under the microscope, then proceeding to the 5% $NH_4Cl$ solution, and so on, it was possible to

identify which of these phases was present.

## 5.5. Microscopic Features of Phases

Eleven solid phases were observed using reflected light microscopy. The appearance of these phases is illustrated by the plates 1 - 15 and described below:

1. Periclase (MgO): This phase occurred usually as well rounded grains. Typical periclase can be seen in Plate 1.

2. Magnesiowustite (MW): This phase occurred as large, well rounded grains, having higher reflectivity than pure periclase. Identifiable using any of the polishing techniques, its typical appearance is illustrated in Plates 10 and 11.

3. Dicalcium Silicate ($C_2S$): This phase occurred as large, partly rounded grains, which, when etched (with 1% Borax solution or by polishing with γ-alumina and water), showed a characteristic dark and light striated appearance, as illustrated in Plate 3. The striated appearance is attributed to twinning (e.g. Prince[31]).

4. Merwinite ($C_3MS_2$): This phase had a platey appearance and on etching (with 5% $NH_4Cl$ solution), displayed a characteristic series of fine criss-cross striations (twinning) on the surface, by which it was readily identified. Its typical appearance is illustrated in Plate 2.

5. Monticellite (CMS): This phase had few features by which it could be identified and difficulty in its identification was enhanced by its occurrence only at low temperatures where the samples inevitably have a very high porosity and poorly developed microstructures. However, by etching successively with 5% $NH_4Cl$, 10% HCl and 5% HF solutions, it could usually be identified by a process of elimination. Plate 4 illustrates its typical appearance.

6. Forsterite ($M_2S$): this phase was readily identified by its blocky, tabular appearance. It was considerably darker in colour than periclase grains. Polishing with γ-alumina gave the grains some relief and enhanced their angular appearance. Its appearance is illustrated in Plate 5.

7. Spinels (MF, MK, MA, $MgAl_{0.5}Cr_{1.2}O_4$ and $MgAl_{1.5}Cr_{0.5}O_4$): These phases were quite distinctive, being highly reflecting and occurring as small angular grains, almost invariably concentrated in localised clusters, as illustrated in Plate 6.

It was found that this concentration of crystals into localised zones occurred when spinel was the second phase (after periclase in the system $MgO-Al_2O_3-CaO-SiO_2$) to crystallise.

The crystals were generally uniformly distributed through the sample when it crystallised after a silicate phase (i.e. appeared as a third or fourth phase).

## 6. COMPATIBILITY RELATIONSHIPS OF PERICLASE IN THE SYSTEM $CaO-MgO-Al_2O_3-SiO_2$ IN AIR

### 6.1. Previous Work

As described in Section 3, the objective of this investigation was to determine the effect of the solid solubility of $Al_2O_3$ in periclase at high temperatures on O'Hara and Biggar's[50] projection of the boundary surface of the periclase phase volume in the system $CaO-MgO-Al_2O_3-SiO_2$.

As described in Section 2.5, previous work on this system was carried out by Solacolu[33] and O'Hara and Biggar[50]. Solacolu[33] investigated the partial system $MgO-MA-M_2S-C_2S$ and Figure 6 shows his phase diagram redrawn by White[32]. His projection through the MgO corner of the tetrahedron of the boundary surface of the primary phase volume of periclase is shown in Figure 21.

O'Hara and Biggar's[50] projection of the same boundary surface is shown in Figure 11. In recent papers[62,63,64] they have revised this diagram for the partial system $MgO-MA-M_2S-C_2S$, projecting on to the plane $MA-M_2S-C_2S$, and expressing compositions in terms of the MA, $M_2S$ and $C_2S$ contents of the mixture recalculated to 100 wt.%. They give the temperatures of the three invariant points as 1425°C ($L_1$), 1410°C ($L_2$) and 1410°C ($L_3$) respectively.

### 6.2. Experimental Procedure and Results

In the present investigation, mixtures containing

80 wt.% MgO with $CaO/SiO_2$ ratios up 2/1 (molecularly) were investigated, their compositions being selected so that they would fall close to phase boundaries in the projected diagram.

Each composition was examined after quenching from a range of temperatures to establish the temperature at which the second phase appeared (periclase being the primary phase in all cases). Table 6 lists all the compositions prepared together with their firing temperatures and the phases identified as having been present at those temperatures. Some of these compositions expressed in terms of their CaO, $Al_2O_3$ and $SiO_2$ contents recalculated to 100 wt.%, and the boundaries of secondary phase fields established by them, are plotted on Figure 17. Five secondary phase fields were established and identified as those of spinel, forsterite, monticellite, merwinite and dicalcium silicate.

Figure 18 shows the positions of the boundaries and the approximate temperatures at which the second phases would appear on cooling (indicated by the isotherms).

Three quaternary invariant points were found, marked b, d and f in Figure 18. These occur where, respectively, (i) spinel, forsterite and monticellite, (ii) spinel, monticellite and merwinite and (iii) spinel, merwinite and dicalcium silicate coexist with periclase and the liquid phase. The temperatures of these points were established as 1415°C, 1390°C and 1410°C respectively,

all within probable limits of approximately ± 5°C.

The compositions and temperatures of these points are given in the table below together with the compositions and temperatures of four ternary invariant points (a, m, n and p) lying on the edges of the diagram.

Also shown are the compositions and temperatures of five points (c, h, e, k and g) in which the joins CMS-$Al_2O_3$, $C_3MS_2$-$Al_2O_3$ and $C_2S$-$Al_2O_3$ intersect the phase boundaries. These joins are respectively the (projected) intersections of the planes MgO-$Al_2O_3$-CS, MgO-$Al_2O_3$-$C_3S_2$ and MgO-$Al_2O_3$-$C_2S$ in the quaternary tetrahedron with the boundary surface. Similarly the points in which the three joins intersect the phase boundaries in Figure 13 are projections of the intersections between these three planes and the boundary lines in the latter surface.

| Points | Compositions in wt.% | | | Temperature °C |
|---|---|---|---|---|
| | CaO | $Al_2O_3$ | $SiO_2$ | |
| a | - | 50.0 | 50.0 | 1710 ± 5 |
| b | 39.0 | 16.0 | 45.0 | 1415 ± 5 |
| c | 40.5 | 15.5 | 44.0 | 1405 ± 5 |
| d | 42.0 | 16.0 | 42.0 | 1390 ± 5 |
| e | 45.0 | 22.0 | 33.0 | 1430 ± 5 |
| f | 47.0 | 26.0 | 27.0 | 1410 ± 5 |
| g | 47.5 | 27.0 | 25.5 | 1415 ± 5 |
| k | 52.0 | 10.0 | 38.0 | 1520 ± 5 |
| p | 53.0 | - | 47.0 | 1575 ± 5 |
| n | 46.5 | - | 53.5 | 1498 ± 5 |
| m | 41.5 | - | 58.5 | 1502 ± 5 |
| h | 46.5 | 2.5 | 51.0 | 1480 ± 5 |

Microstructural features are shown in Plates 1, 2, 3, 4, 5 and 6.

## 6.3. Discussion

Comparisons between O'Hara and Biggar's projections

through MgO of the boundary surface of the periclase field and the results of the present investigation are shown in Figures 19 and 20 (the latter, as explained in Section 6.1, being a projection through the MgO corner on to the plane $MA-M_2S-C_2S$). In their projection on to the plane $CaO-Al_2O_3-SiO_2$ shown in Figure 19 they included a secondary crystallization field of the phase T mentioned in Section 2.1, but omitted it from later diagrams so it does not occur in their version of Figure 20. This phase is difficult to detect and has not been observed during the present investigation although it is stable up to 1400°C as shown by Schlaudt and Roy[25] and Gutt[26].

As a consequence the single invariant point f in Figure 18 (and in the versions of Figures 19 and 20 based on the present work) at which MgO, $C_2S$, $C_3MS_2$, spinel and liquid coexist is replaced in their version of Figure 19 by two points, f' at which MgO, $C_3MS_2$, T, spinel and liquid coexist, and f" at which MgO, $C_2S$, T, spinel and liquid coexist.

It will be seen in Figure 19 that the boundary of the secondary field of spinel established by the present work, i.e. abdf deviates progressively, as the temperature increases, towards higher $Al_2O_3$ contents from a'b'd'f'f", the boundary in O'Hara and Biggar's projection.

This deviation can be attributed to solid solution of the sesquioxide in periclase at high temperatures.

The nature of the effect is shown in Figure 22 in the ternary system $MgO-Al_2O_3-SiO_2$[65] which forms a section of the quaternary system $CaO-MgO-Al_2O_3-SiO_2$, Figure 22 shows the boundary of the primary field of periclase and of the ternary eutectic at which MgO, $M_2S$ and MA coexist with liquid and it will be seen that a projection of the eutectic point E through the MgO corner falls at $\underline{e}_1$ (41 wt.% $Al_2O_3$ and 59 wt.% $SiO_2$), the position of which agrees closely with the position indicated in O'Hara and Biggar's projection [ $\underline{a'}$ (41 wt.% $Al_2O_3$ and 59 wt.% $SiO_2$) in Figure 19] .

If the solid solubility of $Al_2O_3$ in MgO at 1710°C, the temperature of $\underline{e}_1$, was negligible, freezing paths of mixtures in the primary field of periclase would radiate from the MgO corner and $\underline{e}_1$ would be the position of the projected eutectic determined experimentally by the methods used in the present investigation.

Actually however the solubility at the temperature of $\underline{e}_1$ will be appreciable. According to Alper et al.[18] the solubility of $Al_2O_3$ is approximately 17 wt.% in the binary system $MgO-MgAl_2O_4$ at 1995°C, the temperature of the $MgO-MgAl_2O_4$ eutectic. At 1710°C, the temperature of the eutectic E in the ternary system, the solubility will be considerably less than this but is still appreciable. According to the diagram of these authors, in the binary system, it is about 4 wt.%.

Hence the conjugation line from the periclase-$MgAl_2O_4$

solid solution phase to the eutectic will not pass through the MgO corner of the diagram but will pass through a point D on the $MgO-Al_2O_3$ edge as shown in Figure 22.

The line ED then divides the primary field of periclase in Figure 22 such that, $M_2S$ will be the secondary phase below ED and spinel the secondary phase above it. In the 80 wt.% MgO series, the change in the secondary phase $M_2S$ from spinel was found to lie at point A, so that D must lie on EA produced as shown and it will be seen that the position of D established in this way agrees well with the solubility of 4 wt.% established for the binary system[18].

Composition "A" will, of course, when projected through the MgO corner of the triangle onto the $Al_2O_3-SiO_2$ edge appear to lie at $\underline{e}_2$ (49 wt.% $Al_2O_3$ and 51 wt.% $SiO_2$) which corresponds with point $\underline{a}$ (50 wt.% $Al_2O_3$ and 50 wt.% $SiO_2$) of Figure 19. Similarly compositions B and C lie on ED at 90 wt.% MgO and 70 wt.% MgO will project to $\underline{e}_3$ and $\underline{e}_4$ respectively. Hence the displacement of the eutectic in the projected diagram will also increase as the MgO content of the series investigated increases.

In the $MgO-Al_2O_3-C_2S$[31] diagram shown in Figure 23 the eutectic occurs at a lower temperature (1417°C) and solid solubility of $Al_2O_3$ in MgO is negligible at this temperature (see below). When the composition of the eutectic established from mixtures lying on the conjugation line to the eutectic are projected through the MgO

corner of the triangle on to the $Al_2O_3$-$C_2S$ edge they will therefore lie at T (26.5 wt.% $Al_2O_3$ and 73.5 wt.% $C_2S$) and the position of T will not depend on the MgO content of the mixtures investigated. This position is in reasonable agreement with that of points g (27 wt.% $Al_2O_3$ and 73 wt.% $C_2S$) and g' (26 wt.% $Al_2O_3$ and 74 wt.% $SiO_2$) in Figure 19 determined respectively from this investigation and from O'Hara and Biggar's projection.

Figure 24 shows the effect of varying the MgO content of the experimental mixtures on the boundary of the spinel field in the projected diagram, as predicted from Figures 22 and 23. It was assumed that solubility of $Al_2O_3$ in MgO would be negligible below 1500°C so that displacement of the boundary should occur above this temperature.

The solid solubility between MgO-$M_2S$ in the system MgO-MA-$M_2S$ reported by Schlaudt and Roy[16] was considered negligible in this investigation because their findings have not been confirmed by other workers[9,10,13,14,15].

Points c and h in Figure 18 belong to the join $Al_2O_3$-CMS and should be piercing points in the ternary system MgO-$Al_2O_3$-CS which forms a section of the quaternary system CaO-MgO-$Al_2O_3$-$SiO_2$. A phase diagram for this section was previously constructed by El-Shahat and White[2], from their diagram for the binary section MA-CMS, which is shown in Figure 25. Their diagram for the ternary section is shown in Figure 26. Figure 27 shows the same

diagram redrawn using results from this investigation. The following data were used in locating the various points in Figures 26 and 27.

| Point | Temperature °C | Composition wt.% | | | Source |
|---|---|---|---|---|---|
| | | MgO | $Al_2O_3$ | CS | |
| E | 1640 ± 10 | 26.0 | 21.0 | 53.0 | Figure 25 (eutectic point e) |
| J | 1410 ± 10 | 26.0 | 7.5 | 66.5 | Figure 25 (reaction point J) |
| G | 1498 | 22.0 | - | 78.0 | Reference number 66 (peritectic point) |
| F | 1995 | 45.0 | 55.0 | - | Reference number 18 (eutectic point) |
| c | 1405 ± 5 | - | 16.0 | 84.0 | Figure 18 |
| h | 1480 ± 5 | - | 2.5 | 97.5 | Figure 18 |

In Figure 26 the composition of R was found by El-Shahat and White[2] approximately by assuming that the eutectic boundary FER was a straight line, R being the intersection between this line and the straight line MgO-J produced. The composition of R located in this way was found to be 19.5% MgO, 8% $Al_2O_3$ and 72.5% CS by weight, i.e. 37.5 $SiO_2$, 19.5% MgO, 35% CaO and 8% $Al_2O_3$ by weight.

R' in Figure 27 was found by drawing a straight line through the MgO corner to point c (the latter corresponding to point c the projection of R' through the MgO corner in Figure 18) and by reading off the MgO content at R' on O'Hara and Biggar's diagram shown in Figure 28, which is approximately 20%, R' has therefore been placed on

the line MgO-c in Figure 27 where it crosses the 20% MgO line. It will be seen that, with R' located in this way, the boundary FER', is slightly curved. The composition of R' obtained in this way is 20% MgO, 13% $Al_2O_3$ and 67% CS by weight, i.e. 32.4% CaO, 20% MgO, 34.6% $SiO_2$ and 13% $Al_2O_3$ by weight.

The piercing points R and R' at which MA, MgO, CMS and liquid coexist in Figures 26 and 27 occur at 1410 $\pm$ 10°C and 1405 $\pm$ 5°C respectively, these being the temperatures of points J and c in Figures 25 and 18. There is thus good agreement in this respect between the present results and those of El-Shahat and White[2].

In drawing the lines MgO-J and MgO-c in Figures 26 and 27 through MgO it was assumed that the solubility of $Al_2O_3$ in MgO in equilibrium with liquidus R and R' was negligible, which appears to be justified by its extremely low solubility in MgO at 1410°C and 1405°C in the binary section MgO-$Al_2O_3$[18].

In both Figures 26 and 27, it will be seen that the field of primary crystallization of MgO overlaps the line of the section in the ternary system.

Point h' shown in Figure 27 was obtained by drawing a straight line from the MgO corner to h, corresponding to point h in Figure 18, and reading off the MgO content at this point on Figure 28, which is approximately 22.5% MgO. h' occurs at 2% $Al_2O_3$, 22.5% MgO and 75.5% CS by weight, i.e. 39% $SiO_2$, 22.5% MgO, 36.5% CaO and 2% $Al_2O_3$ by weight. At this point MgO, $C_3MS_2$, $C_2S$ and liquid are in equilibrium.

Figure 29 shows the phase diagram of the section MA-CMS (see Figure 25) redrawn using the results of the present investigation.

Similarly Figure 31, which shows the boundary of the primary field of periclase in the section $MgO-Al_2O_3-C_3S_2$, was also constructed from El-Shahat and White's[3] phase diagram for the join $MA-C_3MS_2$, shown in Figure 30, and the results of the present investigation, using O'Hara and Biggar's data for the MgO contents of the liquid phase (Figure 28) as in constructing Figure 27.

In Figure 18 points e and k are piercing points in the section $MgO-Al_2O_3-C_3S_2$. The following data from these sources were used in locating the various points in Figure 31.

| Point | Temperature °C | Composition wt.% | | | Source |
|---|---|---|---|---|---|
| | | MgO | $Al_2O_3$ | $C_3S_2$ | |
| A | 1995 | 45.0 | 55.0 | - | Reference number 18 (eutectic point) |
| H | 1720 | 15.6 | - | 84.4 | Reference number 66 (peritectic point |
| e | 1430 ± 5 | - | 22.0 | 78.0 | Figure 18 |
| k | 1520 ± 5 | - | 10.0 | 90.0 | Figure 18 |
| E | 1560 ± 10 | 17.5 | 24.1 | 58.4 | Figure 30 |
| F | 1575 ± 10 | 14.2 | 9.0 | 76.8 | Figure 30 |

Point R in Figure 31, which corresponds to point e, the maximum in the projected $MA-C_3MS_2$ boundary in Figure 18, is a reaction point at which MA, MgO, $C_3MS_2$ and liquid

coexist occurs at 1430 ± 5°C (being the temperature of the point e). Its composition and position were found using similar procedures to those described above for the ternary system $MgO-Al_2O_3-CS$. The composition of the liquid at point R, was found to be 13% MgO, 19% $Al_2O_3$ and 68% $C_3S_2$ by weight, i.e. 39.6% CaO, 13% MgO, 28.4% $SiO_2$ and 19% $Al_2O_3$ by weight.

As shown in Figure 31 the field of primary crystallisation of MgO overlaps the line of the section in the ternary system agreeing with the results of El-Shahat and White[3] and Gutt[67].

The latter established the partial system $3CaO.MgO.2SiO_2$-$MgO.Al_2O_3$-$2CaO.Al_2O_3.SiO_2$ of the quaternary system $CaO-MgO-Al_2O_3-SiO_2$. Points e and k also correspond to piercing points in Gutt's[67] diagram. His compositions for these points, expressed in terms of the contents of CaO, $Al_2O_3$ and $SiO_2$ of his mixtures recalculated to 100%, are shown below together with those from the present investigation.

| Point | CaO Wt.% | $Al_2O_3$ Wt.% | $SiO_2$ Wt.% | Temp. °C | Phases | Source |
|---|---|---|---|---|---|---|
| e | 46.0 | 22.5 | 31.5 | 1424 | MgO, $C_3MS_2$ | Inferred point from Gutt's diagram[67] |
| | 45.0 | 22.0 | 33.0 | 1430±5 | Spinel & liquid | From Figure 18 |
| k | 52.5 | 10.5 | 37.0 | 1530 | MgO, $C_2S$ | Inferred point Gutt's diagram[67] |
| | 52.0 | 10.0 | 38.0 | 1520±5 | $C_3MS_2$ & liquid | From Figure 18 |

In Figure 31, point F at which the join MgO-k intersects the boundary H-R, agrees closely with the corresponding point in the binary section MA-$C_3MS_2$ investigated by El-Shahat and White[3].

The difference between Solacolu's[33] diagram and the results of the present investigation is shown in Figure 21. Solacolu's diagram similarly seems to have been based on the projection through the MgO corner of the boundary surface of the periclase phase volume in the system MgO-$C_2S$-$M_2S$-MA and he did not allow for the effect of solution of $Al_2O_3$ in MgO at high temperatures.

## 6.4. The Effect of the Relative Solid Solubilities of $Al_2O_3$, $Cr_2O_3$ and $Fe_2O_3$ at high temperatures on the projected diagrams

A feature of interest in Figure 18 is the extension of the spinel phase field, particularly when compared with the areas occupied by the spinel phase in the projected diagrams for the systems CaO-MgO-$Cr_2O_3$-$SiO_2$ (Figure 13) and CaO-MgO-$Fe_2O_3$-$SiO_2$ (Figure 12) as obtained by Tarboton[52] and Crookes[51] respectively. In the former system, where the spinel is $MgCr_2O_4$, the spinel field occupies less area than in the present investigation (Figure 18), whereas in the latter it is entirely absent, i.e. the areas decrease in the order $Al_2O_3$ > $Cr_2O_3$ > $Fe_2O_3$. Significantly, this relationship correlates with the relative solubilities of the three

spinels in periclase at elevated temperatures, shown in Figure 3, where $Al_2O_3 < Cr_2O_3 << Fe_2O_3$.

Tarboton[52] and Crookes[51] investigated the effect on the area of the spinel field in their projected diagrams of replacing half the $Cr_2O_3$ and $Fe_2O_3$ by $Al_2O_3$.

Their results are shown in Figure 32 together with the results of the present investigation. Although Crooke's[51] results, which were established for 70 wt.% MgO, are not strictly comparable with those of Tarboton[52] and of the present work, which were established for 80 wt.% MgO, it will be clear that partial replacement of $Al_2O_3$ by either $Cr_2O_3$ or $Fe_2O_3$ decreases the area of the spinel field markedly.

Quaternary invariant points and other points in Figure 32 were not established by Tarboton[52] and Crookes[51] accurately because only small numbers of samples were examined, but their temperatures would probably be between those established for the single sesquioxides. This assumption is confirmed by the results of El-Shahat and White[1,2,3] as described in Section 2.3. and illustrated by Figures 7, 8 and 9.

It is important to note that Richmond[5] found that the solid-solid bonding between spinel and MgO decreased, in mixtures fired for 2 hrs. at 1700°C, when $Cr_2O_3$ was replaced wholly or partially by $Al_2O_3$ or $Fe_2O_3$, in mixtures containing 15 wt.% CMS, the remainder being MgO and sesquioxide. The greatest degree of periclase-spinel

bonding was found to occur when the spinel was $MgCr_2O_4$ and the least when it was $MgAl_2O_4$.

On the other hand a possible benefit of $Al_2O_3$ in the spinel is that, at temperatures at which a liquid phase is present, a spinel phase will occur at lower sesquioxide contents.

## 6.5. Crystallisation Paths Within the System CaO-MgO-$Al_2O_3$-$SiO_2$

For all compositions studied in the primary phase volume of periclase, 80 wt.% MgO in the quaternary system CaO-MgO-$Al_2O_3$-$SiO_2$ the first solid phase to separate on equilibrium cooling, will be periclase and the freezing path will be a straight line passing through the MgO corner of the composition tetrahedron and the composition of the mixtures. On further cooling a second solid phase will separate at the boundary surface and the temperatures at which these secondary phases will start to crystallise on cooling, and up to which they will exist in the mixtures on heating, are indicated by the isotherms, which are shown in Figure 18 with temperatures alongside.

Once separation of a secondary phase has begun, the direction of the freezing path in Figure 18 at any temperature will lie along the straight line drawn through the point representing the composition of the secondary phase separating at that temperature and that representing the

composition of the mixture in the diagram. When the secondary phase has a fixed composition, this part of the freezing path in the diagram will therefore be a straight line, when the composition of the separating phase varies with temperature due to solid solution, it will be slightly curved.

On intersecting a phase boundary surface a third phase will start to separate and the freezing path will follow the boundary in the direction of falling temperature. Thereafter three possibilities exist:

(1) The freezing path may continue along the boundary to the nearest invariant point, where freezing will be completed. This will occur when the three phases coexisting with periclase and liquid at the invariant point are the same as those that will coexist with periclase in the completely solidified mixtures as indicated by the projected compatibility triangles in Figure 18.

(2) The freezing path may continue to the nearest invariant point but freezing may not be complete there. This will occur when the invariant point is a peritectic reaction point, if the three solid phases coexisting with periclase and liquid are not the same as will coexist with periclase in the completely solid mixture. Then, when reaction at the invariant point has been completed, liquid will still remain while complete resolution of the secondary

phase and separation of a new phase will have occurred. The freezing path will then follow that boundary whose temperature decreases away from the reaction point until it reaches the next reaction point where freezing will be completed as in (1).

(3) The freezing path may leave the boundary before it reaches an invariant point. This will occur, when the boundary line is a reaction line, if the secondary phase that had separated previously is completely redissolved before the invariant point is reached. The freezing path will then leave the boundary in the direction of the line passing through the point representing the composition of the solid phase now crystallising along with periclase and that representing the composition of the mixture. The freezing path will continue along this line until it intersects another boundary and proceeds again as in (1) or (2).

# 7. COMPATIBILITY RELATIONSHIPS IN THE SYSTEM $MgO-MgCr_2O_4-Ca_2SiO_4$ IN AIR

## 7.1. Previous Work

The objective of this investigation was described in Section 3.

The binary section $MgO-MgCr_2O_4$ was investigated by Alper et al.[20] who found the eutectic point at 2355°C, its composition being 35 wt.% MgO and 65 wt.% $Cr_2O_3$.

Wilde and Rees[68], who studied the system $MgO-Al_2O_3-Cr_2O_3$ found the same composition for the eutectic point reported by Alper et al.[20] but its temperature was 2120°C instead of 2355°C.

Keith[69], who investigated the system $MgO-Cr_2O_3-SiO_2$, concluded that their melting points for both the eutectic and for $MgCr_2O_4$, were probably low because of reduction of their specimens in the graphite-tube resistor furnace.

The liquidus temperature of Alper et al.[20] are also higher than those established by Gee[70] and by Wilde and Rees[68].

Investigations in the binary section $MgCr_2O_4-Ca_2SiO_4$ were previously carried out by Rigby et al.[71] who found that the refractoriness of the spinel-silicate mixtures progressively increased with the amount of spinel, indicating that the eutectic composition was low in MK. This agrees with the diagram established by Keith[69]. Rigby et al.[71] found that no melting occurred at any temperature up to 1700°C with specimens containing either

dicalcium silicate or forsterite.

The position of the eutectic point in the system MK-$C_2S$ was determined by El-Shahat and White[1]. Its composition was reported to be 21.5 wt.% $MgCr_2O_4$ and 78.5 wt.% $Ca_2SiO_4$ and its melting temperature 1700°C ± 10°C.

The eutectic point between MgO and $Ca_2SiO_4$ in the binary section was determined by Ricker and Osborn[11], its temperature and composition being respectively 1800°C ± 20°C and 85.9 wt.% $Ca_2SiO_4$: 14.1 wt.% MgO.

As described in Section 2.5, Tarboton[52] investigated melting relationships in CaO-MgO-$Cr_2O_3$-$SiO_2$ mixtures containing 80 wt.% MgO. This projection, through the MgO corner of the boundary surface of the primary field of periclase, is shown in Figure 13. Point B, which lies on the join $Cr_2O_3$-$C_2S$, is a temperature maximum and is therefore a ternary eutectic point in the section MgO-$Cr_2O_3$-$C_2S$.

## 7.2. Experimental Prodedure and Results

The composition of the mixtures investigated, their firing temperatures and the phases present at the temperatures are shown in Tables 7, 8 and 9 respectively.

Initially isoplethal sections were investigated at constant MgO contents, of 60 wt.% and 40 wt.% respectively, the remainder being $Cr_2O_3$ and $C_2S$.

The isoplethal sections at 60 wt.% MgO and 40 wt.% MgO are shown respectively in Figures 33 and 34. Figure 35 shows a similar isoplethal section at 80 wt.%

MgO constructed from Tarboton's diagram[52] (shown in Figure 13). It may be noted that the temperature of point F in Figure 35 was not established by Tarboton's diagram. It must however occur at the same temperature as the invariant points in Figures 33 and 34 and Figure 35 was constructed on this basis. The points M and N, O and P in each Figure were obtained from the binary diagram $MgO-MgCr_2O_4$ of Alper et al.[20] and from the join $MgO-C_2S$ of the ternary system $CaO-MgO-SiO_2$ established by Ricker and Osborn[11].

Points G, H and F of Figure 36 represent the compositions of the invariant points in these sections and lie on a straight line which must be the conjugation line joining the composition of the ternary eutectic in Figure 36 and the composition of the $MgO-Cr_2O_3$ solid solution in equilibrium with the eutectic liquid (see also Section 6.3. and Figure 22). When the compositions of these points are expressed in terms of their $Cr_2O_3$ and $C_2S$ contents recalculated to 100 wt.%, which is equivalent to projecting them through the MgO corner on to the $Cr_2O_3$-$C_2S$ edge of Figure 36, the compositions fall at points C, D and B which are the apparent positions of the invariant points in Figures 33, 34 and 35.

Point A in Figure 36 thus represents the composition of the $MgO-Cr_2O_3$ solid solution which is in equilibrium with the eutectic E. It occurs at approximately 12 wt.% $Cr_2O_3$ which is in close agreement with the limit of the

$MgO-Cr_2O_3$ solid solution series in the binary system $MgO-MgCr_2O_4$ established by Alper et al.[20]. The temperature of E was already known from the temperature of the invariant points in Figures 33 and 34 and its composition was established by quenching suitable mixtures of MgO, $Cr_2O_3$ and $C_2S$ and determining the primary phase occurring in them. Some of the compositions investigated are shown in Figure 36. A similar procedure was used to establish the composition of K, the binary eutectic in the pseudo-binary join $MK-C_2S$. As already described El-Shahat and White[1] found the temperature of this point to be 1700°C ± 10°C. Its composition (80 wt.% $C_2S$ and 20 wt.% MK) agrees well with the eutectic point (78.5 wt.% $C_2S$ and 21.5 wt.% MK) established by the latter investigations.

It should be noted that the line AE divides the primary field of periclase, such that $C_2S$ is the secondary phase in compositions falling below the line and spinel in compositions falling above the line.

The compositions and temperatures of the various labelled points in Figure 36 are shown below:

| Point | Composition (wt.%) | | | Temperature °C |
|---|---|---|---|---|
| | MgO | $Cr_2O_3$ | $C_2S$ | |
| F | 30.0 | 12.4 | 7.6 | 1620 ± 10 |
| G | 60.0 | 13.4 | 26.6 | 1620 ± 10 |
| H | 40.0 | 14.4 | 45.6 | 1620 ± 10 |
| B | - | 62.0 | 38.0 | - |
| C | - | 33.5 | 66.5 | - |
| D | - | 24.0 | 76.0 | - |
| E | 15.0 | 17.0 | 68.0 | 1620 ± 10 |
| I | 35.0 | 65.0 | - | 2355 |
| J | 14.1 | - | 85.9 | 1800 ± 20 |
| K | 4.0 | 16.0 | 80.0 | 1700 ± 10 |
| A | 88.0 | 12.0 | - | - |

There was no "dusting" in any of the compositions investigated during cooling, presumably because, as was shown by Newman and Wells[55], $Cr_2O_3$ stabilized the $Ca_2SiO_4$. Figure 37 shows the diagram with the liquidus isotherms drawn in tentatively. Microstructural features are shown in Plates 7, 8 and 9.

## 7.3. Discussion

IEJ, the boundary of the periclase field in Figure 36, locates the boundary surface of the primary phase volume of periclase in the quaternary composition tetrahedron of the system $CaO-MgO-Cr_2O_3-SiO_2$ where that surface is intersected by the plane of the section $MgO-MK-C_2S$. In Figure 38, this intersection is represented by the join $C_2S-Cr_2O_3$, and B is the apparent position of E on this join after projection through the MgO corner. E' is the position it would have if no solid solubility existed. E' would then have the composition of E, i.e. 15 wt.% MgO, 17 wt.% $Cr_2O_3$ and 68 wt.% $Ca_2SiO_4$.

Point P' in Figure 38, similarly shows the "true" position of $MgO-MK-M_2S$ eutectic in the ternary system $MgO-Cr_2O_3-SiO_2$[69] as shown in Figure 39 and has the composition 59 wt.% MgO, 1 wt.% $Cr_2O_3$ and 40 wt.% $SiO_2$. P' is thus also the position the latter eutectic would have in the projected diagram if no solid solubility occurred.

It follows that the boundary of the spinel field in the boundary surface of the periclase phase volume must pass through E' and P' as indicated by the dashed line in Figure 38. E'P' thus represents the true position of the spinel boundary in the boundary surface. It should be emphasized, however, that the observed freezing behaviour in the 80 wt.% MgO section is as

described by Tarboton's boundaries, not by the boundary E'P'.

From the constructions shown in Figures 36 and 39 it is possible to predict what the apparent positions of E' and P' would be in any other section of constant MgO content. Thus in the Figure 39 the line MgO-N must intersect the conjugate line TP at 80 wt.% MgO, thus fixing the position of N. Similarly the position of O, the apparent position of P, in mixtures containing 70 wt.% MgO is obtained by drawing a straight line for the MgO corner through R, the point of intersection of PT with the 70 wt.% MgO line. Similar predictions can be made from Figure 36.

It is of practical as well as theoretical interest to compare the compatibility relationships of periclase established in the system $MgO-CaO-Cr_2O_3-SiO_2$ with the corresponding relationships in the systems $MgO-CaO-Al_2O_3-SiO_2$ and $MgO-CaO-Fe_2O_3-SiO_2$.

Phase relationships in the section $MgO-Al_2O_3-C_2S$ of the second of these systems were investigated by Prince[31] while Taylor[72] established isothermal relationships in this section at 1550°C. Taylor's diagram is shown in Figure 40.

The latter author also established the isothermal diagram of the section $MgO-Fe_2O_3-C_2S$ of the last system in air at 1550°C and his diagram is shown in Figure 41.

Comparison of the three $MgO-R_2O_3-C_2S$ sections shows that the ternary eutectic points occur as shown below:

| Diagrams | Composition wt.% | | | | | Temp.°C |
|---|---|---|---|---|---|---|
| | MgO | $Fe_2O_3$ | $Al_2O_3$ | $Cr_2O_3$ | $C_2S$ | |
| MgO-$Fe_2O_3$-$C_2S$ | 10.0 | 36.0 | - | - | 54.0 | 1380 |
| MgO-$Al_2O_3$-$C_2S$ | 10.4 | - | 23.9 | - | 65.9 | 1417 |
| MgO-$Cr_2O_3$-$C_2S$ | 15.0 | - | - | 17.0 | 68.0 | 1620 |

The temperature of initial liquid formation in the primary field of periclase thus increases in the order

$$Fe_2O_3 < Al_2O_3 << Cr_2O_3$$

From the compositions of the eutectic points it will be seen that for compositions lying in the primary field of periclase the range of $C_2S/R_2O_3$ ratios over which spinel is the secondary phase also increases in the order $Fe_2O_3 < Al_2O_3 < Cr_2O_3$ (the limiting value of the ratios being 60/40, 72/28 and 80/20 respectively). It should be noted that these ratios refer to the true compositions in the boundary surface of the periclase phase volume.

In mixtures of constant MgO content, however, the composition range within which spinel is found occurs as the secondary phase, increases in the inverse order to the solid solubility of the sesquioxide, i.e.

$$Fe_2O_3 << Cr_2O_3 < Al_2O_3$$

## 8. COMPATIBILITY RELATIONSHIPS OF PERICLASE IN THE SYSTEM $MgO-Fe_2O_3-C_3MS_2$ IN AIR

### 8.1. Previous Work

The objective of this investigation was described in Section 3.

As described in Section 2.5., previous work was carried out by Crookes[51], who investigated melting relationships in $CaO-MgO-Fe_2O_3-SiO_2$ mixtures containing 70 wt.% MgO. His projection through the MgO corner of the boundary surface of the primary field of periclase is shown in Figure 12. As described in Section 6.4., it differs from similar projections of the systems $CaO-MgO-Al_2O_3-SiO_2$ and $CaO-MgO-Cr_2O_3-SiO_2$ in that, because of the extensive solid solubility of $Fe_2O_3$ in MgO at high temperatures, no spinel field appears.

As described in Section 3, the present investigation was carried out to supplement the work of Crookes[51]. For this purpose the binary section $MF-C_3MS_2$ was investigated and an attempt was made to establish the isothermal diagram of the system $MgO-Fe_2O_3-C_3MS_2$ at 1550°C.

### 8.2. Experimental Results

Table 10 and Figure 42 show the compositions of the mixtures examined in the binary section $MF-C_3MS_2$, their firing temperatures and phases present.

Points h, g and a in Figure 42 represent respectively

the invariant equilibrium between magnesiowustite, MF and liquid in air at 1717°C in the system $MgO-Fe_2O_3$ in air[22,30] (see Figures 4 and 5) and the melting points of $MgFe_2O_4$[22,30] and $C_3MS_2$[67].

Figure 42 also shows fields of MF + MW + liquid; MW + liquid; MW + $C_3MS_2$ + liquid; MW + $C_2S$ + $C_3MS_2$ + liquid; MW + $C_2S$ + liquid and $C_2S$ + liquid. The phases MW + $C_2S$ coexist with liquid at 1580°C ± 10°C; MW + $C_2S$ + $C_3MS_2$ coexist with liquid at 1525 ± 10°C and MW + MF + $C_3MS_2$ coexist with liquid at 1425 ± 10°C.

The compositions of the mixtures examined in the system $MgO-Fe_2O_3-C_3MS_2$ and the phases identified as having been present in them at 1550°C after quenching in air and water are shown respectively in Tables 11 and 12 and in Figures 43 and 44.

In Figures 43 and 44 the triangles MF-K-L and MF-K-$L_1$, are the tie triangles within which MF, MW and liquid coexist as established by quenching in air and in water respectively. It will be seen that the position of L and $L_1$ differ considerably. Water quenching was therefore used to establish the relationships shown in Figure 44. It was generally observed that specimens containing $C_3MS_2$ must be quenched in water prior to examination since this phase and also spinel (MF) tend to crystallize from the melt during air-quenching as shown in Plates 10, 11, 12 and 13.

It should be noted that since some dissociation of $Fe_2O_3$ would occur at 1550°C in air, all the mixtures would contain some ferrous oxide.

Points $L_1$ and $L_2$ therefore will not actually lie in the composition triangle $MgO-Fe_2O_3-C_3MS_2$ but respectively on the boundary surface between the primary crystallization volumes of magnesiowustite and spinel and magnesiowustite and dicalcium silicate inside the composition tetrahedron of the quaternary system $MgO-FeO-Fe_2O_3-C_3MS_2$. It should be noted that since the four phases, MW, $C_3MS_2$, $C_2S$ and liquid coexist in the area $X-L_2-C_3MS_2$, it is not actually a compatibility triangle. This position is discussed below.

It will be seen that point X does not coincide with the MgO corner of the diagram in Figure 44, showing that the magnesiowustite coexisting with the liquid $L_2$ at 1550°C contained approximately 3 wt.% iron oxide in solid solution. The latter finding is of potential practical importance. Stephenson and White[47] and Taylor[72] found that in $CaO-MgO-Fe_2O_3$ and $C_2S-MgO-Fe_2O_3$ mixtures in air at 1550°C, magnesiowustite in equilibrium with liquids which were saturated respectively with MgO and CaO, and with MgO and $C_2S$ had dissolved of the order of 3 wt.% of iron oxide in the former case and 8 wt.% of iron oxide in the latter case. The liquids contained 42 wt.% CaO : 12 wt.% MgO : 46 wt.% iron oxide and 61 wt.% $C_2S$ : 13 wt.% MgO : 26 wt.% iron oxide respectively.

Those results can be compared with a solubility of 52 wt.% iron oxide in magnesiowustite when it is in equilibrium with MF at 1550°C in air (point K of Figure 44).

White[73] concluded from these results that, in magnesite refractories in service, the distribution of iron oxide between the magnesiowustite and the liquid phase would depend on the $CaO/SiO_2$ ratio in the latter. When the ratio was high, a higher proportion of the iron oxide would be found in the liquid phase and would tend to increase the amount of liquid formed. Conversely, the addition of $SiO_2$ would tend to displace iron oxide from the liquid phase into the magnesiowustite. The finding that, in the Figure 44, point X occurs at only 3 wt.% iron oxide does not agree with this suggestion. The situation is complicated however by the fact that the triangle $X-C_3MS_2-L_2$ in Figure 44 is not a tie triangle.

Microstructural features are shown in Plates 10, 11, 12, 13 and 14.

## 8.3. Discussion

An explanation of the form of the phase relationships shown in Figure 42 is shown in Figure 45A. The latter shows diagrammatically boundary surfaces which are expected to exist within the composition tetrahedron of the quaternary system $CaO-MgO-Fe_2O_3-SiO_2$ and is not to scale. The position of the section $MgO-C_3S_2-Fe_2O_3$ is indicated and also that of the join $C_3MS_2$-MF (line ag) which lies in this plane. The latter join intersects GdNM, the boundary surface between the primary phase volumes of $C_2S$ and MW, at c. The plane $C_3S_2$-MW-$Fe_2O_3$ intersects

the surfaces GdNM, GdFE (the MW-$C_3MS_2$ boundary surface) and ghSO (the MW-MF boundary surface) in me, ef and fh respectively.

The freezing path of a mixture lying between a and c and having the composition (1), will, on cooling from the liquid state, initially move from (1) to (2) on the $C_2S$-MW boundary with $C_2S$ separating. MW and $C_2S$ will then separate together and the freezing path will follow the line (2) - (3). The latter point lies on the boundary line dG in which the $C_2S$-MW boundary surface (GdNM), the $C_2S$-$C_3MS_2$ boundary surface (GdJH) and the MW-$C_3MS_2$ boundary surface (GdFE) intersect. $C_3MS_2$ will then start to separate and the freezing path will then follow dG until it reaches e. Since the latter lies in the plane $C_3MS_2$-MW-$Fe_2O_3$, as does the composition of mixture (1), the last traces of $C_2S$ will disappear as e is reached, leaving MW, $C_3MS_2$ and liquid. The freezing path will then move from e to f, where peritectic reaction will be completed with separation of MF and solution of MW, leaving therefore a mixture of solid $C_3MS_2$ and MF.

Other mixtures between a and c will behave similarly. Mixture c which lies on the $C_2S$-MW boundary will start to freeze immediately along the line c to (4) separating $C_2S$ and MW. It will then follow line de and so on.

Mixtures between c and g will start to freeze MW initially, their freezing paths following the dashed

lines radiating from MW until they intersect cefg. Those intersecting ce and ef will then move towards f where freezing will be completed as before. Those intersecting hf, eg. composition (5), will then move towards f where freezing will be completed.

Figure 45B shows the phase diagram of section $C_3MS_2$-MF which results from these various transitions. The compositions (1), (c) and (5) are indicated by vertical lines and the intersections of these with the boundary lines indicate the various transitions occurring on cooling. It will be seen that the form of Figure 45B is identical with that of Figure 42.

The primary crystallization fields which will occur in the section MgO-$C_3S_2$-$Fe_2O_3$ can also be deduced from the intersections of the plane of the latter section with the various boundary surfaces in Figure 45A. In the latter Figure these intersections are represented by the lines me, ef, fh, fw, ew and wv. Of these, me, ef and fh have already been defined. fw, ew and wv are the intersections of the plane of the section with the boundary surfaces $C_3MS_2$-spinel (EGHT), $C_3MS_2$-$C_2S$ (GHJd) and $C_2S$-spinel (GKRM). The approximate positions of these phase boundaries in the liquidus surface of the section MgO-$C_3MS_2$-$Fe_2O_3$ are shown in Figure 46, where they are labelled to correspond to the labelling of the intersections of Figure 45A.

Figure 46 shows the boundaries of the primary phase fields of spinel, magnesiowustite, dicalcium silicate and

merwinite. The compositions of points $\underline{f}$, $\underline{e}$, $\underline{c}$, $\underline{L}_1$ and $\underline{L}_3$ are respectively :

f : 12wt.% MgO : 40wt.% $Fe_2O_3$ : 48wt.% $C_3S_2$

e : 11wt.% MgO : 22wt.% $Fe_2O_3$ : 67wt.% $C_3S_2$

c : 13wt.% MgO : 12wt.% $Fe_2O_3$ : 75wt.% $C_3S_2$

$L_1$ : 15wt.% MgO : 52wt.% $Fe_2O_3$ : 33wt.% $C_3S_2$

$L_3$ : 12wt.% MgO : 20wt.% $Fe_2O_3$ : 68wt.% $C_3S_2$

$hL_1feL_3cm$, the boundary of the magnesiowustite field in Figure 46 locates the boundary surface of the primary phase volume of magnesiowustite in the quaternary composition tetrhaedron of the system $CaO-MgO-Fe_2O_3-SiO_2$ where that surface is intersected by the plane of the section $MgO-Fe_2O_3-C_3S_2$.

Point $\underline{e}$ in Figure 46 should correspond to the point D in Crookes's projection (see Figure 12) where the join $C_3MS_2-Fe_2O_3$ crosses the boundary between fields 3 and 4. These two points agree well in terms of phases and temperature but from the position of $\underline{e}$ in Figure 46 (it occurs at 22 wt.% $Fe_2O_3$ while Crookes's point D is at 18 wt.% $Fe_2O_3$) it would appear that on the projection of the 70 wt.% MgO section it should occur at a much higher $Fe_2O_3$ content.

Figure 47 shows an attempt to construct the 1550°C isotherm of the section on the basis of Figures 42, 44, 45 and 46. Figure 47 shows an area $utL_1L_3$ in which only liquid would be present at this temperature, the positions of $\underline{u}$ and $\underline{t}$ being tentative. The position of $L_1$ is as indicated on Figure 44, but $L_3$ does correspond to $L_2$ in

the latter diagram. Evidence for this conclusion was obtained from Figure 42, in which it will be seen that the 1550°C isotherm passes through the field of MW + $C_2S$ + liquid between the fields of MW + $C_2S$ + $C_3MS_2$ + liquid and MW + liquid. It follows that a triangular area $XL_2L_3$, in which MW + $C_2S$ + liquid exist, must occur in Figure 47. (It should be noted that the location of $XL_2$ in Figure 44 is inconsistent with the curvature of the continuous line de in Figure 42 and it is suggested that the line shape of this line is as indicated by the dashed line de. The points of intersection of the isotherm with de and ce in Figure 42, which are labelled y and z, correspond to points y and z in Figure 47.

The reason for the occurrence of the field $XL_2L_3$ is shown in Figure 48, which again shows the plane of the section MgO-$C_3S_2$-$Fe_2O_3$ in the tetrahedron CaO-MgO-$Fe_2O_3$-$SiO_2$ and is labelled similarly to Figure 45A. Point q' on line de is the point at which the temperature is 1550°C and q'$L_3$ is the 1550°C isotherm on the boundary surface $C_2S$-MW. Composition $L_2$ on me on the other hand is the composition in the section on the boundary $C_2S$-MW whose freezing path passes through q' at 1550°C.

Mixtures in the section lying in the area MgO-m-$L_2$, will deposit MgO (actually MW of composition X in Figure 47) until the freezing path reaches $mL_2$ and will then freeze along a path indicating from n with

separation of MgO and $C_2S$ until they intersected de. They will then separate MgO, $C_2S$ and $C_3MS_2$ along de until they reach q' at 1550°C, so that they will then consist of the four phases MgO, $C_2S$, $C_3MS_2$ and liquid as was found in the area $XmL_2$ in Figure 44. The area MgO-m-$L_2$ in Figure 48 thus corresponds to $XmL_2$ in Figure 47.

Mixtures lying in the area MgO-$L_2$-$L_3$ of the section will also deposit MgO until their freezing path intersects $L_2L_3$ and will then freeze along paths radiating from n with separation of MgO and $C_2S$ but at 1550°C they will only have reached the isotherm q'$L_3$ so that no separation of $C_3MS_2$ will occur. MgO-$L_2$-$L_3$ thus corresponds to $XL_2L_3$ in Figure 47, while the area MgO-$L_3$-$L_1$-K corresponds to the area $XL_3L_1K$ in the latter figure.

Mixtures lying in the area $C_3S_2$-m-$L_3$-t of Figure 48 on the other hand will freeze initially with separation of $C_2S$ along paths radiating from $C_2S$. Those whose paths intersect the $C_2S$-$C_3MS_2$ boundary surface (GHJd) within the area dq'r' where q'r' is the 1550°C isotherm in the surface will then deposit $C_3MS_2$ and $C_2S$ and when they have reached the isotherm will consist of $C_2S$ + $C_3MS_2$ + liquid.

This will thus be an area sqr in the section, where sq projects (through $C_2S$) into dq' and rq projects into q'r', in which $C_2S$, $C_3MS_2$ and liquid coexist at 1550°C.

Mixtures lying in the area $mL_2qs$, where $qL_2$ projects into $q'L_2$ will freeze along paths which will intersect the $C_2S$-MW boundary surface in the area $mdq'L_2$. They will then freeze along paths which will intersect de between d and q' and then will reach q' at 1550°C, when they will consist of MW + $C_2S$ + $C_3MS_2$ + liquid.

There will thus be an additional area $mL_2qs$ in the section in which their four phases coexist at 1550°C.

Mixtures lying in the area $qL_2L_3$ where $qL_3$ projects into the 1550°C isotherm $q'L_3$ will also separate $C_2S$ initially along paths which intersect the MW-$C_2S$ boundary surface. At 1550°C the freezing paths will only have reached the isotherm $q'L_3$ and will consist of $C_2S$, MW and liquid only, as in the case of mixtures falling in the area MgO-$L_2$-$L_3$.

Finally, mixtures lying in the section to the left of the line $L_3qr$ will separate $C_2S$ until they reach the 1550°C isothermal surface and will consist of $C_2S$ and liquid only.

It will be seen by comparing Figures 44 and 47 that, while the predicted four phases were found to occur in the area $XmL_2$ the 3-phase areas $XL_2qL_3$ and sqr were not detected. This is attributed partially to the narrowest of the areas involved and also to the compexity of the reactions leading to equilibrium.

It will be seen from Figure 44 that somewhat confusing results were obtained in mixtures approaching $C_3MS_2$ in composition.

# 9. COMPATIBILITY RELATIONSHIPS IN THE PSEUDO-TERNARY SYSTEM $MgAl_2O_4$-$MgCr_2O_4$-$Ca_3MgSi_2O_8$ IN AIR

## 9.1. Previous Work

Previous work and the objective of this investigation was described in Section 3.

## 9.2. Experimental Procedure

To establish the phase equilibrium relationships in the pseudo-ternary system $MgAl_2O_4$-$MgCr_2O_4$-$Ca_3MgSi_2O_8$, four sections were investigated, these being :

(1) $MgAl_2O_4$-$C_3MS_2$

(2) $MgCr_2O_4$-$C_3MS_2$

(3) $MgAl_{1.5}Cr_{0.5}O_4$-$C_3MS_2$

(4) $MgAl_{0.8}Cr_{1.2}O_4$-$C_3MS_2$

The sections 1, 2 and 3 were investigated by El-Shahat and White[3] who used air quenching and they were re-investigated with Section 4 using water quenching (as described in Section 8.2).

Sections 1 and 2 are respectively sections of the systems $CaO$-$MgO$-$Al_2O_3$-$SiO_2$ and $CaO$-$MgO$-$Cr_2O_3$-$SiO_2$, while 3 and 4 are sections of the system $CaO$-$MgO$-$Al_2O_3$-$Cr_2O_3$-$SiO_2$.

## 9.3. Experimental Results

The compositions of the mixtures used in investigating the four sections, their firing temperatures and the phases present at the firing temperatures are shown in Tables 13, 14, 15 and 16 respectively. The phase diagrams

of these sections are shown in Figures 49, 50, 51 and 52 respectively. The solid phases existing in the compositions investigated at various firing temperatures, which were used to establish the phase boundaries are indicated on the diagrams. The indicated temperatures of complete melting of the mixed spinel phases are based on a linear interpolation between published melting points of the end members and are approximate.

Figures 30, 53 and 54 show respectively the sections $MgAl_2O_4$-$C_3MS_2$, $MgCr_2O_4$-$C_3MS_2$ and $MgAl_{1.5}Cr_{0.5}O_4$-$C_3MS_2$ investigated by El-Shahat and White[3] using air quenching. Comparison between the diagrams proposed by the latter authors and present results shows that points E and F in sections MA-$C_3MS_2$ and $MgAl_{1.5}Cr_{0.5}O_4$-$C_3MS_2$ and point T in section MK-$C_3MS_2$ occur at temperatures slightly lower than reported by El-Shahat and White[3].

The temperature (1540°C ± 10°C) and composition of the eutectic point R of the section MK-$C_3MS_2$ at which MgO, $C_2S$, $C_3MS_2$, spinel and liquid coexist (see Figures 50 and 53) agree with those reported by the latter authors although on their diagram the wrong temperature is quoted. The temperature of R also agrees with that of point C in Tarboton's projected diagram[52] (see Figure 13 and Sections 2.5 and 7.1).

The temperature (1430°C ± 10°C) of the eutectic point R in the section MA-$C_3MS_2$ (see Figures 30 and 49) where MA, MgO, $C_3MS_2$, $C_2S$ and liquid coexist, also agrees with that of point g (1415 ± 5°C) in Figure 18. Point g was

established in the quaternary system $CaO-MgO-Al_2O_3-SiO_2$ as described in Section 6.2.

Microstructural features are shown in Plate 15.

## 9.4. Discussion of Sections

From a comparison of Figures 49, 50, 51 and 52, the following features will be seen:

(1) Replacement of $Al_2O_3$ by $Cr_2O_3$ in the spinel phase raises the temperature of initial melting, complete replacement causing an increase of 110°C.

(2) The temperatures of the points E and F in the sections $MA-C_3MS_2$ and $MgAl_{1.5}Cr_{0.5}-C_3MS_2$ and of point T in Section $MgAl_{0.8}Cr_{1.2}O_4-C_3MS_2$ increase progressively as $Al_2O_3$ is replaced by $Cr_2O_3$.

(3) The solubility of the spinel in the liquid phase at constant temperature above these points decreases as the $Cr_2O_3$ content of the spinel increases.

The freezing paths in the sections investigated were described in El-Shahat and White's paper[3].

## 9.5. The Phase Diagram of the System $MA-MK-C_3MS_2$

Figure 55 shows the position of the phase boundaries between the primary fields of crystallization of MgO, spinel and dicalcium silicate in the liquidus surface of the pseudo-ternary system $MA-MK-C_3MS_2$ as established by the phase diagrams shown in Figures 49, 50, 51 and 52.

Isotherms on the liquidus surface derived from the

liquidus curves of the sections are also shown. As $Al_2O_3$ in the spinel is replaced by $Cr_2O_3$, the phase boundaries of the MgO field rapidly converge and intersection when approximately two-thirds of the $Al_2O_3$ has been replaced.

The temperatures along both boundaries increase as the $\frac{Cr_2O_3}{Al_2O_3}$ ratio increases. It will be evident from the direction of the boundary between the MgO field and the spinel field and the fact that it drops only 20°C between A and E that the liquidus isotherms in the latter field must run in a direction roughly parallel to it, so that the solubility of the spinel in the liquid phase must decrease rapidly with increasing $Cr_2O_3$ content.

## 10. PRACTICAL APPLICATIONS OF PHASE RELATIONSHIPS ESTABLISHED TO TECHNOLOGY OF BASIC REFRACTORIES

A projected diagram of the boundary surface of the periclase phase volume in the system $CaO-MgO-Al_2O_3-SiO_2$ for mixtures containing 80 wt.% MgO has been established (Figure 18) and compared with the diagram of the boundary surface derived by O'Hara and Biggar[50] (Figure 19). The comparison shows that displacement of the boundary lines in the projected diagram due to solid solubility of $Al_2O_3$ in periclase only becomes appreciable at temperatures above 1500°C. The main effect is to cause a progressive displacement of the boundary of the spinel field to higher $Al_2O_3$ contents as the temperature of the boundary rises above 1500°C (see Figures 18 and 19).

At comparable MgO contents, however, the area of the spinel field in the projected diagrams of the systems $CaO-MgO-Fe_2O_3-SiO_2$ (Figure 12), $CaO-MgO-Cr_2O_3-SiO_2$ (Figure 13) and $CaO-MgO-Al_2O_3-SiO_2$ (Figure 18), and hence the range of $R_2O_3/CaO+SiO_2$ ratios over which spinel is the secondary phase in the three systems, decreases in the order

$$Al_2O_3 > Cr_2O_3 \gg Fe_2O_3$$

which is the order of increasing solid solubility of the sesquioxides in periclase at high temperatures.

An explanation for this dependence on the solid solubility of the sesquioxide has been advanced and a graphical method of predicting the displacement of spinel-silicate boundary with varying MgO content has been described

(see Figures 22, 23, 24, 36 and 39).

As a consequence of these effects partial replacement of $Cr_2O_3$ or $Fe_2O_3$ or both by $Al_2O_3$ (see Figure 32) in the spinel phase in chrome-magnesite or magnesite-chrome refractories will displace the boundary downwards, and at temperatures above those of initial melting, spinel will occur at lower $R_2O_3/CaO + SiO_2$ ratios, i.e. at lower contents of $Al_2O_3$ in the mixture. Any advantage from this effect would however have to be balanced against possible disadvantages of lower temperatures of initial melting.

Thus it will be seen in Figure 13 that the temperatures of initial melting in the phase assemblages of Table 1, when $Cr_2O_3$ is the only sesquioxide present are, moving from left to right of the Table, 1490°C (point A), 1480°C (point C) and 1540°C (point D) whereas in Figure 18 when $Al_2O_3$ is the only sesquioxide present, the temperatures of the corresponding points are 1415°C (point b), 1390°C (point d) and 1410°C (point f).

Further, when the comparison is extended to include $Fe_2O_3$ [(see projected diagrams of Figures 12, 13 and 18 and also the diagrams of the systems $MgO-Cr_2O_3-C_2S$ (Figure 36), $MgO-Al_2O_3-C_2S$ (Figure 40) and $MgO-Fe_2O_3-C_2S$ (Figure 41)] the temperatures of initial melting in the primary phase volume of periclase, with a given silicate composition, are found to decrease in the order

$$Cr_2O_3 >> Al_2O_3 > Fe_2O_3$$

This relationship was also found to apply to replacement of $Cr_2O_3$ by $Al_2O_3$ in the system $MgAl_2O_4$-$MgCr_2O_4$-$C_3MS_2$ (see Figure 55) confirming the findings of El-Shahat and White[1,2,3] for spinel-silicate systems.

In addition, from the boundaries of the area of primary crystallization of periclase established in the systems MgO-$Cr_2O_3$-$C_2S$ (see Figure 36), MgO-$Al_2O_3$-CS (Figure 27), MgO-$Al_2O_3$-$C_3S_2$ (see Figure 31) and MgO-$Fe_2O_3$-$C_3S_2$ (Figure 48), the boundary surface of the primary phase volume of periclase in the quaternary tetrhedra CaO-MgO-$Cr_2O_3$-$SiO_2$, CaO-MgO-$Al_2O_3$-$SiO_2$ and CaO-MgO-$Fe_2O_3$-$SiO_2$ have been located, where these surfaces are intersected by the planes of these systems.

An important conclusion from this work is that the finding by El-Shahat and White[1,2,3] that in the spinel-silicate systems investigated by them, the solubility of the spinel in the liquid phase increases in the order

$$Cr_2O_3 << Al_2O_3 < Fe_2O_3$$

so that the content of $R_2O_3$ required to retain spinel at temperatures above that of initial melting, will not apply when large amounts of periclase are also present, as in most basic refractories.

As explained above, the present work has demonstrated that in such bodies the relative solubility of sesquioxide in the periclase is the dominant factor so that the order of the $R_2O_3$ requirement is

$$Al_2O_3 < Cr_2O_3 << Fe_2O_3$$

REFERENCES


1. El-Shahat, R.M., and White, J., "The Systems $MgAl_2O_4$-$MgCr_2O_4$-$Ca_2SiO_4$ and $MgFe_2O_4$-$MgCr_2O_4$-$Ca_2SiO_4$", Trans. Brit. Ceram. Soc., 63, 313-330, 1964.
2. El-Shahat, R.M., and White, J., "Phase Equilibrium Relationships in Spinel-Silicate Systems (Part 2)", Trans. Brit. Ceram. Soc., 65, 309-336, 1966.
3. El-Shahat, R.M., and White, J., "Phase Equilibrium Relationships in Spinel-Silicate Systems (Parts 3 and 4)", Trans. Brit. Ceram. Soc., 65, 497-519, 1966.
4. Hatfield, T., "Phase Equilibrium and Microstructure in Systems Containing Periclase and Silicates", M.Sc.Tech. Thesis, University of Sheffield, 1969.
5. Richmond, C., "Microstructural Parameters of Basic Refractory Compositions", Ph.D. Thesis, University of Sheffield, 1970.
6. Brampton, E.C., Parnham, H., and White, J., "Dolomite Linings for Basic Electric Arc Furnaces", J.I.S. Inst., 152, 341-372, 1945.
7. White, J., "Basic Refractories: a Survey of Present Knowledge", J. Iron and Steel Inst., 200, 611-621, 1962.
8. Rait, J.R., "Basic Refractories, their Chemistry and their Performance", Iliffe, London, 410pp, 1950.
9. Hatfield, T., and Richmond, C., "The Solubility of Monticellite in Forsterite", Trans. Brit. Ceram. Soc., 69, (3), 99-101, 1970.
10. Biggar, G.M., and O'Hara, M.J., "Monticellite and Forsterite Crystalline Solutions", J. Amer. Ceram. Soc., 52, (5), 249-253, 1969.

11. Ricker, R.W., and Osborn, E.F., "Additional Phase Equilibrium Data for the System $CaO-MgO-SiO_2$", J. Amer. Ceram. Soc., 37, (3), 133-139, 1954.

12. Doman, R.C., Barr, J.B., McNally, R.N., and Alper, A.M., "Phase Equilibria in the System CaO-MgO", J. Amer. Ceram. Soc., 46, (7), 313-316, 1963.

13. Jones, D.G., and Melford, D.A., "Comparison of the High Temperature Constitution of Sea-Water Magnesites with that of Natural Greek Material", Trans. Brit. Ceram. Soc., 68, 241-247, 1969.

14. Henney, J.W., and Jones, J.W.S., "The Solid Solubility of CaO and $SiO_2$ in MgO and its Effect on the $MgO-CaO-SiO_2$ System at 1750°C", Trans. Brit. Ceram. Soc., 68, 201-203, 1969.

15. Spencer, D.R.F., Beamond, T.W., and Coleman, D.S., "The Solubility of CaO in MgO and its Effect on the $CaO-MgO-SiO_2$ System at 1800°C", Trans. Brit. Ceram. Soc., 70, 31-33, 1971.

16. Schlaudt, C.M., and Roy, D.M., "Crystalline Solution in the System $MgO-Mg_2SiO_4-MgAl_2O_4$", J. Amer. Ceram. Soc., 48, (5), 248-251, 1965.

17. Hatfield, T., Richmond, C., Ford, W.F., and White, J., "Compatibility Relationships Between Periclase and Silicate Phases in Magnesite Refractories at High Temperatures", Trans. Brit. Ceram. Soc., 69, 53-58, 1970.

18. Alper, A.M., McNally, R.N., Ribbe, P.H., and Doman, R.C., "The System $MgO-MgAl_2O_4$", J. Amer. Ceram. Soc.,45, (6), 263-268, 1962.

19. Hayhurst, A., "An Investigation into the Effect of Bond Type and Distribution on the High Temperature Mechanical Properties of Basic Refractory Materials", Ph.D. Thesis, University of Sheffield. 1961.

20. Alper, A.M., McNally, R.N., Doman, R.C., and Keihn, F.G., "Phase Equilibria in the System MgO-$MgCr_2O_4$", J. Amer. Ceram. Soc., 47, (1), 30-33, 1964.

21. Woodhouse, D., and White, J., "Phase Relationships in Iron Oxide Containing Spinels (Part 3)", Trans. Brit. Ceram. Soc., 54, (6), 333-366, 1955.

22. Phillips, B., Somiya, S., and Muan, A., "Melting Relationships of Magnesia Oxide-Iron Oxide Mixtures in Air", J. Amer. Ceram. Soc., 44, (4), 167-169, 1961.

23. Stubican, V.S., and Menezes, de I., "Grain Boundary Reactions in Magnesia-Chrome Refractories" : Application of the Electron Probe, I", J. Amer. Ceram. Soc., 49, (10), 535-540, 1966.

24. Menezes, de I., and Stubican, V.S., "Grain Boundary Reactions in Magnesia-Chrome Refractories : Application of the Electron Probe, II", J. Amer. Ceram. Soc., 49, (11), 609-612, 1966.

25. Schlaudt, C.M., and Roy, D.M., "The Join $Ca_2SiO_4$-$CaMgSiO_4$", J. Amer. Ceram. Soc., 49, (8), 430-432, 1966.

26. Gutt, W., "A New Calcium Magnesiosilicate", Nature, (London), 190 (4773), 339-340, 1961.

27. Gutt, W., "The System Dicalcium Silicate-Merwinite", Nature (London),207 (4993), 184-185, 1965.

28. Richards, R.G., and White, J., "Phase Relationships of Iron Oxide-Containing Spinels : Part II", Trans. Brit. Ceram. Soc., 53 (7), 422-459, 1954.

29. Paladino, A.E., "Phase Equilibria in the Ferrite Region of the System FeO-MgO-$Fe_2O_3$", J. Amer. Ceram. Soc., 43 (4), 183-191, 1960.

30. Willshee, J.C., and White, J., "An Investigation of Equilibrium Relationships in the System $MgO-FeO-Fe_2O_3$ up to 1750°C in Air", Trans. Brit. Ceram. Soc., 66, 541-555, 1967.

31. Prince, A.T., "Phase Equilibrium Relationships in a Portion of the System $MgO-Al_2O_3-2CaO.SiO_2$", J. Amer. Ceram. Soc., 34 (2), 44-51, 1951.

32. White, J., "High Temperature Oxides", Chapter 2 : Magnesia Based Refractories, Volume 5-1, Ed. A.M. Alper, Academic Press, N.Y. 358pp., 1970.

33. Solacolu, S., "Thermal Equilibria of the System $MgO-MgO.Al_2O_3-(MgO.Fe_2O_3)-2MgO.SiO_2-2CaO.SiO_2$ with Applications to the Reaction Mechanism of the Magnesite Refractories", Revue Roumaine de Mètallurgie, Acad. R.P.R., 7, 105-129, 1962.

34. Berry, T.F., Allen, W.G. and Snow, R.B., "Chemical Changes in Basic Bricks During Service", J. Amer. Ceram. Soc., 33 (4), 121-132, 1950.

35. Houseman, D.H., and White, J., "Development of Bond Strength During Firing - A New Approach and its Technical Implications", Trans. Brit. Ceram. Soc., 58, 231-276, 1959.

36. Allison, E.B., Brock, P., and White, J., "The Rheology of Aggregates Containing a Liquid Phase with Special Reference to the Mechanical Properties of Refractories at High Temperatures", Trans. Brit. Ceram. Soc., 58, 495-521, 1959.

37. Rigby, G.R., and Richardson, H.M., "Roof Performance in the Third Campaign of an All-basic Open-Hearth Furnace", Trans. Brit. Ceram. Soc., 56, 22-36, 1957.

38. Laming, J., "Recent Work on Chrome-Magnesite Bricks", Refractories J., 35, 3, 116-118, 1959.

39. Richardson, H.M., "Discussion on Recent Work on Chrome-Magnesite Bricks", Refractories J., 35 (3), 118-120, 1959.

40. Ford, W.F., Hayhurst, A., and White, J., "The Effect of Bond Structure on the High Temperature Tensile Behaviour of Basic Bricks", Trans. Brit. Ceram. Soc., 60, 581-601, 1961.

41. Hayhurst, A., and Laming, J., "The Effect of Firing Temperature on the Properties of Chrome-Magnesite Bricks", Refractories J., March, 80-97, 1963.

42. Hayhurst, A., and Laming, J., "The Structure of Chrome-Magnesite Refractories at High Temperatures", Trans. Brit. Ceram. Soc., 62, 989-1005, 1963.

43. Smith, C.S., "Grains, Phases and Interfaces : An Interpretation of Microstructure", Trans. A.I.M.E., 175, 15-51, 1948.

44. Van Vlack, L.H., "Microstructure of Silica in the Presence of Iron Oxide", J. Amer. Ceram. Soc., 43, 140-145, 1960.

45. Jackson, B., Ford, W.F., and White, J., "The Influence of $Cr_2O_3$ and $Fe_2O_3$ on the Wetting of Periclase Grains by Liquid Silicate", Trans. Brit. Ceram. Soc., 62, 577-601, 1963.

46. Jackson, B., and Ford, W.F., "A Quantitative Study of Bonding in Basic Refractories", Trans. Brit. Ceram. Soc., 65, 19-39, 1966.

47. Stephenson, I.M., and White, J., "Factors Controlling Microstructure and Grain Growth in Two-Phase (one solid and one liquid) and (one liquid) Systems", Trans. Brit. Ceram. Soc., 66, 443-483, 1967.

48. McMurdie, H.F., and Insley, H., "Studies on the Quaternary System $CaO-MgO-2CaO.SiO_2-5CaO.3Al_2O_3$", J. Research Nat. Bur. Standards, 16, 467-474, 1936.

49. de Aza, S., Richmond, C., and White, J., unpublished work, 1970.

50. O'Hara, M.J. and Biggar, G.M., "Phase Equilibria Aspects of the Performance of Basic Refractories", Trans. Brit. Ceram. Soc., 69, 243-251, 1970.

51. Crookes, E., "An Investigation of the Phase Boundaries in the Boundary Surface of the Primary Phase Volume of Magnesiowustite in the System CaO-MgO-Iron Oxide-$SiO_2$ in Air", M.Sc.Tech. Thesis, University of Sheffield, 1971.

52. Tarboton, W.R., "Compatibility Relationships of Periclase in the system CaO-MgO-$Cr_2O_3$-$SiO_2$ in Air", M.Sc.Tech. Thesis, University of Sheffield, 1972.

53. Bredig, M.A., "Polymorphism of Calcium Orthosilicate", J. Amer. Ceram. Soc., 33, 188-192, 1950.

54. Zerfoss, S., and Davis, H.M., "Observations on Solid Phase Inversions of Calcium Orthosilicate, Constituent of Dolomite-Silica Brick", J. Amer. Ceram. Soc., 26, 302-307, 1943.

55. Newman, E.S., and Wells, L.S., "Effect of Some Added Materials on Dicalcium Silicate", J. Research Nat. Bur. Standards, 36, 137-158, 1946.

56. Glasser, F.P., "Phase Diagrams,Materials Science and Technology", Chapter V, pages 147-190, Volume 6 -II, Ed.A.M. Alper, Academic Press, N.Y., 1970.

57. Schouten, C., "The Reflecting Microscope as Applied to Some Ceramic Products", Bull. Amer. Ceram. Soc., 30 (4), 130-136, 1951.

58. Snow, R.B., "Examination of Refractory Specimens in Reflected Light, J. Amer. Ceram. Soc., 36 (9), 299-304, 1953.

59. Roberts, E.W., "Preparing Polished Surfaces for Microscopic Examination in Reflected Light", Trans. Brit. Ceram. Soc., 54, 120-136, 1955.

60. Treffner, W.S., "Behaviour of Chromite Spinel as Related to Microstructure, J. Amer. Ceram. Soc., 44 (12), 583-591, 1961.

61. Pressley, H., "Phase Equilibrium Relationships and Microstructure inSystems Formed by Magnesia, Copper Oxide and Spinels, M.Sc.Tech. Thesis, University of Sheffield, 1972.

62. Biggar, G.M., and O'Hara, M.J., "Melting of Forsterite, Monticellite, Merwinite, Spinel and Periclase Assemblages", J. Amer. Ceram. Soc. (53), 534-537, 1970.

63. Biggar, G.M., and O'Hara, M.J., "Retrograde Solubility of Periclase, Forsterite and Dicalcium Silicate", J. Amer. Ceram. Soc. (53), 538-540, 1970.

64. Biggar, G.M., "Phase Equilibria in Chrome-Bearing Basic Refractories", Refractories J., January, 6-9, 1972.

65. Rankin, G.A., and Merwin, H.E., "The Ternary System $MgO-Al_2O_3-SiO_2$", Amer. J. Sci. (4th Series) 45, 301-325, 1918".

66. Osborn, E.F., and Muan, A., "Phase Equilibrium Diagrams of Oxide Systems", Plate 2, Amer. Ceram. Soc., and Edward Orton, Jr., Ceramics Foundation, 1960.

67. Gutt, W., "High Temperature Phase Equilibria for the Partial System $3CaO.MgO.2SiO_2$-$MgO.Al_2O_3$-$2CaO.Al_2O_3.SiO_2$ in the quaternary system $CaO-SiO_2-Al_2O_3-MgO$", J. of the Iron and Steel Institute (9), 770-774, 1964.

68. Wilde, W.T., and Rees, W.J., "The Ternary System $MgO-Al_2O_3-Cr_2O_3$", Trans. Brit. Ceram. Soc., 42 (7), 123-155, 1943.

69. Keith, M.L., "Phase Equilibria in the System $MgO-Cr_2O_3-SiO_2$", J. Amer. Ceram. Soc., 37 (10),490-496, 1954.

70. Gee, K.W., "The System $MgO-SiO_2-Cr_2O_3$", Ph.D. Thesis, University of Sheffield, 1940.

71. Rigby, G.R., Hutton, R.F., and Hamilton, G.B., "Reactions Occurring in Basic Brick", J. Amer. Ceram. Soc. (46), 332-342, 1963.

72. Taylor, M.I., "Phase Relationships in the System $CaO-MgO-B_2O_3-SiO_2$ Relevant to Magnesite Refractories Containing $B_2O_3$", Ph.D. Thesis, University of Sheffield, 1971.

73. White, J., Unpublished work, 1972.

## TABLE 1

## PHASE COMBINATIONS IN BASIC REFRACTORIES

| Molar Ratio $CaO/SiO_2$ | | | | | |
|---|---|---|---|---|---|
| 0 - 1.0 | 1.0 - 1.5 | 1.5 - 2.0 | Greater than 2.0 | | |
| (1) | (2) | (3) | (4) | (5) | (6) |
| Magnesio-wustite | Magnesio-wustite | Magnesio-wustite | Magnesio-wustite | Magnesio-wustite | Magnesio-wustite |
| Spinel | Spinel | Spinel | Spinel | Dicalcium Silicate | Lime |
| Forsterite | Monticellite | Merwinite | Dicalcium Silicate | Tricalcium Silicate | Tricalcium Silicate |
| Monticellite | Merwinite | Dicalcium-Silicate | Ca Ferrites, Aluminates and Chromites | Ca Ferrites, Aluminates and Chromites | Ca Ferrites, Aluminates and Chromites |

## TABLE 2

### PHASE FIELDS EXISTING IN THE SYSTEM MgO-FeO-$Fe_2O_3$

| Single Phase | Double Phase | Triple Phase |
|---|---|---|
| $Fe_2O_3$ (small, shown as corner of diagram) | $Fe_2O_3$ + spinel (area $Fe_2O_3$- H - J) | Spinel E + magnesiowustite D + liquid L (D - E - L) |
| Spinel | Spinel + magnesiowustite ($MgFe_2O_4$- MgO - D - E) | |
| Magnesiowustite liquid to right of line F' - L - J - MgO) | Spinel + liquid (F - E - L - F') | |

TABLE 3

Chemical Analysis* of the Magnesium Ingot

| | | |
|---|---|---|
| Zn | → | 0.006% |
| Al | → | 0.007% |
| Si | → | 0.006% |
| Cu | → | <0.001% |
| Mn | → | 0.006% |
| Fe | → | 0.003% |
| Sn | → | 0.001% |
| Ni | → | <0.001% |
| Ca | → | 0.002% |
| Pb | → | 0.003% |
| Cd | → | 0.0005% |
| | → | 0.0365% |
| Mg | | remainder |

*Chemical Analysis supplied by Magnesium Electron Ltd.

TABLE 4

Chemical Analysis of the MgO Powder

Estimated Quantity Present

Result as parts per million - weight for weight

| Element | |
|---|---|
| Aluminium | 100 |
| Calcium | 30 |
| Copper | 3 |
| Iron | 10 |
| Lead | 20 |
| Magnesium | 50 |
| Silicon | 70 |

The following elements were specifically sought but not detected:-

Ag, As, Au, B, Ba, Be, Bi, Cd, Co, Cr, Cs, Ga, Ge, Hf, Hg, In, Ir, K, Li, Mo, Na, Nb, Ni, Os, P, Pd, Pt, Rb, Re, Rh, Ru, Sb, Se, Sn, Sr, Ta, Te, Ti, Tl, V, W, Zn, Zr.

Chemical Analysis supplied by
W. & C. Spicer Ltd.

TABLE 5

Compositions and Constitution of Materials Used

| Sample | Chemical Analysis* (wt.%) | | | | | | | | Composition by Chemical Anaylsis | Phases detected by X-Rays* |
|---|---|---|---|---|---|---|---|---|---|---|
| | Ign. Loss | $SiO_2$ | $Al_2O_3$ | $Cr_2O_3$ | $Fe_2O_3$ | CaO | MgO | Alkalis | | |
| Alumina | - | 0.13 | 99.78 | - | - | 0.01 | - | 0.05 | - | Corundum |
| Belgian sand | - | 98.76 | 0.09 | - | 0.81 | 0.28 | - | 0.11 | - | Quartz |
| Belgian sand washed | - | 99.64 | - | - | 0.14 | 0.09 | - | 0.05 | - | Quartz |
| Chromium oxide | - | - | - | 99.43 | - | - | - | - | - | Chromic Oxide |
| Ferric oxide | - | - | - | - | 99.34 | - | - | - | - | Hematite |
| Calcium Carbonate | 45.10 | 0.04 | 0.39 | - | 0.29 | 54.03 | - | 0.19 | - | Calcite |
| Magnesium Oxide | - | - | 0.11 | - | 0.03 | - | 99.80 | - | - | Periclase |
| Merwinite | - | 34.20 | 1.00** | - | - | 50.94 | 12.81 | - | - | Merwinite + dicalcium silicate + unidentified lines |
| Magnesio-ferrite | - | - | - | - | 79.27 | - | 20.72 | - | $MgO.(Fe_2O_3)0.965$ | Magnesioferrite |
| Spinel | - | - | 70.40 | - | - | - | 29.91 | - | $MgO.(Al_2O_3)0.931$ | Spinel + periclase (small) |
| Picro Chromite | - | - | 0.32 | 77.08 | - | - | 22.65 | - | $MgO.(Cr_2O_3)0.902$ | Pirochromite |
| Spinel s.s. $MgAl_{1.5}Cr_{0.5}O_4$ | - | - | 48.25 | 24.20 | - | - | 28.42 | - | $MgO.(Al_2O_3)0.671$ $(Cr_2O_3)0.226$ | Spinel solid solution |
| Spinel s.s. $MgAl_{0.8}Cr_{1.2}O_4$ | - | 0.37 | 23.60 | 52.39 | 0.48 | 0.17 | 22.96 | - | $MgO.(Al_2O_3)0.405$ $(Cr_2O_3)0.605$ | Spinel solid solution |

*From Department of Research of Magnesita S.A., Brazil.

**$Al_2O_3 + Fe_2O_3$

TABLE 6

Experimental compositions and phases identified in mixtures containing 80% MgO. Compositions expressed in terms of their CaO, $Al_2O_3$ and $SiO_2$ contents recalculated to 100%.

Note: The temperatures given are those at which the samples were soaked prior to quenching in water.

| $Al_2O_3$ wt.% | $SiO_2$ wt.% | CaO wt.% | Firing Temp. °C | Soaking Time (hours) | Phases present at the firing temperature |
|---|---|---|---|---|---|
| 20.0 | 28.0 | 52.0 | 1425 | 24 | MgO + $C_2S$ + liquid |
| | | | 1461 | 15 | MgO + $C_2S$ + liquid |
| | | | 1522 | 10 | MgO + $C_2S$ + liquid |
| 25.0 | 26.0 | 49.0 | 1425 | 24 | MgO + $C_2S$ + liquid |
| | | | 1432 | 20 | MgO + $C_2S$ + liquid |
| | | | 1461 | 15 | MgO + liquid |
| | | | 1522 | 10 | MgO + liquid |
| 30.0 | 24.5 | 45.5 | 1420 | 15 | MgO + spinel + $C_2S$ + liquid |
| | | | 1425 | 24 | MgO + liquid |
| | | | 1461 | 15 | MgO + liquid |
| | | | 1522 | 10 | MgO + liquid |
| 34.0 | 23.0 | 43.0 | 1417 | 20 | MgO + $C_2S$ + spinel |
| | | | 1420 | 15 | MgO + spinel + liquid |
| | | | 1425 | 24 | MgO + liquid |
| | | | 1461 | 15 | MgO + liquid |
| | | | 1522 | 10 | MgO + liquid |
| 40.0 | 21.0 | 39.0 | 1417 | 20 | MgO + spinel + $C_2S$ |
| | | | 1448 | 17 | MgO + spinel + liquid |
| 17.0 | 35.0 | 48.0 | 1440 | 24 | MgO + $C_3MS_2$ + $C_2S$ + liquid |
| | | | 1455 | 24 | MgO + $C_3MS_2$ + liquid |
| | | | 1485 | 24 | MgO + $C_3MS_2$ + liquid |
| | | | 1515 | 24 | MgO + liquid |
| 21.0 | 33.0 | 46.0 | 1440 | 24 | MgO + $C_3MS_2$ + $C_2S$ + liquid |
| | | | 1455 | 24 | MgO + $C_3MS_2$ + liquid |
| | | | 1485 | 24 | MgO + liquid |
| | | | 1515 | 24 | MgO + liquid |
| 31.0 | 29.0 | 40.0 | 1440 | 24 | MgO + spinel + liquid |
| | | | 1455 | 24 | MgO + spinel + liquid |
| | | | 1485 | 24 | MgO + spinel + liquid |
| | | | 1515 | 24 | MgO + spinel + liquid |

Contd.../

TABLE 6 - cond. 1

| $Al_2O_3$ wt.% | $SiO_2$ wt.% | CaO wt.% | Firing Temp. °C | Soaking Time (hours) | Phases present at the firing temperature |
|---|---|---|---|---|---|
| 12.0 | 37.0 | 51.0 | 1495 | 24 | MgO + $C_3MS_2$ + liquid |
| | | | 1500 | 24 | MgO + $C_3MS_2$ + liquid |
| | | | 1520 | 24 | MgO + liquid |
| 15.0 | 36.0 | 49.0 | 1495 | 24 | MgO + liquid |
| | | | 1520 | 24 | MgO + liquid |
| 5.0 | 41.0 | 54.0 | 1495 | 24 | MgO + $C_3MS_2$ ?? |
| | | | 1520 | 24 | MgO + $C_3MS_2$ ?? |
| | | | 1570 | 24 | MgO + $C_3MS_2$ + $C_2S$ |
| | | | 1595 | 24 | MgO + $C_3MS_2$ + $C_2S$ + liquid |
| | | | 1610 | 15 | MgO + $C_2S$ + liquid |
| 5.0 | 43.0 | 52.0 | 1495 | 24 | MgO + $C_3MS_2$ |
| | | | 1520 | 24 | MgO + $C_3MS_2$ + liquid ?? |
| | | | 1570 | 24 | MgO + $C_3MS_2$ + liquid |
| | | | 1595 | 24 | MgO + $C_3MS_2$ + liquid |
| 5.0 | 45.0 | 50.0 | 1495 | 24 | MgO + $C_3MS_2$ + liquid |
| | | | 1520 | 24 | MgO + $C_3MS_2$ + liquid |
| | | | 1570 | 24 | MgO + liquid |
| 20.0 | 30.0 | 50.0 | 1455 | 24 | MgO + $C_2S$ + liquid |
| 20.0 | 32.0 | 48.0 | 1455 | 24 | MgO + $C_3MS_2$ + liquid |
| 10.0 | 60.0 | 30.0 | 1530 | 24 | MgO + $M_2S$ + liquid |
| 15.0 | 55.0 | 30.0 | 1530 | 24 | MgO + $M_2S$ + liquid |
| 20.0 | 50.0 | 30.0 | 1485 | 18 | MgO + spinel + $M_2S$ + liquid |
| | | | 1500 | 24 | MgO + $M_2S$ + liquid |
| | | | 1530 | 24 | MgO + $M_2S$ + liquid |
| 25.0 | 45.0 | 30.0 | 1485 | 18 | MgO + spinel + $M_2S$ + liquid |
| | | | 1500 | 24 | MgO + spinel + liquid |
| | | | 1530 | 24 | MgO + spinel + liquid |
| 30.0 | 40.0 | 30.0 | 1485 | 18 | MgO + spinel + liquid |
| | | | 1500 | 24 | MgO + spinel + liquid |
| | | | 1530 | 24 | MgO + liquid |
| 20.0 | 60.0 | 20.0 | 1575 | 24 | MgO + $M_2S$ + liquid |
| 23.0 | 57.0 | 20.0 | 1575 | 24 | MgO + $M_2S$ + liquid |
| 26.0 | 54.0 | 20.0 | 1565 | 18 | MgO + spinel + $M_2S$ + liquid |
| | | | 1575 | 18 | MgO + $M_2S$ + liquid |
| | | | 1585 | 17 | MgO + $M_2S$ + liquid |

TABLE 6 - contd. 2

| $Al_2O_3$ wt.% | $SiO_2$ wt.% | CaO wt.% | Firing Temp. °C | Soaking Time (hours) | Phases present at the firing temperature |
|---|---|---|---|---|---|
| 30.0 | 50.0 | 20.0 | 1565 | 18 | MgO + spinel + $M_2S$ + liquid |
| | | | 1575 | 18 | MgO + spinel + $M_2S$ + liquid |
| | | | 1580 | 8 | MgO + spinel + $M_2S$ + liquid |
| | | | 1585 | 14 | MgO + liquid |
| | | | 1590 | 14 | MgO + $M_2S$ + liquid |
| 28.0 | 62.0 | 10.0 | 1625 | 24 | MgO + $M_2S$ + spinel + liquid |
| | | | 1645 | 19 | MgO + $M_2S$ + liquid |
| 32.0 | 58.0 | 10.0 | 1640 | 18 | MgO + spinel + $M_2S$ + liquid |
| | | | 1645 | 24 | MgO + $M_2S$ + liquid |
| | | | 1650 | 10 | MgO + $M_2S$ + liquid |
| | | | 1665 | 18 | MgO + liquid |
| 36.0 | 54.0 | 10.0 | 1640 | 18 | MgO + $M_2S$ + spinel + liquid |
| | | | 1645 | 24 | MgO + $M_2S$ + liquid |
| | | | 1650 | 10 | MgO + $M_2S$ + liquid |
| | | | 1665 | 18 | MgO + liquid |
| 18.0 | 47.0 | 35.0 | 1440 | 18 | MgO + spinel + $M_2S$ + liquid |
| | | | 1445 | 16 | MgO + $M_2S$ + liquid |
| | | | 1450 | 24 | MgO + liquid |
| | | | 1455 | 18 | MgO + liquid |
| 21.0 | 44.0 | 35.0 | 1420 | 19 | MgO + spinel + $M_2S$ + liquid |
| | | | 1440 | 18 | MgO + spinel + $M_2S$ + liquid |
| | | | 1450 | 24 | MgO + spinel + liquid |
| | | | 1460 | 24 | MgO + liquid |
| 24.0 | 41.0 | 35.0 | 1420 | 19 | MgO + spinel + $M_2S$ + liquid |
| | | | 1440 | 18 | MgO + spinel + $M_2S$ + liquid |
| | | | 1448 | 18 | MgO + spinel + liquid |
| | | | 1480 | 24 | MgO + liquid |
| 38.0 | 52.0 | 10.0 | 1640 | 18 | MgO + $M_2S$ + spinel + liquid |
| | | | 1645 | 24 | MgO + $M_2S$ + liquid |
| | | | 1665 | 18 | MgO + liquid |
| 40.0 | 50.0 | 10.0 | 1640 | 18 | MgO + $M_2S$ + spinel + liquid |
| | | | 1645 | 24 | MgO + spinel + liquid |
| | | | 1650 | 10 | MgO + spinel + liquid |
| | | | 1665 | 18 | MgO + spinel + liquid |
| 27.0 | 38.0 | 35.0 | 1448 | 18 | MgO + spinel + liquid |
| 33.0 | 47.0 | 20.0 | 1565 | 18 | MgO + $M_2S$ + liquid + spinel |
| | | | 1575 | 18 | MgO + spinel + $M_2S$ + liquid |
| | | | 1585 | 14 | MgO + spinel + liquid |

Contd.../

TABLE 6 - contd. 3

| $Al_2O_3$ wt.% | $SiO_2$ wt.% | CaO wt.% | Firing Temp. °C | Soaking Time (hours) | Phases present at the firing temperature |
|---|---|---|---|---|---|
| 23.0 | 35.0 | 42.0 | 1425 | 15 | MgO + spinel + liquid |
| 25.0 | 35.0 | 40.0 | 1425 | 15 | MgO + spinel + liquid |
| 20.0 | 38.0 | 42.0 | 1425 | 15 | MgO + spinel + liquid |
| | | | 1450 | 27 | MgO + liquid |
| 22.0 | 38.0 | 40.0 | 1425 | 15 | MgO + spinel + liquid |
| | | | 1450 | 27 | MgO + spinel + liquid |
| 38.0 | 57.0 | 5.0 | 1670 | 6 | MgO + liquid |
| 40.0 | 55.0 | 5.0 | 1660 | 8 | MgO + spinel + $M_2S$ + liquid |
| | | | 1670 | 6 | MgO + spinel + $M_2S$ + liquid |
| | | | 1680 | 3 | MgO + liquid |
| 42.0 | 53.0 | 5.0 | 1660 | 8 | MgO + spinel + $M_2S$ + liquid |
| | | | 1680 | 3 | MgO + $M_2S$ + liquid |
| 44.0 | 51.0 | 5.0 | 1660 | 8 | MgO + spinel + $M_2S$ + liquid |
| | | | 1670 | 6 | MgO + spinel + $M_2S$ + liquid |
| | | | 1680 | 3 | MgO + spinel + $M_2S$ + liquid |
| 21.0 | 35.0 | 44.0 | 1420 | 15 | MgO + $C_3MS_2$ + spinel + liquid |
| | | | 1430 | 20 | MgO + liquid |
| | | | 1445 | 7 | MgO + liquid |
| 18.0 | 38.0 | 44.0 | 1410 | 20 | MgO + $C_3MS_2$ + spinel + liquid |
| | | | 1420 | 15 | MgO + $C_3MS_2$ + liquid |
| 10.0 | 45.0 | 45.0 | 1420 | 15 | MgO + $C_3MS_2$ + liquid |
| 10.0 | 47.0 | 43.0 | 1410 | 15 | MgO + CMS + liquid |
| | | | 1420 | 20 | MgO + CMS + liquid |
| 10.0 | 49.0 | 41.0 | 1410 | 15 | MgO + CMS + liquid |
| | | | 1420 | 20 | MgO + CMS + liquid |
| 15.0 | 42.0 | 43.0 | 1400 | 18 | MgO + $C_3MS_2$ + liquid |
| | | | 1410 | 18 | MgO + $C_3MS_2$ + liquid |
| 17.0 | 42.0 | 41.0 | 1400 | 18 | MgO + spinel + liquid |
| | | | 1410 | 18 | MgO + liquid |

Contd.../

TABLE 6 - contd. 4

| $Al_2O_3$ wt.% | $SiO_2$ wt.% | CaO wt.% | Firing Temp. °C | Soaking Time (hours) | Phases present at the firing temperature |
|---|---|---|---|---|---|
| 14.0 | 44.0 | 42.0 | 1410 | 18 | MgO + CMS + liquid |
| 17.0 | 44.0 | 39.0 | 1400 | 15 | MgO + spinel + liquid |
| | | | 1432 | 20 | MgO + liquid |
| 16.0 | 46.0 | 38.0 | 1400 | 15 | MgO + spinel + liquid |
| | | | 1432 | 20 | MgO + liquid |
| 49,0 | 51.0 | - | 1690 | 15 | MgO + $M_2S$ + liquid ?? |
| | | | 1710 | 6 | MgO + $M_2S$ + liquid |
| | | | 1725 | 6 | MgO + $M_2S$ + liquid |
| 47.0 | 53.0 | - | 1690 | 15 | MgO + $M_2S$ + liquid ?? |
| | | | 1710 | 6 | MgO + $M_2S$ + liquid |
| | | | 1725 | 6 | MgO + $M_2S$ + liquid |
| 45.0 | 55.0 | - | 1690 | 15 | MgO + $M_2S$ + liquid ?? |
| | | | 1710 | 6 | MgO + $M_2S$ + liquid |
| | | | 1725 | 6 | MgO + $M_2S$ + liquid |
| 28.0 | 52.0 | 20.0 | 1590 | 10 | MgO + $M_2S$ + liquid |
| - | 45.0 | 55.0 | 1590 | 10 | MgO + $C_2S$ + liquid |
| - | 48.0 | 52.0 | 1560 | 3 | MgO + $C_3MS_2$ + liquid |
| - | 52.0 | 48.0 | 1480 | 18 | MgO + $C_3MS_2$ + liquid + CMS |
| | | | 1490 | 20 | MgO + $C_3MS_2$ + liquid |
| | | | 1500 | 5 | MgO + liquid |
| - | 57.0 | 43.0 | 1490 | 20 | MgO + CMS + liquid |
| | | | 1500 | 15 | MgO + CMS + liquid |
| - | 54.0 | 46.0 | 1490 | 20 | MgO + CMS + liquid |
| 13.0 | 35.0 | 52.0 | 1490 | 20 | MgO + $C_2S$ + liquid |
| | | | 1500 | 15 | MgO + liquid |
| 22.0 | 48.0 | 30.0 | 1490 | 20 | MgO + spinel + $M_2S$ + liquid |
| | | | 1500 | 18 | MgO + spinel + $M_2S$ + liquid |
| | | | 1520 | 3 | MgO + $M_2S$ + liquid |
| 10.0 | 50.0 | 40.0 | 1400 | 15 | Poor structure |
| | | | 1420 | 18 | MgO + CMS + liquid |
| | | | 1430 | 20 | MgO + CMS + liquid |

Contd.../

TABLE 6 - contd. 5

| $Al_2O_3$ wt.% | $SiO_2$ wt.% | CaO wt.% | Firing Temp. °C | Soaking Time (hours) | Phases present at the firing temperature |
|---|---|---|---|---|---|
| 26.0 | 29.0 | 45.0 | 1400 | 15 | No structure |
| | | | 1410 | 15 | MgO + $C_2S$ + $C_3MS_2$ + liquid |
| | | | 1420 | 18 | MgO + spinel + $C_3MS_2$ + liquid + $C_2S$ ?? |
| | | | 1430 | 20 | MgO + spinel + liquid |
| 24.0 | 29.0 | 47.0 | 1400 | 15 | No structure |
| | | | 1410 | 15 | MgO + $C_2S$ + $C_3MS_2$ + liquid |
| | | | 1420 | 18 | MgO + $C_2S$ + $C_3MS_2$ + liquid |
| | | | 1430 | 20 | MgO + $C_3MS_2$ + liquid |
| 32.0 | 22.0 | 46.0 | 1400 | 15 | MgO + $C_2S$ + spinel + liquid |
| | | | 1410 | 15 | MgO + spinel + liquid |
| | | | 1420 | 18 | MgO + liquid |
| 30.0 | 22.0 | 48.0 | 1400 | 15 | MgO + $C_2S$ + spinel + liquid |
| | | | 1410 | 15 | MgO + $C_2S$ + liquid |
| | | | 1420 | 18 | MgO + $C_2S$ + liquid |
| 51.0 | 49.0 | - | 1713 | 3 | MgO + spinel + liquid |
| 53.0 | 47.0 | - | 1713 | 3 | MgO + spinel + liquid |
| 55.0 | 45.0 | - | 1713 | 3 | MgO + spinel + liquid |
| - | 58.0 | 42.0 | 1490 | 15 | MgO + $M_2S$ + CMS + liquid |
| | | | 1500 | 18 | MgO + CMS + liquid |
| 10.0 | 51.0 | 39.0 | 1430 | 20 | MgO + $M_2S$ + liquid |
| - | 60.0 | 40.0 | 1490 | 15 | MgO + $M_2S$ + liquid |
| - | 59.0 | 41.0 | 1490 | 15 | MgO + $M_2S$ + liquid |

TABLE 7

Experimental compositions and phases identified in mixtures belonging to the isoplethal section at 60 wt.% MgO in the system $MgO-Cr_2O_3-C_2S$.

Note: The temperatures given are those at which the samples were soaked prior to quenching in water.

| MgO wt.% | $Cr_2O_3$ wt.% | $C_2S$ wt.% | Firing Temp. °C | Soaking Time (hours) | Phases present at the firing temperature |
|---|---|---|---|---|---|
| 60 | 22 | 18 | 1550 | 15 | MgO + spinel + $C_2S$ |
| | | | 1590 | 20 | MgO + spinel + $C_2S$ |
| | | | 1620 | 15 | MgO + spinel + liquid |
| | | | 1655 | 15 | MgO + spinel + liquid |
| | | | 1700 | 4 | MgO + spinel + liquid |
| 60 | 20 | 20 | 1655 | 15 | MgO + spinel + liquid |
| | | | 1680 | 15 | MgO + spinel + liquid |
| | | | 1700 | 4 | MgO + spinel + liquid |
| | | | 1700 | 15 | MgO + spinel + liquid |
| 60 | 18 | 22 | 1655 | 15 | MgO + spinel + liquid |
| | | | 1680 | 15 | MgO + liquid |
| | | | 1700 | 4 | MgO + liquid |
| 60 | 16 | 24 | 1620 | 15 | MgO + spinel + liquid |
| | | | 1655 | 15 | MgO + liquid |
| | | | 1700 | 4 | MgO + liquid |
| 60 | 14 | 26 | 1600 | 22 | MgO + spinel + $C_2S$ |
| | | | 1620 | 15 | MgO + liquid |
| | | | 1630 | 22 | MgO + liquid |
| | | | 1640 | 22 | MgO + liquid |
| | | | 1700 | 6,5 | MgO + liquid |
| | | | 1700 | 22 | MgO + liquid |
| 60 | 12 | 28 | 1600 | 22 | MgO + spinel + $C_2S$ |
| | | | 1610 | 15 | MgO + spinel + $C_2S$ |
| | | | 1630 | 22 | MgO + $C_2S$ + liquid |
| | | | 1640 | 22 | MgO + liquid |
| | | | 1700 | 6,5 | MgO + liquid |
| | | | 1700 | 22 | MgO + liquid |

Contd.../

Table 7 - contd.

| MgO wt.% | $Cr_2O_3$ wt.% | $C_2S$ wt.% | Firing Temp. °C | Soaking Time (hours) | Phases present at the firing temperature |
|---|---|---|---|---|---|
| 60 | 10 | 30 | 1600 | 22 | MgO + spinel + $C_2S$ |
| | | | 1610 | 15 | MgO + spinel + $C_2S$ |
| | | | 1620 | 15 | MgO + $C_2S$ + liquid |
| | | | 1640 | 22 | MgO + $C_2S$ + liquid |
| | | | 1680 | 15 | MgO + liquid |
| | | | 1700 | 6,5 | MgO + liquid |
| | | | 1700 | 22 | MgO + liquid |
| 60 | 8 | 32 | 1600 | 22 | MgO + spinel + $C_2S$ |
| | | | 1620 | 15 | MgO + $C_2S$ + liquid |
| | | | 1680 | 15 | MgO + $C_2S$ + liquid |
| | | | 1700 | 5 | MgO + liquid |
| | | | 1696 | 2 | MgO + liquid |
| 60 | 6 | 34 | 1700 | 5 | MgO + $C_2S$ + liquid |
| 60 | 4 | 36 | 1620 | 15 | MgO + $C_2S$ + liquid |
| | | | 1700 | 5 | MgO + $C_2S$ + liquid |
| 60 | 15 | 25 | 1620 | 15 | MgO + spinel + $C_2S$ + liquid |
| 60 | 13 | 27 | 1620 | 15 | MgO + $C_2S$ + liquid |

TABLE 8

Experimental compositions and phases identified in mixtures belonging to the isoplethal section at 40 wt.% MgO in the system $MgO-Cr_2O_3-C_2S$.

Note: The temperatures given are those at which the samples were soaked prior to quenching in water.

| MgO wt.% | $Cr_2O_3$ wt.% | $C_2S$ wt.% | Firing Temp. °C | Soaking Time (hours) | Phases present at the firing temperature |
|---|---|---|---|---|---|
| 40 | 19.2 | 40.8 | 1635 | 15 | MgO + spinel + liquid |
| | | | 1640 | 5 | MgO + spinel + liquid |
| | | | 1647 | 15 | MgO + spinel + liquid |
| 40 | 16.8 | 43.2 | 1622 | 13 | MgO + $C_2S$ + spinel |
| | | | 1627 | 8 | MgO + spinel + $C_2S$ + liquid |
| | | | 1635 | 15 | MgO + spinel + liquid |
| | | | 1640 | 5 | MgO + spinel + liquid |
| | | | 1647 | 15 | MgO + liquid |
| 40 | 14.4 | 45.6 | 1622 | 13 | MgO + $C_2S$ + spinel |
| | | | 1627 | 8 | MgO + spinel + $C_2S$ + liquid |
| | | | 1635 | 15 | MgO + liquid |
| | | | 1640 | 5 | MgO + liquid |
| | | | 1647 | 15 | MgO + liquid |
| 40 | 12.0 | 48.0 | 1635 | 15 | MgO + $C_2S$ + liquid |
| | | | 1640 | 5 | MgO + $C_2S$ + liquid |
| | | | 1647 | 15 | MgO + liquid |

TABLE 9

Experimental compositions and phases identified in mixtures used to locate the eutectic point of the system $MgO-Cr_2O_3-C_2S$

| MgO wt.% | $Cr_2O_3$ wt.% | $C_2S$ wt.% | Firing Temp. °C | Soaking Time (hours) | Phases present at the firing temperature |
|---|---|---|---|---|---|
| 16.0 | 14.0 | 70.0 | 1630 | 3 | $C_2S$ + MgO + liquid |
| | | | 1645 | 1 | $C_2S$ + MgO + liquid |
| | | | 1655 | 1½ | MgO + liquid |
| 13.0 | 14.0 | 73.0 | 1630 | 3 | $C_2S$ + MgO + liquid |
| | | | 1645 | 1 | $C_2S$ + MgO + liquid |
| | | | 1650 | 1 | $C_2S$ + MgO + liquid |
| 10.0 | 14.0 | 76.0 | 1630 | 3 | $C_2S$ + spinel + liquid |
| | | | 1635 | 1 | $C_2S$ + spinel + liquid |
| | | | 1647 | 1 | $C_2S$ + liquid |
| | | | 1662 | 1½ | liquid |
| 6.0 | 14.0 | 80.0 | 1630 | 3 | $C_2S$ + spinel + liquid |
| 12.0 | 10.0 | 78.0 | 1620 | 13 | $C_2S$ + MgO + spinel + liquid |
| | | | 1635 | 1 | $C_2S$ + MgO + liquid |
| | | | 1670 | 1½ | $C_2S$ + MgO + liquid |
| | | | 1700 | 1 | $C_2S$ + MgO + liquid |
| | | | 1720 | 1½ | liquid |
| 18.0 | 10.0 | 72.0 | 1620 | 13 | MgO + $C_2S$ + spinel + liquid |
| | | | 1670 | 1½ | MgO + $C_2S$ + liquid |
| | | | 1685 | 1 | MgO + $C_2S$ + liquid |
| | | | 1700 | 1 | MgO + $C_2S$ + liquid |
| | | | 1720 | 1½ | liquid |
| 13.0 | 16.0 | 71.0 | 1620 | 13 | $C_2S$ + MgO + spinel + liquid |
| | | | 1645 | 1 | $C_2S$ + spinel + liquid |
| | | | 1662 | 1½ | $C_2S$ + liquid |

Contd.../

Table 9 - contd.

| MgO wt.% | $Cr_2O_3$ wt.% | $C_2S$ wt.% | Firing Temp. °C | Soaking Time (hours) | Phases present at the firing temperature |
|---|---|---|---|---|---|
| 19.0 | 16.0 | 65.0 | 1620 | 13 | $C_2S$ + MgO + spinel + liquid |
| | | | 1660 | 2 | MgO + spinel + liquid |
| | | | 1674 | 2 | MgO + spinel + liquid |
| 15.0 | 5.0 | 80.0 | 1630 | 3 | $C_2S$ + MgO + liquid |
| | | | 1683 | 2 | $C_2S$ + MgO + liquid |
| | | | 1713 | 2 | $C_2S$ + MgO + liquid |
| 25.0 | 5.0 | 70.0 | 1630 | 3 | $C_2S$ + MgO + liquid |
| | | | 1683 | 2 | $C_2S$ + MgO + liquid |
| | | | 1713 | 2 | $C_2S$ + MgO + liquid |
| 20.0 | 25.0 | 55.0 | 1635 | 2 | MgO + spinel + liquid |
| | | | 1666 | 2 | MgO + spinel + liquid |
| 30.0 | 25.0 | 45.0 | 1635 | 2 | MgO + spinel + liquid |
| | | | 1666 | 2 | MgO + spinel + liquid |
| 30.0 | 5.0 | 65.0 | 1630 | 2 | $C_2S$ + MgO + liquid |
| | | | 1683 | 2 | $C_2S$ + MgO + liquid |
| | | | 1713 | 2 | $C_2S$ + MgO + liquid |
| 35.0 | 5.0 | 60.0 | 1630 | 2 | $C_2S$ + MgO + liquid |
| | | | 1683 | 2 | $C_2S$ + MgO + liquid |
| | | | 1713 | 2 | $C_2S$ + MgO + liquid |
| 6.0 | 15.0 | 79.0 | 1630 | 2 | $C_2S$ + spinel + liquid |
| | | | 1674 | 2 | $C_2S$ + spinel + liquid |
| | | | 1680 | ½ | $C_2S$ + spinel + liquid |
| | | | 1690 | 1 | $C_2S$ + spinel + liquid |
| | | | 1693 | 1 | $C_2S$ + liquid |
| 40.0 | 30.0 | 30.0 | 1630 | 2 | MgO + spinel + liquid |
| 25.0 | 10.0 | 65.0 | 1645 | 2½ | MgO + $C_2S$ + liquid |
| | | | 1690 | 2 | MgO + $C_2S$ + liquid |
| | | | 1720 | 1½ | MgO + liquid |
| 30.0 | 10.0 | 60.0 | 1645 | 2½ | MgO + $C_2S$ + liquid |
| | | | 1690 | 2 | MgO + $C_2S$ + liquid |
| 24.0 | 16.0 | 60.0 | 1647 | 2 | MgO + spinel + liquid |
| | | | 1660 | 2 | MgO + spinel + liquid |
| 30.0 | 16.0 | 54.0 | 1647 | 2 | MgO + spinel + liquid |
| 13.0 | 18.0 | 69.0 | 1645 | 1 | spinel + $C_2S$ + liquid |
| | | | 1660 | 2 | spinel + liquid |
| 17.0 | 18.0 | 65.0 | 1660 | 2 | MgO + spinel + liquid |
| 6.0 | 16.0 | 78.0 | 1670 | 1 | spinel + $C_2S$ + liquid |
| | | | 1680 | 1½ | spinel + liquid |
| | | | 1690 | 1 | liquid |
| 6.0 | 17.0 | 77.0 | 1680 | 1½ | spinel + liquid |
| | | | 1690 | 1 | liquid |

TABLE 10

Experimental compositions and phases identified in mixtures of the system MF-$C_3MS_2$.

Note: The temperatures given are those at which the samples were soaked prior to quenching in water.

| MF Wt.% | $C_3MS_2$ Wt.% | Firing Temp. °C | Soaking Time (hours) | Phases present at the firing temperature |
|---|---|---|---|---|
| 60.0 | 40.0 | 1430 | 12 | MF + MW + liquid |
| | | 1450 | 2 | MF + MW + liquid |
| 40.0 | 60.0 | 1424 | 16 | MF + $C_3MS_2$ |
| | | 1430 | 12 | MF + MW + liquid |
| | | 1440 | 2 | MW + liquid |
| 30.0 | 70.0 | 1430 | 12 | MW + $C_3MS_2$ + liquid |
| | | 1440 | 2 | MW + $C_3MS_2$ + liquid |
| | | 1485 | 1 | MW + liquid |
| 20.0 | 80.0 | 1406 | 12 | MF + $C_3MS_2$ |
| | | 1415 | 15 | MF + $C_3MS_2$ |
| | | 1424 | 16 | MF + $C_3MS_2$ |
| | | 1430 | 12 | MW + $C_3MS_2$ + liquid |
| | | 1450 | 2 | MW + $C_3MS_2$ + liquid |
| | | 1500 | 2 | MW + $C_3MS_2$ + liquid |
| | | 1510 | 2 | MW + $C_3MS_2$ + liquid |
| | | 1525 | 1 | MW + $C_2S$ + liquid |
| | | 1548 | 1 | MW + liquid |
| | | 1560 | 1 | MW + liquid |
| | | 1590 | 1 | MW + liquid |
| | | 1605 | 1 | liquid |
| | | 1620 | 1 | liquid |
| 10.0 | 90.0 | 1430 | 12 | MW + $C_3MS_2$ + liquid |
| | | 1450 | 2 | MW + $C_3MS_2$ + liquid |
| | | 1500 | 2 | MW + $C_3MS_2$ + liquid |
| | | 1525 | 2 | MW + $C_3MS_2$ + liquid |
| | | 1540 | 2 | MW + $C_2S$ + liquid |
| | | 1550 | 2 | MW + $C_2S$ + liquid |
| | | 1600 | 1 | MW + $C_2S$ + liquid |
| | | 1610 | 1 | MW + $C_2S$ + liquid |
| | | 1700 | 1 | liquid |
| 5.0 | 95.0 | 1430 | 12 | MW + $C_3MS_2$ + liquid |
| | | 1450 | 2 | MW + $C_3MS_2$ + liquid |
| | | 1500 | 2 | MW + $C_3MS_2$ + liquid |
| | | 1520 | 2 | MW + $C_3MS_2$ + liquid |
| | | 1530 | 2 | MW + $C_3MS_2$ + $C_2S$ + liquid |
| | | 1540 | 2 | MW + $C_3MS_2$ + $C_2S$ + liquid |
| | | 1550 | 2 | MW + $C_3MS_2$ + $C_2S$ + liquid |
| | | 1575 | 2 | MW + $C_2S$ + liquid |
| | | 1600 | 1 | MW + $C_2S$ + liquid |
| | | 1625 | 2 | MW + $C_2S$ + liquid |

Contd.../

**Table 10** - contd.

| MF Wt.% | $C_3MS_2$ Wt.% | Firing Temp. °C | Soaking Time (hours) | Phases present at the firing temperature |
|---|---|---|---|---|
| | | 1645 | 1 | MW + $C_2S$ + liquid |
| | | 1650 | 2 | MW + $C_2S$ + liquid |
| | | 1680 | 1 | MW + $C_2S$ + liquid |
| 15.0 | 85.0 | 1518 | 2 | MW + $C_3MS_2$ + liquid |
| | | 1532 | 2 | MW + $C_2S$ + liquid |
| | | 1548 | 1 | MW + $C_2S$ + liquid |
| | | 1575 | 1 | MW + $C_2S$ + liquid |
| | | 1590 | 1 | liquid |
| | | 1605 | 1 | liquid |
| | | 1645 | 1 | liquid |
| 35.0 | 65.0 | 1544 | 1 | MW + liquid |
| | | 1560 | 1 | MW + liquid |
| | | 1600 | 1 | MW + liquid |
| 12.5 | 87.5 | 1530 | 2 | MW + $C_3MS_2$ + $C_2S$ + liquid |
| | | 1540 | 2 | MW + $C_2S$ + liquid |
| | | 1560 | 1 | MW + $C_2S$ + liquid |
| | | 1610 | 1 | MW + $C_2S$ + liquid |
| | | 1645 | 1 | liquid |
| 7.5 | 92.5 | 1540 | 2 | MW + $C_3MS_2$ + $C_2S$ + liquid |
| | | 1550 | 2 | MW + $C_2S$ + liquid |
| | | 1560 | 1 | MW + $C_2S$ + liquid |
| | | 1620 | 1 | MW + $C_2S$ + liquid |
| | | 1645 | 1 | MW + $C_2S$ + liquid |
| | | 1700 | 1 | $C_2S$ + liquid |
| 2.5 | 97.5 | 1520 | 1 | MW + $C_3MS_2$ + liquid |
| | | 1530 | 1 | MW + $C_3MS_2$ + $C_2S$ + liquid |
| | | 1540 | 1 | MW + $C_3MS_2$ + $C_2S$ + liquid |
| | | 1550 | 2 | MW + $C_3MS_2$ + $C_2S$ + liquid |
| | | 1560 | 1 | MW + $C_3MS_2$ + $C_2S$ + liquid |
| | | 1600 | 1 | MW + $C_2S$ + liquid |
| | | 1690 | 1 | MW + $C_2S$ + liquid |
| | | 1710 | 1 | $C_2S$ + liquid |
| 25.0 | 75.0 | 1482 | 2 | MW + $C_3MS_2$ + liquid |
| | | 1510 | 1 | MW + liquid |
| 35.0 | 65.0 | 1455 | 1 | MW + $C_3MS_2$ + liquid |
| 45.0 | 55.0 | 1455 | 1 | MW + MF + liquid |
| | | 1690 | 1 | MW + liquid |
| | | 1710 | 1 | liquid |
| 50.0 | 50.0 | 1480 | 2 | MW + liquid |
| - | 100.0 | 1680 | 2 | MgO + $C_2S$ + liquid |
| | | 1700 | 2½ | $C_2S$ + liquid |
| | | 1705 | 1 | $C_2S$ + liquid |
| | | 1715 | 2 | $C_2S$ + liquid |

TABLE 11

Experimental compositions and phases identified in mixtures of the system $MgO-Fe_2O_3-C_3MS_2$ after firing at 1550°C - 2 hrs. - and quenching in air.

| $Fe_2O_3$ wt.% | MgO wt.% | $C_3MS_2$ wt.% | Phases present at the firing temperature |
|---|---|---|---|
| 10.0 | 80.0 | 10.0 | MW + $C_3MS_2$ + liquid |
| 20.0 | 70.0 | 10.0 | MW + $C_3MS_2$ + liquid |
| 20.0 | 60.0 | 20.0 | MW + $C_3MS_2$ + liquid |
| 30.0 | 50.0 | 20.0 | MW + $C_3MS_2$ + liquid |
| 10.0 | 10.0 | 80.0 | MW + $C_3MS_2$ + $C_2S$ + liquid |
| 20.0 | 10.0 | 70.0 | MW + $C_3MS_2$ + liquid |
| 20.0 | 20.0 | 60.0 | MW + $C_3MS_2$ + liquid |
| 10.0 | 20.0 | 70.0 | MW + $C_3MS_2$ + $C_2S$ + liquid |
| 10.0 | 60.0 | 30.0 | MW + $C_3MS_2$ + liquid |
| 20.0 | 50.0 | 30.0 | MW + $C_3MS_2$ + liquid |
| 30.0 | 40.0 | 30.0 | MW + $C_3MS_2$ + liquid |
| 40.0 | 30.0 | 30.0 | MW + liquid |
| 10.0 | 50.0 | 40.0 | MW + $C_3MS_2$ + liquid |
| 20.0 | 40.0 | 40.0 | MW + $C_3MS_2$ + liquid |
| 30.0 | 30.0 | 40.0 | MW + $C_3MS_2$ + liquid |
| 40.0 | 20.0 | 40.0 | MW + MF + liquid |
| 5.0 | 85.0 | 10.0 | MW + $C_3MS_2$ + liquid |
| 5.0 | 65.0 | 30.0 | MW + $C_3MS_2$ + liquid |
| 5.0 | 45.0 | 50.0 | MW + $C_3MS_2$ + liquid |
| 5.0 | 35.0 | 60.0 | MW + $C_3MS_2$ + liquid |
| 30.0 | 60.0 | 10.0 | MW + $C_3MS_2$ + liquid |
| 40.0 | 50.0 | 10.0 | MW + liquid |
| 50.0 | 40.0 | 10.0 | MW + MF + liquid |
| 60.0 | 30.0 | 10.0 | MW + MF + liquid |
| 2.5 | 87.5 | 10.0 | MW + $C_3MS_2$ + liquid |
| 1.0 | 89.0 | 10.0 | MW + $C_3MS_2$ + liquid |
| 2.5 | 67.5 | 30.0 | MW + $C_3MS_2$ + liquid |
| 1.0 | 69.0 | 30.0 | MW + $C_3MS_2$ + liquid |
| 65.0 | 25.0 | 10.0 | MW + MF + liquid |
| 70.0 | 20.0 | 10.0 | MW + MF + liquid |
| 75.0 | 15.0 | 10.0 | MF + liquid |
| 80.0 | 10.0 | 10.0 | MF + liquid |
| 40.0 | 40.0 | 20.0 | MW + liquid |
| 50.0 | 30.0 | 20.0 | MW + MF + liquid |
| 60.0 | 20.0 | 20.0 | MW + MF + liquid |
| 70.0 | 10.0 | 20.0 | MF + liquid |
| 50.0 | 45.0 | 5.0 | MW + liquid + MF (traces) |
| 54.0 | 41.0 | 5.0 | MW + MF + liquid |
| 75.0 | 20.0 | 5.0 | MW + MF + liquid |

Contd.../

Table 11 - contd.

| $Fe_2O_3$ wt.% | MgO wt.% | $C_3MS_2$ wt.% | Phases present at the firing temperature |
|---|---|---|---|
| 80.0 | 15.0 | 5.0 | MF + liquid |
| 52.0 | 43.0 | 5.0 | MW + MF + liquid |
| 51.0 | 39.0 | 10.0 | MW + MF + liquid |
| 71.0 | 19.0 | 10.0 | MW + MF + liquid |
| 76.0 | 19.0 | 5.0 | MF + MW + liquid |
| 46.0 | 34.0 | 20.0 | MW + liquid + MF (traces) |
| 48.0 | 32.0 | 20.0 | MW + liquid + MF (traces) |
| 62.0 | 18.0 | 20.0 | MW + MF + liquid |
| 64.0 | 16.0 | 20.0 | MW + MF + liquid |
| 72.0 | 18.0 | 10.0 | MW + MF + liquid |
| 73.0 | 17.0 | 10.0 | MF + liquid |
| 65.0 | 15.0 | 20.0 | MW + MF + liquid |
| 66.0 | 14.0 | 20.0 | MF + liquid |
| 12.0 | 48.0 | 40.0 | MW + $C_3MS_2$ + liquid |
| 14.0 | 46.0 | 40.0 | MW + $C_3MS_2$ + liquid |
| 16.0 | 44.0 | 40.0 | MW + $C_3MS_2$ + liquid |
| 18.0 | 42.0 | 40.0 | MW + $C_3MS_2$ + liquid |
| 7.0 | 33.0 | 60.0 | MW + $C_3MS_2$ + liquid |
| 9.0 | 31.0 | 60.0 | MW + $C_3MS_2$ + liquid |
| 9.0 | 41.0 | 50.0 | MW + $C_3MS_2$ + liquid |
| 11.0 | 39.0 | 50.0 | MW + $C_3MS_2$ + liquid |
| 22.0 | 48.0 | 30.0 | MW + $C_3MS_2$ + liquid |
| 24.0 | 46.0 | 30.0 | MW + $C_3MS_2$ + liquid |
| 23.0 | 37.0 | 40.0 | MW + $C_3MS_2$ + liquid |
| 26.0 | 34.0 | 40.0 | MW + $C_3MS_2$ + liquid |
| 22.0 | 68.0 | 10.0 | MW + $C_3MS_2$ + liquid |
| 24.0 | 66.0 | 10.0 | MW + $C_3MS_2$ + liquid |
| 26.0 | 64.0 | 10.0 | MW + $C_3MS_2$ + liquid |
| 28.0 | 62.0 | 10.0 | MW + $C_3MS_2$ + liquid |
| 22.0 | 58.0 | 20.0 | MW + $C_3MS_2$ + liquid |
| 24.0 | 56.0 | 20.0 | MW + $C_3MS_2$ + liquid |
| 26.0 | 54.0 | 20.0 | MW + $C_3MS_2$ + liquid |
| 28.0 | 52.0 | 20.0 | MW + $C_3MS_2$ + liquid |
| 61.0 | 14.0 | 25.0 | MW + MF + liquid |
| 62.0 | 13.0 | 25.0 | MF + liquid |
| 55.0 | 12.0 | 33.0 | MW + MF + liquid |
| 56.0 | 11.0 | 33.0 | MF + liquid |
| 2.0 | 38.0 | 60.0 | MW + $C_3MS_2$ + liquid |
| 4.0 | 36.0 | 60.0 | MW + $C_3MS_2$ + liquid |
| 6.0 | 34.0 | 60.0 | MW + $C_3MS_2$ + $C_2S$ + liquid |
| 8.0 | 32.0 | 60.0 | MW + $C_3MS_2$ + $C_2S$ + liquid |
| 1.0 | 9.0 | 90.0 | MW + $C_3MS_2$ + liquid |
| 3.0 | 7.0 | 90.0 | MW + $C_3MS_2$ + $C_2S$ + liquid |
| 5.0 | 5.0 | 90.0 | MW + $C_3MS_2$ + liquid |
| 8.0 | 2.0 | 90.0 | $C_3MS_2$ + $C_2S$ + liquid |

Contd.../

Table 11 - contd.

| $Fe_2O_3$ wt.% | MgO wt.% | $C_3MS_2$ wt.% | Phases present at the firing temperature |
|---|---|---|---|
| 22.0 | 28.0 | 50.0 | MW + $C_3MS_2$ + liquid |
| 24.0 | 26.0 | 50.0 | MW + $C_3MS_2$ + liquid |
| 26.0 | 24.0 | 50.0 | MW + $C_3MS_2$ + liquid |
| 28.0 | 22.0 | 50.0 | MW + $C_3MS_2$ + liquid |
| 3.0 | 27.0 | 70.0 | MW + $C_3MS_2$ + liquid |
| 5.0 | 25.0 | 70.0 | MW + $C_3MS_2$ + $C_2S$ + liquid |
| 2.0 | 18.0 | 80.0 | MW + $C_3MS_2$ + liquid |
| 4.0 | 16.0 | 80.0 | MW + $C_3MS_2$ + $C_2S$ + liquid |
| 11.0 | 4.0 | 85.0 | MW + $C_3MS_2$ + $C_2S$ + liquid |
| 13.0 | 2.0 | 85.0 | MW + $C_3MS_2$ + $C_2S$ + liquid |
| 7.0 | 3.0 | 90.0 | MW + $C_3MS_2$ + $C_2S$ + liquid |
| 9.0 | 1.0 | 90.0 | MW + $C_3MS_2$ + $C_2S$ + liquid |
| 2.0 | - | 98.0 | $C_3MS_2$ + liquid |
| 2.0 | 2.0 | 96.0 | $C_3MS_2$ + liquid |
| 6.0 | 1.0 | 93.0 | $C_2S$ + liquid |
| 2.0 | 28.0 | 70.0 | MW + $C_3MS_2$ + liquid |
| 3.0 | 37.0 | 60.0 | MW + $C_3MS_2$ + liquid |
| 5.0 | 30.0 | 65.0 | MW + $C_3MS_2$ + liquid |
| 4.0 | 1.0 | 95.0 | $C_3MS_2$ + $C_2S$ + liquid |
| 1.0 | 29.0 | 70.0 | MW + $C_3MS_2$ + liquid |
| 1.0 | 39.0 | 60.0 | MW + $C_3MS_2$ + liquid |
| 12.0 | 58.0 | 30.0 | MW + $C_3MS_2$ + liquid |
| 14.0 | 56.0 | 30.0 | MW + $C_3MS_2$ + liquid |
| 16.0 | 54.0 | 30.0 | MW + $C_3MS_2$ + liquid |
| 18.0 | 52.0 | 30.0 | MW + $C_3MS_2$ + liquid |
| 79.8 | 20.2 | - | MF + liquid + MW (traces) |
| 52.5 | 47.5 | - | MW + liquid + MF (traces) |

TABLE 12

Experimental compositions and phases identified in mixtures of the system $MgO-Fe_2O_3-C_3MS_2$ after firing at 1550°C and quenching in water.

| $Fe_2O_3$ wt.% | MgO wt.% | $C_3MS_2$ wt.% | Soaking Time (hrs.) | Phases present at the firing temperature |
|---|---|---|---|---|
| 12.0 | 58.0 | 30.0 | 15 | MW + liquid |
| 14.0 | 56.0 | 30.0 | 15 | MW + liquid |
| 16.0 | 54.0 | 30.0 | 15 | MW + liquid |
| 18.0 | 52.0 | 30.0 | 15 | MW + liquid |
| 2.0 | - | 98.0 | 2 | $C_2S$ + liquid |
| 2.0 | 2.0 | 96.0 | 2 | MW + $C_3MS_2$ + $C_2S$ + liquid |
| 6.0 | 1.0 | 93.0 | 2 | $C_2S$ + liquid |
| 2.0 | 38.0 | 60.0 | 2 | MW + $C_3MS_2$ + $C_2S$ + liquid |
| 4.0 | 36.0 | 60.0 | 2 | MW + $C_3MS_2$ + $C_2S$ + liquid |
| 6.0 | 34.0 | 60.0 | 2 | MW + $C_3MS_2$ + $C_2S$ + liquid |
| 8.0 | 32.0 | 60.0 | 2 | MW + $C_3MS_2$ + $C_2S$ + liquid |
| 1.0 | 9.0 | 90.0 | 2 | MW + $C_3MS_2$ + $C_2S$ + liquid |
| 3.0 | 7.0 | 90.0 | 2 | MW + $C_3MS_2$ + $C_2S$ + liquid |
| 5.0 | 5.0 | 90.0 | 2 | MW + $C_2S$ + liquid |
| 50.0 | 45.0 | 5.0 | 14 | MW + liquid |
| 52.0 | 43.0 | 5.0 | 14 | MW + liquid + MF (traces) |
| 46.0 | 34.0 | 20.0 | 14 | MW + liquid |
| 48.0 | 32.0 | 20.0 | 14 | MW + liquid |
| 12.0 | 48.0 | 40.0 | 4 | MW + liquid |
| 14.0 | 46.0 | 40.0 | 4 | MW + liquid |
| 16.0 | 44.0 | 40.0 | 4 | MW + liquid |
| 18.0 | 42.0 | 40.0 | 4 | MW + liquid |
| 1.0 | 29.0 | 70.0 | 2 | MW + $C_3MS_2$ + liquid |
| 1.0 | 39.0 | 60.0 | 2 | MW + $C_3MS_2$ + liquid |
| 7.0 | 33.0 | 60.0 | 2 | MW + $C_3MS_2$ + $C_2S$ + liquid |
| 9.0 | 31.0 | 60.0 | 2 | MW + $C_3MS_2$ + $C_2S$ + liquid |
| 9.0 | 41.0 | 50.0 | 2 | MW + $C_3MS_2$ + $C_2S$ + liquid |
| 11.0 | 39.0 | 50.0 | 2 | MW + $C_3MS_2$ + $C_2S$ + liquid |
| 8.0 | 2.0 | 90.0 | 4 | MW + $C_2S$ + liquid |
| 2.0 | - | 98.0 | 4 | $C_2S$ + liquid |
| 6.0 | 1.0 | 93.0 | 4 | $C_2S$ + liquid |
| 76.0 | 19.0 | 5.0 | 2 | MF + liquid + MW (traces) |
| 75.0 | 20.0 | 5.0 | 2 | MF + MW + liquid |
| 51.0 | 39.0 | 10.0 | 2 | MW + liquid |
| 75.0 | 15.0 | 10.0 | 2 | MF + liquid |
| 10.0 | 60.0 | 30.0 | 15 | MW + liquid |
| 10.0 | 50.0 | 40.0 | 15 | MW + liquid |
| 5.0 | 45.0 | 50.0 | 15 | MW + $C_3MS_2$ + $C_2S$ + liquid |
| 5.0 | 85.0 | 10.0 | 15 | MW + $C_3MS_2$ + $C_2S$ + liquid |
| 22.0 | 28.0 | 50.0 | 2 | MW + liquid |
| 71.0 | 19.0 | 10.0 | 2 | MW + MF + liquid |
| 64.0 | 16.0 | 20.0 | 2 | MW + MF + liquid |

Contd.../

Table 12 - contd.

| $Fe_2O_3$ wt.% | MgO wt.% | $C_3MS_2$ wt.% | Soaking Time (hrs.) | Phases present at the firing temperature |
|---|---|---|---|---|
| 65.0 | 15.0 | 20.0 | 2 | MF + MW + liquid |
| 3.0 | 27.0 | 70.0 | 2 | MW + $C_3MS_2$ + liquid + $C_2S$ |
| 2.0 | 18.0 | 80.0 | 2 | MW + $C_3MS_2$ + liquid + $C_2S$ |
| 2.0 | 28.0 | 70.0 | 2 | MW + $C_3MS_2$ + $C_2S$ + liquid |
| 3.0 | 37.0 | 60.0 | 2 | MW + $C_3MS_2$ + $C_2S$ + liquid |
| 50.0 | 30.0 | 20.0 | 2 | MW + liquid |
| 66.0 | 14.0 | 20.0 | 2 | MF + liquid |
| 62.0 | 13.0 | 25.0 | 2 | MF + liquid |
| 2.0 | 58.0 | 40.0 | 15 | MW + $C_3MS_2$ + $C_2S$ + liquid |
| 4.0 | 56.0 | 40.0 | 15 | MW + $C_3MS_2$ + $C_2S$ + liquid |
| 6.0 | 54.0 | 40.0 | 15 | MW + $C_3MS_2$ + $C_2S$ + liquid |
| 8.0 | 52.0 | 40.0 | 15 | MW + $C_3MS_2$ + $C_2S$ + liquid |
| 10.0 | 10.0 | 80.0 | 2 | MW + $C_3MS_2$ + $C_2S$ + liquid |
| 20.0 | 10.0 | 70.0 | 2 | liquid |
| 20.0 | 20.0 | 60.0 | 2 | liquid |
| 10.0 | 20.0 | 70.0 | 2 | MW + $C_3MS_2$ + $C_2S$ + liquid |
| 52.0 | 28.0 | 20.0 | 2 | MW + liquid |
| 52.0 | 38.0 | 10.0 | 2 | MW + MF + liquid |
| 1.0 | 59.0 | 40.0 | 2 | MW + $C_3MS_2$ + liquid + $C_2S$ (traces) |
| 9.0 | 51.0 | 40.0 | 2 | MW + $C_3MS_2$ + $C_2S$ + liquid |
| 7.0 | 63.0 | 30.0 | 2 | MW + $C_3MS_2$ + $C_2S$ + liquid |
| 8.0 | 62.0 | 30.0 | 2 | MW + liquid |
| 5.0 | 85.0 | 10.0 | 2 | MW + $C_3MS_2$ + $C_2S$ + liquid |
| 5.0 | 65.0 | 30.0 | 2 | MW + $C_3MS_2$ + $C_2S$ + liquid |
| 1.0 | 89.0 | 10.0 | 2 | MW + $C_3MS_2$ + liquid |
| 1.0 | 69.0 | 30.0 | 2 | MW + $C_3MS_2$ + liquid |

TABLE 13

Experimental compositions and phases identified in mixtures of the system $MgAl_2O_4$-$C_3MS_2$.

Note: The temperatures given are those at which the samples were soaked prior to quenching in water.

| MA wt.% | $C_3MS_2$ wt.% | Firing Temp. °C | Soaking Time (hours) | Phases present at the firing temperature |
|---|---|---|---|---|
| 40 | 60 | 1526 | 1½ | MgO + spinel + liquid |
| | | 1540 | 2½ | MgO + spinel + liquid |
| | | 1555 | 2 | spinel + liquid |
| 70 | 30 | 1430 | 20 | spinel + $C_3MS_2$ |
| | | 1440 | 2 | spinel + MgO + liquid |
| | | 1450 | 2 | spinel + MgO + liquid |
| | | 1545 | 2 | spinel + MgO + liquid |
| 50 | 50 | 1420 | 15 | MgO + spinel + $C_3MS_2$ + $C_2S$ + liquid ? |
| | | 1440 | 3 | MgO + spinel + $C_2S$ + liquid |
| | | 1450 | 4 | spinel + MgO + liquid |
| | | 1465 | 4 | spinel + MgO + liquid |
| | | 1545 | 2 | spinel + MgO + liquid |
| | | 1560 | 2 | spinel + liquid |
| 10 | 90 | 1480 | 2 | $C_2S$ + MgO + $C_3MS_2$ + liquid |

TABLE 14

Experimental compositions and phases identified in mixtures of the system $MgCr_2O_4$-$C_3MS_2$.

Note: The temperatures given are those at which the samples were soaked prior to quenching in water.

| MK wt.% | $C_3MS_2$ wt.% | Firing Temp. °C | Soaking Time (hours) | Phases present at the firing temperature |
|---|---|---|---|---|
| 15 | 85 | 1508 | 15 | spinel + $C_3MS_2$ + $C_2S$ |
| | | 1530 | 2½ | spinel + $C_3MS_2$ + $C_2S$ |
| | | 1545 | 2 | $C_2S$ + spinel + MgO + liquid |
| 50 | 50 | 1555 | 2 | spinel + $C_2S$ + MgO + liquid |
| 35 | 65 | 1485 | 15 | spinel + $C_3MS_2$ |
| | | 1545 | 2 | spinel + $C_2S$ + MgO + liquid |
| | | 1580 | 2 | spinel + $C_2S$ + MgO + liquid |
| | | 1603 | 2 | spinel + liquid |
| 20 | 80 | 1530 | 15 | spinel + $C_3MS_2$ |
| | | 1543 | 4 | spinel + $C_2S$ + MgO + liquid |
| | | 1575 | 3 | spinel + $C_2S$ + MgO + liquid |
| | | 1595 | 3 | spinel + $C_2S$ + liquid |

TABLE 15

Experimental compositions and phases identified in mixtures of the system $MgAl_{1.5}Cr_{0.5}O_4$-$C_3MS_2$.

Note: The temperatures given are those at which the samples were soaked prior to quenching in water.

| Spinel s.s. wt.% | $C_3MS_2$ wt.% | Firing Temp. °C | Soaking Time (hours) | Phases present at the firing temperature |
|---|---|---|---|---|
| 30.0 | 70.0 | 1550 | 1½ | MgO + spinel + liquid |
| | | 1565 | 2 | spinel + liquid |
| 12.5 | 87.5 | 1555 | 2 | MgO + $C_2S$ ? + liquid |
| | | 1565 | 2 | liquid |
| 70.0 | 30.0 | 1470 | 3 | spinel + MgO + $C_2S$?+ liquid ? |
| | | 1545 | 2 | spinel + MgO + liquid |
| | | 1555 | 2 | spinel + MgO + liquid |
| 55.0 | 45.0 | 1545 | 2 | spinel + MgO + liquid |
| | | 1560 | 2 | spinel + MgO + liquid |
| 5.0 | 95.0 | 1465 | 15 | MgO + $C_3MS_2$+ $C_2S$ + spinel + liquid |
| | | 1480 | 15 | MgO + $C_3MS_2$ + $C_2S$ + spinel + liquid |
| | | 1505 | 2 | MgO + $C_3MS_2$ + $C_2S$ + spinel + liquid |
| | | 1515 | 2 | MgO + $C_3MS_2$ + $C_2S$ + liquid |
| | | 1560 | 2 | MgO + $C_2S$ + $C_3MS_2$ + liquid |
| | | 1570 | 2 | MgO + $C_2S$ + liquid |
| | | 1580 | 2 | $C_2S$ + MgO + liquid |
| | | 1620 | 1 | $C_2S$ + liquid |
| | | 1630 | 1 | $C_2S$ + liquid |
| | | 1645 | 1 | $C_2S$ + liquid |
| | | 1695 | 1 | $C_2S$ + liquid |
| | | 1705 | 1 | liquid |

TABLE 16

Experimental compositions and phases identified in mixtures of the system $MgAl_{0.8}Cr_{1.2}O_4$-$C_3MS_2$.

Note: The temperatures given are those at which the samples were soaked prior to quenching in water.

| Spinel s.s. wt.% | $C_3MS_2$ wt.% | Firing Temp. °C | Soaking Time (hours) | Phases present at the firing temperature |
|---|---|---|---|---|
| 40.0 | 60.0 | 1520 | 17 | Spinel + MgO + $C_2S$ + liquid |
| | | 1575 | 2 | Spinel + liquid |
| | | 1590 | 2 | Spinel + liquid |
| | | 1610 | 2 | Spinel + liquid |
| 20.0 | 80.0 | 1520 | 17 | Spinel + MgO + $C_2S$ + liquid |
| | | 1570 | 2 | Spinel + liquid |
| | | 1585 | 2 | Spinel + liquid |
| | | 1625 | 2 | Spinel + liquid |
| | | 1670 | 1 | Spinel + liquid |
| | | 1690 | 1 | Liquid |
| 7.5 | 92.5 | 1515 | 10 | Spinel + MgO + $C_2S$ + $C_3MS_2$ + liquid |
| | | 1520 | 17 | Spinel + MgO + $C_2S$ + liquid |
| | | 1530 | 3 | Spinel + MgO + $C_2S$ + liquid |
| | | 1535 | 4½ | Spinel + MgO + $C_2S$ + liquid |
| | | 1537 | 2½ | Spinel + MgO + $C_2S$ + liquid |
| | | 1543 | 3 | $C_2S$ + MgO + liquid |
| | | 1548 | 5½ | $C_2S$ + MgO + liquid |
| | | 1550 | 3 | $C_2S$ + MgO + liquid |
| | | 1556 | 2½ | $C_2S$ + MgO + liquid |
| | | 1560 | 3 | $C_2S$ + MgO + liquid |
| | | 1571 | 2 | $C_2S$ + liquid |
| | | 1585 | 2 | $C_2S$ + liquid |
| 2.5 | 97.5 | 1520 | 17 | $C_3MS_2$ + $C_2S$ + MgO + liquid |
| | | 1520 | 5 | $C_3MS_2$ + $C_2S$ + MgO + liquid |
| | | 1525 | 4 | $C_3MS_2$ + $C_2S$ + MgO + liquid |
| | | 1530 | 3 | $C_3MS_2$ + $C_2S$ + MgO + liquid |
| | | 1537 | 2½ | $C_3MS_2$ + $C_2S$ + MgO + liquid |
| | | 1545 | 2 | $C_3MS_2$ + $C_2S$ + MgO + liquid |
| | | 1560 | 2 | $C_2S$ + MgO + liquid |
| | | 1565 | 2 | $C_2S$ + MgO + liquid |
| | | 1575 | 2 | $C_2S$ + MgO + liquid |
| | | 1615 | 2 | $C_2S$ + MgO + liquid |
| | | 1660 | 1½ | $C_2S$ + liquid |
| | | 1685 | 1 | $C_2S$ + liquid |

Contd.../

Table 16 - contd.

| Spinel s.s. wt.% | $C_3MS_2$ wt.% | Firing Temp. °C | Soaking Time (hours) | Phases present at the firing temperature |
|---|---|---|---|---|
| 5.0 | 95.0 | 1515 | 10 | $C_3MS_2$ + $C_2S$ + spinel + MgO + liquid |
| | | 1520 | 17 | $C_3MS_2$ + $C_2S$ + spinel + MgO + liquid |
| | | 1530 | 3 | $C_3MS_2$ + $C_2S$ + MgO + liquid |
| | | 1535 | 4½ | $C_2S$ + MgO + liquid |
| | | 1545 | 3½ | $C_2S$ + MgO + liquid |
| | | 1585 | 2 | $C_2S$ + MgO + liquid |
| | | 1605 | 2 | $C_2S$ + MgO + liquid |
| | | 1615 | 2 | $C_2S$ + liquid |
| | | 1660 | 1½ | $C_2S$ + liquid |
| | | 1685 | 1 | $C_2S$ + liquid |
| 10.0 | 90.0 | 1535 | 4½ | Spinel + $C_2S$ + MgO + liquid |
| | | 1562 | 2 | Spinel + $C_2S$ + liquid |
| | | 1597 | 2 | Liquid |
| | | 1600 | 1 | Liquid |
| | | 1617 | 1½ | Liquid |
| | | 1622 | 1½ | Liquid |
| 15.0 | 85.0 | 1520 | 5 | Spinel + $C_2S$ + MgO + liquid |
| | | 1530 | 3 | Spinel + $C_2S$ + MgO + liquid |
| | | 1537 | 2½ | Spinel + $C_2S$ + MgO + liquid |
| | | 1543 | 3 | Spinel + $C_2S$ + MgO + liquid |
| | | 1597 | 2 | Liquid + spinel ? ? ? |
| | | 1617 | 1½ | Liquid |
| 27.5 | 72.5 | 1570 | 2 | Spinel + liquid |
| | | 1585 | 2 | Spinel + liquid |
| | | 1680 | 1 | Spinel + liquid |
| | | 1690 | 1 | Spinel + liquid |
| 1.5 | 98.5 | 1525 | 4 | $C_3MS_2$ + $C_2S$ + MgO + liquid |
| | | 1530 | 3½ | $C_3MS_2$ + $C_2S$ + MgO + liquid |
| | | 1545 | 2 | $C_3MS_2$ + $C_2S$ + MgO + liquid |
| 4.0 | 96.0 | 1525 | 4 | $C_3MS_2$ + $C_2S$ + MgO + liquid |
| | | 1530 | 3½ | $C_3MS_2$ + $C_2S$ + MgO + liquid |
| | | 1548 | 5½ | $C_2S$ + MgO + liquid |
| 12.5 | 87.5 | 1575 | 2 | Spinel + liquid |
| | | 1585 | 2 | Liquid |
| 11.0 | 89.0 | 1545 | 2 | Spinel + $C_2S$ + MgO + liquid |
| | | 1550 | 2 | Spinel + $C_2S$ + MgO + liquid |
| | | 1571 | 2 | Liquid |
| | | 1605 | 2 | Liquid |
| 8.5 | 91.5 | 1571 | 2 | $C_2S$ + liquid |
| | | 1600 | 1½ | $C_2S$ + liquid |

FIGURE 1

Phase relationships in the solid state in the system $CaO-MgO-Fe_2O_3-SiO_2$. Phase volumes shown are those in which free MgO (periclase) occurs.

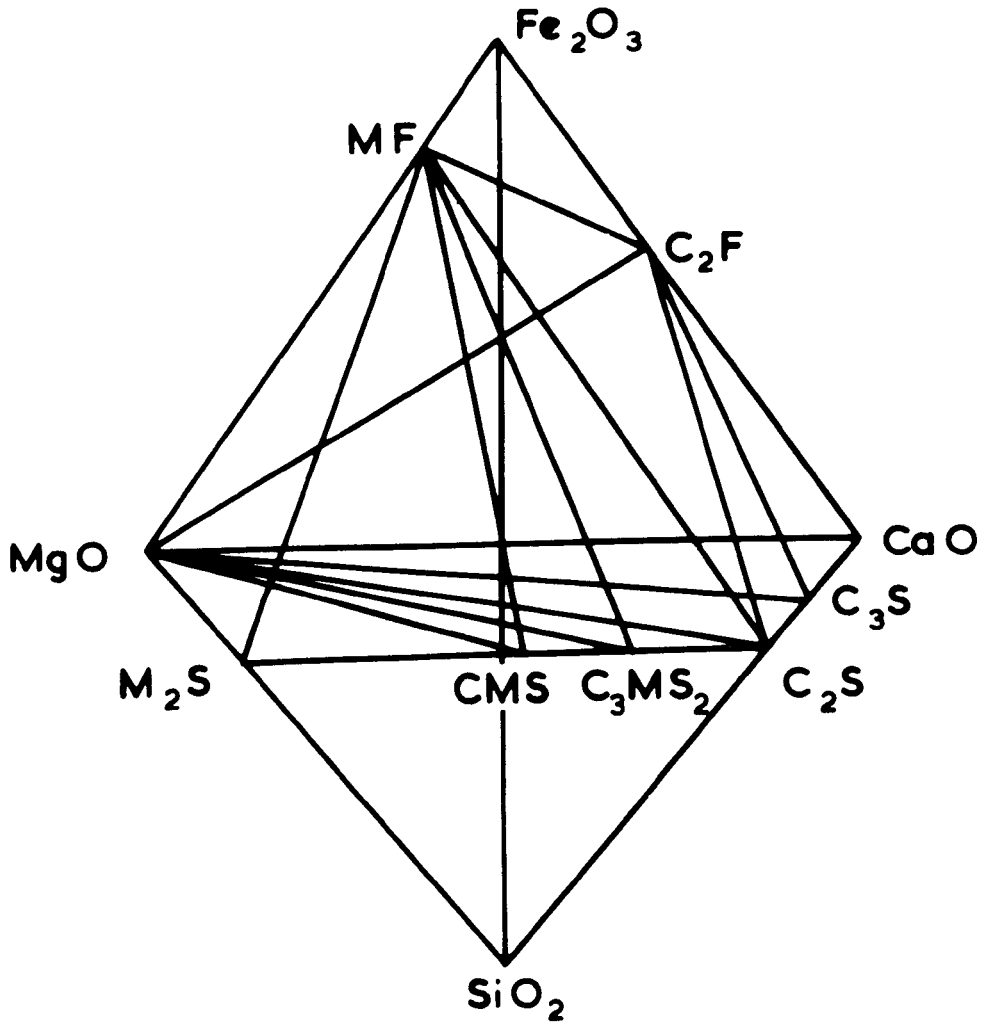
$Fe_2O_3$
MF
$C_2F$
MgO
CaO
$C_3S$
$M_2S$
CMS
$C_3MS_2$
$C_2S$
$SiO_2$

FIGURE 2

Isoplethal sections in the ternary system $CaO-MgO-SiO_2$ at

(A) 5% $SiO_2$

(B) 2% $SiO_2$

(C) 1% $SiO_2$

Showing the effect of CaO solubility in periclase, with compositions expressed in terms of the $CaO/SiO_2$ ratio in the mixtures. (From Hatfield et al.[17].)

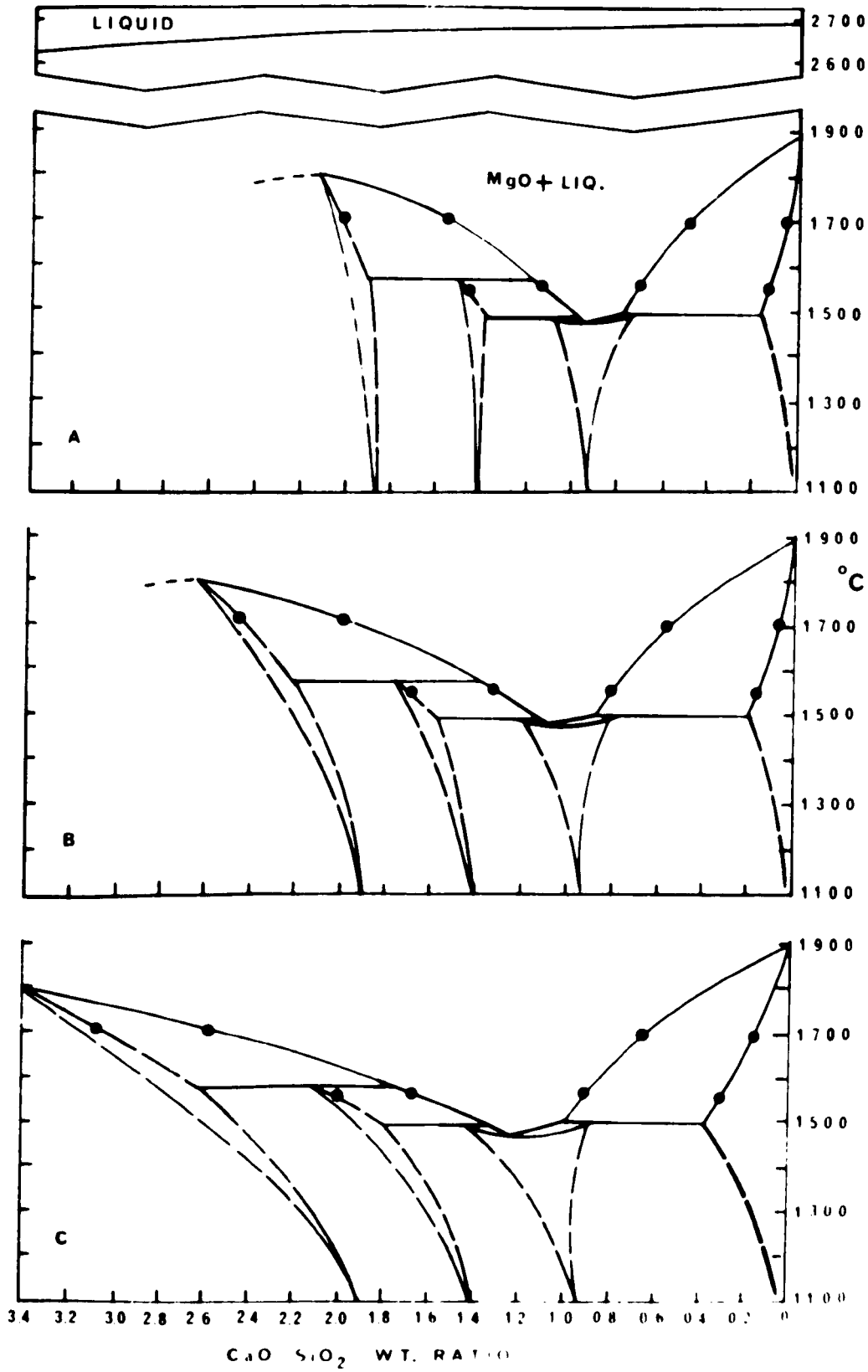
LIQUID
2700
2600
1900
MgO + LIQ.
1700
1500
1300
A
1100
1900
°C
1700
1500
1300
B
1100
1900
1700
1500
1300
C
1100
3.4 3.2 3.0 2.8 2.6 2.4 2.2 2.0 1.8 1.6 1.4 1.2 1.0 0.8 0.6 0.4 0.2 0
CaO SiO2 WT. RATIO

FIGURE 3

Solid solubilities of sesquioxides in periclase between 1000-2400°C.

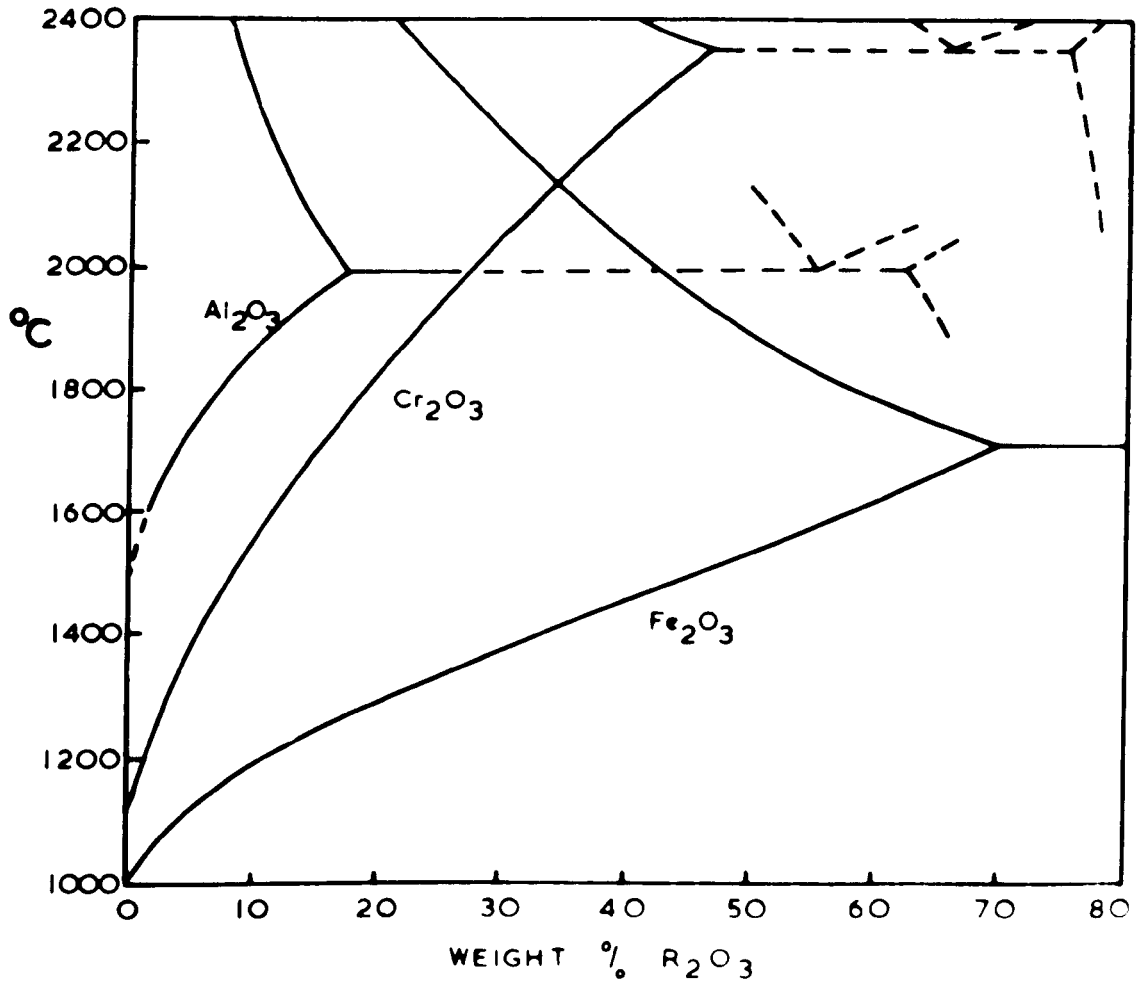
2400
2200
2000
1800
1600
1400
1200
1000
°C
$Al_2O_3$
$Cr_2O_3$
$Fe_2O_3$
0
10
20
30
40
50
60
70
80
WEIGHT % $R_2O_3$

FIGURE 4

Isobaric ternary diagram of the system MgO-FeO-$Fe_2O_3$ in air. Dashed lines are reaction paths. (SP = spinel. MW = magnesiowustite.)

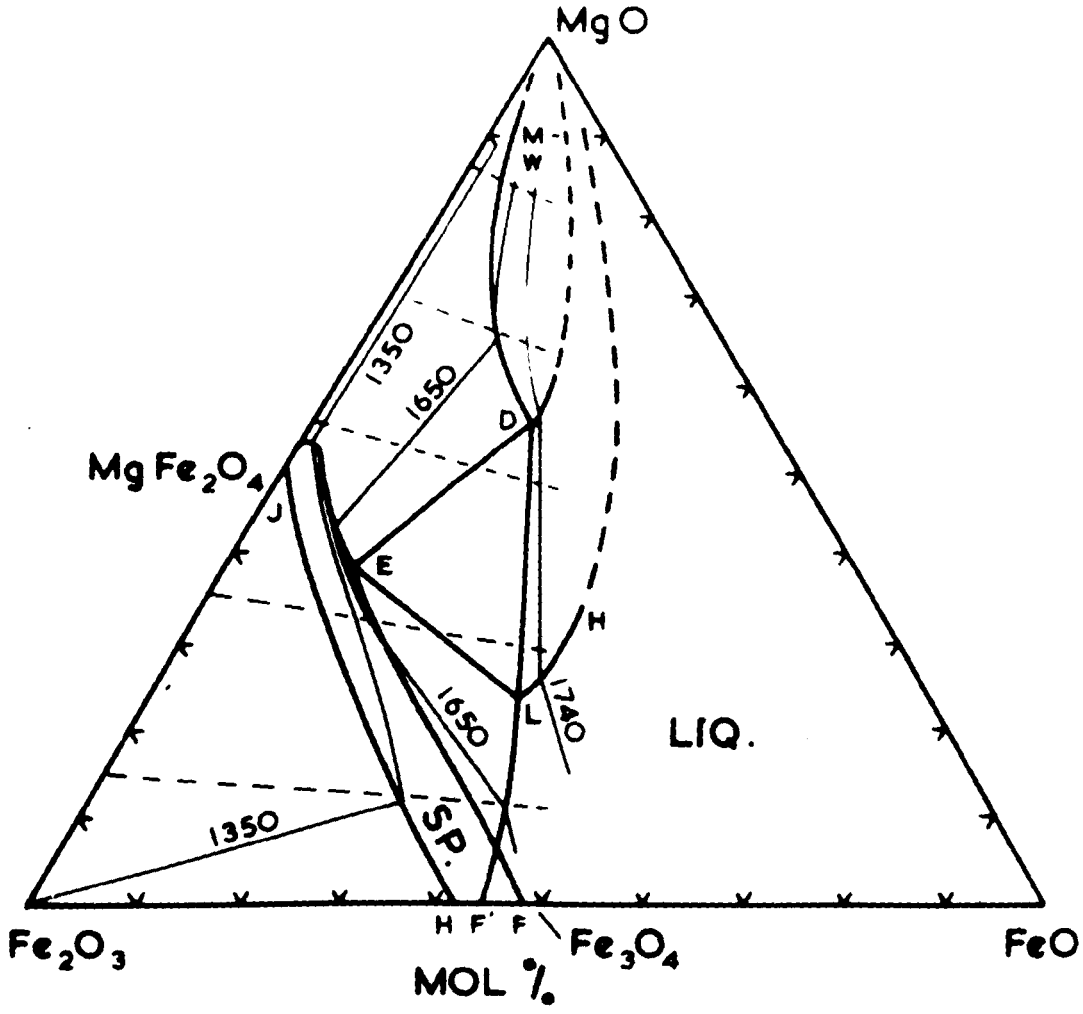
MgO
M
W
1350
1650
D
MgFe2O4
J
E
H
1650
L
1740
LIQ.
SP.
1350
H F' F
Fe2O3
Fe3O4
FeO
MOL %

FIGURE 5

Temperature-composition diagram of the system $MgO-FeO-Fe_2O_3$ in air derived from Figure 4. (Lettering corresponds to that in Figure 4.)

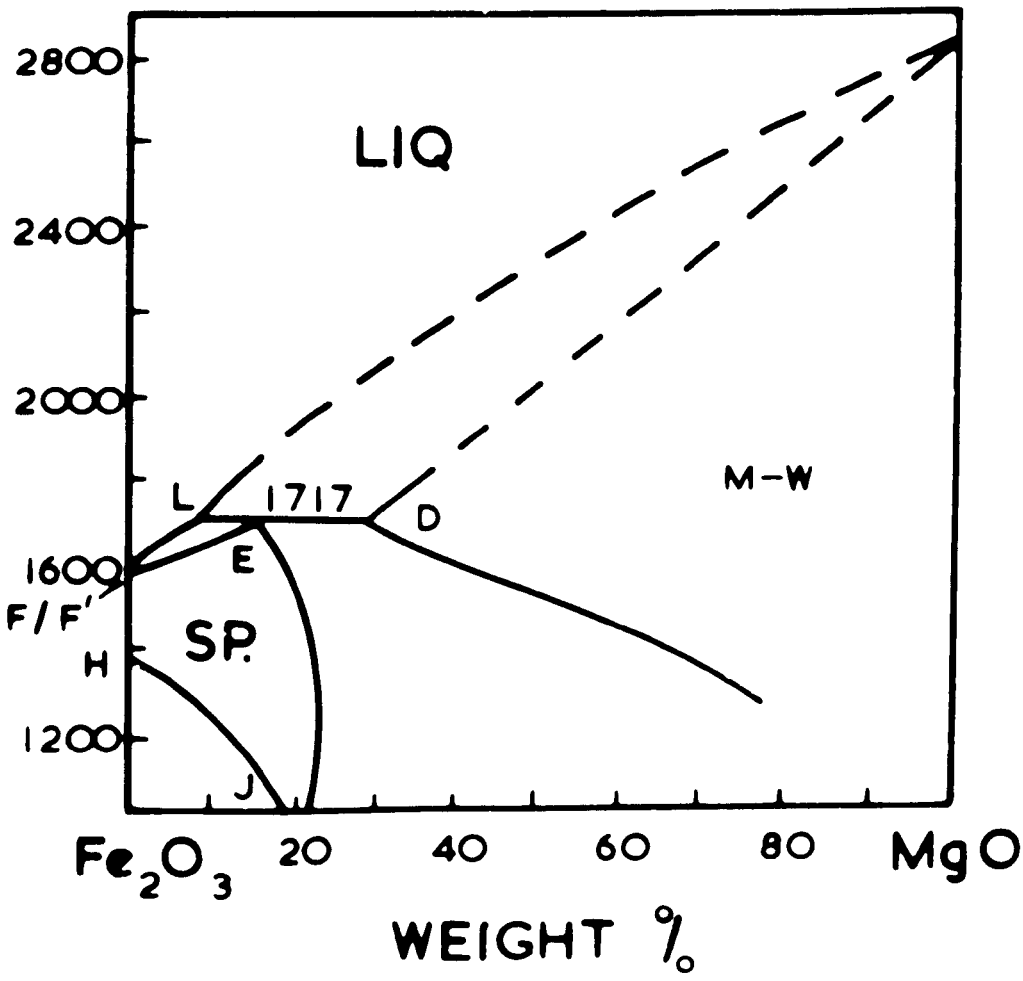
2800
2400
2000
1600
1200
LIQ
L
1717
D
E
F/F'
SP.
H
J
M-W
Fe2O3
20
40
60
80
MgO
WEIGHT %

FIGURE 6

Melting relationships in the quaternary system $MgO-Mg_2SiO_4-Ca_2SiO_4-MgAl_2O_4$ (from White[32]).

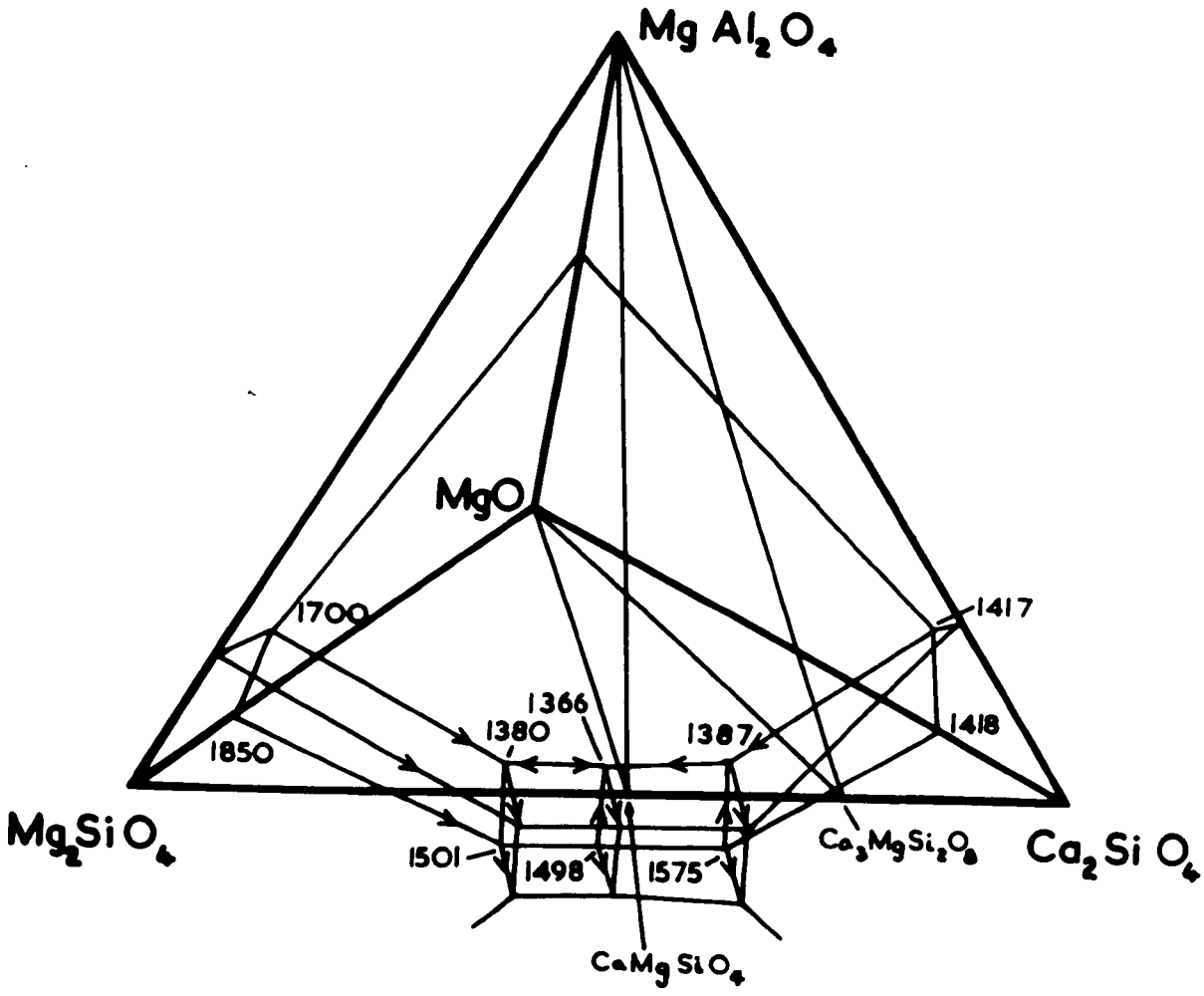
Mg Al2 O4
MgO
1700
1417
1366
1380
1387
1418
1850
Mg2 Si O4
1501
1498
1575
Ca3 Mg Si2 O8
Ca2 Si O4
Ca Mg Si O4

FIGURE 7

Liquidus surface and isotherms in the system $MgAl_2O_4$-$MgCr_2O_4$-$C_2S$ (from El-Shahat and White[1]).

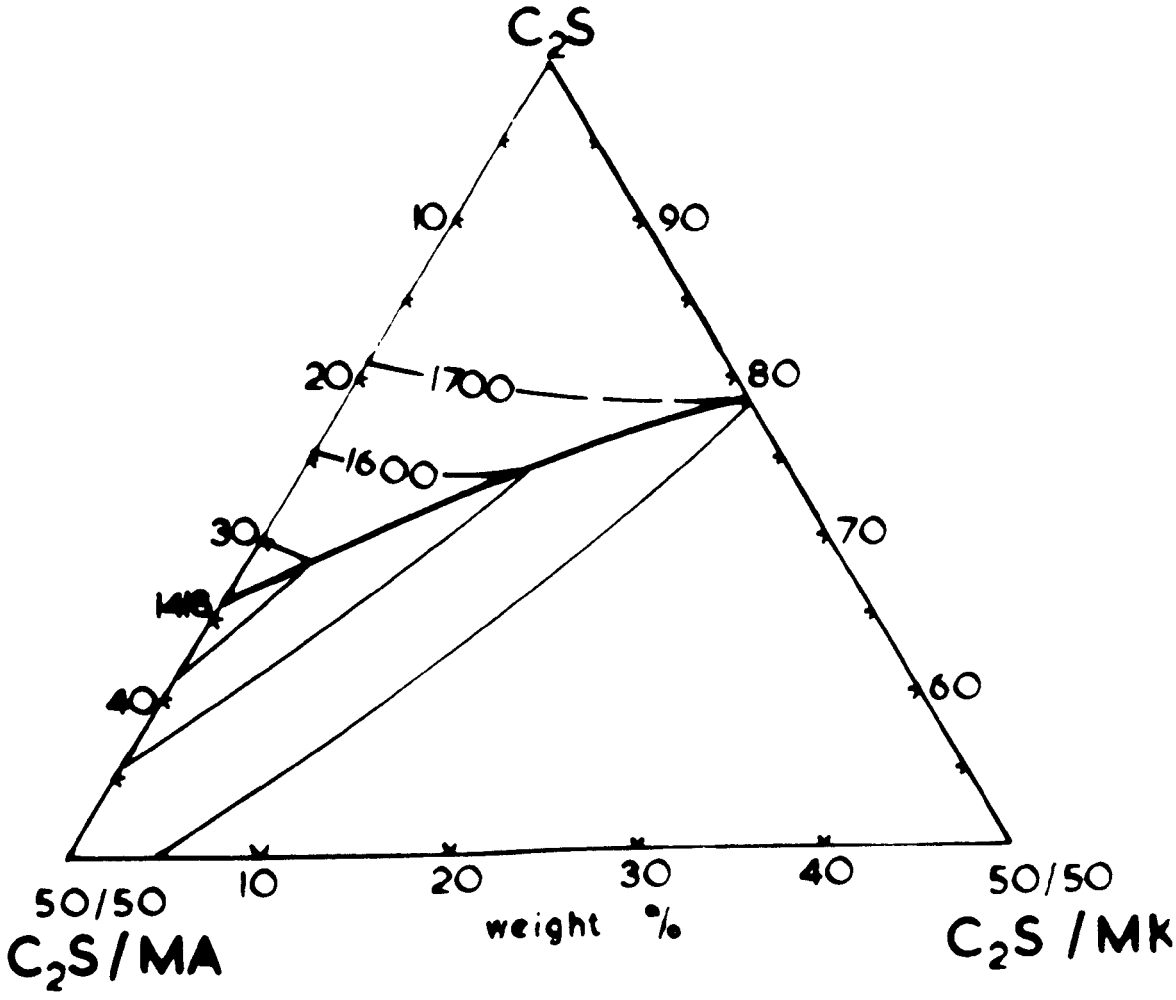
C2S
10
90
20
1700
80
1600
30
70
1418
40
60
50/50
C2S/MA
10
20
30
40
weight %
50/50
C2S/MK

FIGURE 8

Liquidus surface and isotherms in the system $MgFe_2O_4$-$MgAl_2O_4$-$C_2S$ (from El-Shahat and White[1]).

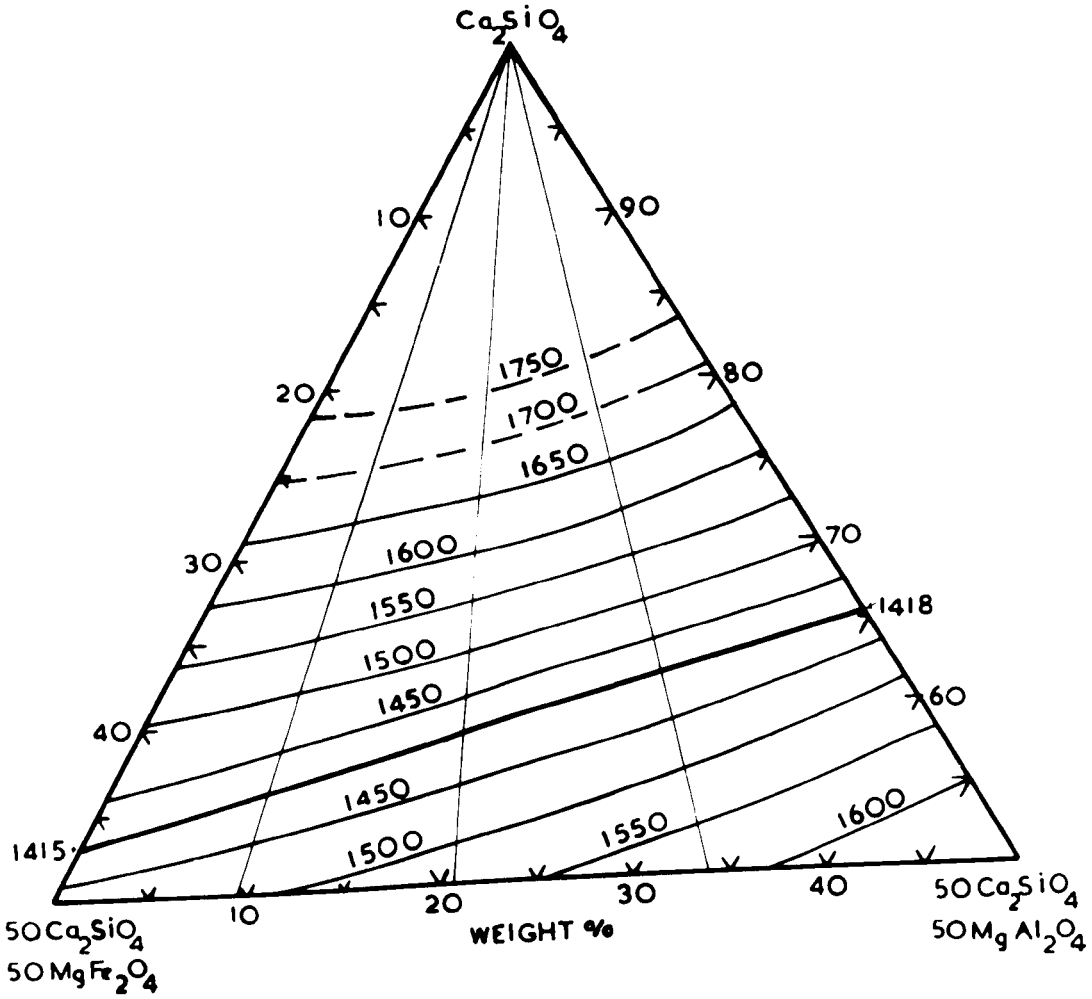
$Ca_2SiO_4$
10
90
20
80
30
70
40
60
1750
1700
1650
1600
1550
1500
1450
1450
1500
1550
1600
1415
1418
10
20
30
40
WEIGHT %
50 $Ca_2SiO_4$
50 $MgFe_2O_4$
50 $Ca_2SiO_4$
50 $MgAl_2O_4$

FIGURE 9

Variation in temperature of melting of eutectic in the system $MgAl_2O_4$-$MgFe_2O_4$-$MgCr_2O_4$-$Ca_2SiO_4$ with variation in composition of spinel solid solution. Compositions giving the same melting temperature are joined by isotherms (from El-Shahat and White[3]).

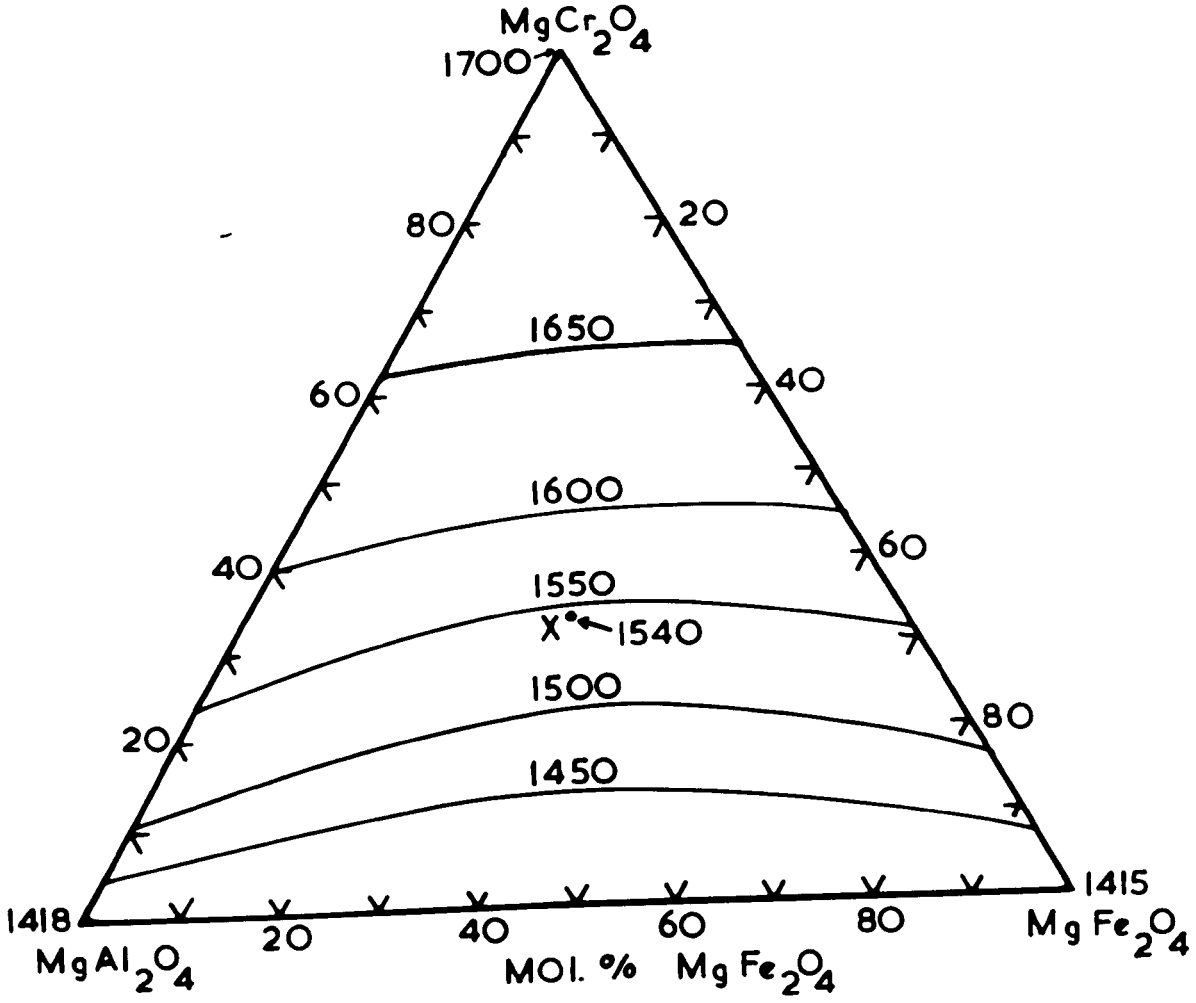
MgCr2O4
1700
80
20
1650
60
40
1600
40
60
1550
X
1540
20
1500
80
1450
1418
1415
20
40
60
80
MgAl2O4
MOL. % MgFe2O4
MgFe2O4

FIGURE 10

Isoplethal sections of the ternary system CaO-MgO-$SiO_2$ at constant $SiO_2$ content of 5% by weight showing the effect of CaO/$SiO_2$ ratio on melting behaviour. The effect of CaO solubility in periclase is ignored (from White[32]).

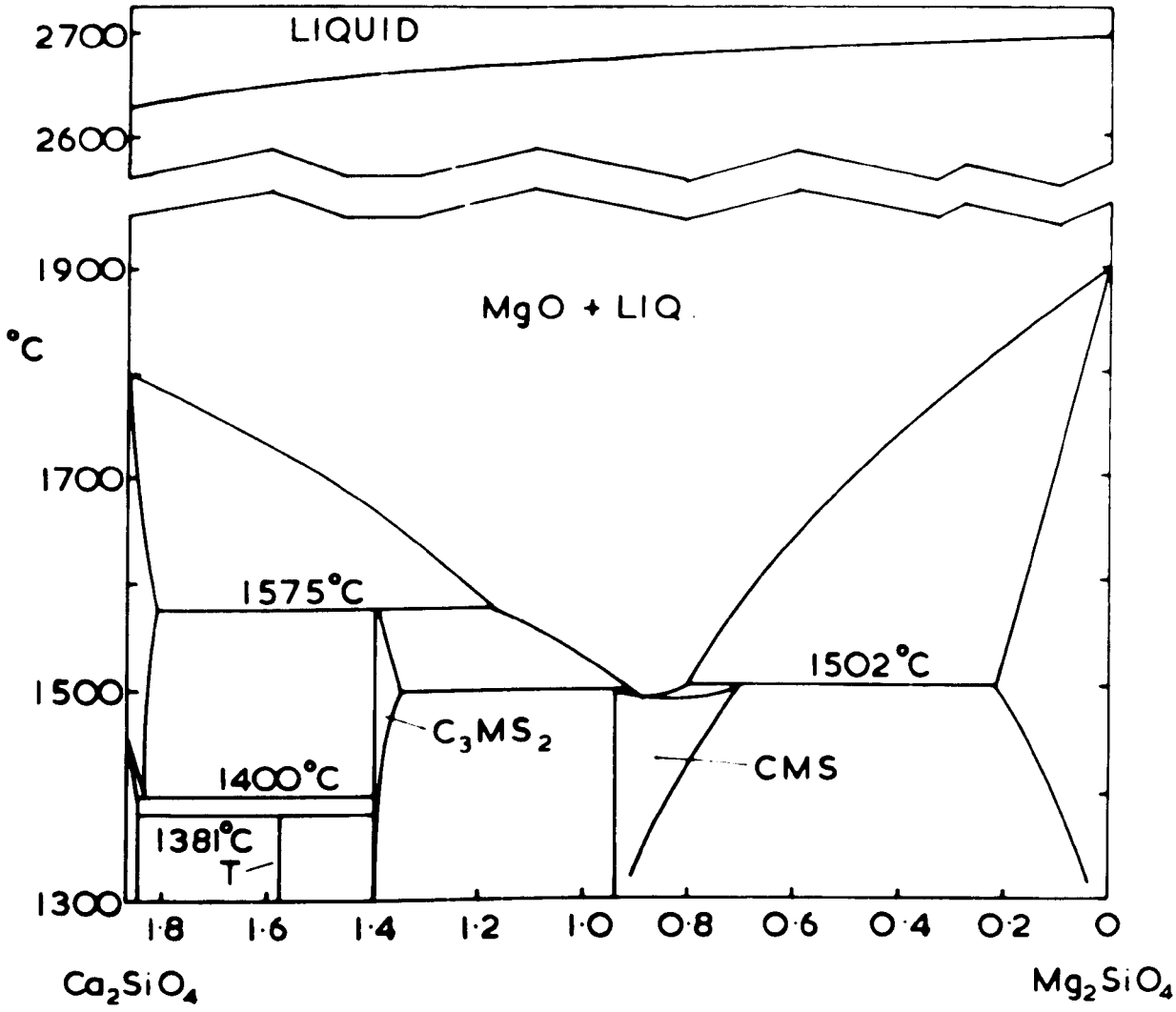
LIQUID
2700
2600
1900
MgO + LIQ
°C
1700
1575°C
1500
1502°C
C3MS2
CMS
1400°C
1381°C
T
1300
1·8
1·6
1·4
1·2
1·0
0·8
0·6
0·4
0·2
0
Ca2SiO4
Mg2SiO4

FIGURE 11

Projection of the boundary surface of primary phase volume of periclase in the system $CaO-MgO-Al_2O_3-SiO_2$ showing the second solid phases to separate on cooling, with the temperatures at which this occurs indicated by isotherms (from O'Hara and Biggar[50]). The various phase fields are numbered as follows:

1 - CaO : 2 - $C_3S$ : 3 - $C_2S$ : 4 - $C_5MS_3$ (Bredigite) :

5 - $C_3MS_2$ : 6 - CMS : 7 - $M_2S$ : 8 MA : 9 - $C_3A$ :

10 - $C_{12}A_7$ : 11 - $C_3A_2M$ : 12-$C_6A_4MS$ : 13 - CA.

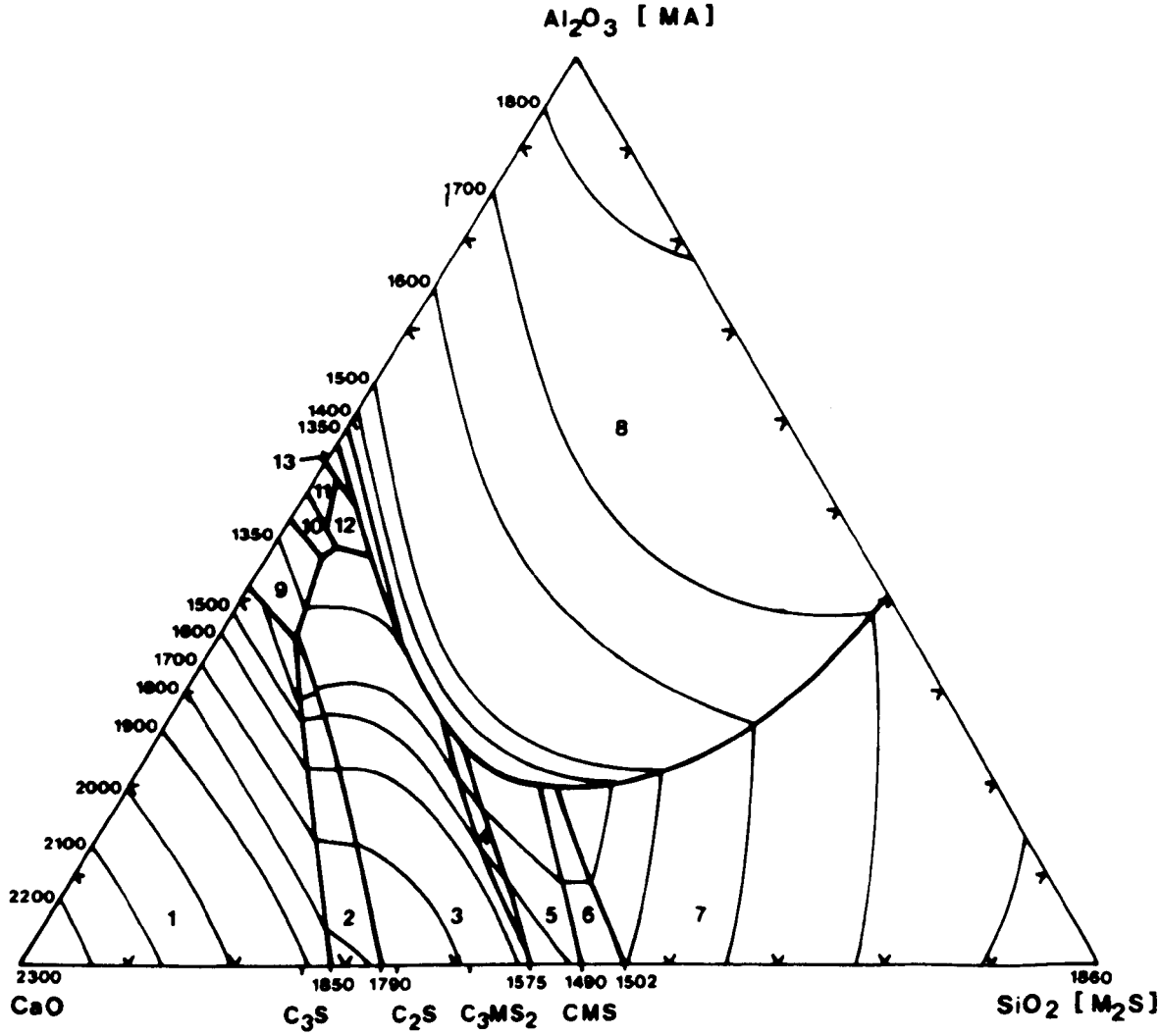
Al2O3 [ MA ]
1800
1700
1600
1500
1400
1350
13
11
10
12
1350
9
1500
1600
1700
1800
1900
2000
2100
2200
8
1
2
3
5
6
7
2300
1850
1790
1575
1490
1502
1860
CaO
C3S
C2S
C3MS2
CMS
SiO2 [ M2S ]

FIGURE 12

Projection showing secondary phases crystallising (in air) from $CaO$-$MgO$-$Fe_2O_3$-$SiO_2$ mixtures containing 70 wt.% MgO. Temperatures of secondary crystallization indicated by isotherms. Compositions of mixtures expressed in terms of CaO + iron oxide + $SiO_2$ recalculated to 100 wt.% (from Crookes[51]).

Point D lies on the join $C_3MS_2$-$Fe_2O_3$.

The various phase fields are numbered as follows:
1 - CaO : 2 - $C_3S$ : 3 - $C_2S$ : 4 - $C_3MS_2$: 5 - CMS : 6 - $M_2S$.

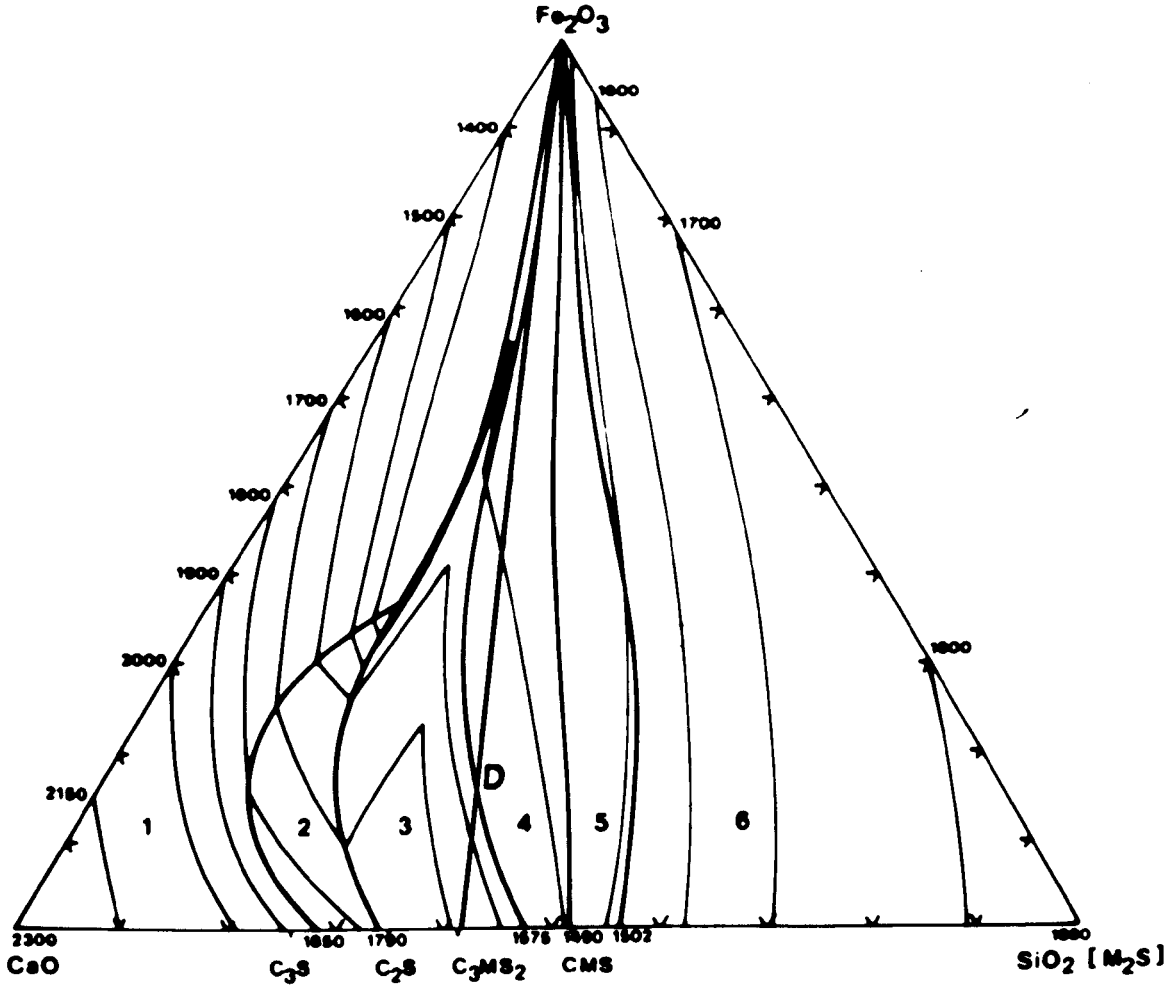
$Fe_2O_3$
1800
1400
1500
1700
1600
1700
1800
1900
2000
1800
2150
D
1
2
3
4
5
6
2300
1680
1790
1575
1680
1502
1680
CaO
$C_3S$
$C_2S$
$C_3MS_2$
CMS
$SiO_2$ [$M_2S$]

FIGURE 13

Projection showing secondary phases crystallizing (in air) from $CaO$-$MgO$-$Cr_2O_3$-$SiO_2$ mixtures containing 80 wt.% MgO. Temperatures of secondary crystallization indicated by isotherms. Compositions of mixtures expressed in terms of $CaO$ + $Cr_2O_3$ + $SiO_2$ recalculated to 100 wt.% (from Tarboton[52]). Points A, C, D are experimentally established invariant points, and E and F are possible invariant points. B lies on join $C_2S$-$Cr_2O_3$. The various phase fields are numbered as follows:

1 - $CaO$ : 2 - $C_3S$ : 3 - $C_2S$ : 4 - $C_3MS_2$ : 5 - CMS : 6 - $M_2S$ : 7 - MK : 8 - "941".

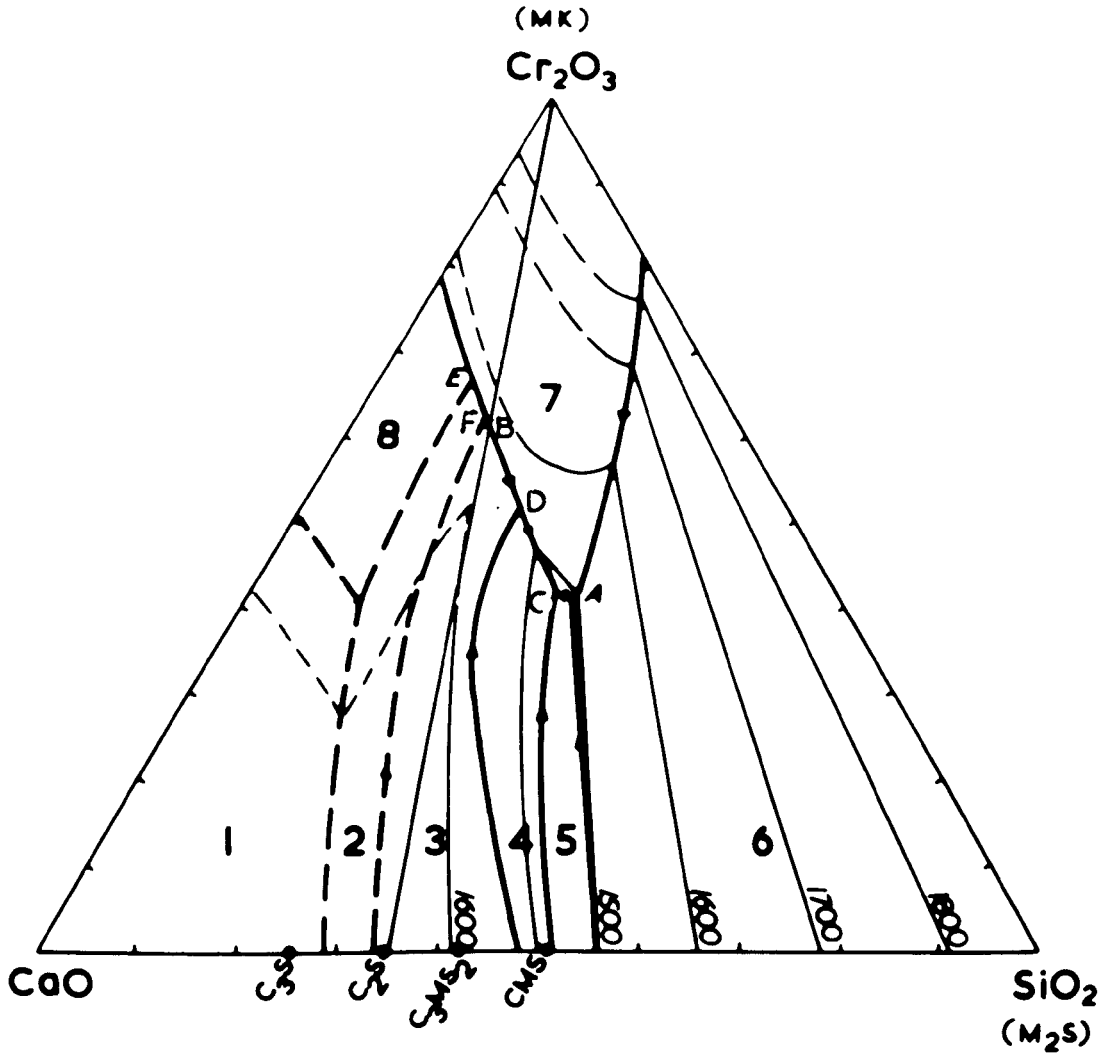
(MK)
$Cr_2O_3$
E'
F
B
8
7
D
C
A
1
2
3
4
5
6
1600
1500
1600
1700
1800
CaO
C3S
C2S
C3MS2
CMS
$SiO_2$
($M_2S$)

FIGURE 14

Free energy-temperature diagram showing the four forms of dicalcium silicate suggested by Bredig[53] and their inversion temperatures. Dashed lines represent metastable equilibrium. The diagram shows the free energies increasing with temperature, whereas it should decrease, but is valid if it is considered to represent vapour pressure instead of free energy.

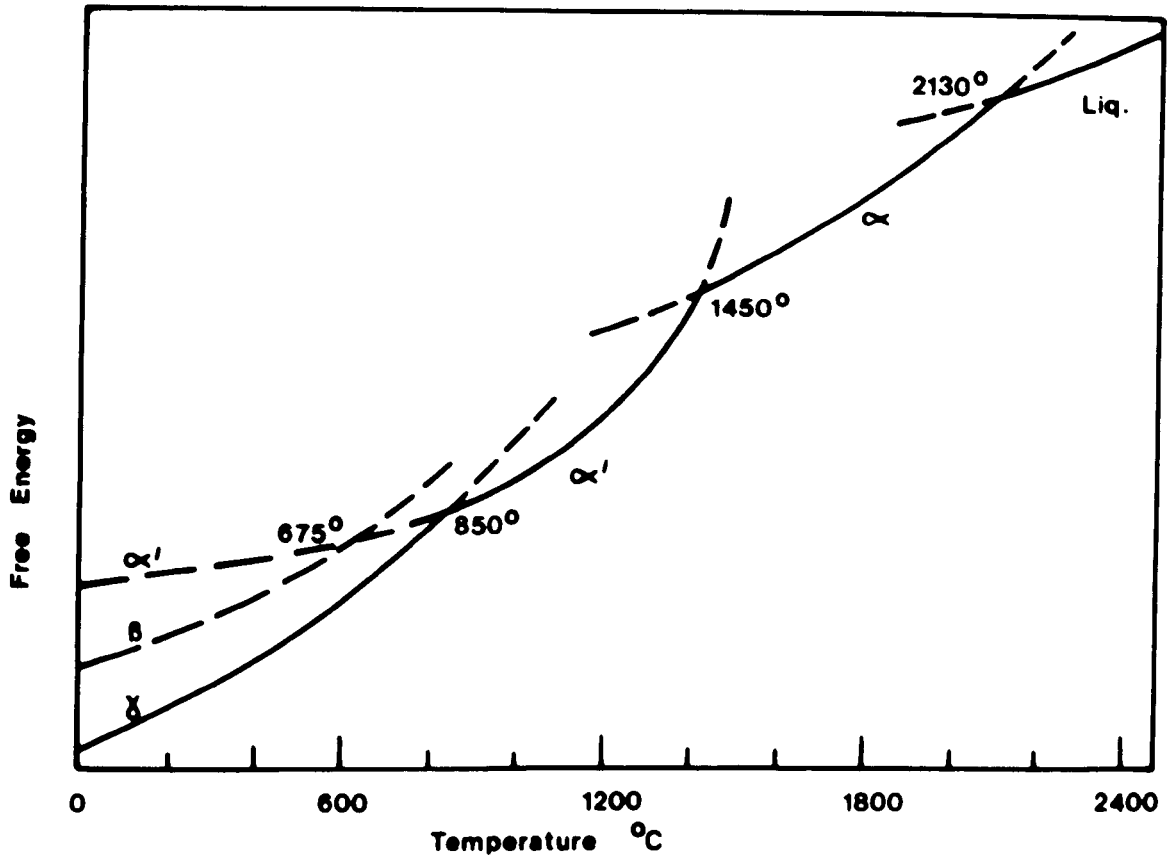
Free Energy
2130°
Liq.
α
1450°
α'
675°
850°
α'
β
γ
0
600
1200
1800
2400
Temperature °C

FIGURE 15

The molybdenum-wound resistance furnace :

A - molybdenum wire lead

B - Pyrex glass T-piece

C - high alumina cement/Autostick seals

D - outer alumina tube

E - $^{1}/4$" alumina tube

F - alumina powder

G - high alumina cement covering the molybdenum wiring

H - thermocouple

J - pellets in platinum boxes

K - high alumina column

L - recrystallized alumina tubes of 1", 1¼" internal diameter

M - high alumina cement

N - rigid syndanio support board

O - insulating brick plug

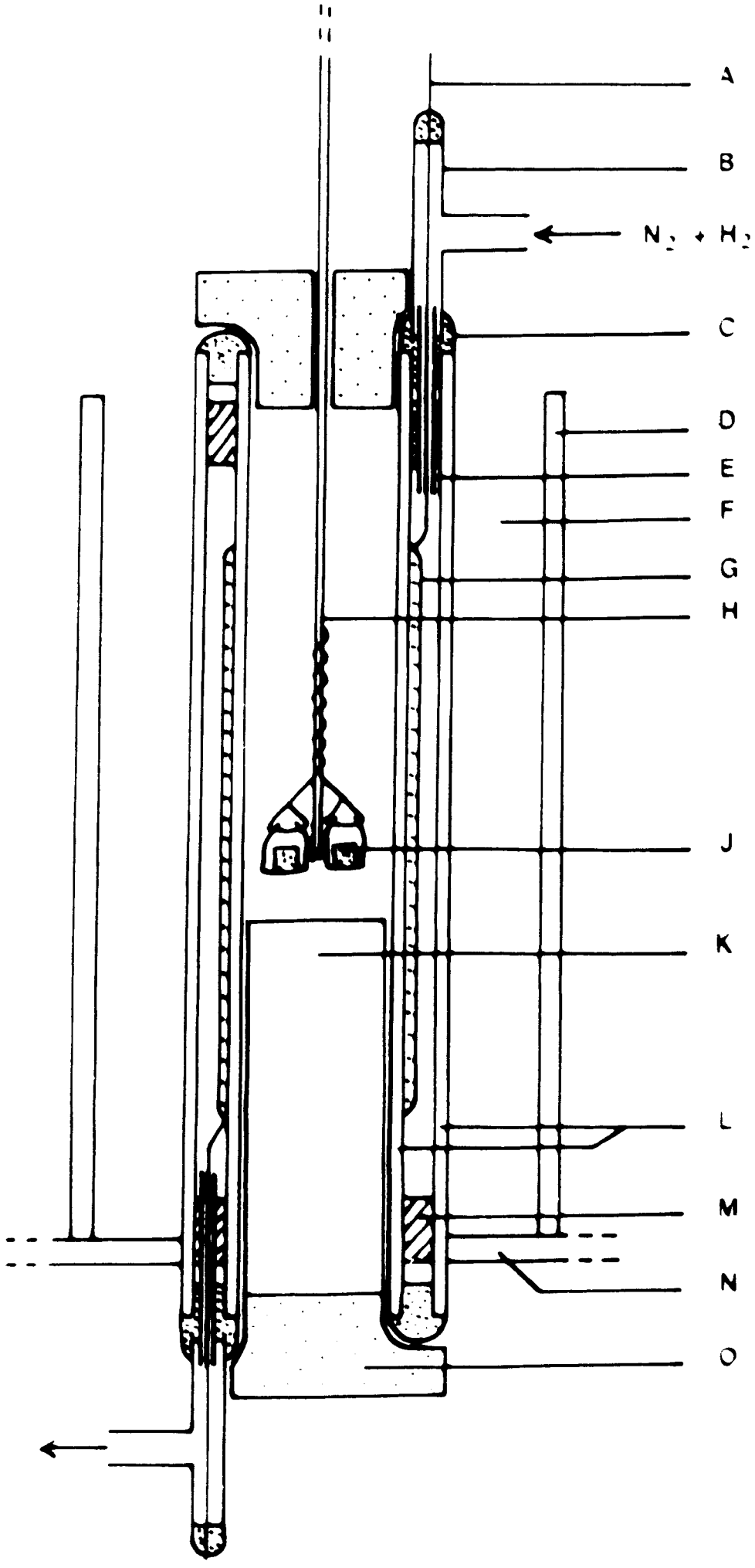
A
B
$N_2 + H_2$
C
D
E
F
G
H
J
K
L
M
N
O

FIGURE 16

Power supply and control circuit for the molybdenum-wound furnace incorporating a motorised variac unit and a West Gardsman controller.

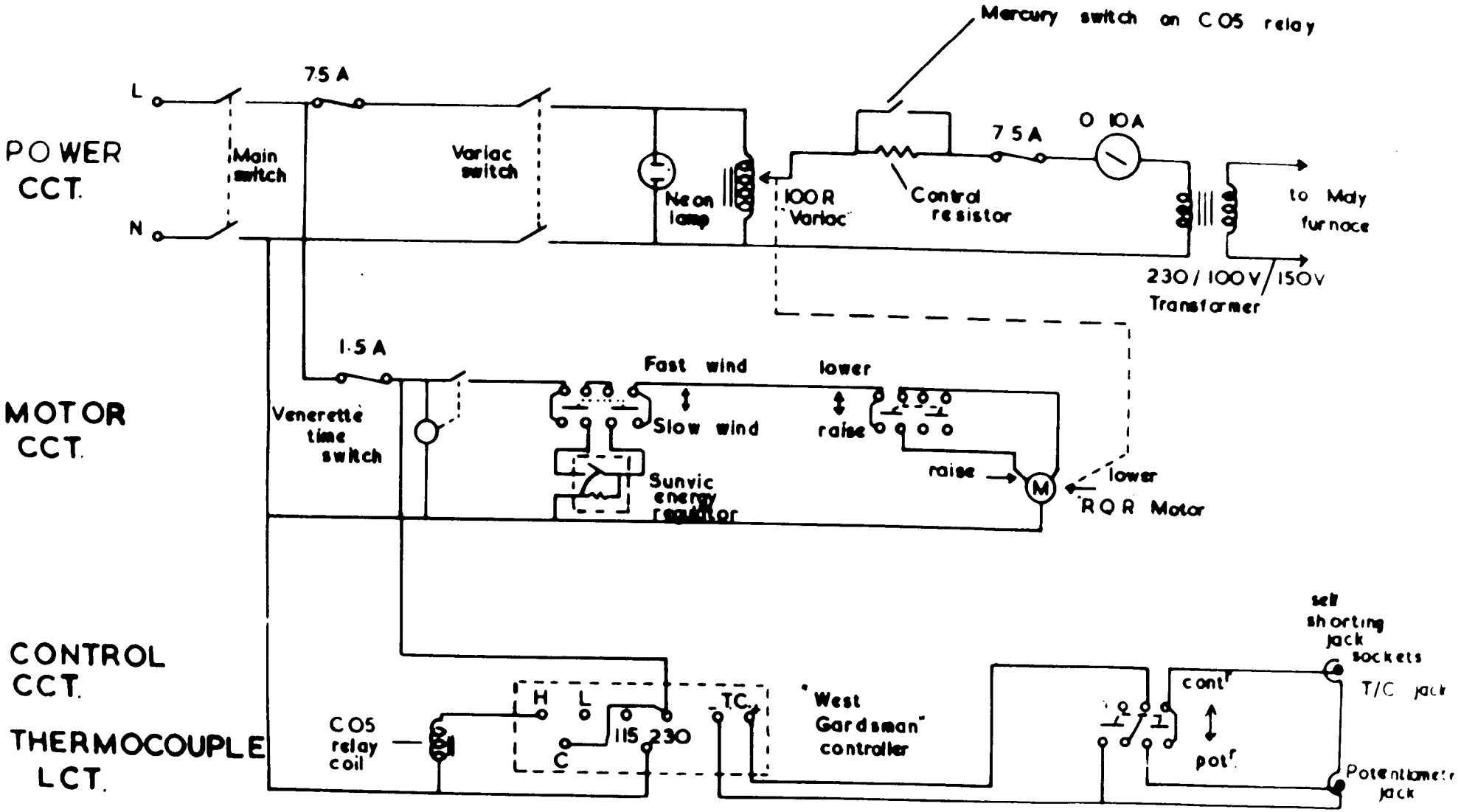
POWER CCT.
MOTOR CCT.
CONTROL CCT.
THERMOCOUPLE LCT.
L
N
7.5 A
Main switch
Variac switch
Neon lamp
Mercury switch on COS relay
100 R Variac
Control resistor
7.5 A
0 10A
to Moly furnace
230/100V/150V Transformer
1.5 A
Venerette time switch
Fast wind
Slow wind
lower
raise
Sunvic energy regulator
raise
lower
M
RQR Motor
COS relay coil
H
L
C
115
230
TC
"West Gardsman" controller
cont.
pot.
self shorting jack sockets
T/C jack
Potentiometer jack

FIGURE 17

Projection of the boundary surface of the primary phase volume of periclase in the system $CaO-MgO-Al_2O_3-SiO_2$ (in air) showing the second solid phases to separate on cooling from mixtures containing 80 wt.% MgO.
The various phase fields are numbered as follows:
1 - MA : 2 - $M_2S$: 3 - CMS : 4 $C_3MS_2$ : 5 - $C_2S$.

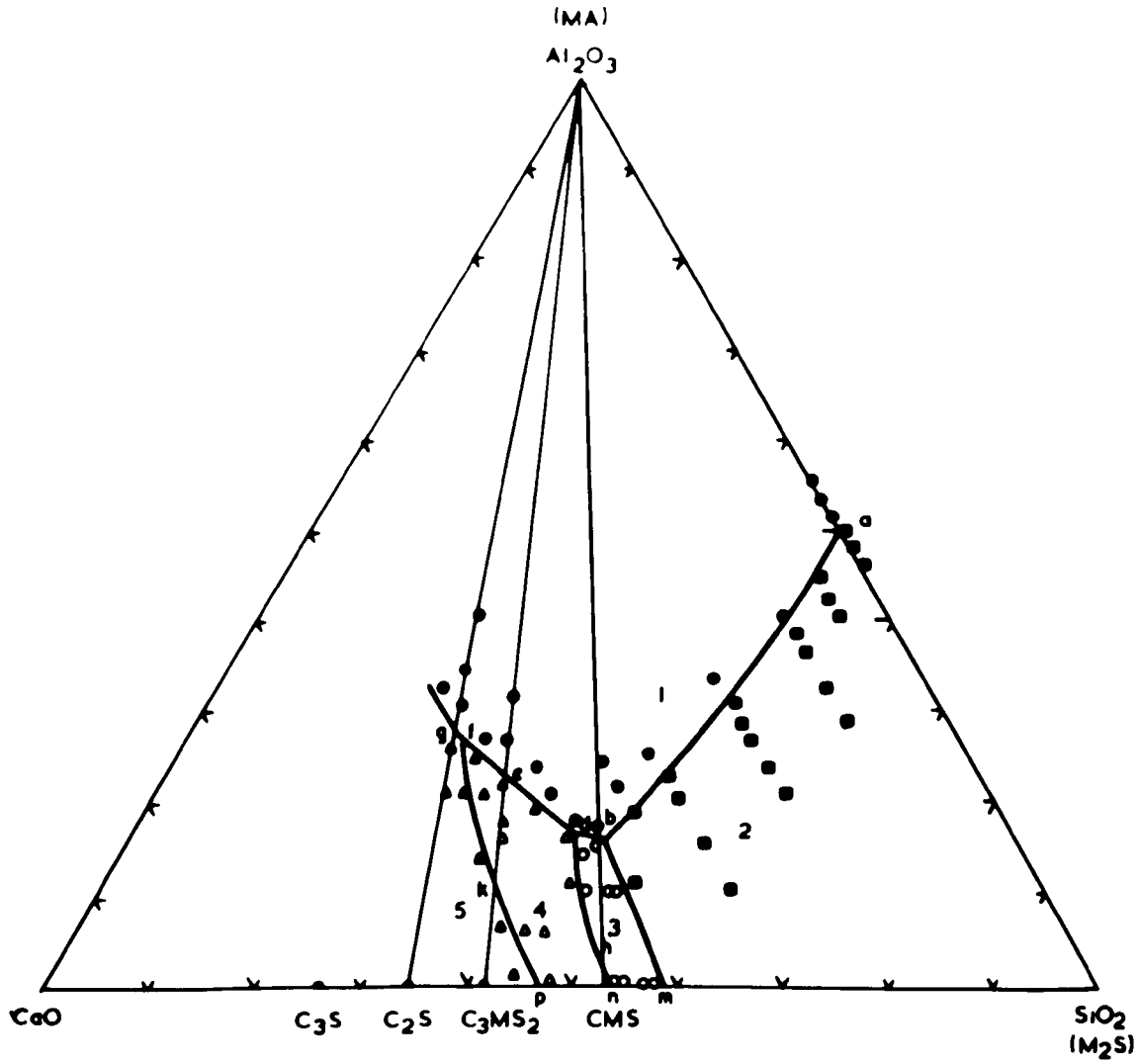
(MA)
Al2O3
CaO
C3S
C2S
C3MS2
CMS
SiO2
(M2S)
a
b
c
d
e
f
g
h
i
k
l
m
n
p
1
2
3
4
5

FIGURE 18

Projection of the boundary surface of the primary phase volume of periclase in the system CaO-MgO-$Al_2O_3$-$SiO_2$ (in air) showing the second solid phases to separate on cooling from mixtures containing 80 wt.% MgO and with the temperatures at which this occurs indicated by isotherms. The various phase fields are numbered as follows:

1 - MA : 2 - $M_2S$ : 3 - CMS : 4 - $C_3MS_2$ : 5 $C_2S$.

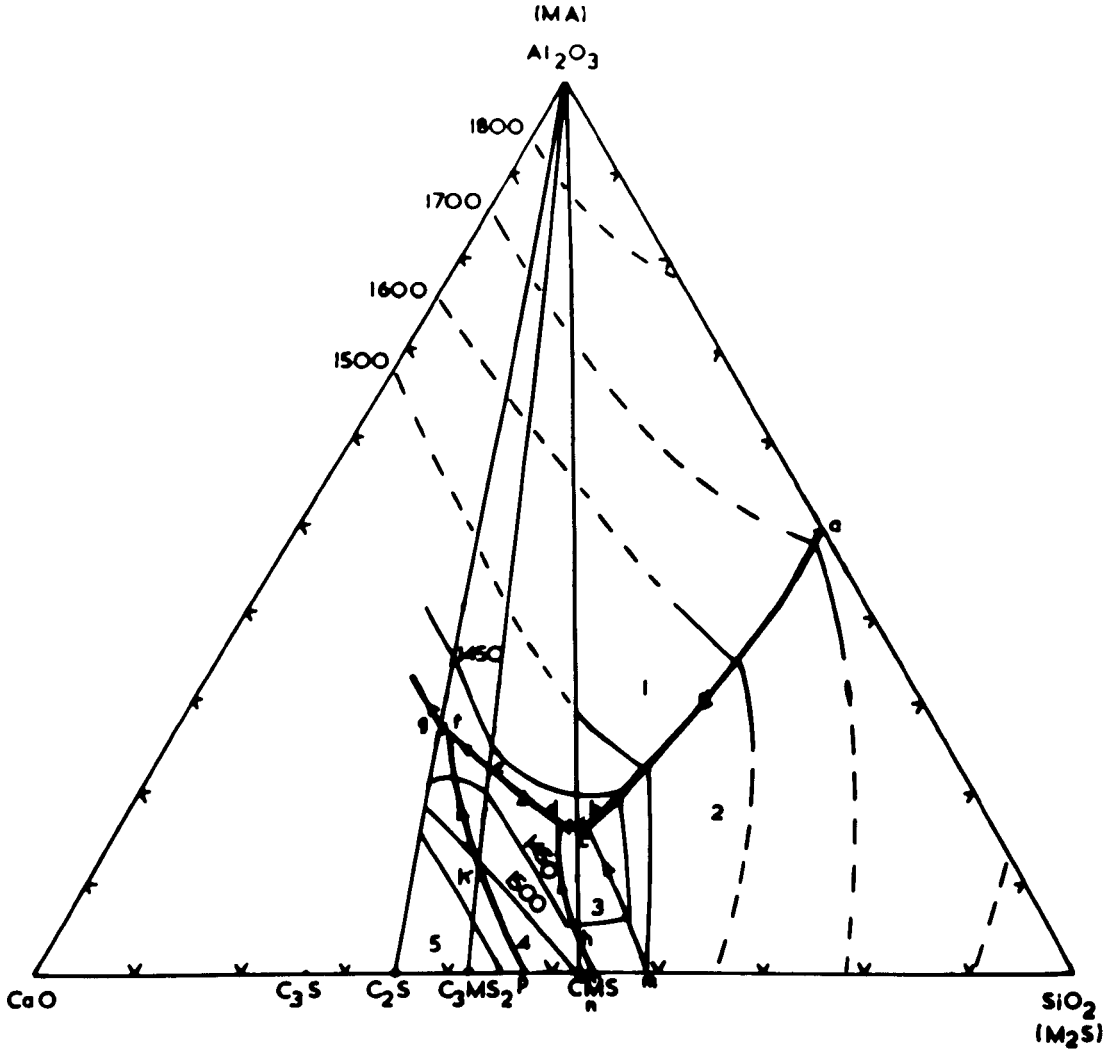
(MA)
$Al_2O_3$
1800
1700
1600
1500
1450
a
g
f
K
E
E'
E''
1
2
3
4
5
CaO
$C_3S$
$C_2S$
$C_3MS_2$
p
CMS
n
m
$SiO_2$
($M_2S$)

FIGURE 19

Projection of the boundary surface of the primary phase volume of periclase in the system CaO-MgO-$Al_2O_3$-$SiO_2$ (in air) showing the second solid phases found to separate on cooling from mixtures containing 80 wt.% MgO (thick lines). Boundaries according to O'Hara and Biggar[50] indicated by thin lines.

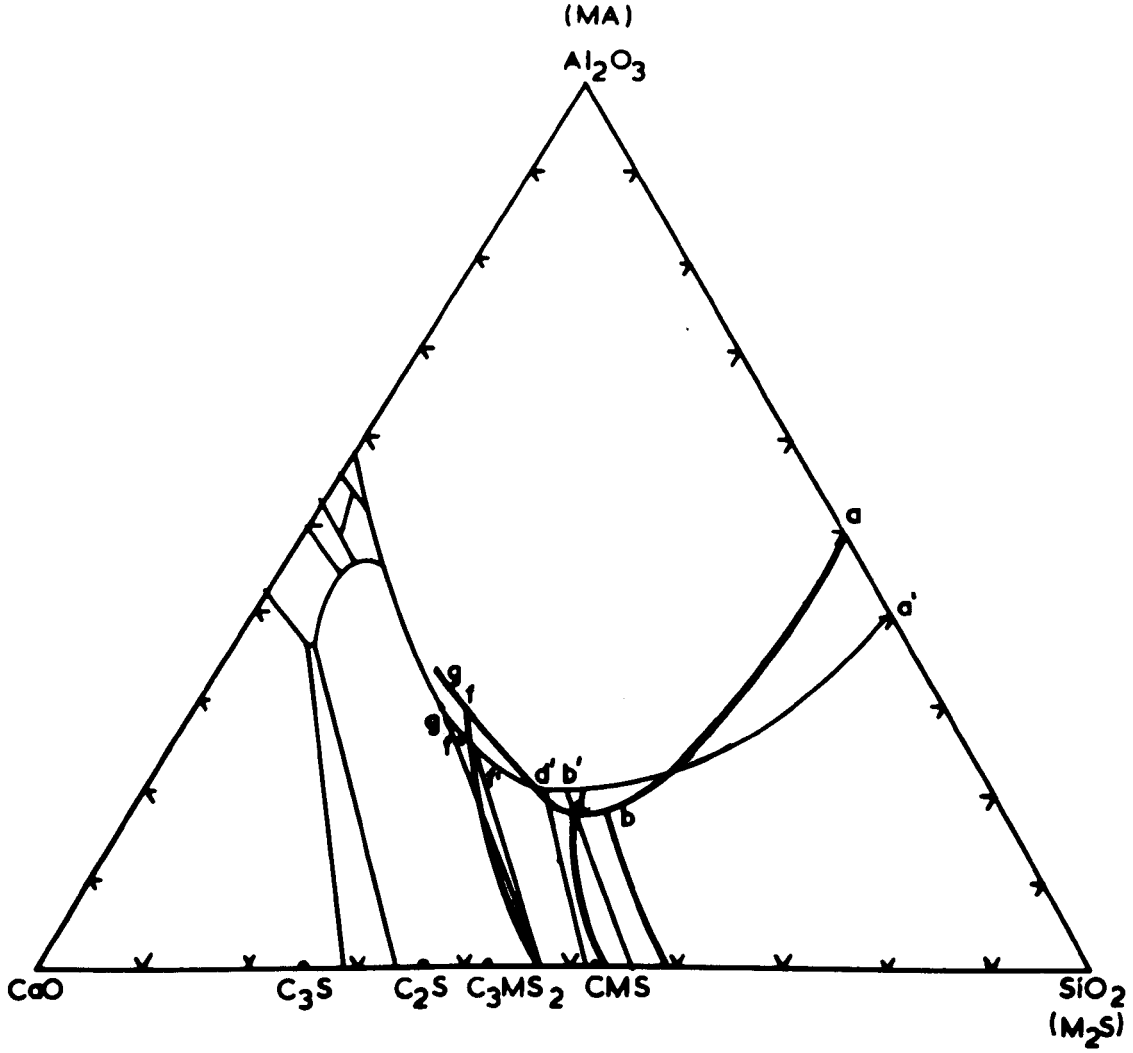
(MA)
$Al_2O_3$
a
a'
$g_1$
g
d' b'
b
CaO
$C_3S$
$C_2S$
$C_3MS_2$
CMS
$SiO_2$
($M_2S$)

FIGURE 20

Projection of the boundary surface of the primary phase volume of periclase in the system $CaO-MgO-Al_2O_3-SiO_2$ projected on to the plane $MA-M_2S-C_2S$. Thick lines show boundaries established by present work for mixtures containing 80 wt.% MgO. Thin lines show boundaries according to Biggar and O-Hara[62, 63, 64].

The various phase fields are numbered as follows:

1 - MA : 2 - $M_2S$ : 3 - CMS : 4 - $C_3MS_2$ : 5 - $C_2S$.

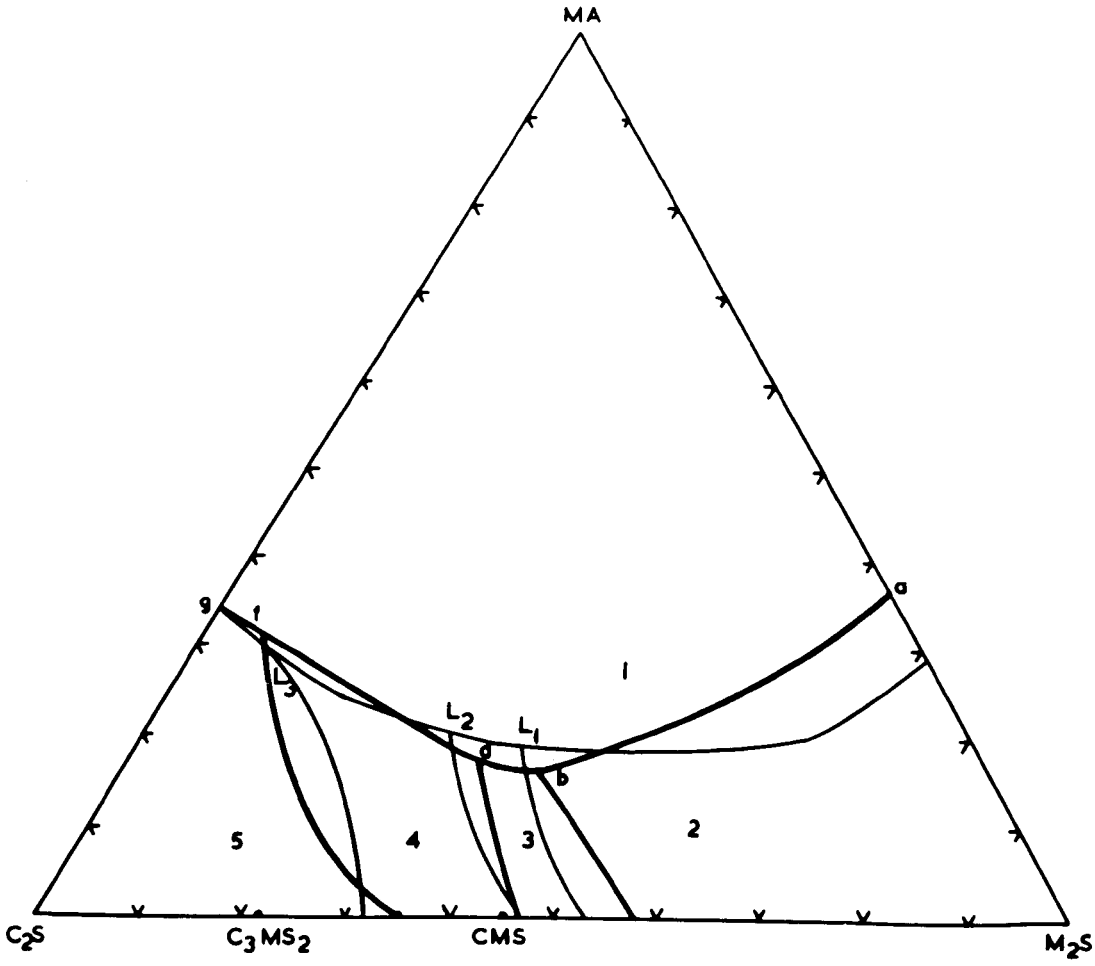
MA
g
f
a
L3
L2
L1
d
b
1
2
3
4
5
C2S
C3MS2
CMS
M2S

FIGURE 21

Projection of the boundary surface of the primary phase volume of periclase in the system $CaO-MgO-Al_2O_3-SiO_2$ according to Solacolu[33] (dashed lines) and as established from mixtures containing 80 wt.% MgO during the present investigation (thick lines).
The various phase fields are numbered as follows:
1 - MA : 2 - $M_2S$ : 3 - CMS : 4 - $C_3MS_2$ : 5 - $C_2S$.

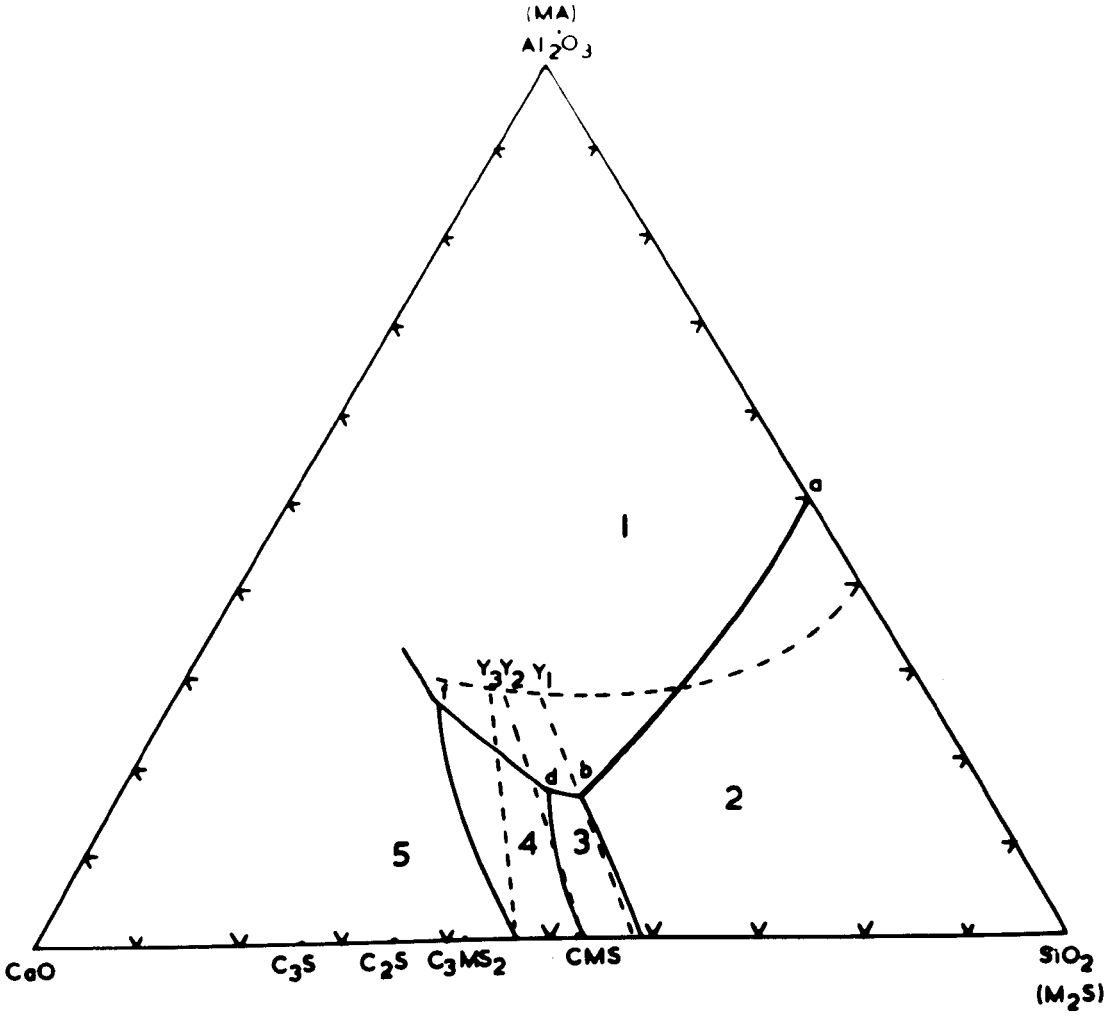
(MA)
$Al_2O_3$
a
1
$Y_3$ $Y_2$ $Y_1$
7
d
b
2
5
4
3
CaO
$C_3S$
$C_2S$
$C_3MS_2$
CMS
$SiO_2$
($M_2S$)

FIGURE 22

Partial phase diagram of the system $MgO-Al_2O_3-SiO_2$[65] showing phase boundaries in liquidus surface and the position of eutectic E. Point D shows composition of periclase phase coexisting with eutectic liquid E. $e_4$, $e_2$ and $e_3$ are apparent positions of the eutectic in mixtures containing 70 wt.%, 80 wt.% and 90 wt.% MgO after projecting through the MgO corner. $e_1$ shows projected composition of E in the absence of solid solubility of $Al_2O_3$ in periclase.

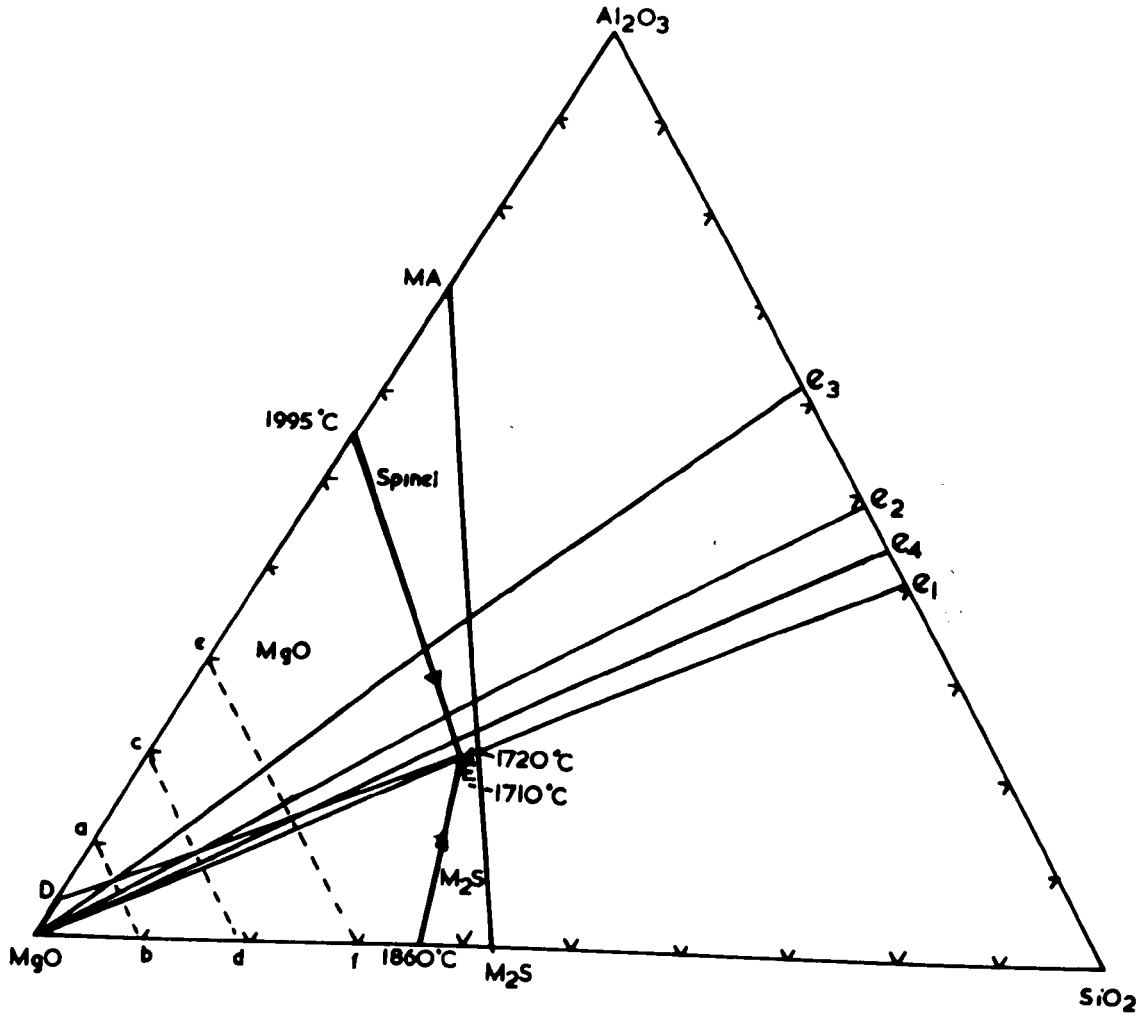
$Al_2O_3$
MA
1995°C
Spinel
$e_3$
$e_2$
$e_4$
$e_1$
MgO
c
a
D
E
1720°C
1710°C
$M_2S$
MgO
b
d
f
1860°C
$M_2S$
$SiO_2$

FIGURE 23

Partial phase diagram of the system $MgO-Al_2O_3-C_2S$[31] showing phase boundaries on the liquidus surface and the position of eutectic E. In the absence of solid solubility of $Al_2O_3$ in MgO the eutectic point E projects to point T which is independent of the MgO content of mixtures.

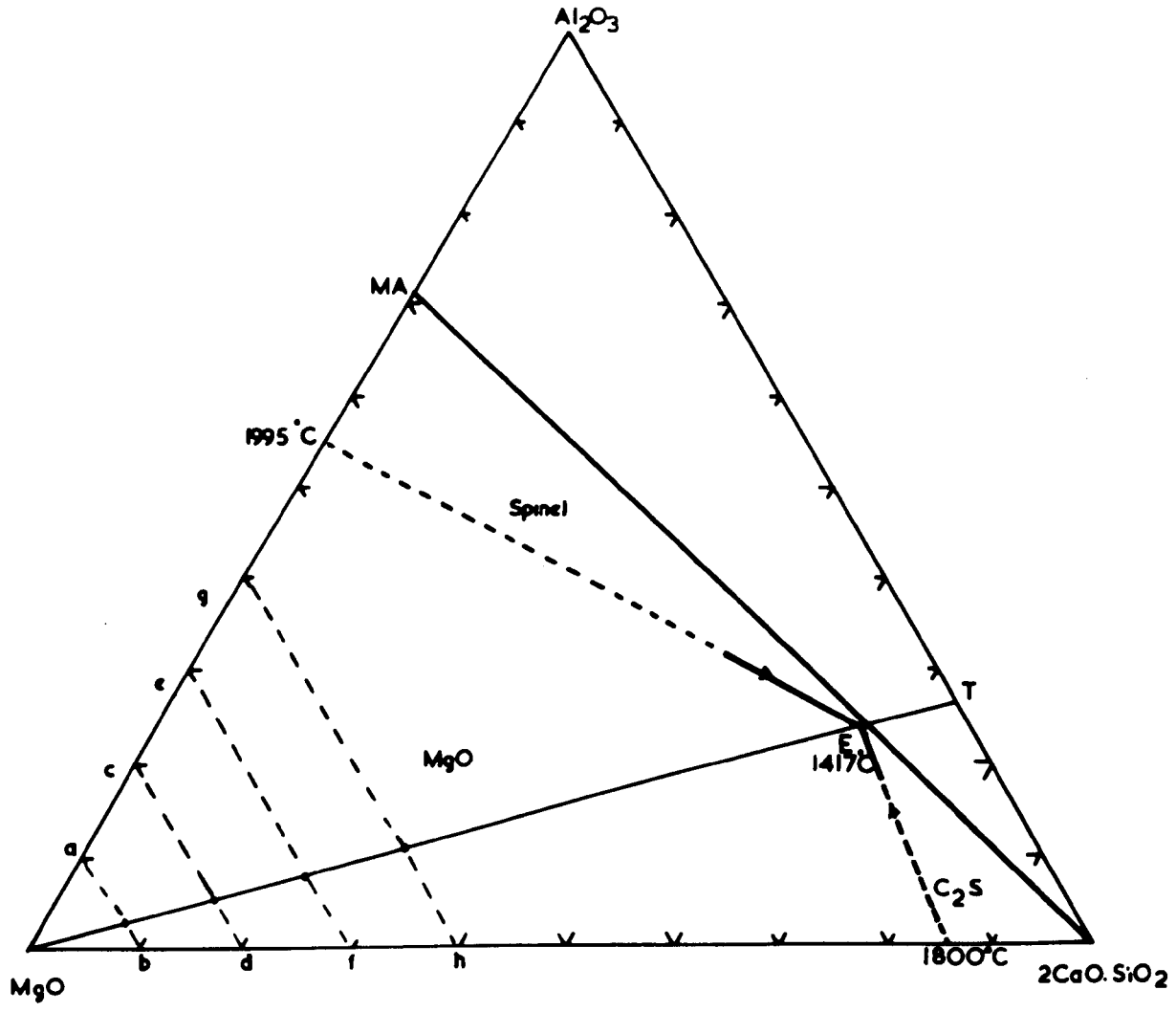
$Al_2O_3$
MA
1995°C
Spinel
g
e
c
a
MgO
T
E
1417°C
$C_2S$
1800°C
MgO
b
d
f
h
$2CaO.SiO_2$

FIGURE 24

Projection of the boundary surface of the primary phase volume of periclase in the system CaO-MgO-$Al_2O_3$-$SiO_2$ showing the progressive displacement of silicate-spinel boundary as MgO content of mixtures increases from 70 wt.% ($e_4$) to 80 wt.% ($e_2$) and 90 wt.% ($e_3$). The various phase fields are numbered as follows:

1 - MA : 2 - $M_2S$ : 3 - CMS : 4 - $C_3MS_2$ : 5 - $C_2S$.

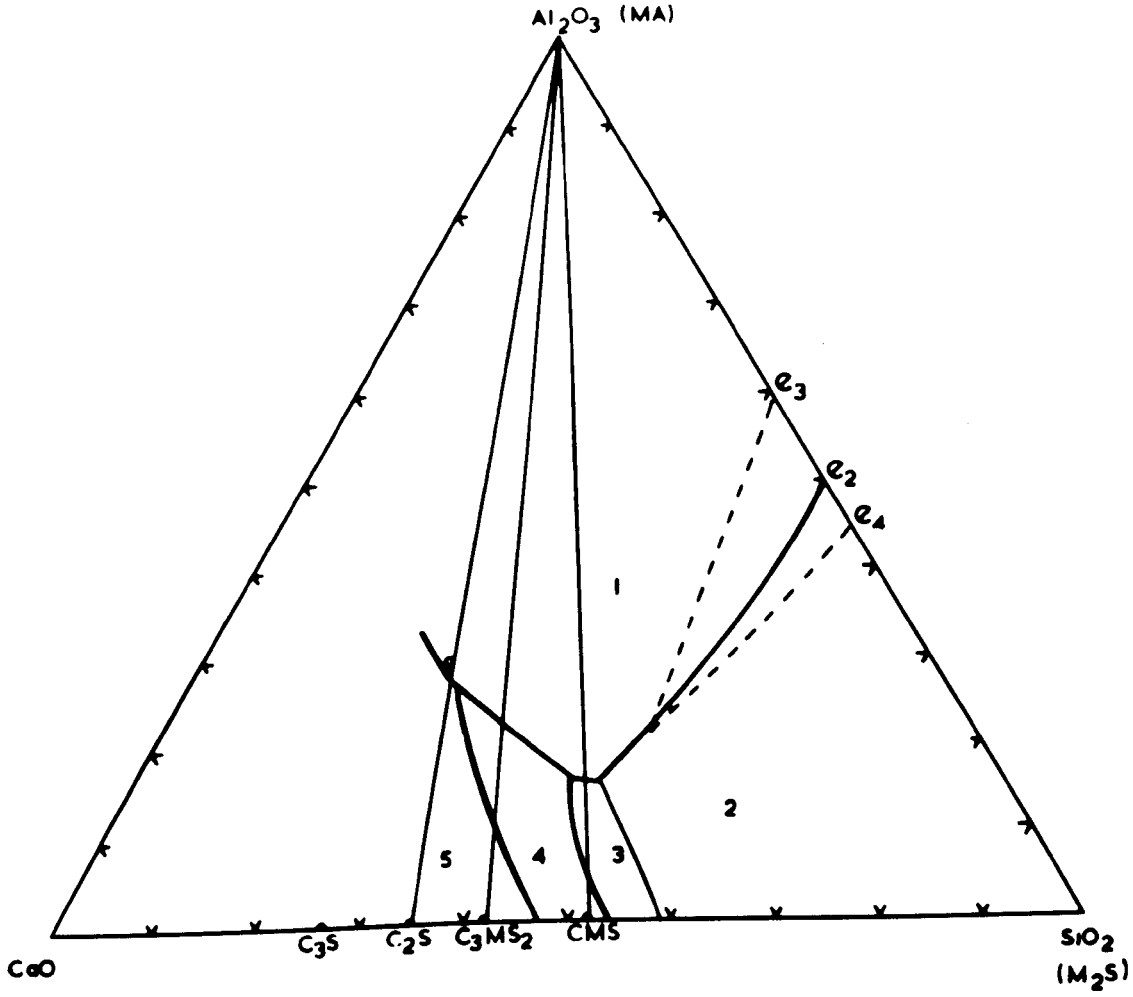
$Al_2O_3$ (MA)
$e_3$
$e_2$
$e_4$
1
2
3
4
5
CaO
$C_3S$
$C_2S$
$C_3MS_2$
CMS
$SiO_2$
($M_2S$)

FIGURE 25

Phase diagram of the system $MgAl_2O_4$-CMS (after El-Shahat and White[2]). Because of the incongruent melting of CMS this system could be treated as a section in the ternary system $MgO$-$Al_2O_3$-CS.

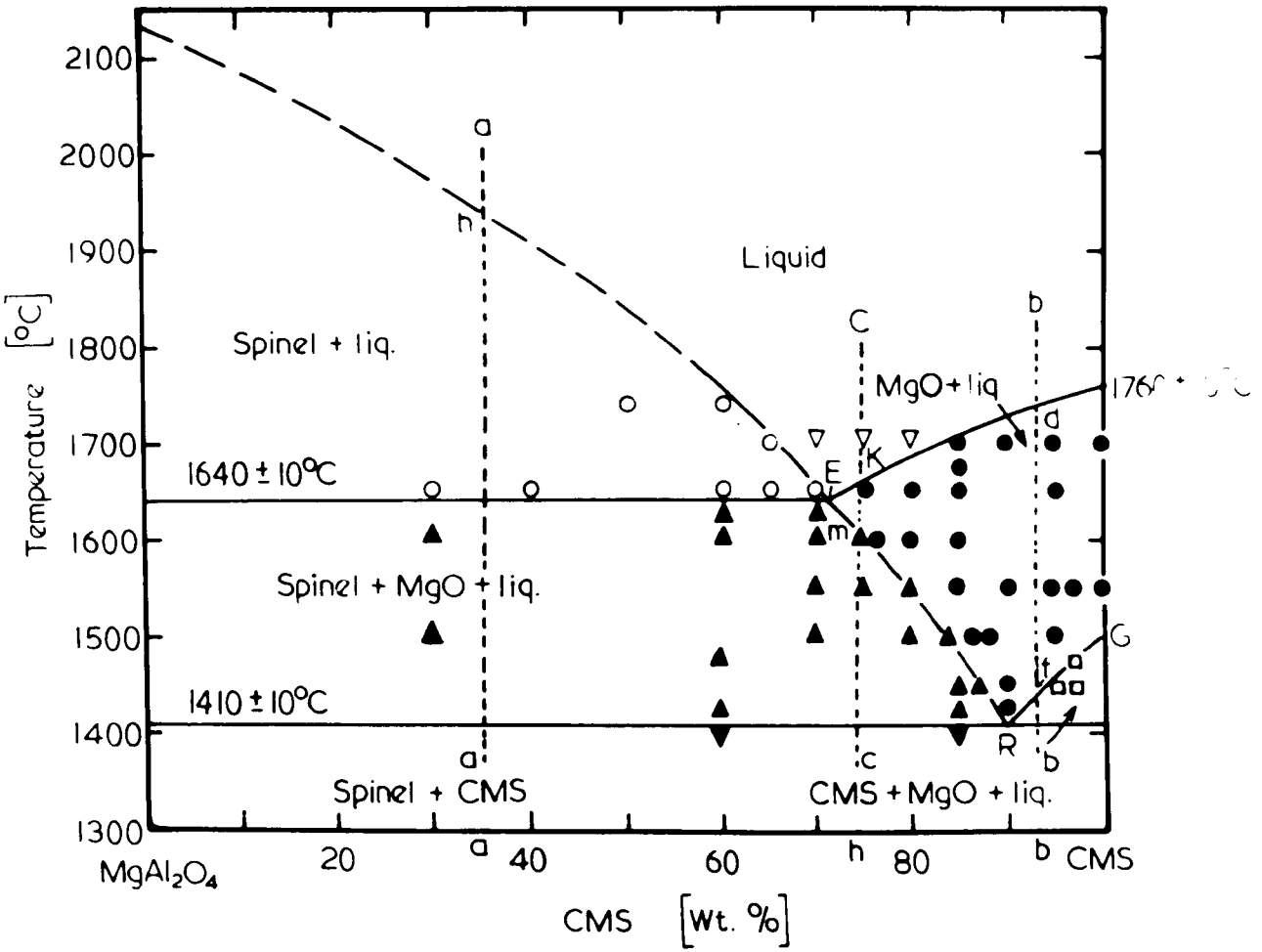
2100
2000
1900
1800
1700
1600
1500
1400
1300
Temperature [°C]
Liquid
Spinel + liq.
MgO + liq
1640 ± 10°C
Spinel + MgO + liq.
1410 ± 10°C
Spinel + CMS
CMS + MgO + liq.
a
h
c
b
K
E
m
R
G
MgAl2O4
20
40
60
80
CMS
CMS [Wt. %]

FIGURE 26

Phase relationships in the system $MgO-Al_2O_3-CS$ (after El-Shahat and White[2]) as indicated by the phase diagram of the section $MgAl_2O_4$-CMS (see Figure 25) and by published data on the systems MgO-CS[66] and $MgO-MgAl_2O_4$[18].

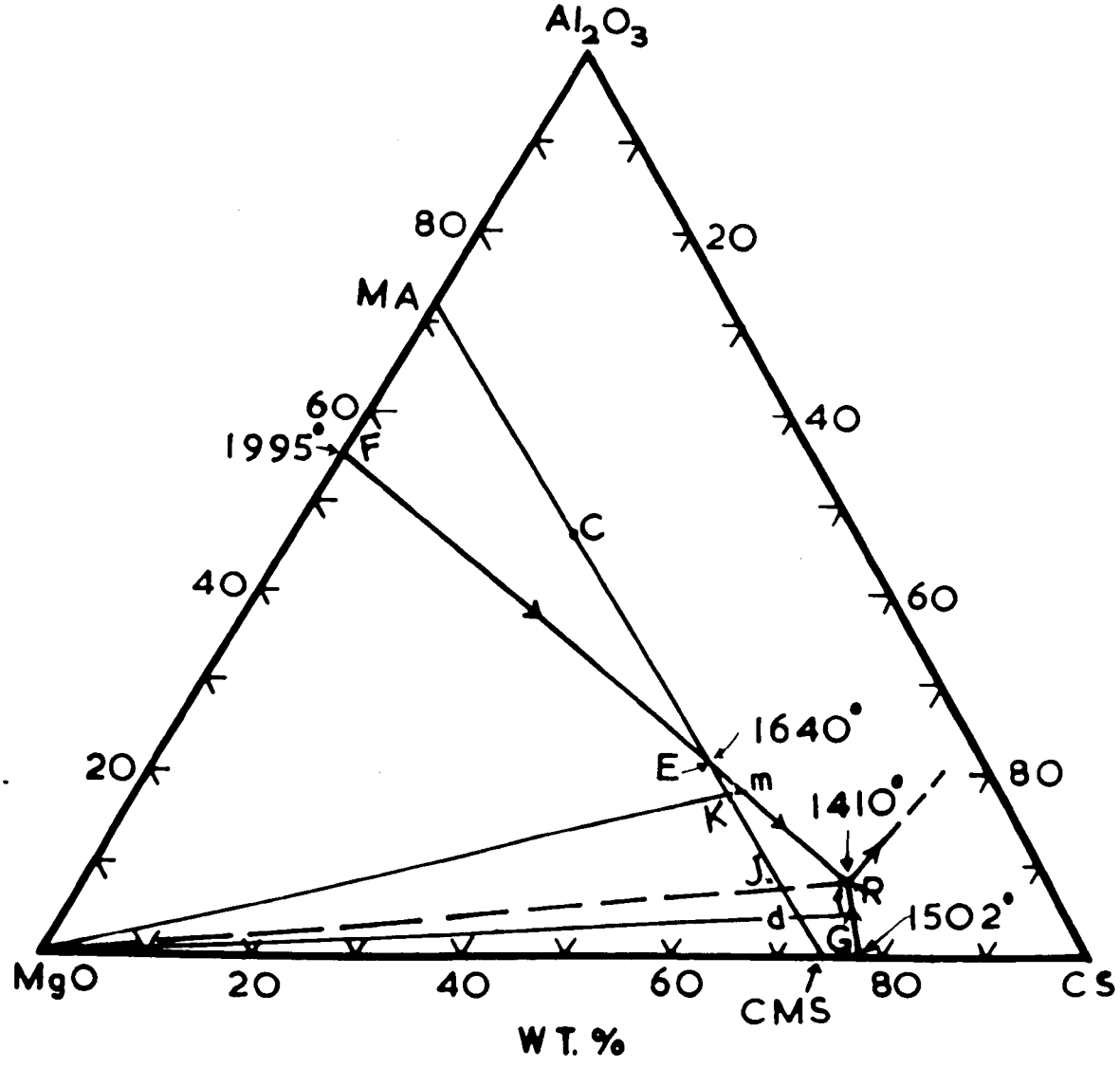
Al2O3
80
20
MA
60
40
1995°
F
C
40
60
20
1640°
E
m
80
1410°
K
J
R
d
1502°
G
MgO
20
40
60
80
CMS
CS
WT. %

FIGURE 27

Phase relationships in the system $MgO-Al_2O_3-CS$ constructed using points c and h on the join $Al_2O_3$-CMS from Figure 18, and published data on the systems MA-CMS (see Figure 25), MgO-CS[66] and $MgO-MgAl_2O_4$[18].

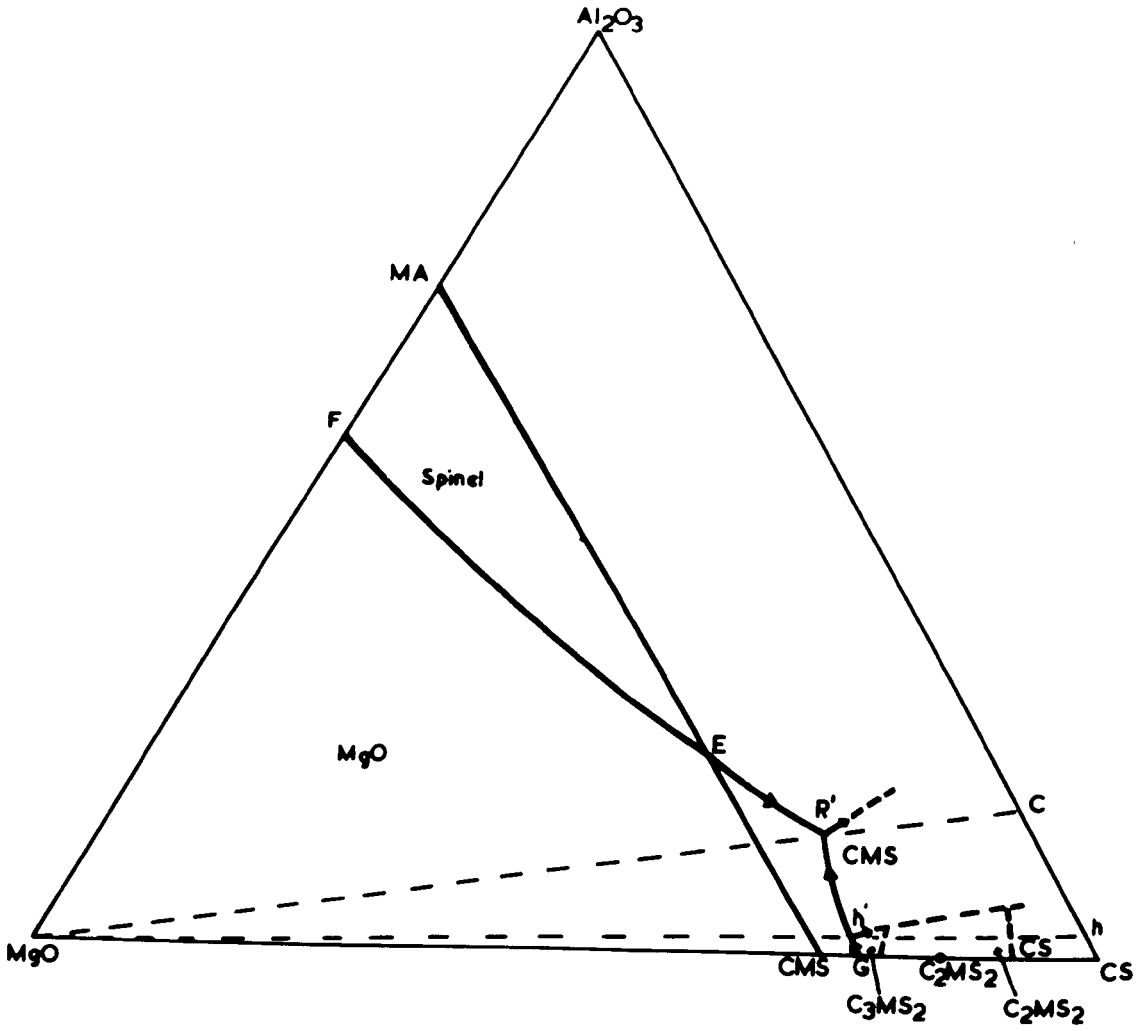
$Al_2O_3$
MA
F
Spinel
MgO
E
R'
C
CMS
h'
h
MgO
CMS
G
CS
CS
$C_2MS_2$
$C_3MS_2$
$C_2MS_2$

FIGURE 28

Projection from periclase on to the plane $CaO-Al_2O_3-SiO_2$ of the liquidus surfaces bounding the primary phase volume of periclase, contoured to show weight % MgO present in the liquid phase on the surface. (From O'Hara and Biggar[50].)

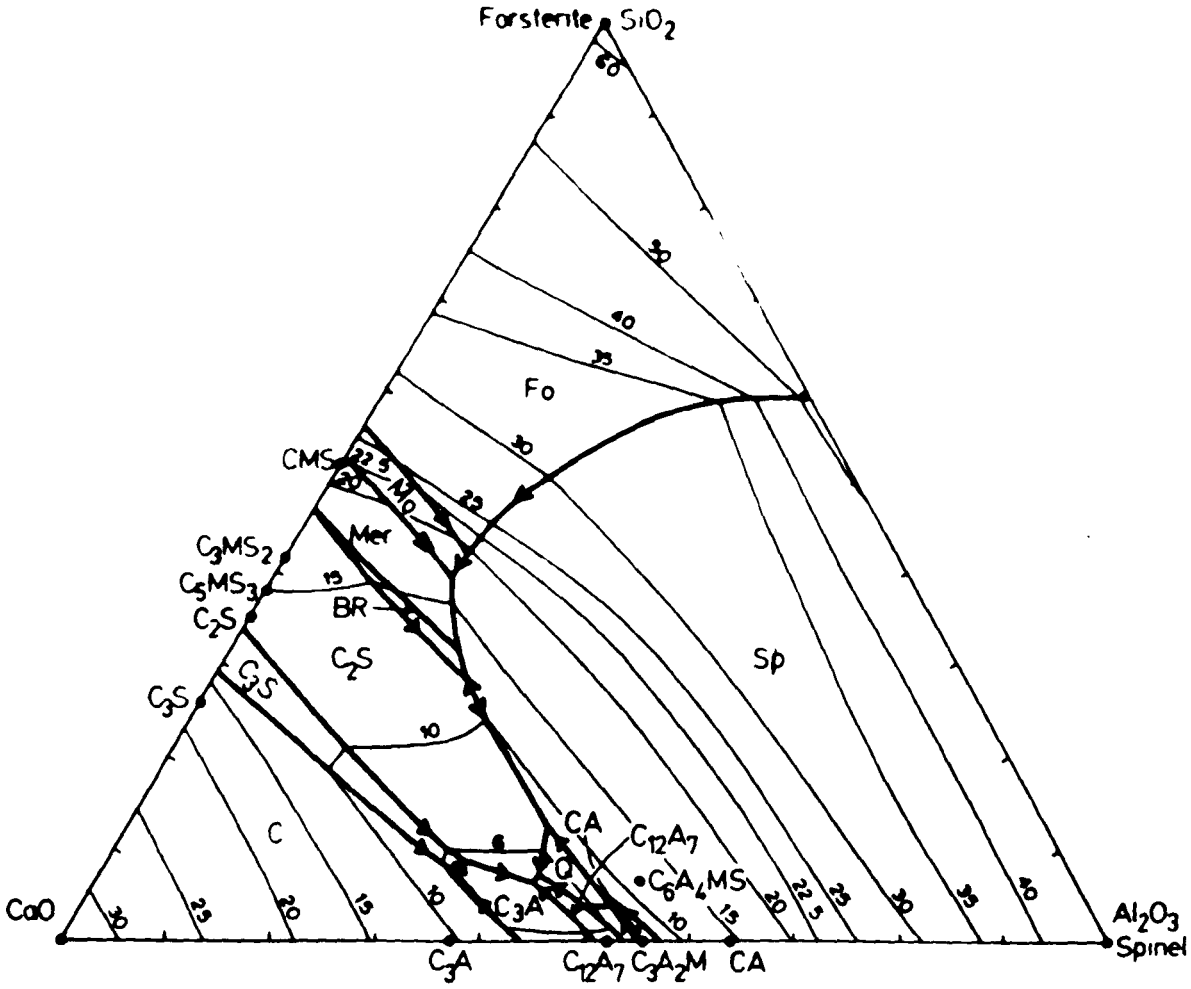
Forsterite
$SiO_2$
50
30
40
35
Fo
30
CMS
22.5
M
22.5
Mer
$C_3MS_2$
$C_5MS_3$
15
$C_2S$
BR
$C_2S$
Sp
$C_3S$
$C_3S$
10
CA
$C_{12}A_7$
C
$C_6A_4MS$
C
$C_3A$
CaO
30
25
20
15
10
10
15
20
22.5
25
30
35
40
$Al_2O_3$
Spinel
$C_3A$
$C_{12}A_7$
$C_3A_2M$
CA

FIGURE 29

Phase diagram of the system $MgAl_2O_4$-CMS constructed from the join $Al_2O_3$-CMS (see Figure 18) and of the system $MgAl_2O_4$-CMS (see Figure 25).

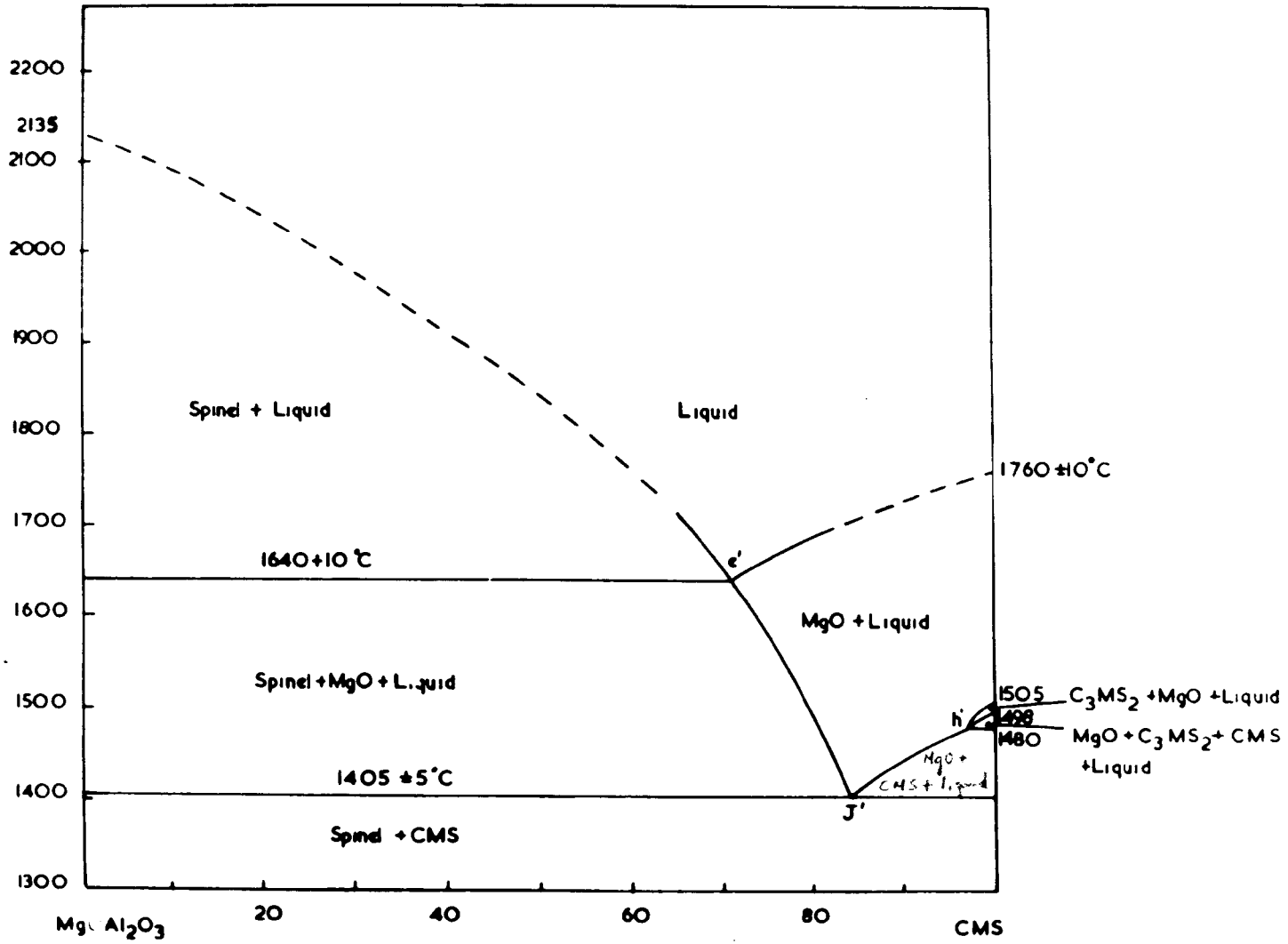
2200
2135
2100
2000
1900
1800
1700
1600
1500
1400
1300
Spinel + Liquid
Liquid
1760±10°C
1640±10°C
e'
MgO + Liquid
Spinel + MgO + Liquid
1505
$C_3MS_2$ + MgO + Liquid
h'
1480
$MgO + C_3MS_2 + CMS$ + Liquid
1405 ± 5°C
J'
Spinel + CMS
MgO · $Al_2O_3$
20
40
60
80
CMS

FIGURE 30

Phase diagram of the system $MgAl_2O_4$-$C_3MS_2$ from El-Shahat and White[3] after quenching in air.

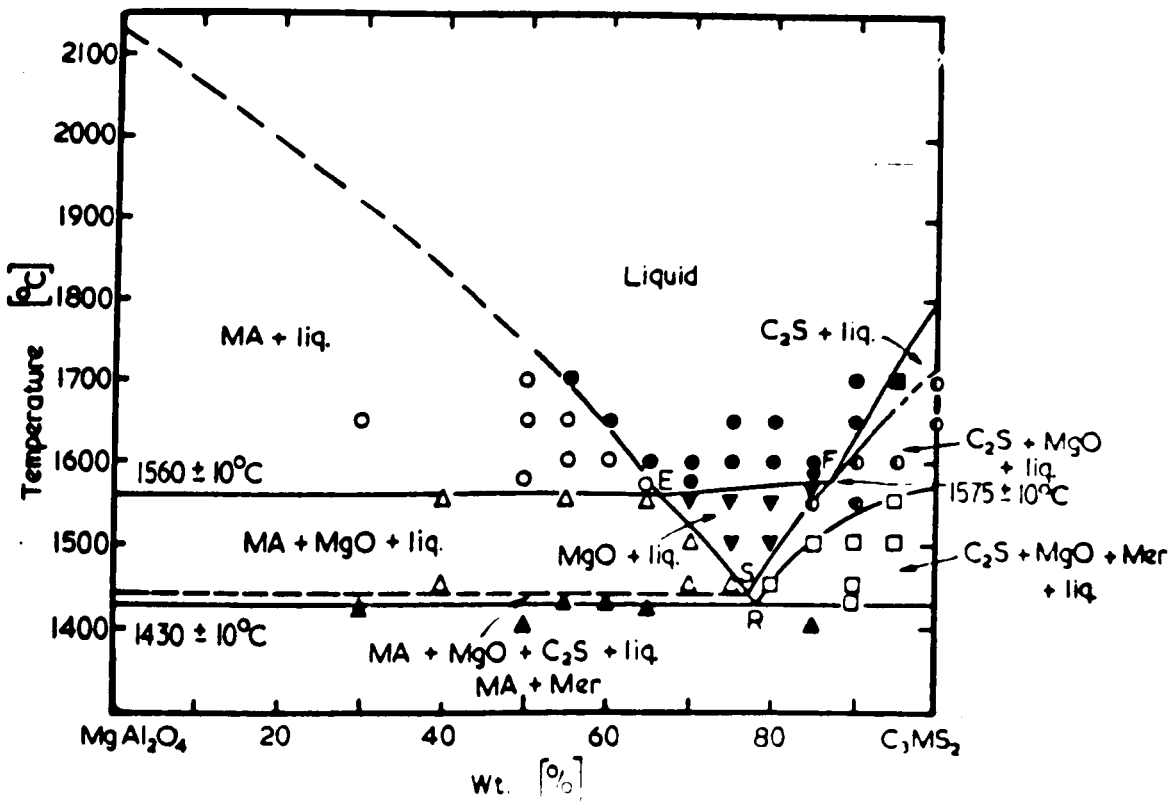
2100
2000
1900
1800
1700
1600
1500
1400
Temperature [°C]
Liquid
MA + liq.
C2S + liq.
C2S + MgO + liq.
1560 ± 10°C
E
F
1575 ± 10°C
MA + MgO + liq.
MgO + liq.
S
C2S + MgO + Mer + liq.
R
1430 ± 10°C
MA + MgO + C2S + liq.
MA + Mer
MgAl2O4
20
40
60
80
C3MS2
Wt. [%]

FIGURE 31

Phase relationships in the system $MgO-Al_2O_3-C_3S_2$ constructed using points e and k on join $Al_2O_3-C_3MS_2$ from Figure 18, and from published data on the systems $MA-C_3MS_2$ (see Figure 30), $MgO-C_3S_2$[66] and $MgO-MgAl_2O_4$[18].

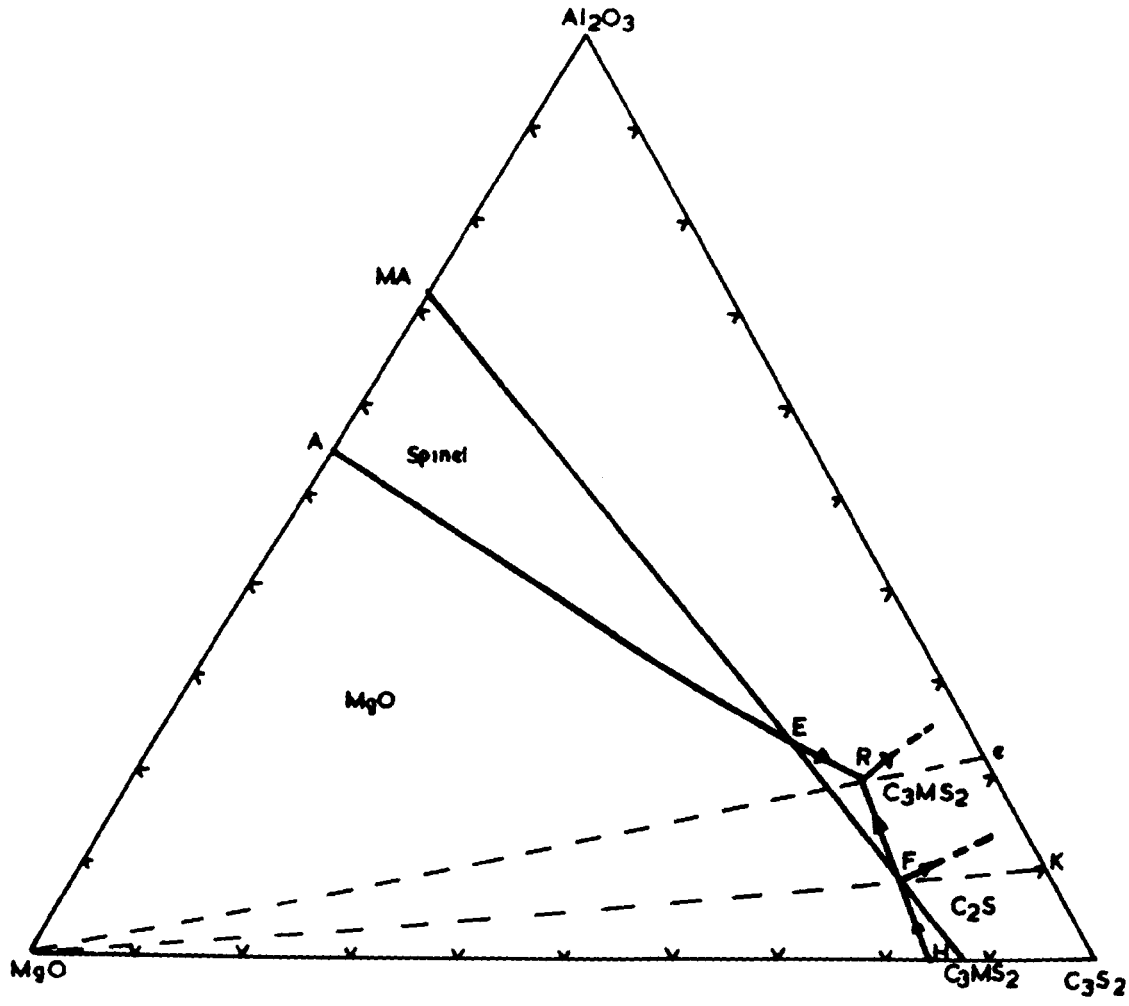
$Al_2O_3$
MA
A
Spinel
MgO
E
R
$C_3MS_2$
e
F
K
$C_2S$
H
MgO
$C_3MS_2$
$C_3S_2$

FIGURE 32

Diagram showing the position of the boundary of the spinel field on the boundary surface of the primary phase volume of periclase, the continuous line representing its position in the system $CaO-MgO-Al_2O_3-SiO_2$ and the broken line and dashed and dotted line showing its approximate displacement when $Al_2O_3$ is partially replaced by $Cr_2C_3$[52] and $Fe_2O_3$[51] respectively.

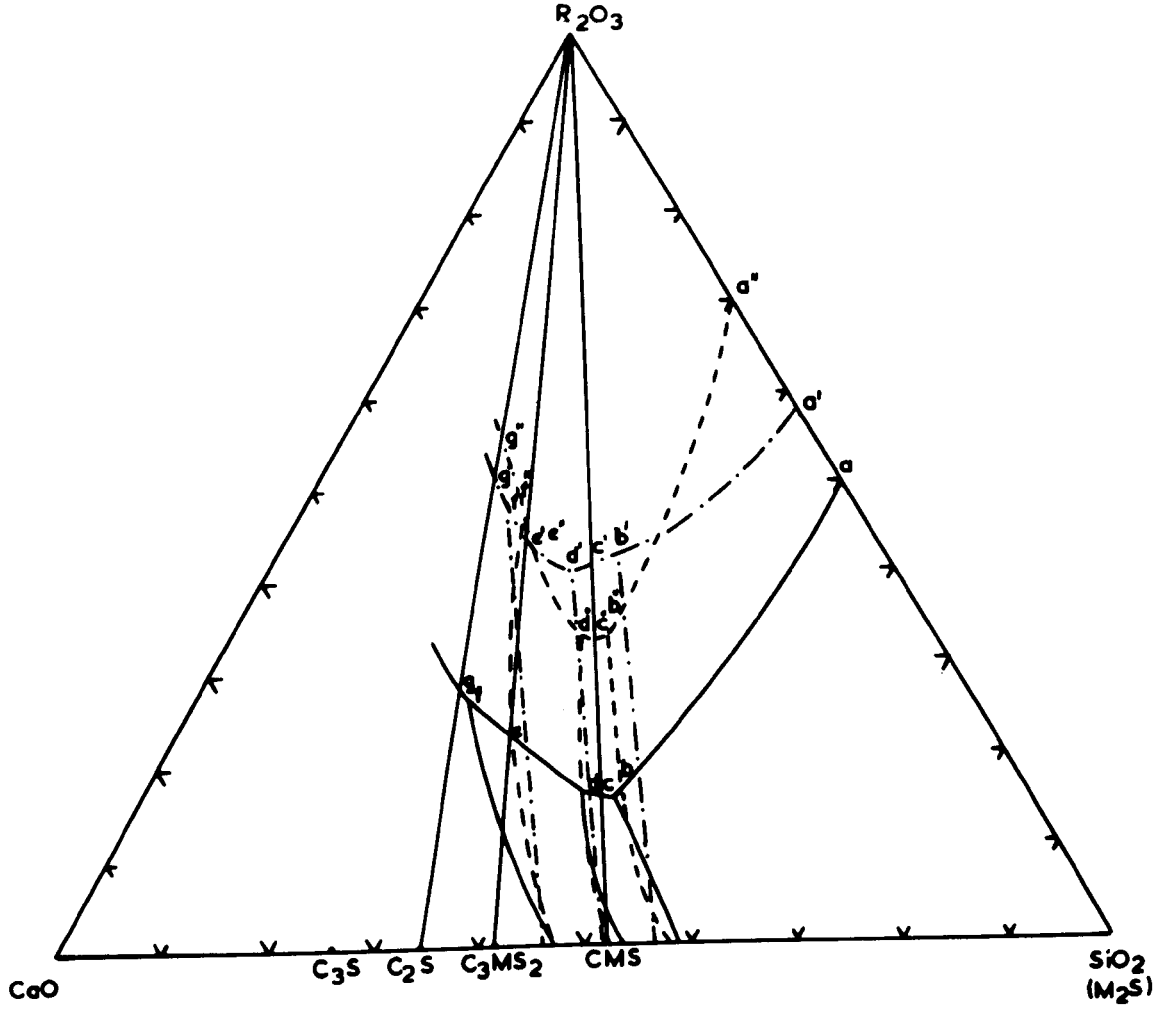
R2O3
a''
a'
a
CaO
C3S
C2S
C3MS2
CMS
SiO2
(M2S)

FIGURE 33

Phase diagram of the isoplethal section at 60 wt.% MgO in the system $MgO-Cr_2O_3-C_2S$. Point G represents the eutectic and points M and N, and O and P were obtained respectively from the systems $MgO-MgCr_2O_4$[20] and $MgO-CaO-SiO_2$[11].

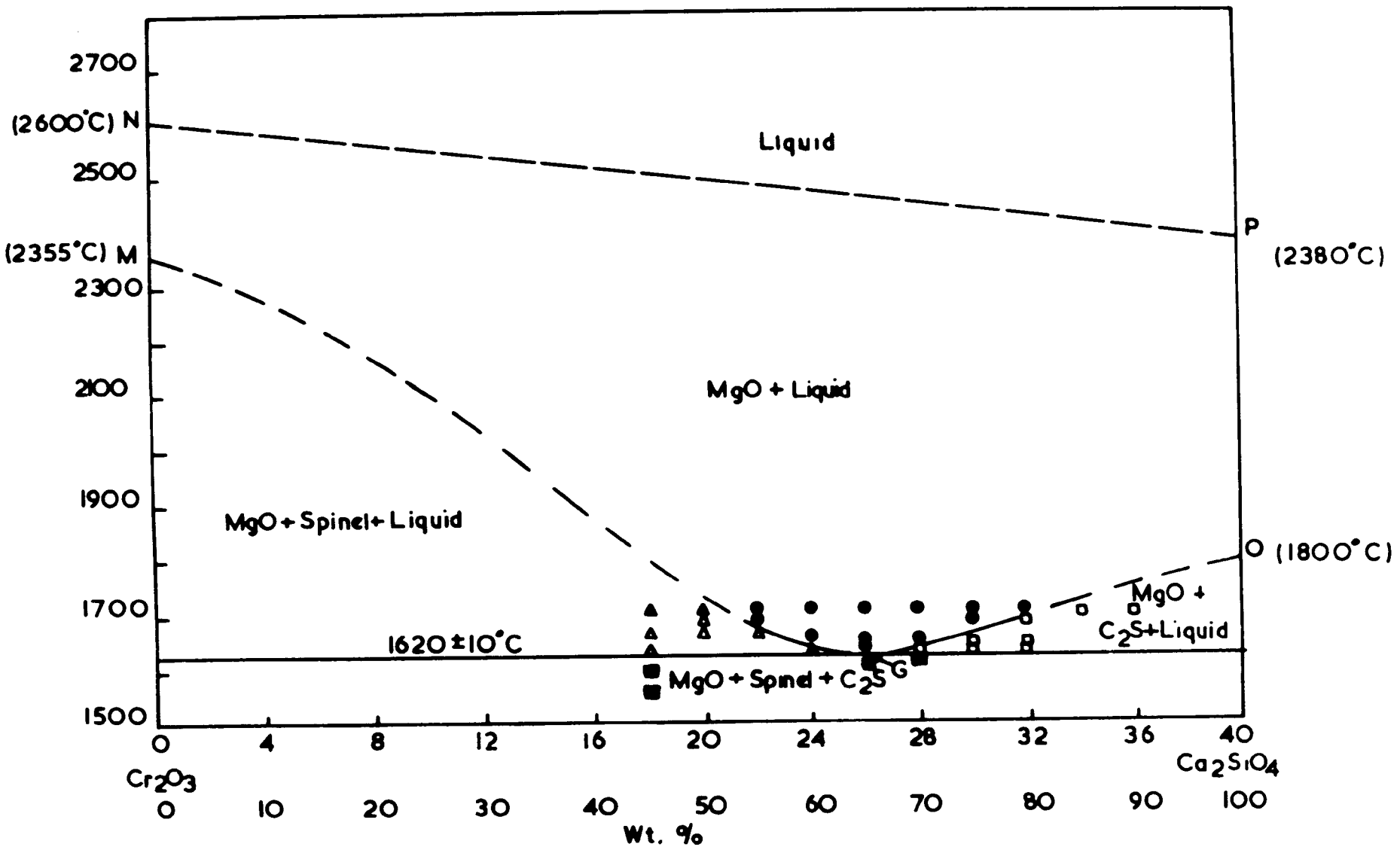
2700
(2600°C) N
2500
(2355°C) M
2300
2100
1900
1700
1500
Liquid
P
(2380°C)
MgO + Liquid
MgO + Spinel + Liquid
O (1800°C)
MgO + C2S + Liquid
1620 ± 10°C
MgO + Spinel + C2S
G
0 4 8 12 16 20 24 28 32 36 40
Ca2SiO4
Cr2O3
0 10 20 30 40 50 60 70 80 90 100
Wt. %

FIGURE 34

Phase diagram of the isoplethal section at 40 wt.% MgO in the system $MgO-Cr_2O_3-C_2S$. Point H represents the eutectic and points M and N, and O and P, were obtained respectively from the systems $MgO-MgCr_2O_4$[20] and $MgO-CaO-SiO_2$[11].

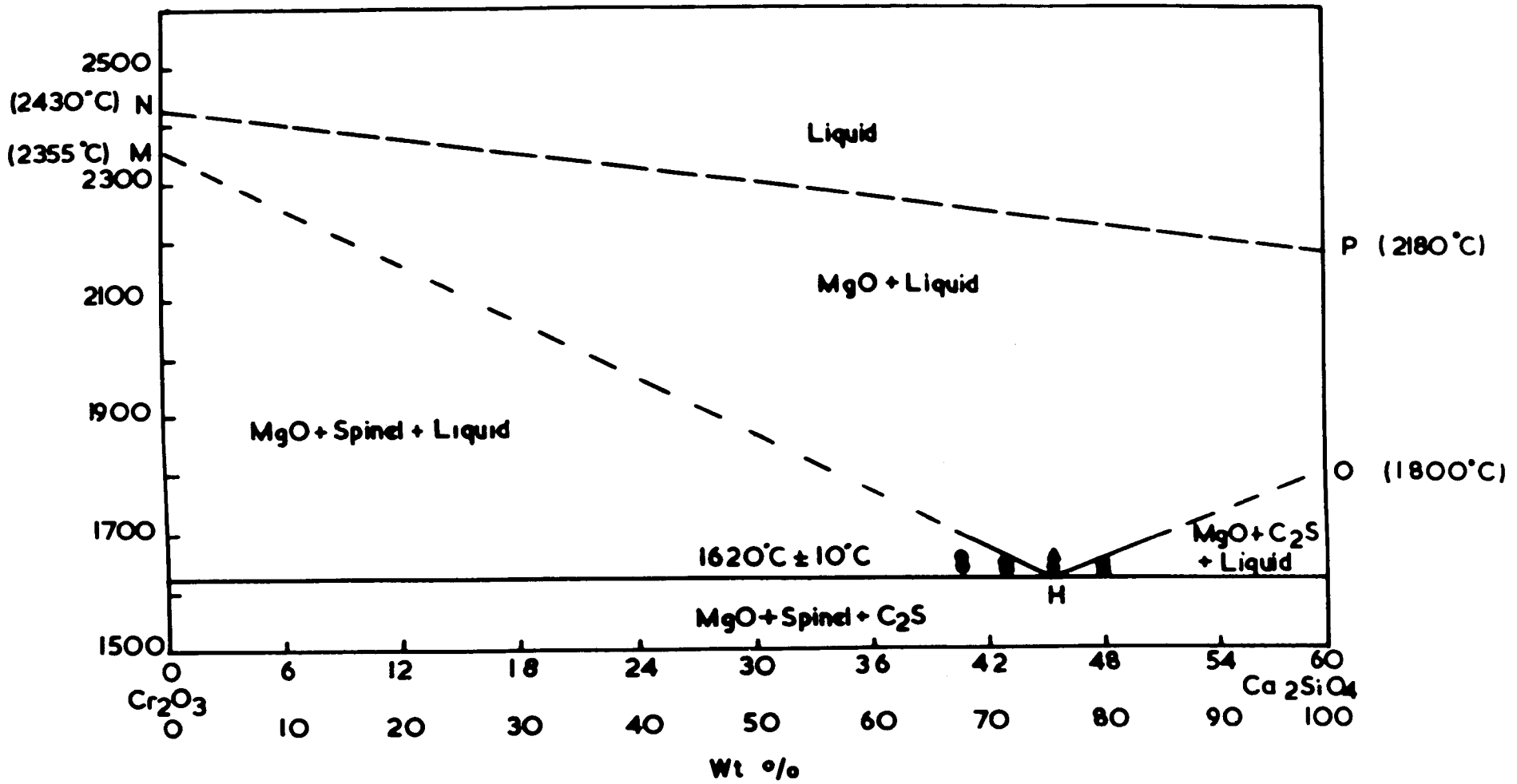
2500
(2430°C) N
(2355°C) M
2300
2100
1900
1700
1500
Liquid
MgO + Liquid
MgO + Spinel + Liquid
P (2180°C)
O (1800°C)
1620°C ± 10°C
MgO + C2S + Liquid
H
MgO + Spinel + C2S
0 6 12 18 24 30 36 42 48 54 60
Ca2SiO4
Cr2O3
0 10 20 30 40 50 60 70 80 90 100
Wt %

FIGURE 35

Phase diagram of the isoplethal section at 80 wt.% MgO in the system $MgO-Cr_2O_3-C_2S$ derived from Tarboton's projection (see Figure 13). Point F represents the eutectic and points M and N, and O and P, were obtained respectively from the systems $MgO-MgCr_2O_4$[20] and $MgO-CaO-SiO_2$[11].

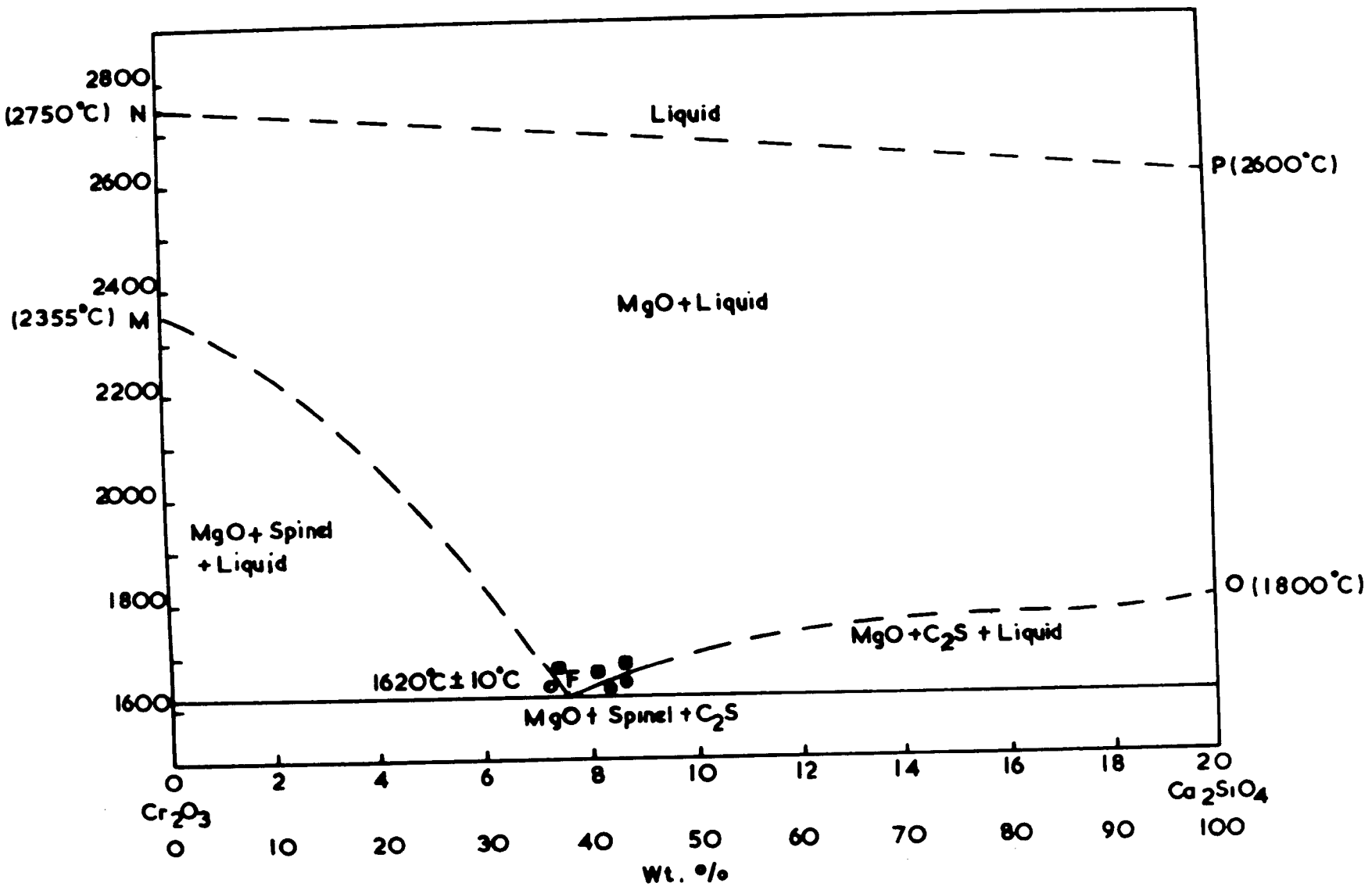
2800
(2750°C) N
2600
2400
(2355°C) M
2200
2000
1800
1600
Liquid
P (2600°C)
MgO + Liquid
MgO + Spinel + Liquid
O (1800°C)
MgO + C2S + Liquid
1620°C ± 10°C
F
MgO + Spinel + C2S
0
2
4
6
8
10
12
14
16
18
20
Ca2SiO4
Cr2O3
0
10
20
30
40
50
60
70
80
90
100
Wt. %

FIGURE 36

Phase diagram of the system $MgO-Cr_2O_3-C_2S$ showing phase boundaries in liquidus surface and the position of eutectic E. Point A shows composition of periclase phase coexisting with eutectic liquid E. B, C and D are apparent positions of the eutectic in mixtures containing 80 wt.% MgO (see Figure 35), 60 wt.% MgO (see Figure 33) and 40 wt.% MgO (see Figure 34) after projecting through the MgO corner. E' shows projected composition of E in the absence of solid solubility of $Cr_2O_3$ in periclase.

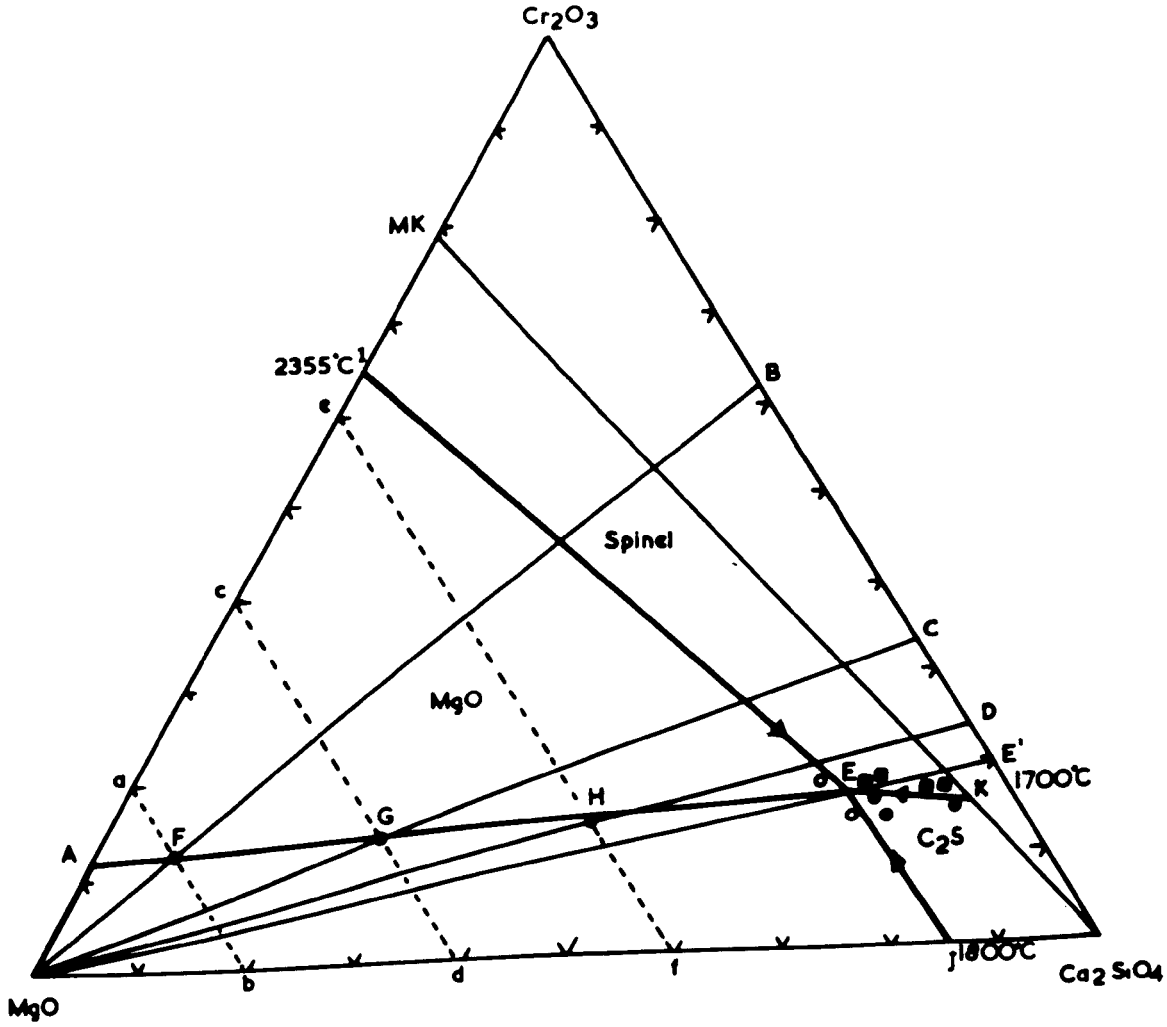
$Cr_2O_3$
MK
2355°C
1
e
B
Spinel
c
C
MgO
D
E'
a
E
K
1700°C
H
G
F
A
$C_2S$
1800°C
MgO
b
d
f
$Ca_2SiO_4$

FIGURE 37

Phase diagram of the system $MgO-Cr_2O_3-C_2S$ with the isotherms drawn in tentatively. The eutectic E occurs at 1620°C $\pm$ 10°C and its composition is 15 wt.% MgO, 17 wt.% $Cr_2O_3$ and 68 wt.% $Ca_2SiO_4$.

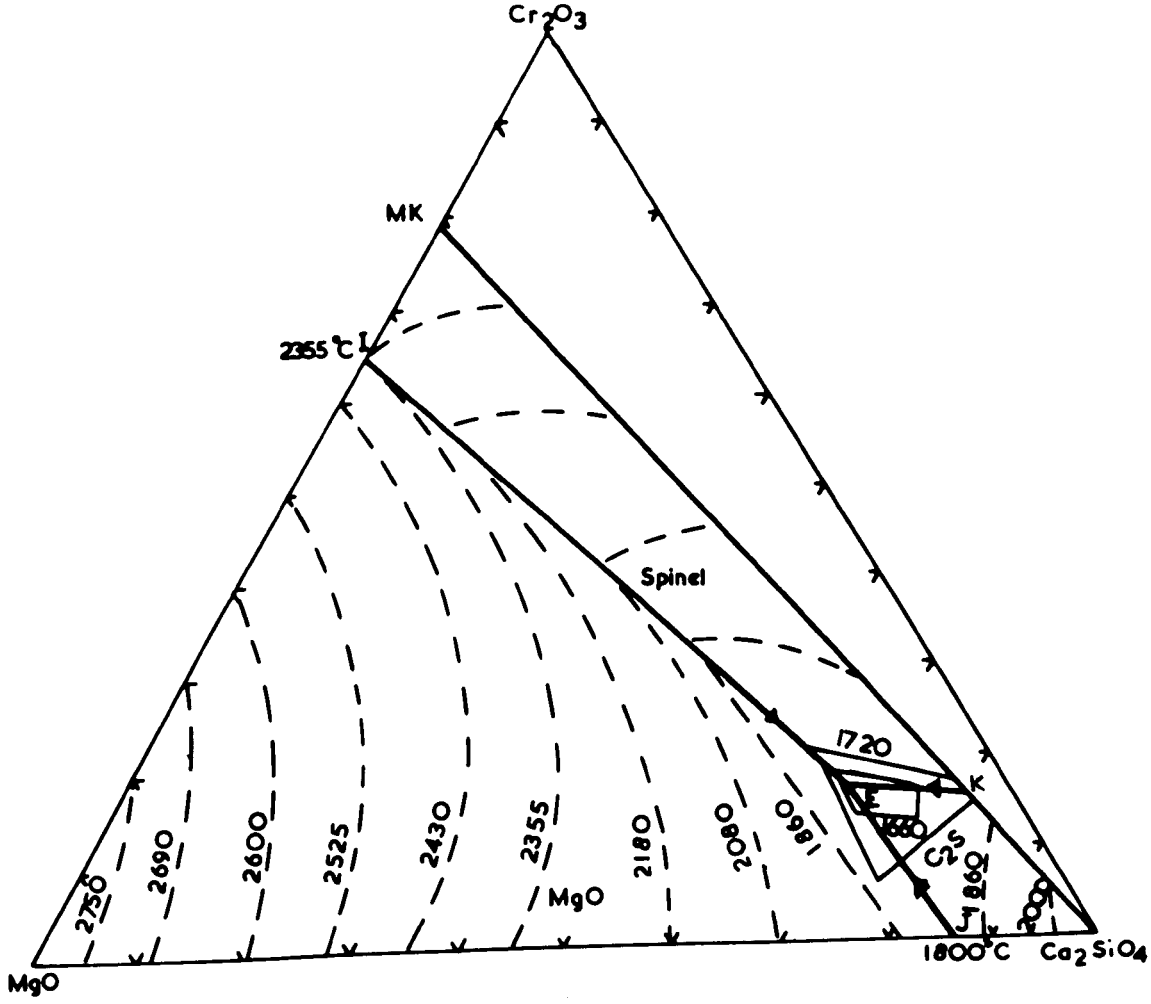
Cr2O3
MK
2355°C
Spinel
1720
K
1860
CS
1860
2000
1800°C
Ca2SiO4
MgO
2750
2690
2600
2525
2430
2355
2180
2080
1980
MgO

FIGURE 38

Projection showing secondary phases crystallising in air from $CaO-MgO-Cr_2O_3-SiO_2$ mixtures containing 80 wt.% MgO (see Figure 13). Points E' and P' show respectively the positions which points B and N would have if the solid solubility of $Cr_2O_3$ in MgO was negligible. (Compare Figures 36 and 39.)

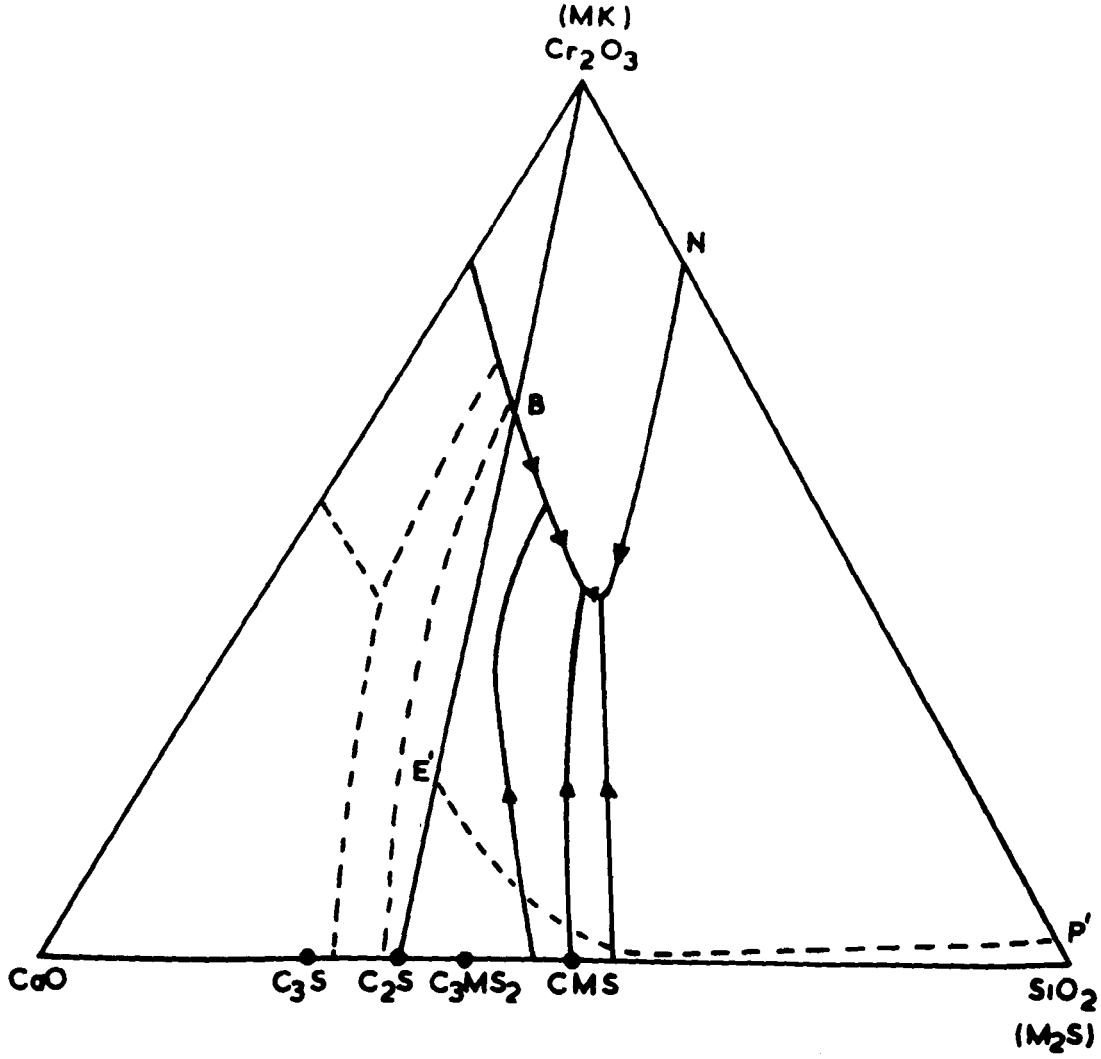
(MK)
$Cr_2O_3$
N
B
E'
P'
CaO
$C_3S$
$C_2S$
$C_3MS_2$
CMS
$SiO_2$
($M_2S$)

FIGURE 39

Partial phase diagram of the system $MgO-Cr_2O_3-SiO_2$ showing phase boundaries in liquidus surface and the position of eutectic P. Point T shows composition of periclase phase coexisting with eutectic liquid P. N and O are apparent positions of the eutectic in mixtures containing 80 wt.% MgO (see Figure 13) and 70 wt.% MgO after projecting through the MgO corner. P' shows projected composition of P in the absence of solid solubility of $Al_2O_3$ in periclase.

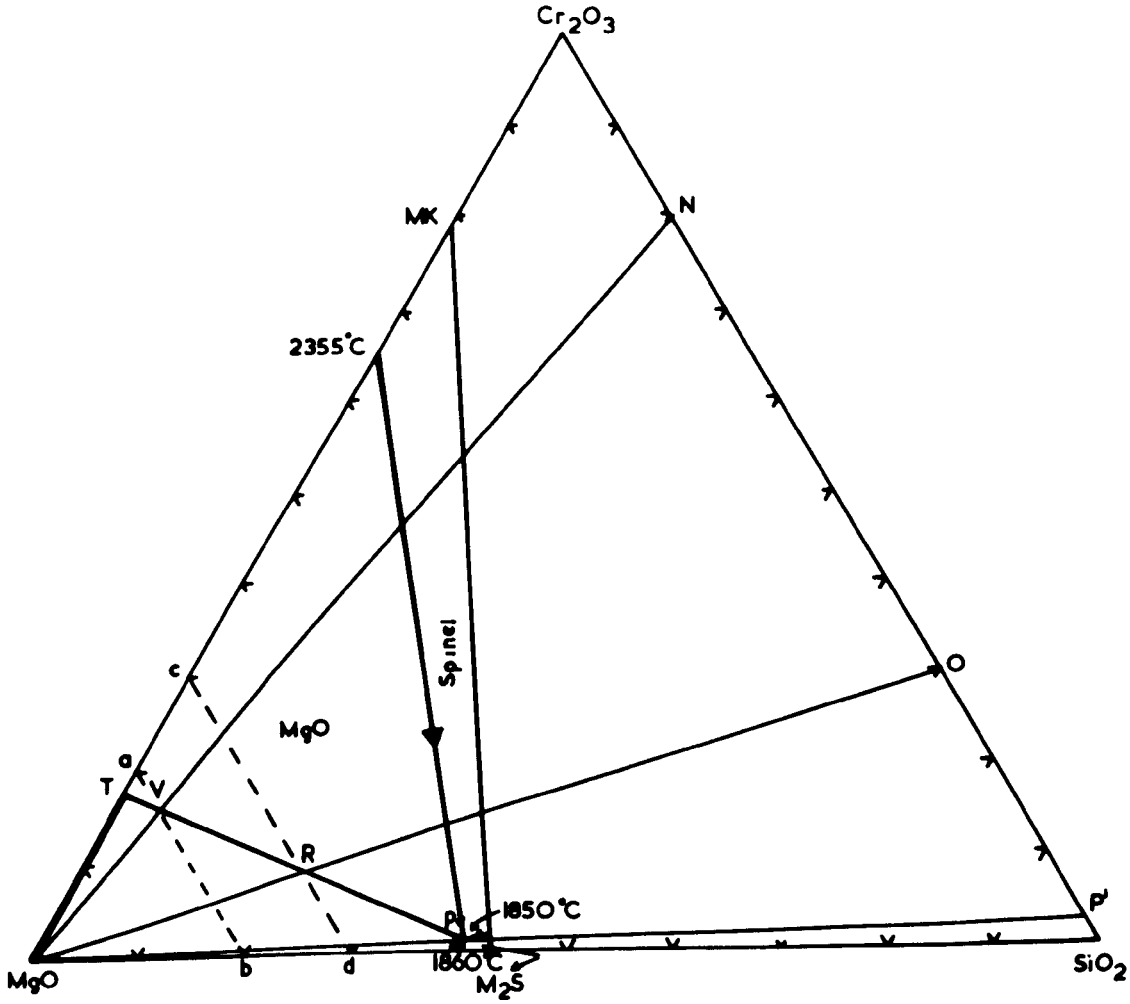
$Cr_2O_3$
MK
N
2355°C
Spinel
c
MgO
a
T
V
R
O
P
1850°C
P'
MgO
b
d
1860°C
$M_2S$
$SiO_2$

FIGURE 40

Phase relationships in the system $MgO-Al_2O_3-C_2S$ at 1550°C. a-L-$C_2S$ is the tie triangle within which MgO and $C_2S$ coexist with liquid L. (From Taylor[72].)

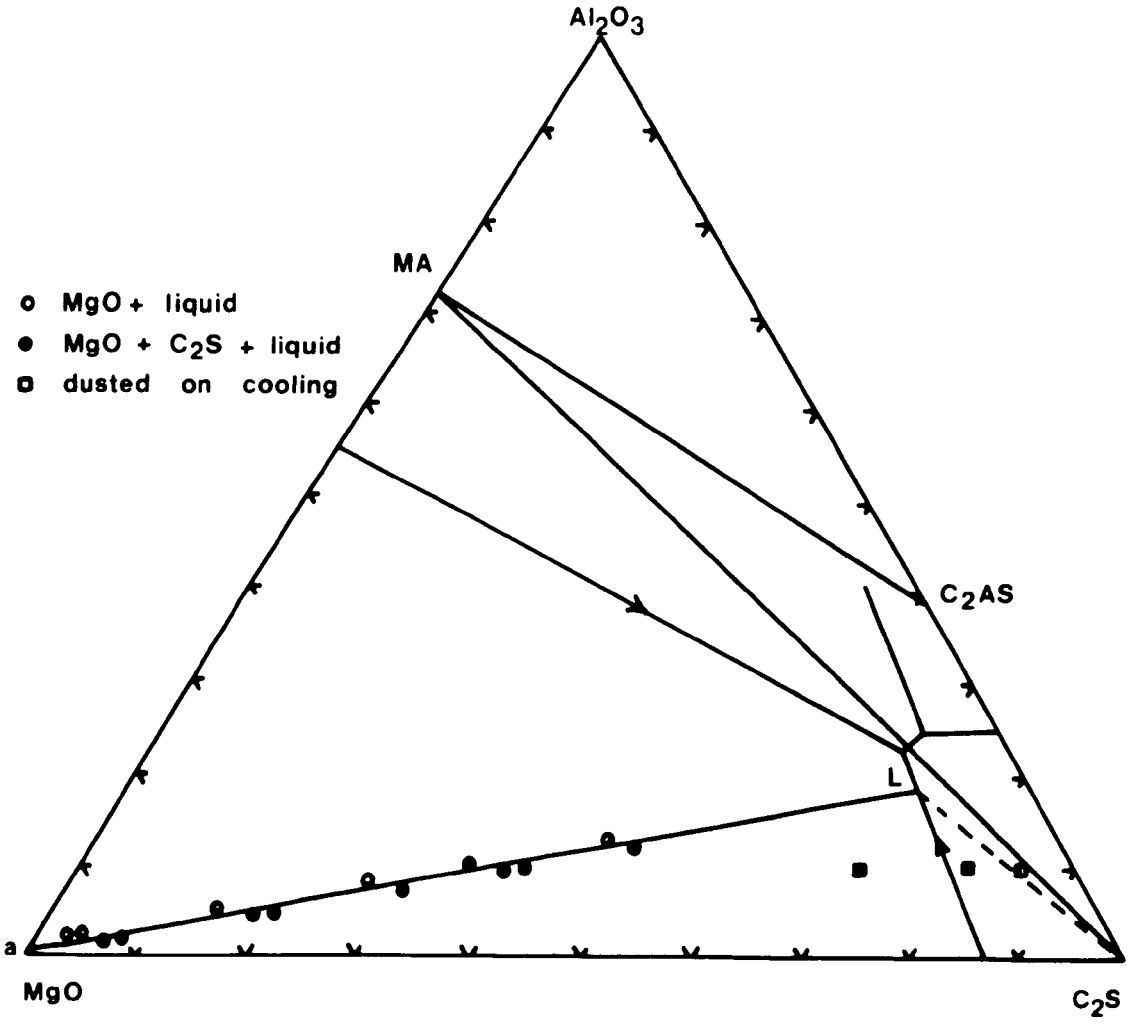
$Al_2O_3$
MA
o MgO + liquid
● MgO + $C_2S$ + liquid
▫ dusted on cooling
$C_2AS$
L
a
MgO
$C_2S$

FIGURE 41

Solid-liquid relationships in air in the system $MgO-Fe_2O_3-C_2S$ (from Taylor[72]). ae, be, en, cn and mn are boundaries on the liquidus surface. Triangles A-L-$C_2S$ and k-f-MF are the tie triangles within which magnesiowustite A and $C_2S$ coexist with liquid L, and magnesiowustite k and MF coexist with liquid f at 1550°C in air. hLfg is the 1550°C isotherm on the liquidus surface.

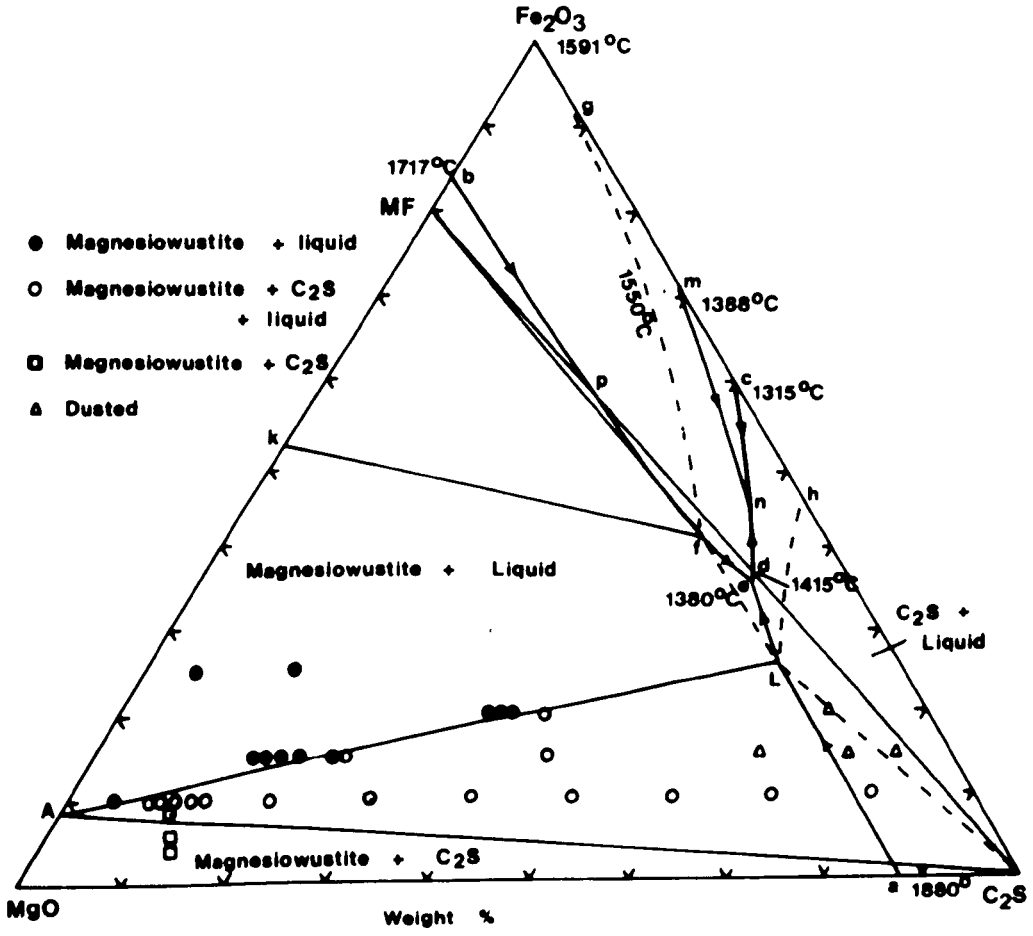
Fe2O3
1591 °C
1717°C
b
MF
g
1550°C
m
1388°C
c
1315°C
p
k
h
n
d
1380°C
e
1415°C
C2S + Liquid
L
Magnesiowustite + Liquid
Magnesiowustite + C2S + liquid
Magnesiowustite + C2S
Dusted
A
Magnesiowustite + C2S
MgO
Weight %
s
1880°
C2S

FIGURE 42

Phase diagram of the section $MgFe_2O_4$-$C_3MS_2$ of the system MgO-$Fe_2O_3$-$C_3MS_2$ after quenching in water.

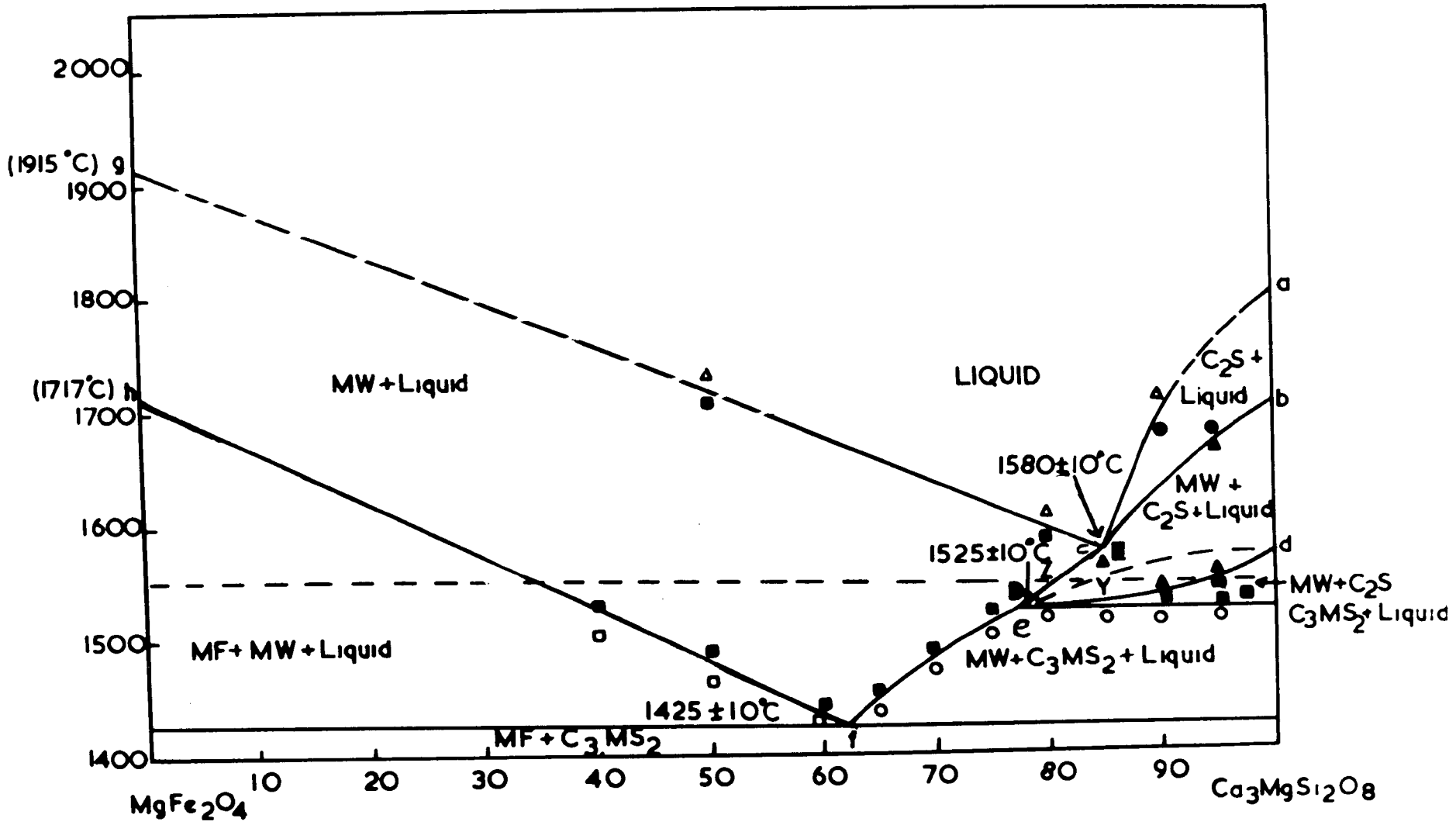
2000
(1915 °C) g
1900
1800
(1717°C) h
1700
1600
1500
1400
MW + Liquid
LIQUID
C2S + Liquid
1580±10°C
MW + C2S + Liquid
1525±10°C
MW+C2S
C3MS2 + Liquid
MF + MW + Liquid
MW+C3MS2 + Liquid
1425 ± 10°C
MF + C3MS2
a
b
c
d
e
f
Y
10
20
30
40
50
60
70
80
90
MgFe2O4
Ca3MgSi2O8

FIGURE 43

The triangle in air at 1550°C in the system MgO-$Fe_2O_3$-$C_3MS_2$ within which magnesiowustite, spinel and liquid L coexist in air at 1550°C. As established by air-quenching.

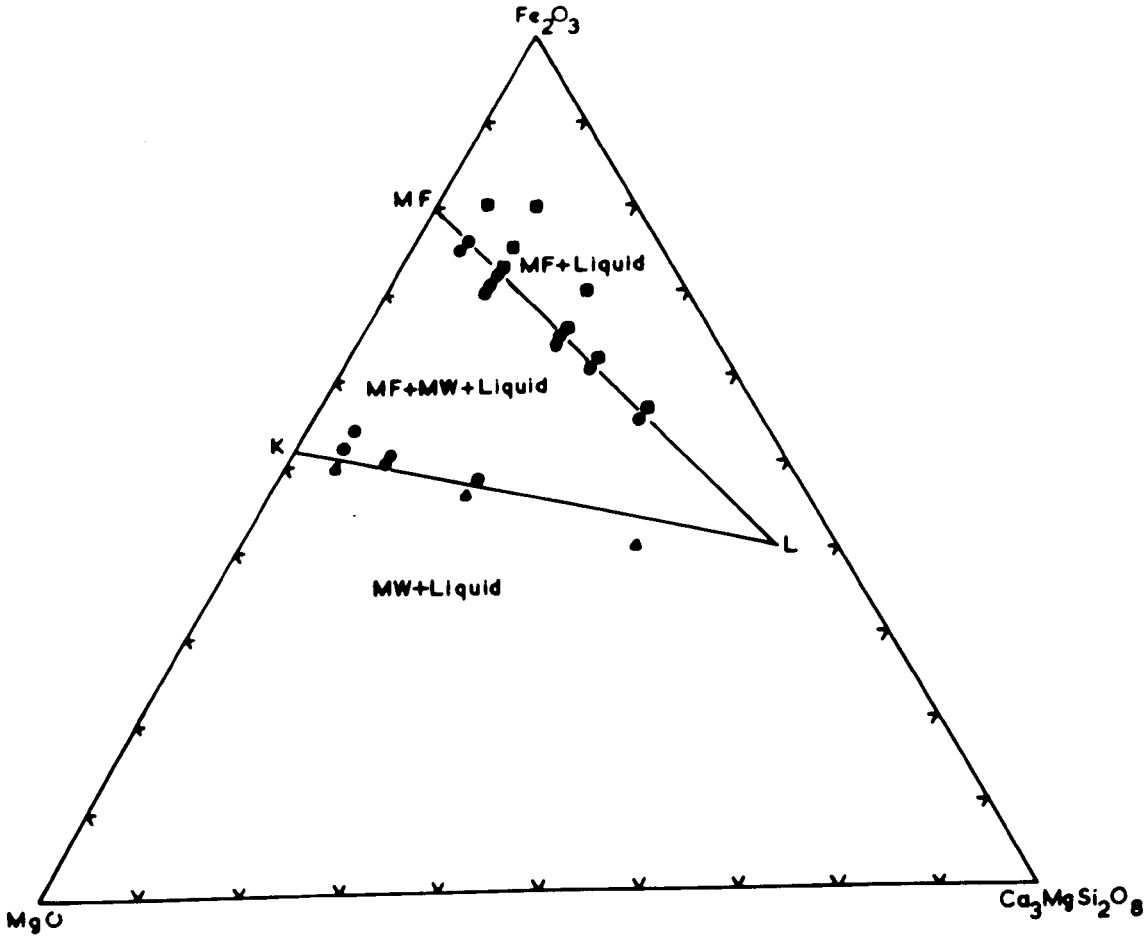
Fe2O3
MF
MF+Liquid
MF+MW+Liquid
K
L
MW+Liquid
MgO
Ca3MgSi2O8

FIGURE 44

The tie triangles in air at 1550°C in the system $MgO-Fe_2O_3-C_3MS_2$ within which magnesiowustite X and $C_3MS_2$ coexist with liquid $L_2$ (triangle $X-L_2-C_3MS_2$) and within which magnesiowustite K and MF coexist with liquid $L_1$ (triangle $K-L_1-MF$). As established by water-quenching.

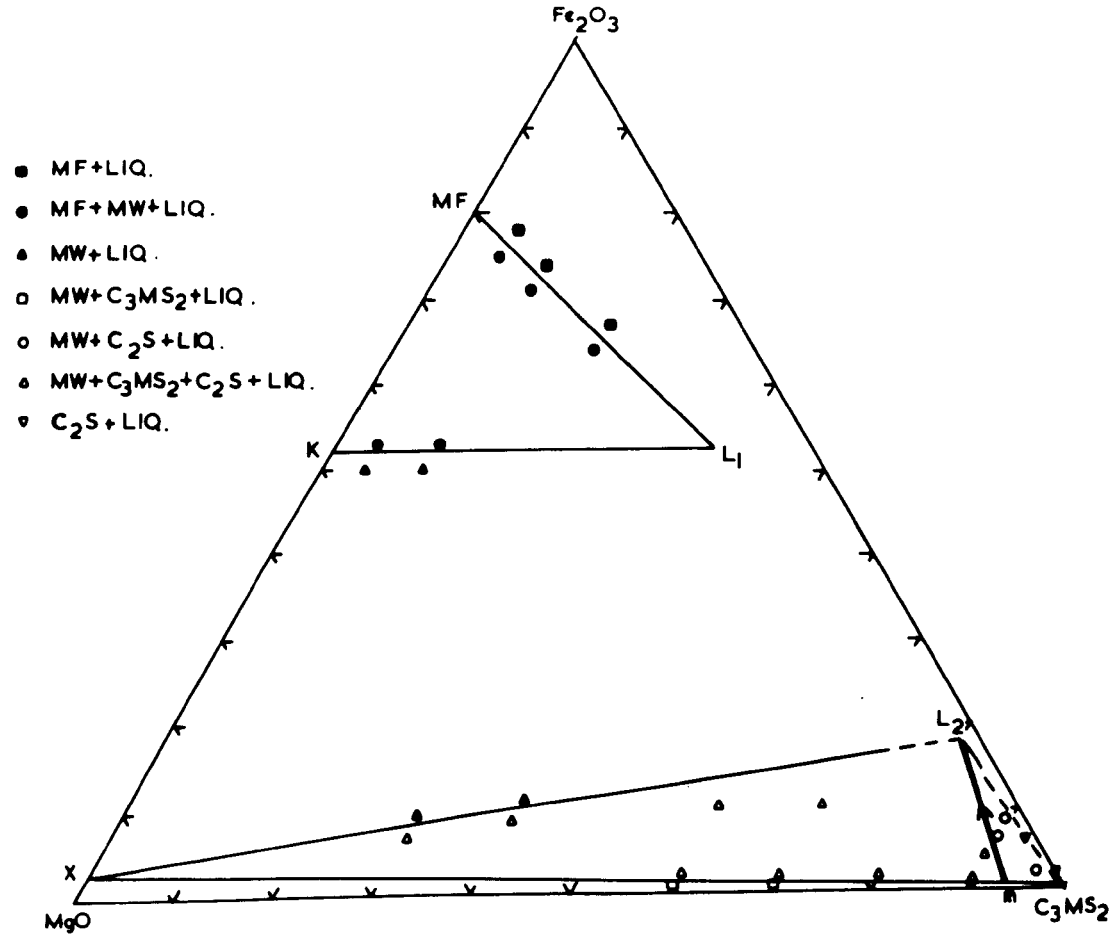
MF+LIQ.
MF+MW+LIQ.
MW+LIQ.
MW+C3MS2+LIQ.
MW+C2S+LIQ.
MW+C3MS2+C2S+LIQ.
C2S+LIQ.
Fe2O3
MF
K
L1
L2
X
MgO
C3MS2

FIGURE 45

A-Boundary surfaces in the composition tetrahedron of the quaternary system $CaO-MgO-Fe_2O_3-SiO_2$ (not to scale) showing their intersections with the plane $MgO-C_3S_2-Fe_2O_3$ and location of the join $MF-C_3MS_2$. B-Section $MF-C_3MS_2$ derived from Figure 15A (see Section 8 for explanation).

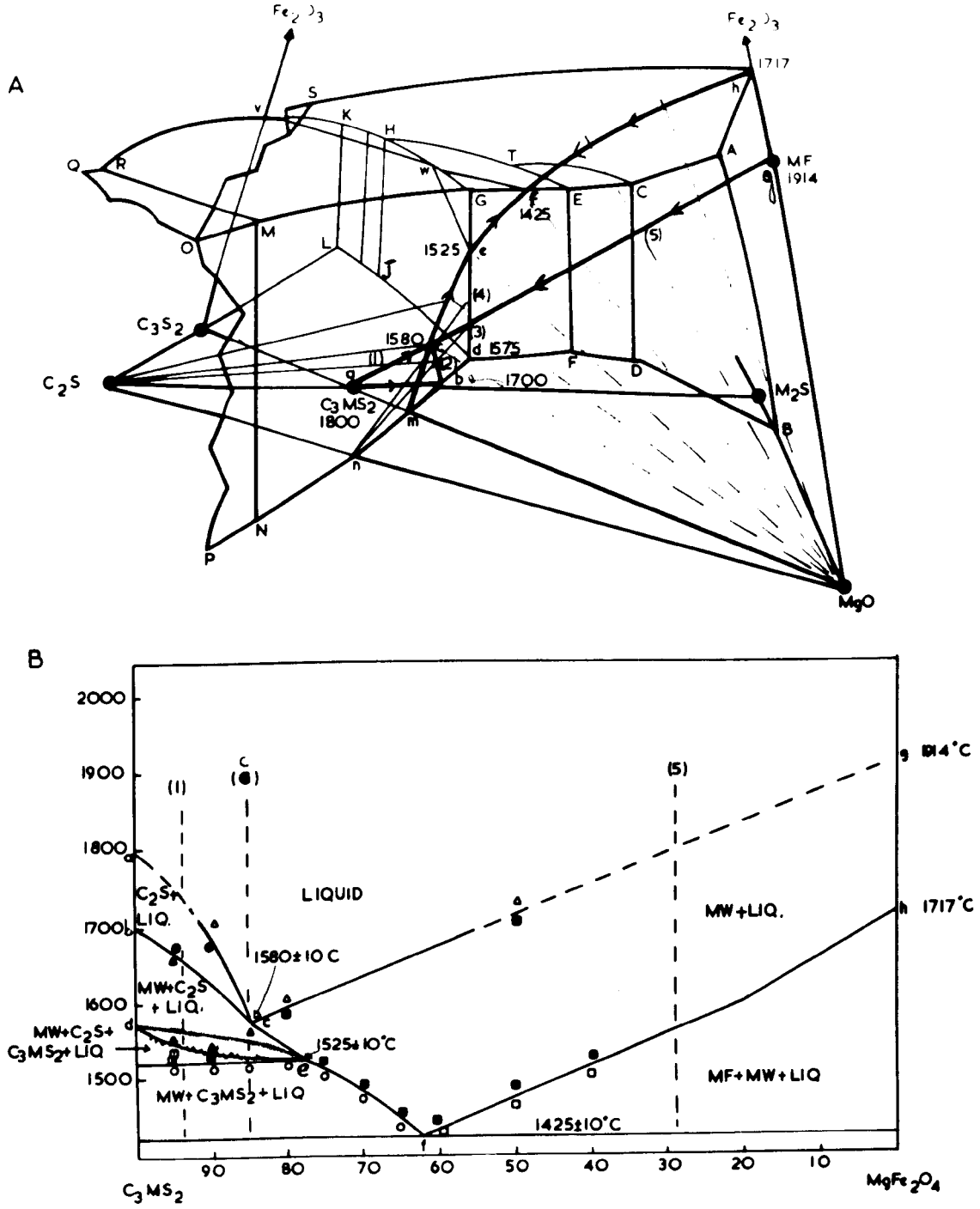
A
$Fe_2O_3$
$Fe_2O_3$
1717
MF
1914
1425
1525
1580
1575
1700
$C_3S_2$
$C_2S$
$C_3MS_2$
1800
$M_2S$
MgO
B
2000
1900
1800
1700
1600
1500
(1)
C
(5)
g 1914°C
h 1717°C
LIQUID
$C_2S$+ LIQ.
1580±10 C
MW+LIQ.
MW+$C_2S$ + LIQ.
MW+$C_2S$+ $C_3MS_2$+LIQ
1525±10°C
MF+MW+LIQ
MW+$C_3MS_2$+LIQ
1425±10°C
90
80
70
60
50
40
30
20
10
$C_3MS_2$
$MgFe_2O_4$

FIGURE 46

Phase diagram of system $MgO-Fe_2O_3-C_3MS_2$ showing boundaries on liquidus surface as deduced from Figures 42 and 45.

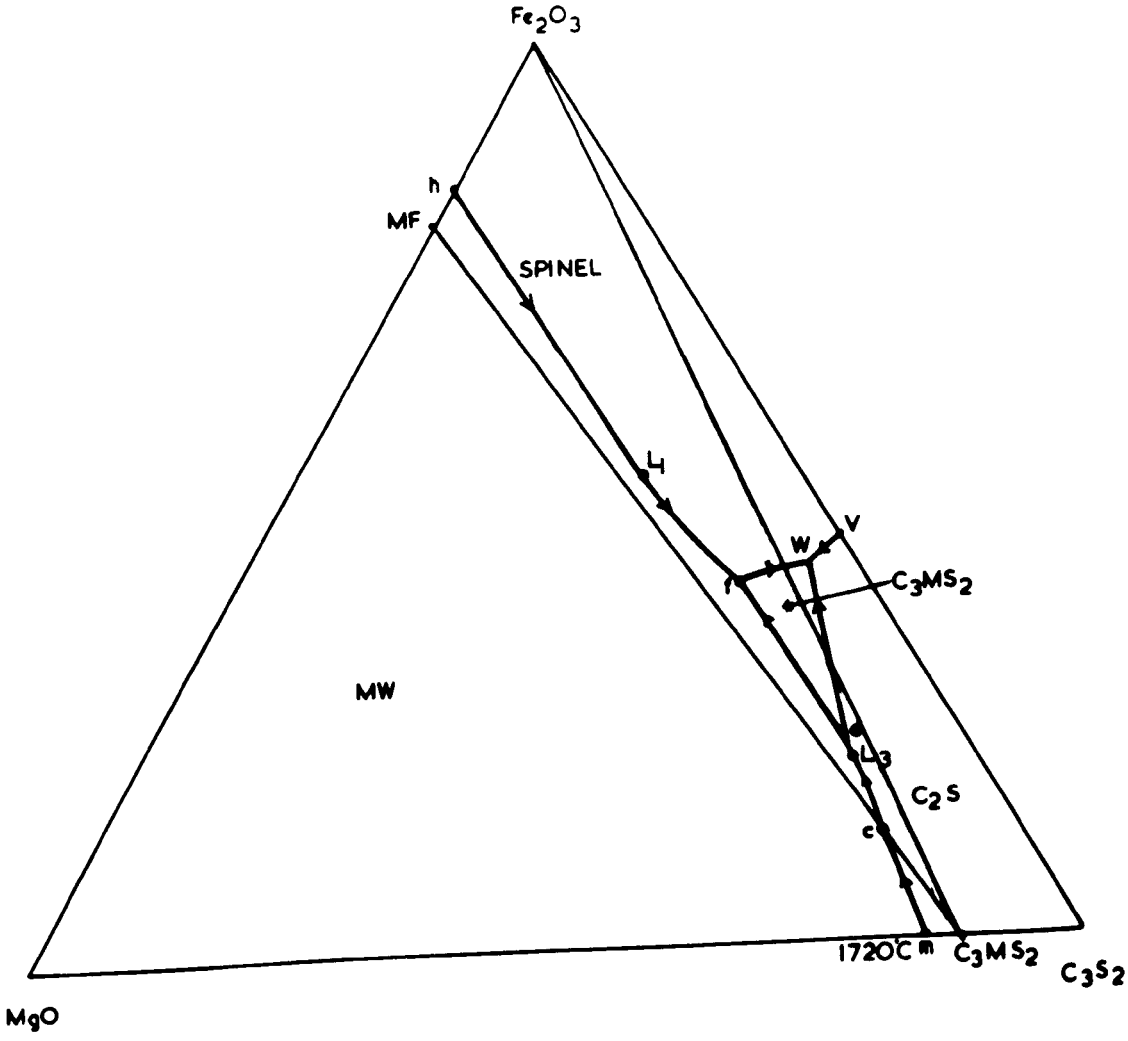
$Fe_2O_3$
h
MF
SPINEL
L4
V
W
r
$C_3MS_2$
MW
L3
$C_2S$
e
1720°C m
$C_3MS_2$
$C_3S_2$
MgO

FIGURE 47

Isotherm at 1550°C in air in the system MgO-$Fe_2O_3$-$C_3S_2$. (See Section 8 for explanation.)

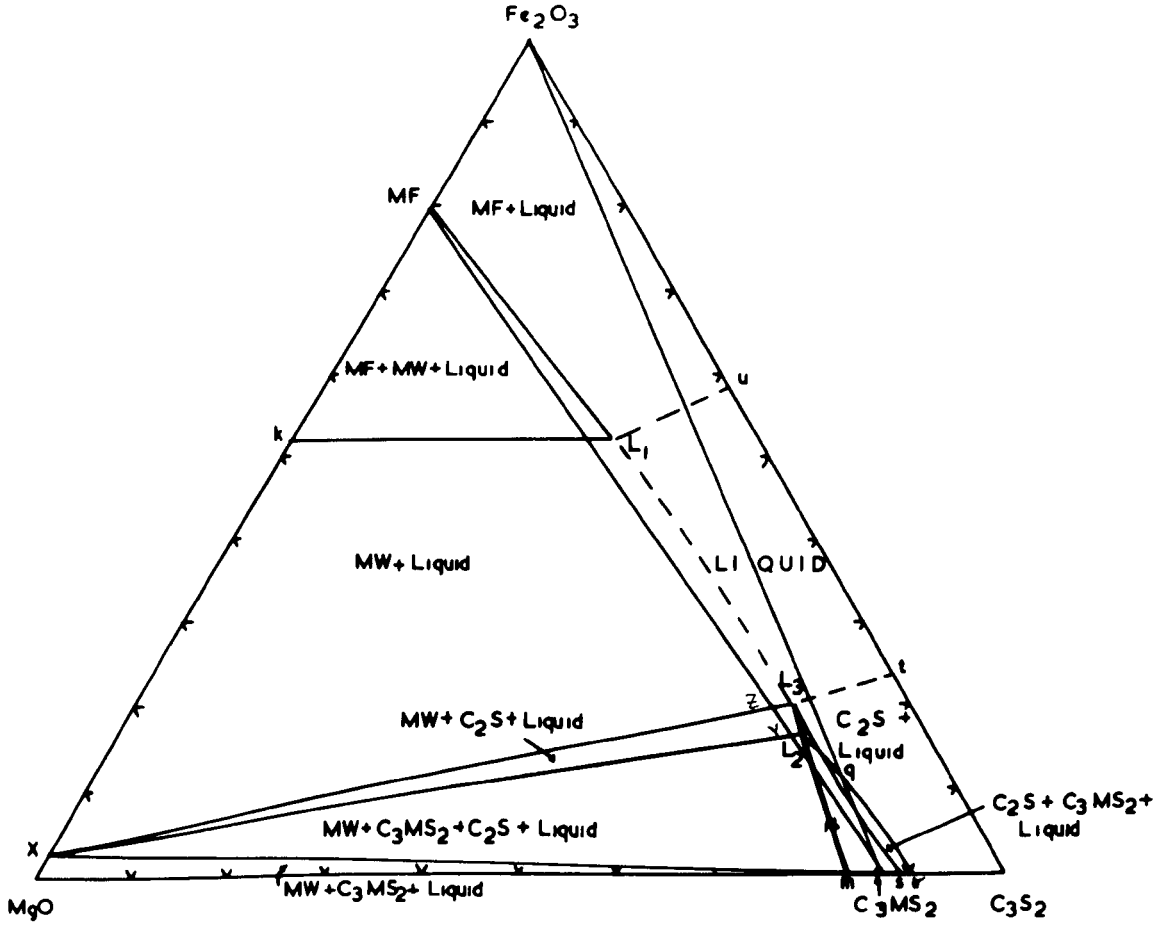
$Fe_2O_3$
MF
MF + Liquid
MF + MW + Liquid
k
u
$L_1$
MW + Liquid
LIQUID
t
$L_3$
z
MW + $C_2S$ + Liquid
$C_2S$ + Liquid
$L_2$
q
$C_2S$ + $C_3MS_2$ + Liquid
MW + $C_3MS_2$ + $C_2S$ + Liquid
x
MW + $C_3MS_2$ + Liquid
MgO
$C_3MS_2$
$C_3S_2$

FIGURE 48

Boundary surfaces in the composition tetrahedron of the quaternary system $CaO-MgO-Fe_2O_3-SiO_2$ as in Figure 45, with isothermal phase boundaries at 1550°C in the section $MgO-C_3S_2-Fe_2O_3$ indicated. (See Section 8 for explanation.)

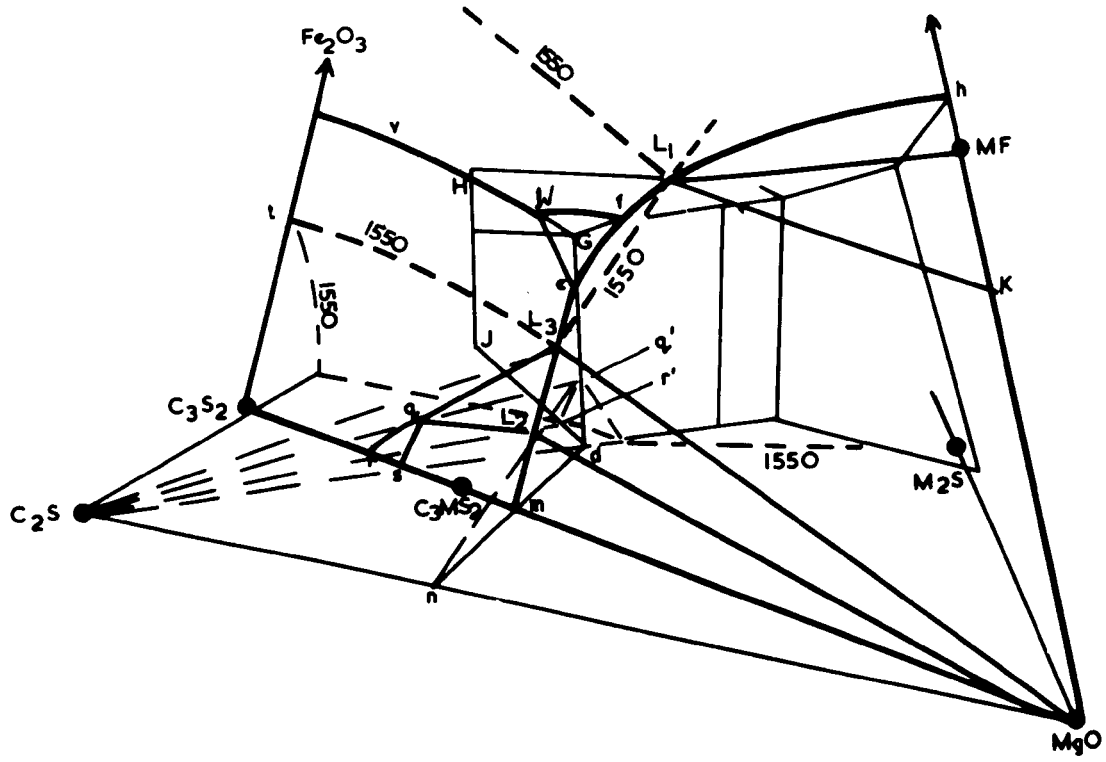
$Fe_2O_3$
1580
h
v
$L_1$
MF
H
W
t
1550
G
K
1550
1550
J
$K_3$
q'
r'
$C_3S_2$
q
$L_2$
1550
$M_2S$
$C_2S$
$C_3MS_2$
m
n
MgO

FIGURE 49

Phase diagram of the system $MgAl_2O_4$-$Ca_2MgSi_2O_8$ as established by water-quenching.

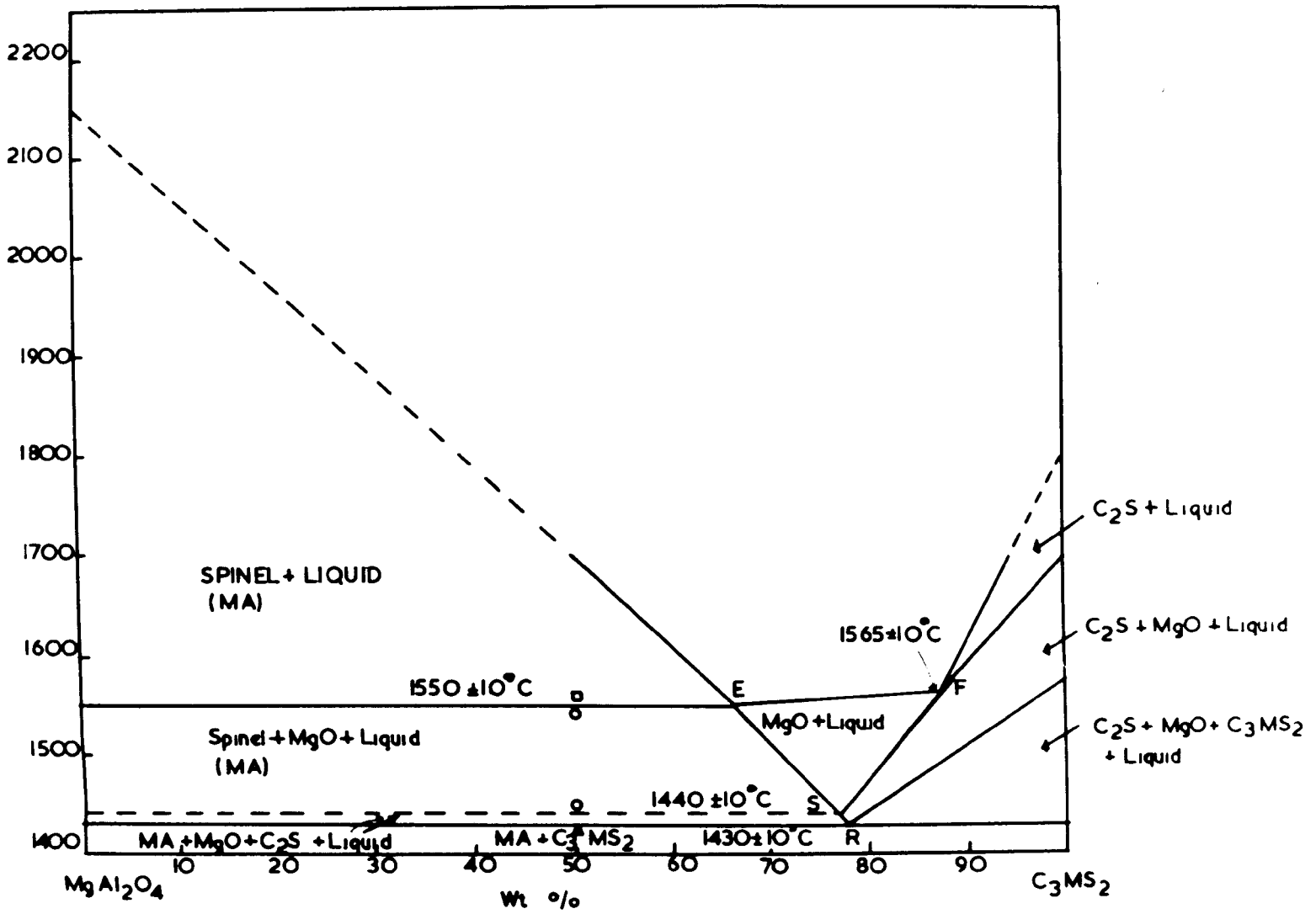
2200
2100
2000
1900
1800
1700
1600
1500
1400
SPINEL + LIQUID
(MA)
1550 ±10°C
D
E
1565±10°C
F
C2S + Liquid
C2S + MgO + Liquid
MgO + Liquid
Spinel + MgO + Liquid
(MA)
C2S + MgO + C3MS2
+ Liquid
1440 ±10°C
S
MA + MgO + C2S + Liquid
MA + C3MS2
1430±10°C
R
10
20
30
40
50
60
70
80
90
MgAl2O4
Wt %
C3MS2

FIGURE 50

Phase diagram of the system $MgCr_2O_4$-$Ca_2MgSi_2O_8$ as established by water-quenching.

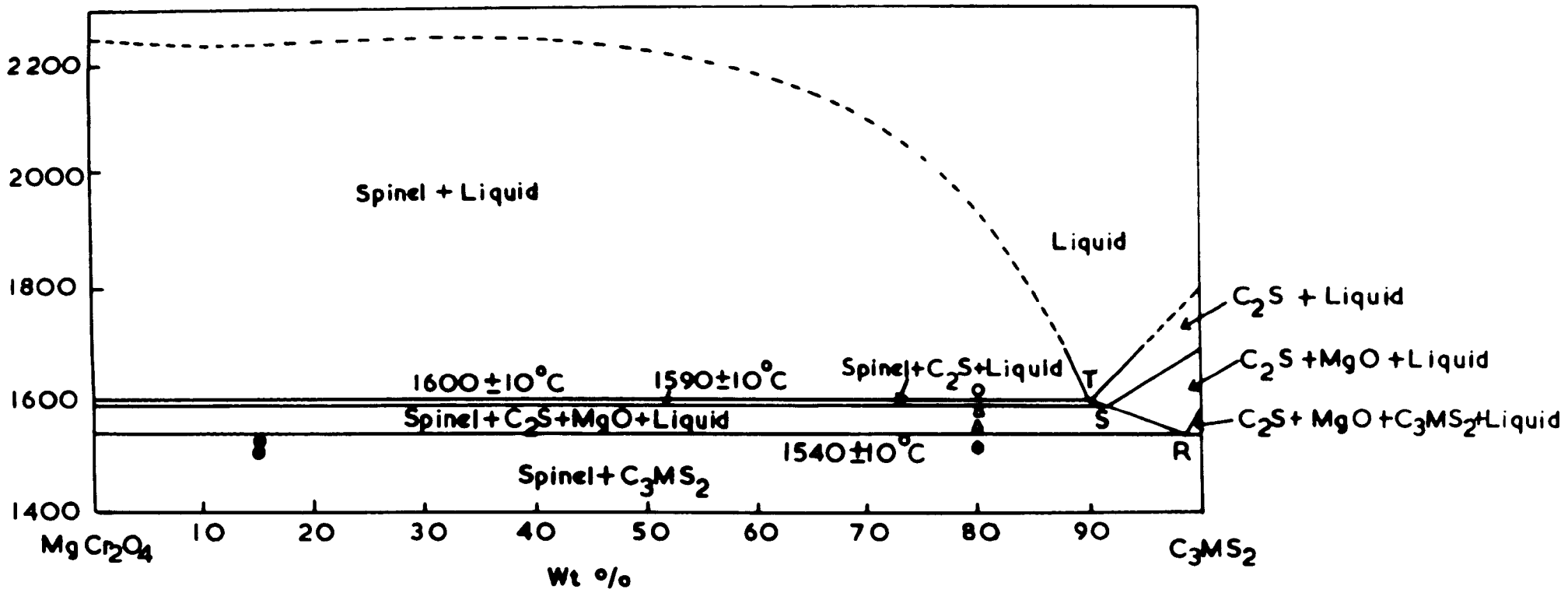
2200
2000
1800
1600
1400
Spinel + Liquid
Liquid
$C_2S$ + Liquid
$C_2S$ + MgO + Liquid
$C_2S$ + MgO + $C_3MS_2$ + Liquid
1600 ± 10°C
1590 ± 10°C
Spinel + $C_2S$ + Liquid
T
Spinel + $C_2S$ + MgO + Liquid
S
1540 ± 10°C
R
Spinel + $C_3MS_2$
$MgCr_2O_4$
10
20
30
40
50
60
70
80
90
$C_3MS_2$
Wt %

FIGURE 51

Phase diagram of the section $MgAl_{1.5}Cr_{0.5}O_4$-$Ca_3MgSi_2O_8$ of the system $MgAl_2O_4$-$MgCr_2O_4$-$Ca_3MgSi_2O_8$ as established by water quenching.

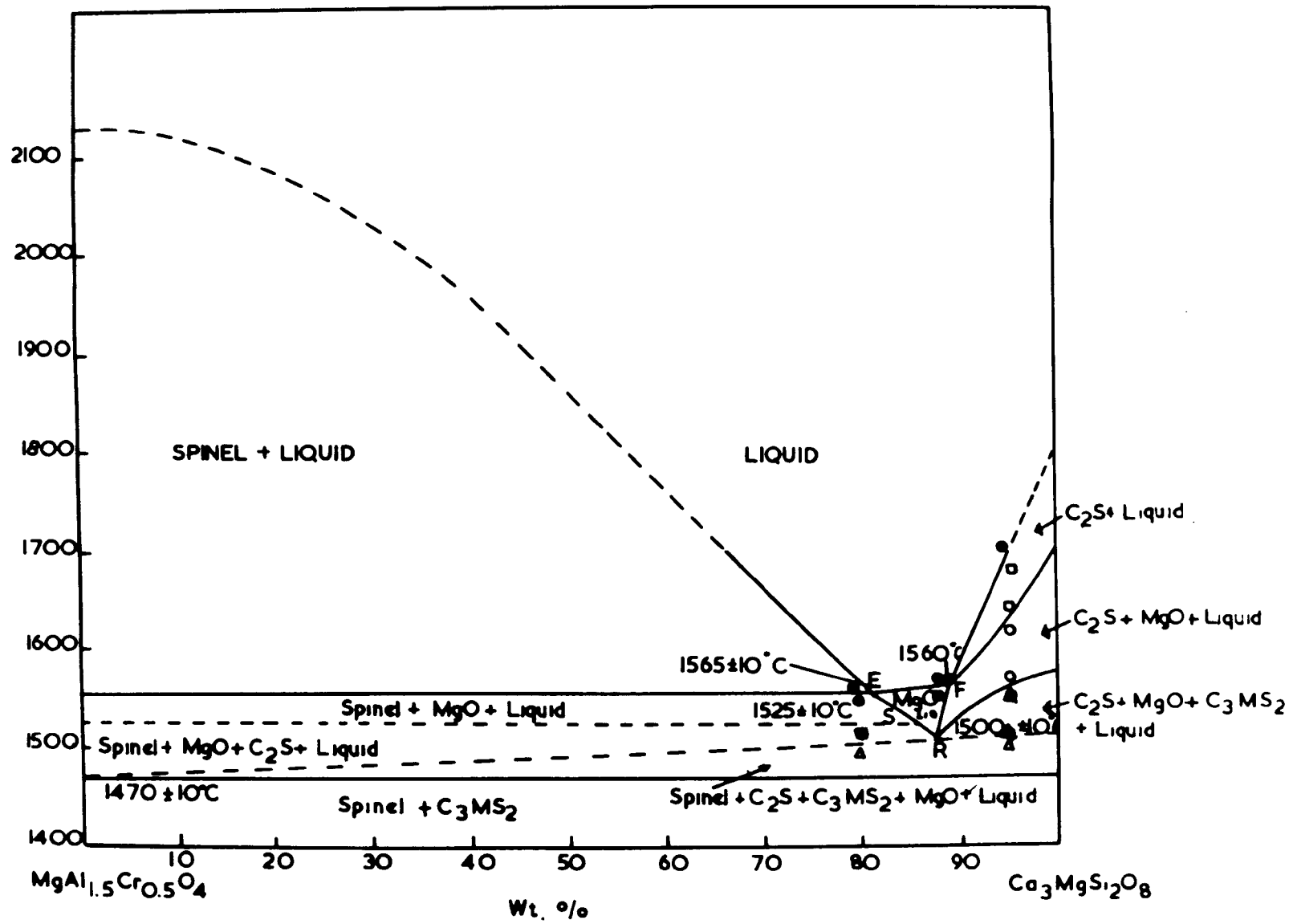
2100
2000
1900
1800
1700
1600
1500
1400
SPINEL + LIQUID
LIQUID
$C_2S$ + Liquid
$C_2S$ + MgO + Liquid
1565±10°C
1560°C
E
F
MgO
Spinel + MgO + Liquid
1525±10°C
S
R
Spinel + MgO + $C_2S$ + Liquid
$C_2S$ + MgO + $C_3MS_2$ + Liquid
1470±10°C
Spinel + $C_3MS_2$
Spinel + $C_2S$ + $C_3MS_2$ + MgO + Liquid
10
20
30
40
50
60
70
80
90
$MgAl_{1.5}Cr_{0.5}O_4$
$Ca_3MgSi_2O_8$
Wt. %

FIGURE 52

Phase diagram of the section $MgAl_{0.8}Cr_{1.2}O_4$-$Ca_3MgSi_2O_8$ of the system $MgAl_2O_4$-$MgCr_2O_4$-$Ca_3MgSi_2O_8$ as established by quenching in water.

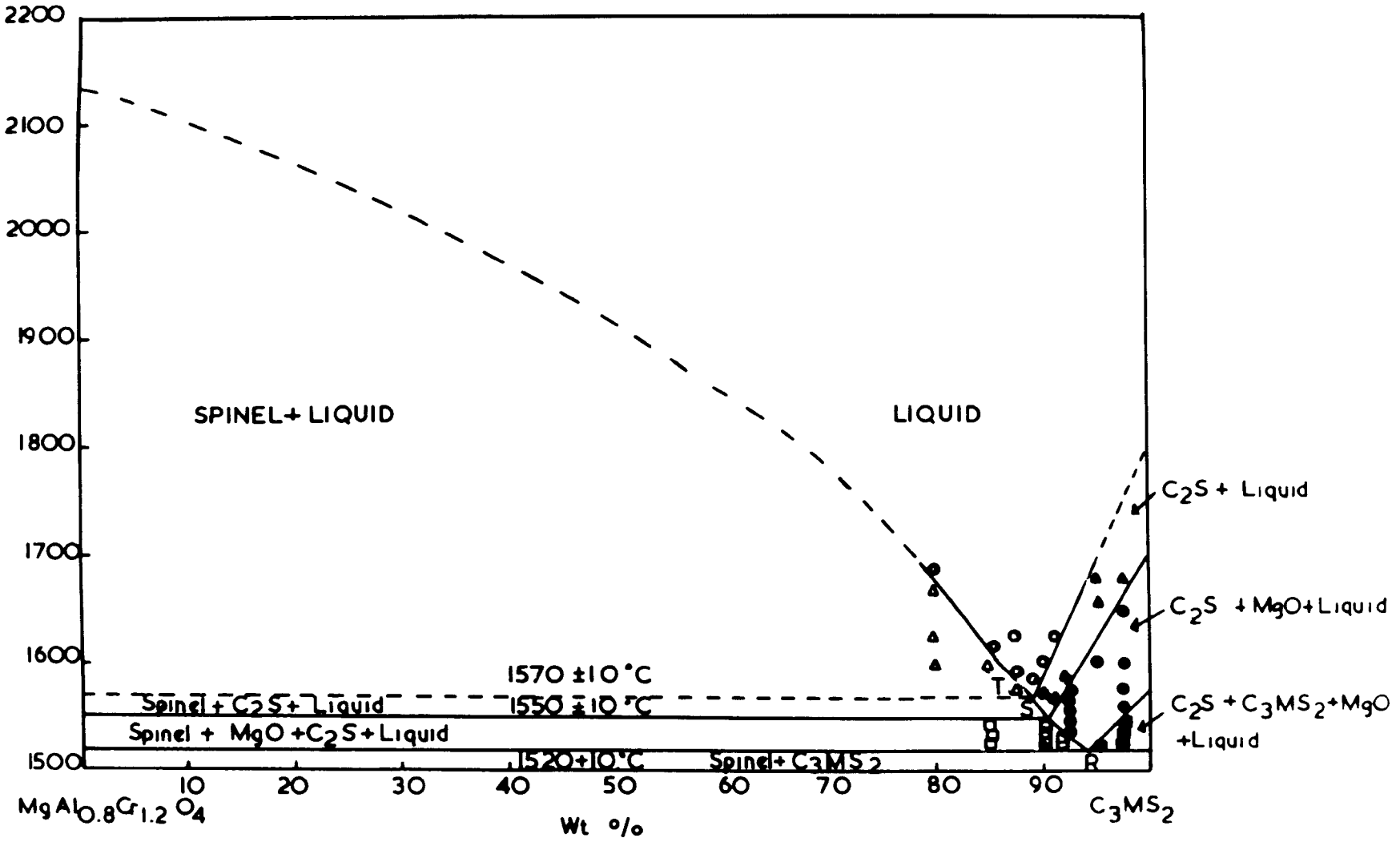
2200
2100
2000
1900
1800
1700
1600
1500
SPINEL + LIQUID
LIQUID
$C_2S$ + Liquid
$C_2S$ + MgO + Liquid
$C_2S$ + $C_3MS_2$ + MgO + Liquid
1570 ±10 °C
1550 ±10 °C
1520 ±10 °C
Spinel + $C_2S$ + Liquid
Spinel + MgO + $C_2S$ + Liquid
Spinel + $C_3MS_2$
T
S
R
10
20
30
40
50
60
70
80
90
$MgAl_{0.8}Cr_{1.2}O_4$
Wt %
$C_3MS_2$

FIGURE 53

Phase diagram of the system $MgCr_2O_4$-$Ca_3MgSi_2O_8$ from El-Shahat and White[3] as established by quenching in air.

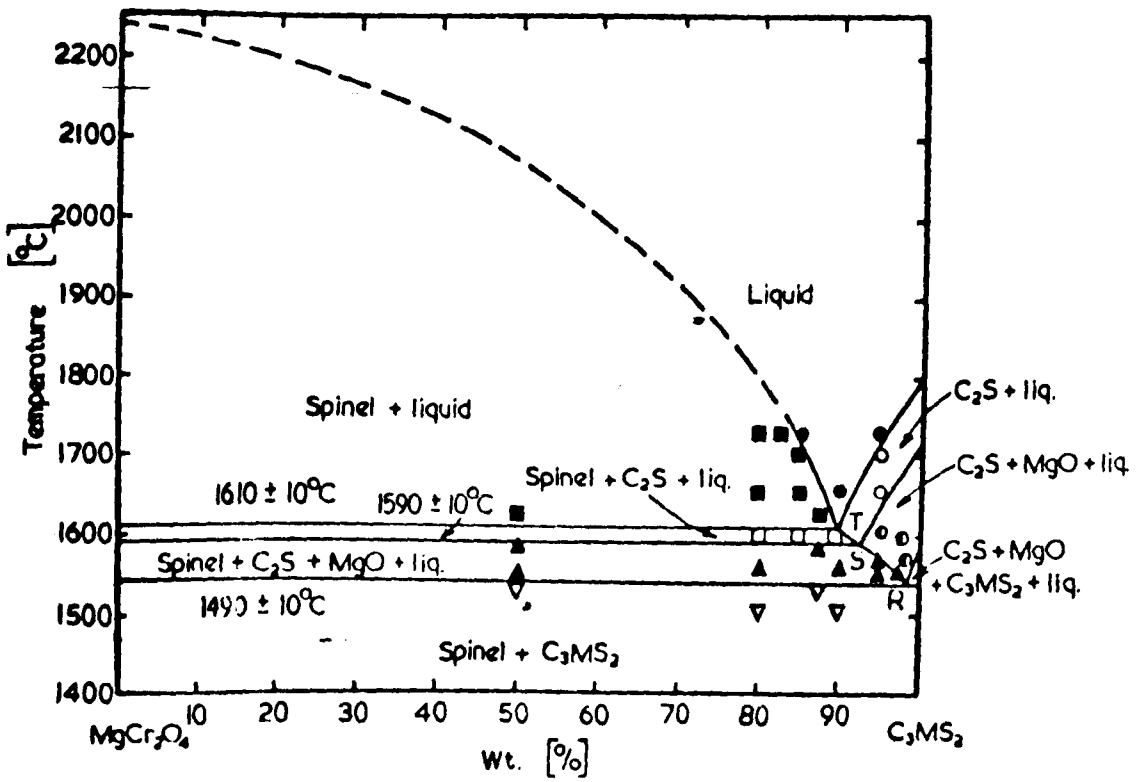
2200
2100
2000
1900
1800
1700
1600
1500
1400
Temperature [°C]
Liquid
Spinel + liquid
Spinel + C2S + liq.
1610 ± 10°C
1590 ± 10°C
Spinel + C2S + MgO + liq.
1490 ± 10°C
Spinel + C3MS2
C2S + liq.
C2S + MgO + liq.
C2S + MgO
+ C3MS2 + liq.
T
S
R
10
20
30
40
50
60
70
80
90
MgCr2O4
C3MS2
Wt. [%]

FIGURE 53

Phase diagram of the system $MgCr_2O_4$-$Ca_3MgSi_2O_8$ from El-Shahat and White[3] as established by quenching in air.

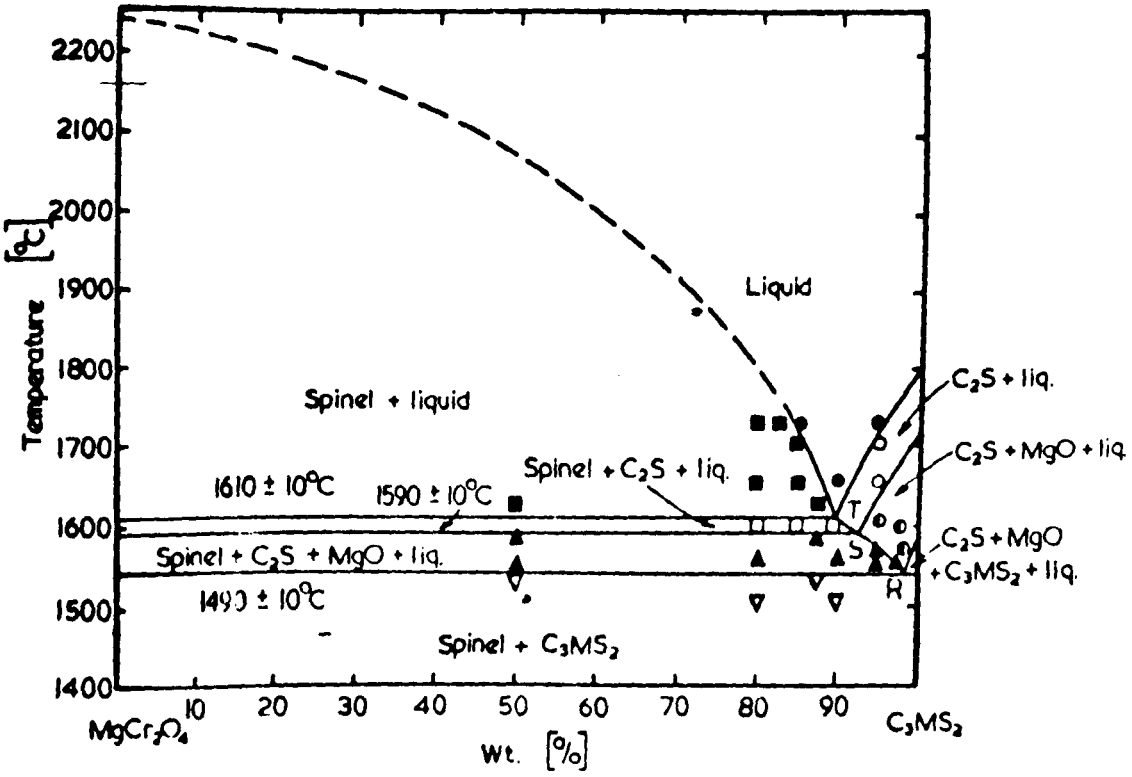
2200
2100
2000
1900
1800
1700
1600
1500
1400
Temperature [°C]
Liquid
Spinel + liquid
Spinel + C2S + liq.
1610 ± 10°C
1590 ± 10°C
Spinel + C2S + MgO + liq.
1490 ± 10°C
Spinel + C3MS2
C2S + liq.
C2S + MgO + liq.
C2S + MgO
+ C3MS2 + liq.
T
S
R
10
20
30
40
50
60
70
80
90
MgCr2O4
C3MS2
Wt. [%]

FIGURE 54

Phase diagram of the section $MgAl_{1.5}Cr_{0.5}O_4$-$Ca_3MgSi_2O_8$ of the system $MgAl_2O_4$-$MgCr_2O_4$-$Ca_3MgSi_2O_8$ from El-Shahat and White[3] as established by quenching in air.

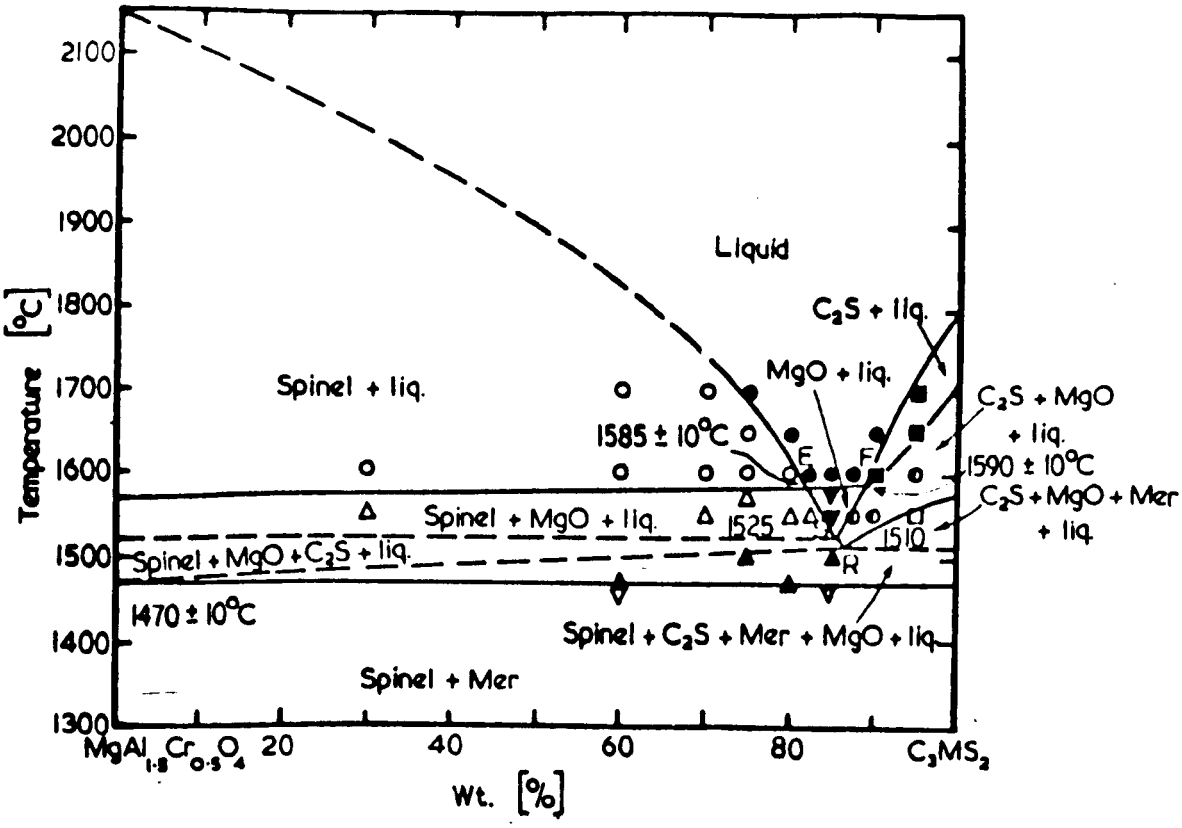
2100
2000
1900
1800
1700
1600
1500
1400
1300
Temperature [°C]
Liquid
C2S + liq.
MgO + liq.
Spinel + liq.
C2S + MgO + liq.
1585 ± 10°C
1590 ± 10°C
E
F
Spinel + MgO + liq.
1525
1510
C2S + MgO + Mer + liq.
Spinel + MgO + C2S + liq.
R
1470 ± 10°C
Spinel + C2S + Mer + MgO + liq.
Spinel + Mer
MgAl1.8Cr0.2O4
20
40
60
80
C3MS2
Wt. [%]

FIGURE 55

Liquidus surface of the pseudo-ternary system $MgAl_2O_4$-$MgCr_2O_4$-$Ca_2MgSi_2O_8$ constructed from Figures 49, 50, 51 and 52 showing primary crystallization fields of MgO, $Ca_2SiO_4$ and spinel. Arrows show direction of falling temperature along phase boundaries. Only the upper part of the composition triangle is shown.

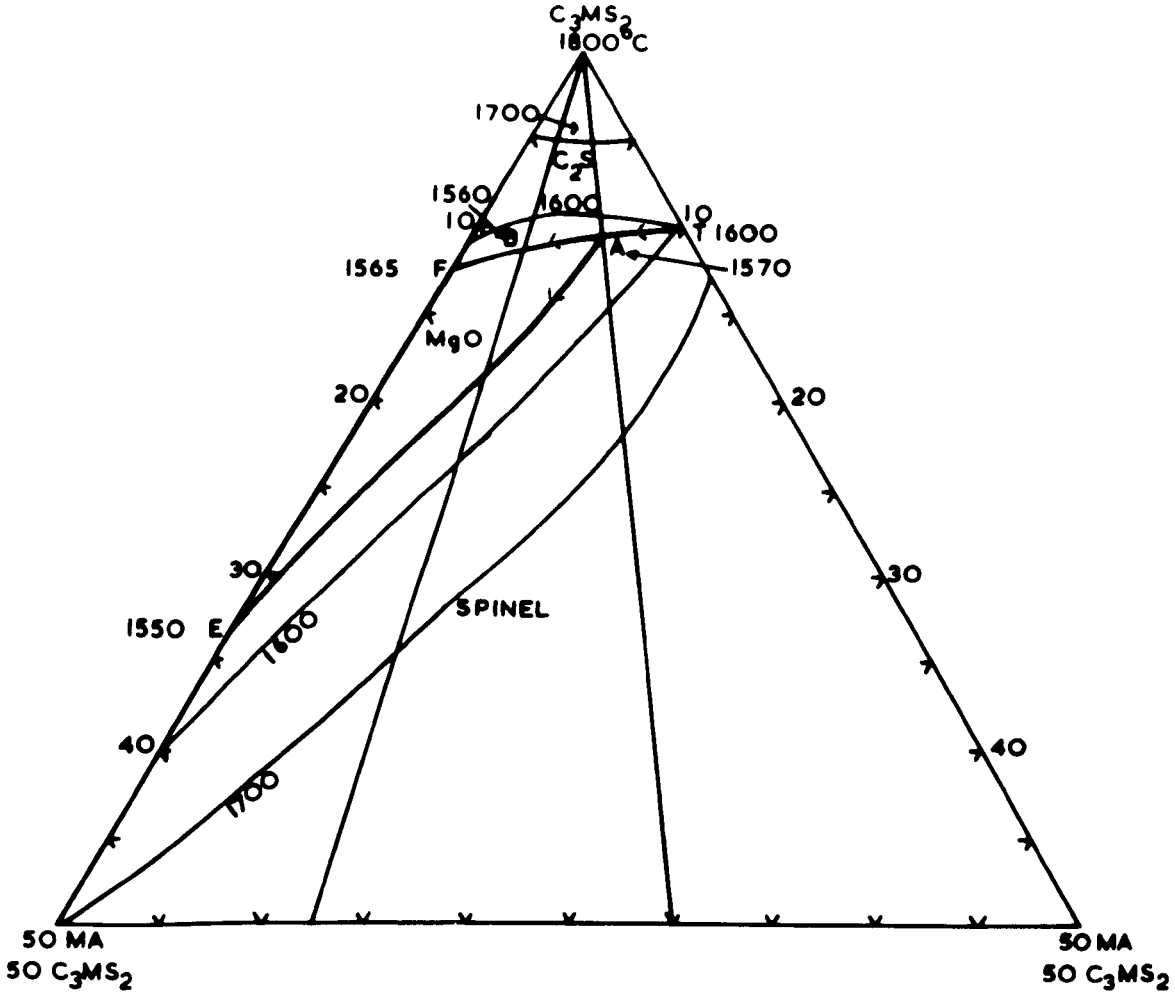
$C_3MS_2$
1800°C
1700
$C_2S$
1560
1600
10
1600
1565
F
1570
MgO
20
20
30
30
1550
E
1600
SPINEL
40
40
1700
50 MA
50 $C_3MS_2$
50 MA
50 $C_3MS_2$

PLATE 1

Micrograph of a specimen containing 80 wt.% MgO and 20 wt.% of a mixture consisting of 13 wt.% $Al_2O_3$ : 35 wt.% $SiO_2$ and 52 wt.% CaO after firing for 15 hrs. at 1500°C. It shows rounded grains of periclase in a matrix that was liquid at 1500°C. Black spots are pores.
(Magnification x 460.)

PLATE 2

Micrograph of a specimen containing 80 wt.% MgO and 20 wt.% of a mixture consisting of 10 wt.% $Al_2O_3$, 45 wt.% $SiO_2$ and 45 wt.% CaO after firing for 15 hrs. at 1420°C. It shows rounded light grey grains of periclase and medium grains (characteristically criss-crossed) of merwinite in a matrix that was liquid at 1420°C. Black spots are pores. Sample etched with Ammonium Chloride Solution.
(Magnification x 460.)

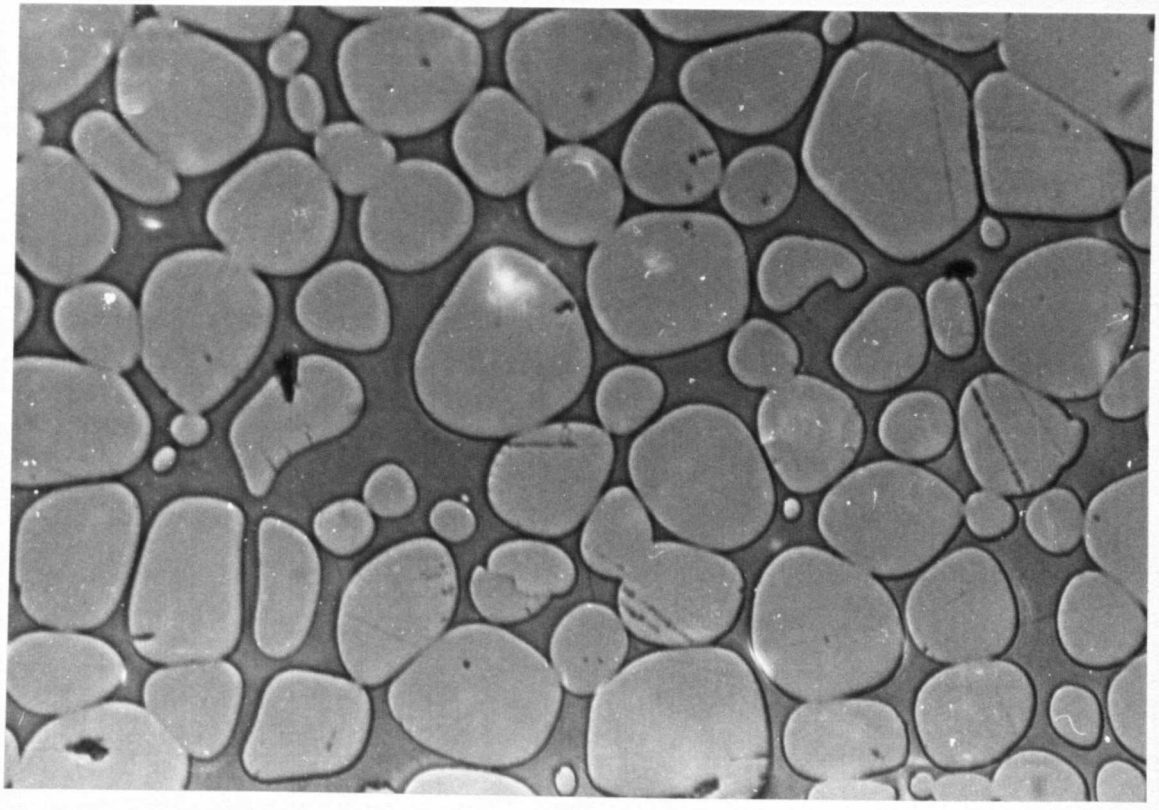

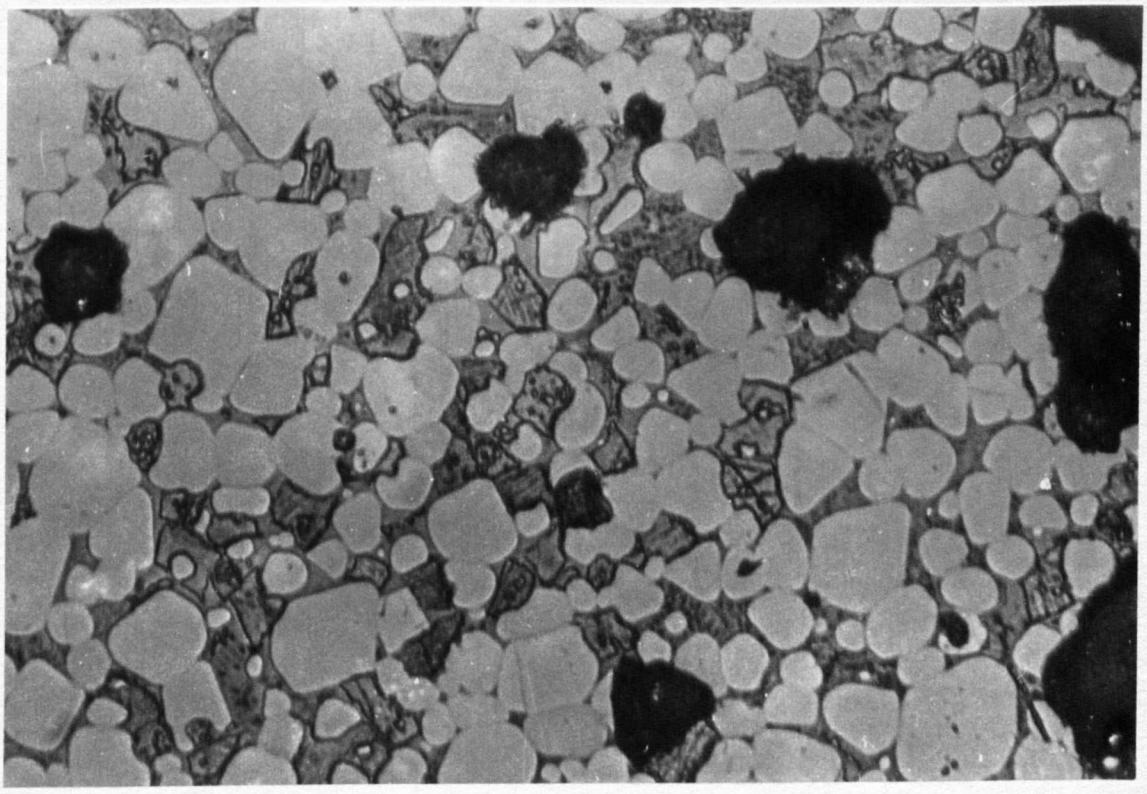

PLATE 3A

Micrograph of the same composition as Plate 1 after firing for 20 hrs. at 1490°C. Final polishing carried out with $\gamma$-$Al_2O_3$. It shows rounded light grey grains of periclase (being the primary phase) and rounded twinned grains of $C_2S$ in a matrix that was liquid at 1490°C. Black spots are pores.
(Magnification x 460.)

PLATE 3B

The same area as in Plate 3A but after etching in Ammonium Chloride Solution. The rounded twinned grains of $C_2S$ are darkened by etching.
(Magnification x 460.)

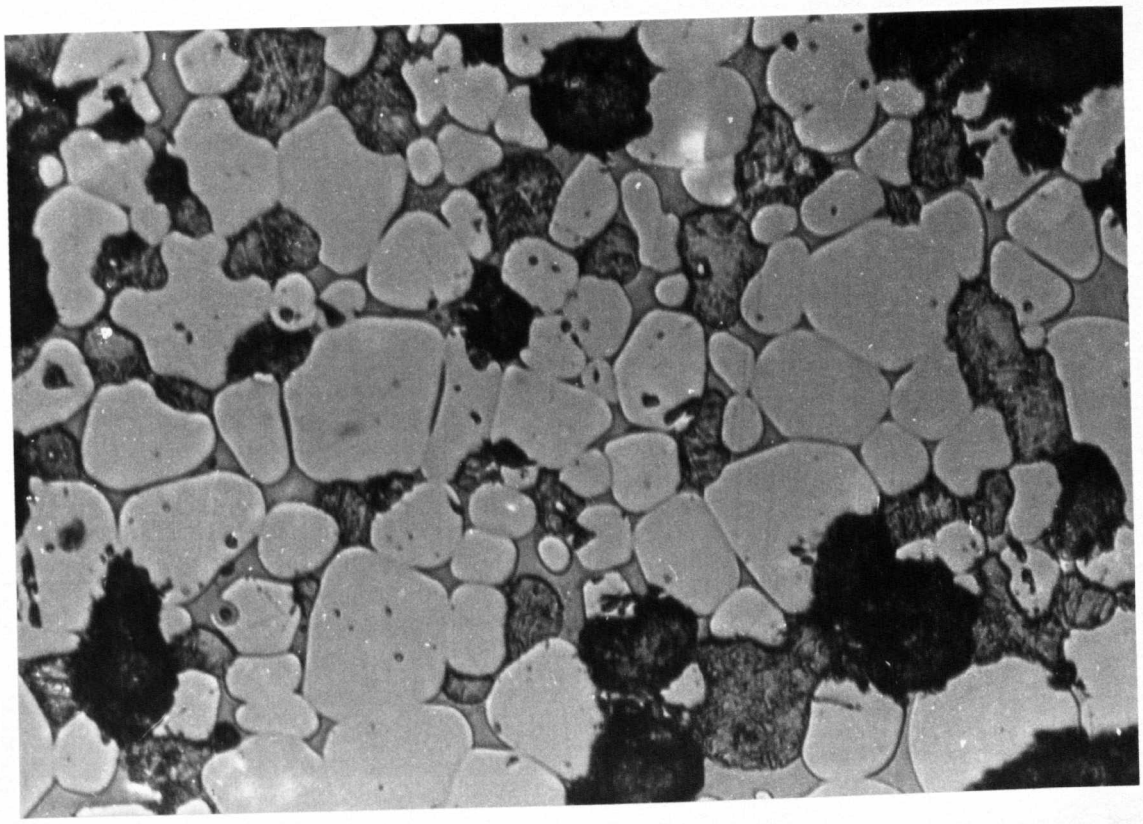

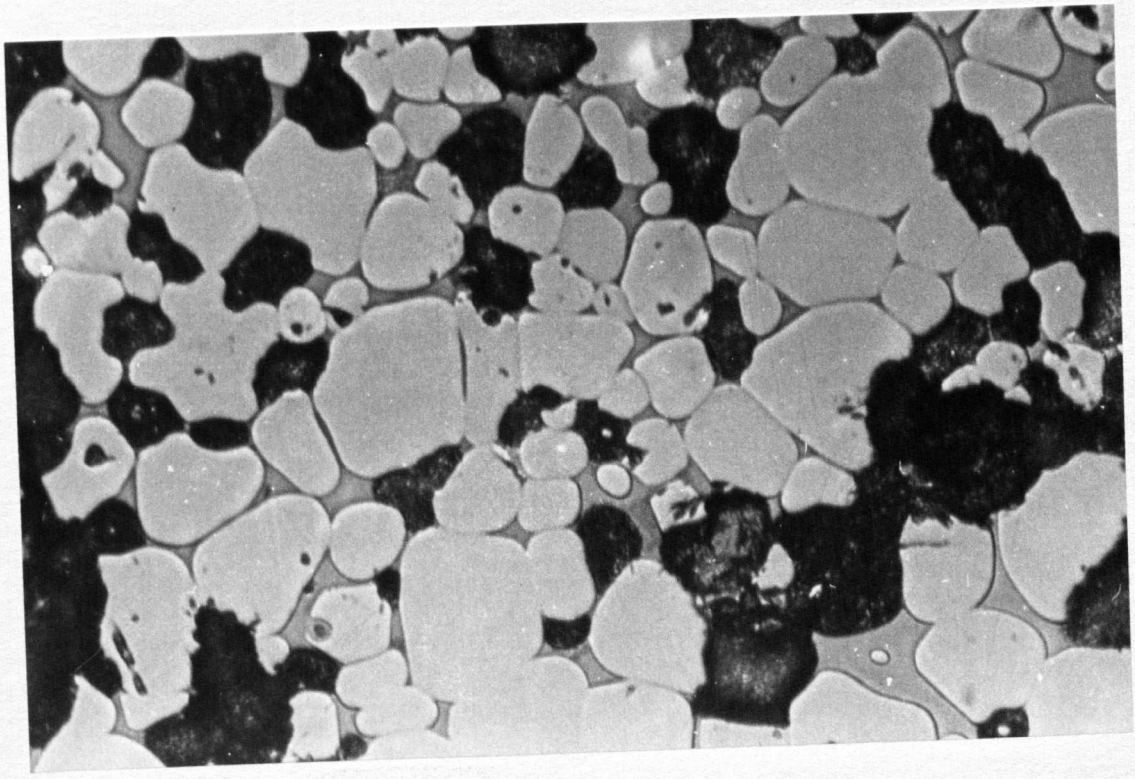

PLATE 4

Micrograph of a specimen containing 80 wt.% MgO and 20 wt.% of a mixture consisting of 10 wt.% $Al_2O_3$, 49 wt.% $SiO_2$ and 41 wt.% CaO after firing 15 hrs. at 1420°C. It shows rounded grains of periclase and large grey grains of monticellite (it has the same appearance as the liquid phase) in a matrix that was liquid at 1420°C. Sample etched with 10% HCl solution. Black areas are pores.
(Magnification x 460.)

PLATE 5

Micrograph of a specimen containing 80 wt.% MgO and 20 wt.% of a mixture consisting of 28 wt.% $Al_2O_3$, 52 wt. % $SiO_2$ and 20 wt.% CaO after firing for 10 hrs. at 1590°C. It shows rounded, light grey grains of periclase and forsterite grains (dark grey - platey) in a matrix that was liquid at 1590°C. Final polishing carried out in $\gamma$-alumina.
Black areas are pores.
(Magnification x 460.)

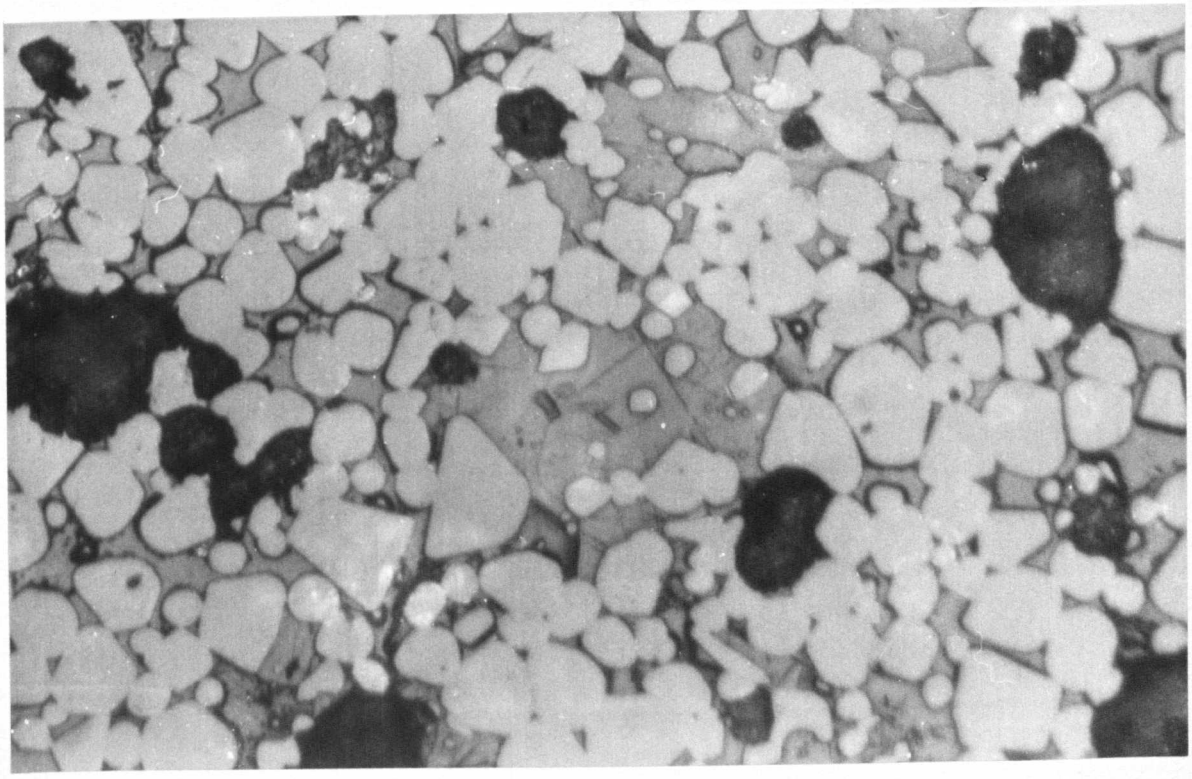

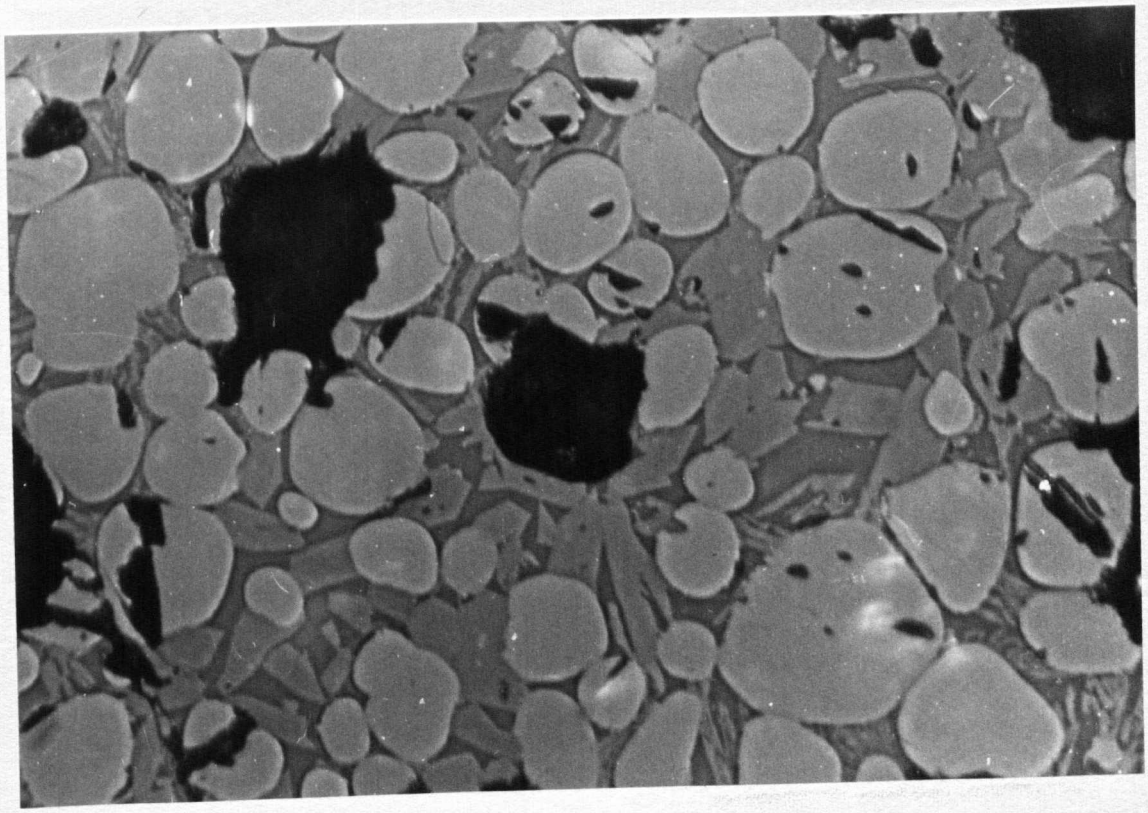

PLATE 6

Micrograph of a specimen containing 80 wt.% MgO and 20 wt.% of a mixture consisting of 25 wt.% $Al_2O_3$, 45 wt.% $SiO_2$ and 30 wt.% CaO after firing for 24 hrs. at 1530°C. It shows rounded light grey grains of periclase and MA spinel (small angular grains) in a matrix that was liquid at 1530°C.

Black spots are pores.

(Magnification x 460.)

PLATE 7

Micrograph of a specimen containing 60 wt.% MgO, 15 wt.% $Cr_2O_3$ and 25 wt.% $C_2S$ of the isoplethal section 60 wt.% MgO and 40 wt.% ($Cr_2O_3$ and $C_2S$) after firing 15 hrs. at 1620°C. It shows rounded light grains of periclase, chrome spinel (angular bright grains) and $C_2S$ (dark grains) in a matrix that was liquid at 1620°C. Large grey grains are resin. Etched in Borax solution.

(Magnification x 460.)

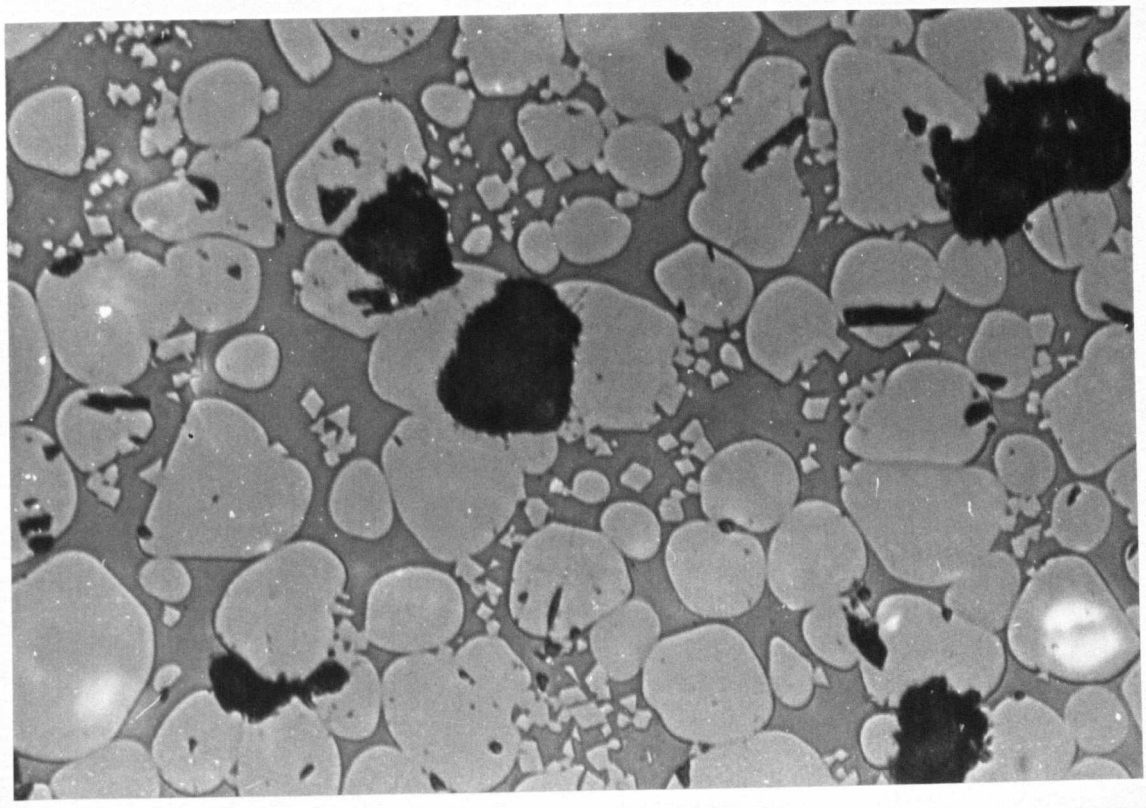

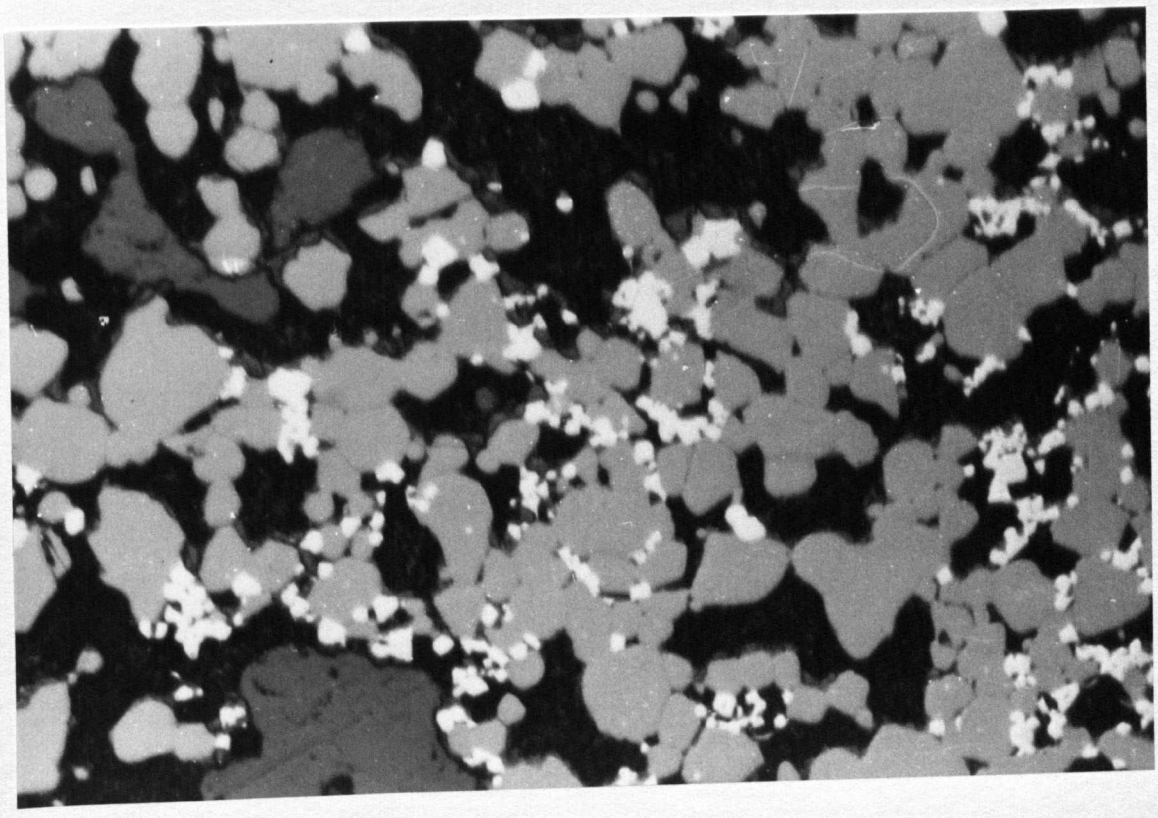

PLATE 8

Micrograph of a specimen containing 60 wt.% MgO, 13 wt.% $Cr_2O_3$ and 27 wt.% $C_2S$ of the isoplethal section at 60 wt.% MgO and 40 wt.% ($Cr_2O_3$ and $C_2S$) after firing 15 hrs. at 1620°C.
It shows rounded light grey grains of periclase and $C_2S$ (dark grey) in a matrix that was liquid at 1620°C. Large grey grains are resin.
Etched in Borax solution.
(Magnification x 460.)

PLATE 9

Micrograph of a specimen containing 24 wt.% MgO, 16 wt.% $Cr_2O_3$ and 60 wt.% $C_2S$ after firing 2 hrs. at 1647°C. It shows angular grey grains of periclase and chrome spinel (angular bright grains) in a matrix that was liquid at 1647°C.
Black spots are pores.
(Magnification x 460.)

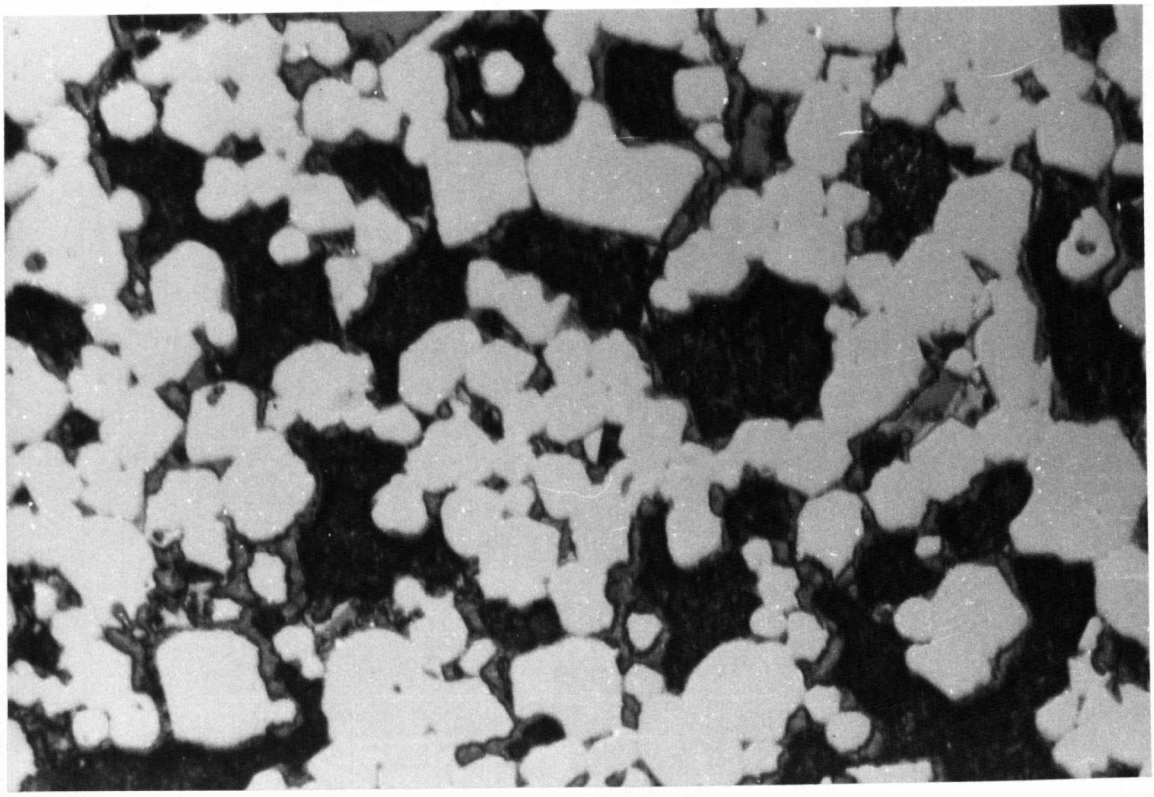

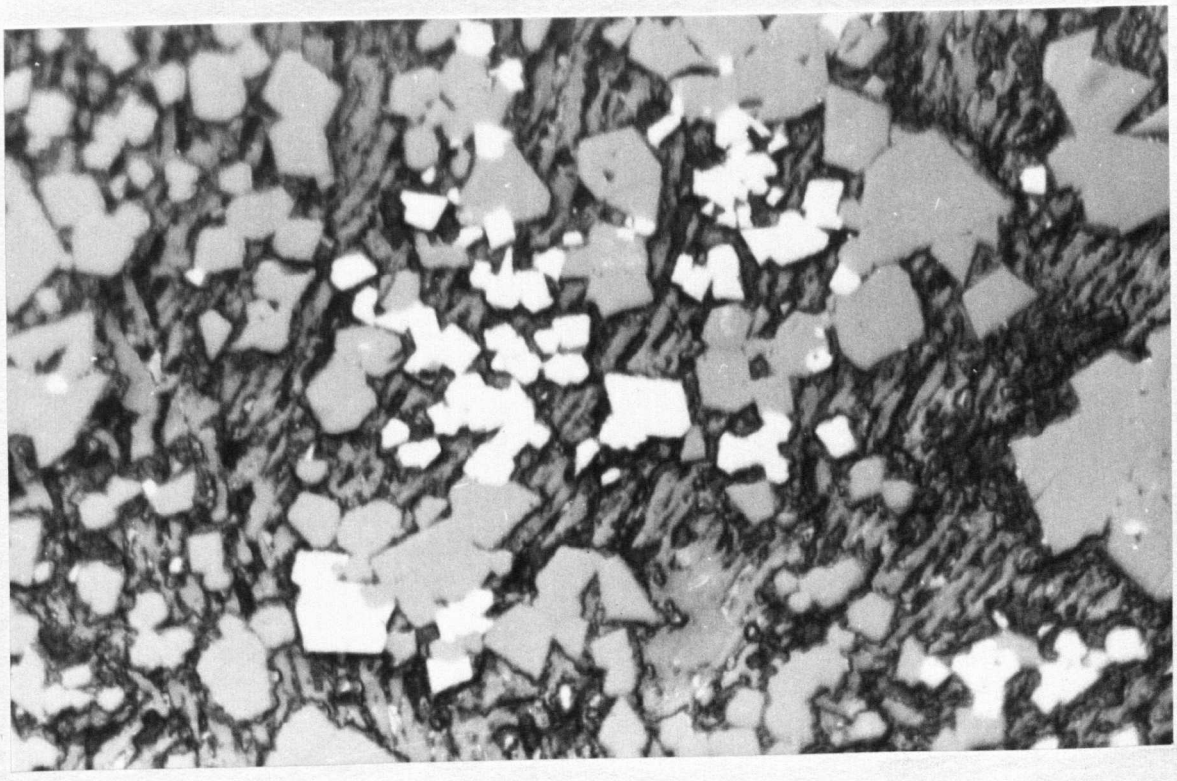

PLATE 10A

Micrograph of a specimen containing 50 wt.% MgO, 10 wt.% $Fe_2O_3$ and 40 wt.% $C_3MS_2$ after firing 2 hrs. at 1550°C and quenching in air. It shows rounded grains of magnesiowustite and grey grains of merwinite (criss-crossed) probably recrystallized from the liquid phase during air quenching.
Black spots are pores.
Sample etched with Ammonium Chloride Solution.
(Magnification x 460.)

PLATE 10B

The same composition of the Plate 10A but after firing 15 hrs. at 1550°C and quenching in water. It shows rounded grains of magnesiowustite in a matrix that was liquid at 1550°C, the large size of the grains being due to the long soaking time.
Black spots are pores.
Sample etched with Ammonium Chloride Solution.
(Magnification x 460.)

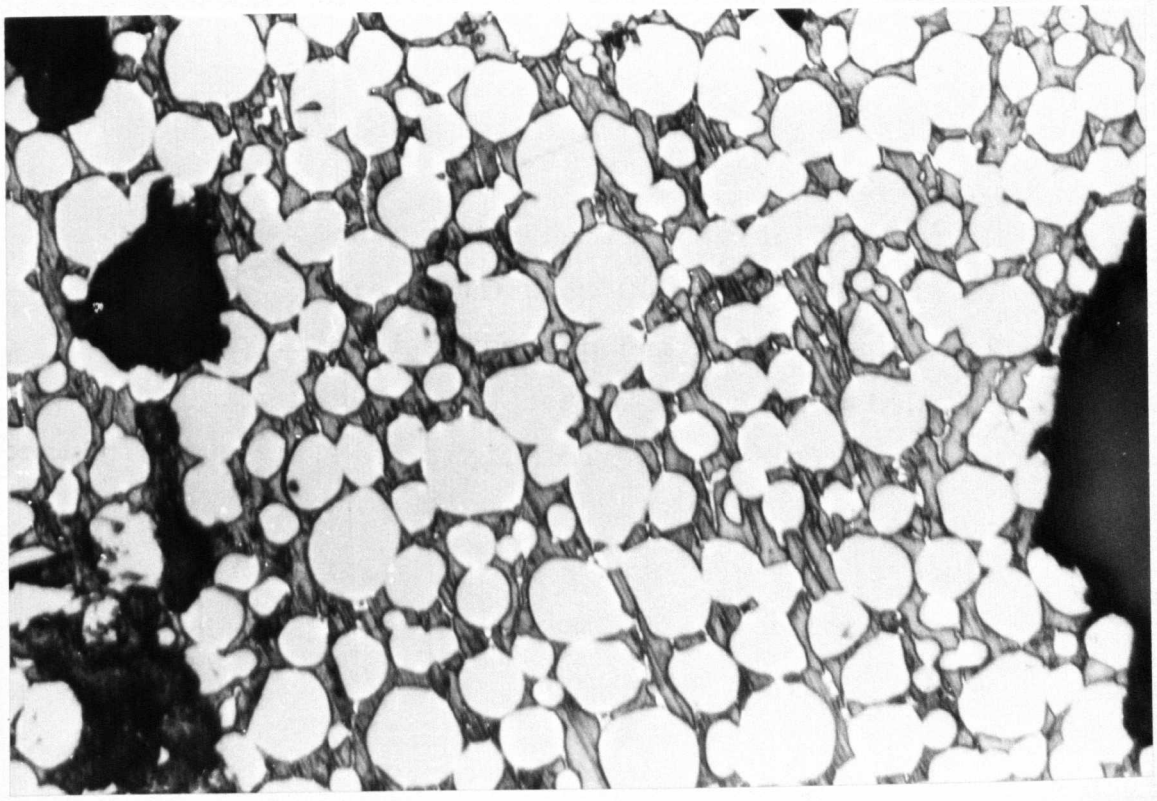

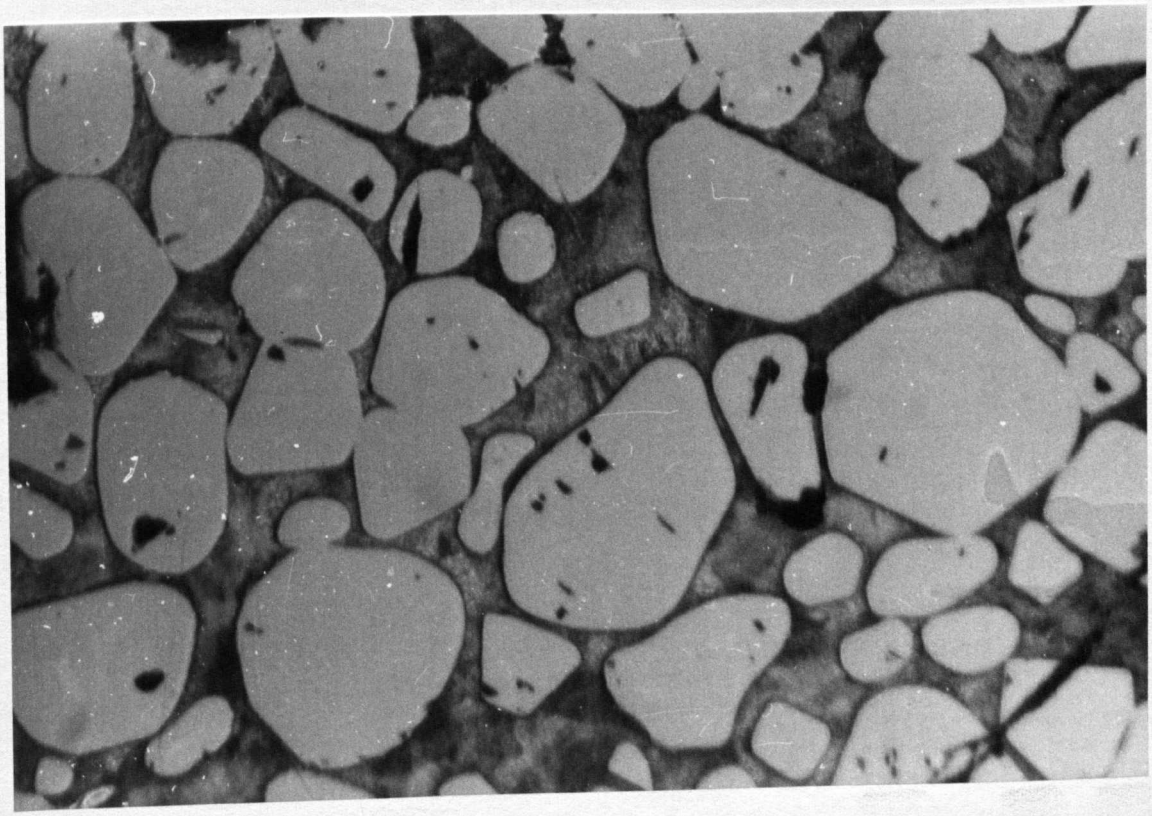

PLATE 11A

Micrograph of a specimen containing 45 wt.% MgO, 50 wt.% $Fe_2O_3$ and 5 wt.% $C_3MS_2$ after firing 2 hrs. at 1550°C and quenching in air. It shows rounded grains of magnesiowustite and magnesioferrite (bright grains), the latter having crystallized during air-quenching in a matrix that was liquid at 1550°C.
Black spots are pores.
(Magnification x 460.)

PLATE 11B

The same composition as Plate 11A but after firing 14 hrs. at 1550°C and quenching in water. It shows rounded grains of magnesiowustite in a matrix that was liquid at 1550°C, the large size of the grain being due to long soaking time.
Black spots are pores.
(Magnification x 460.)

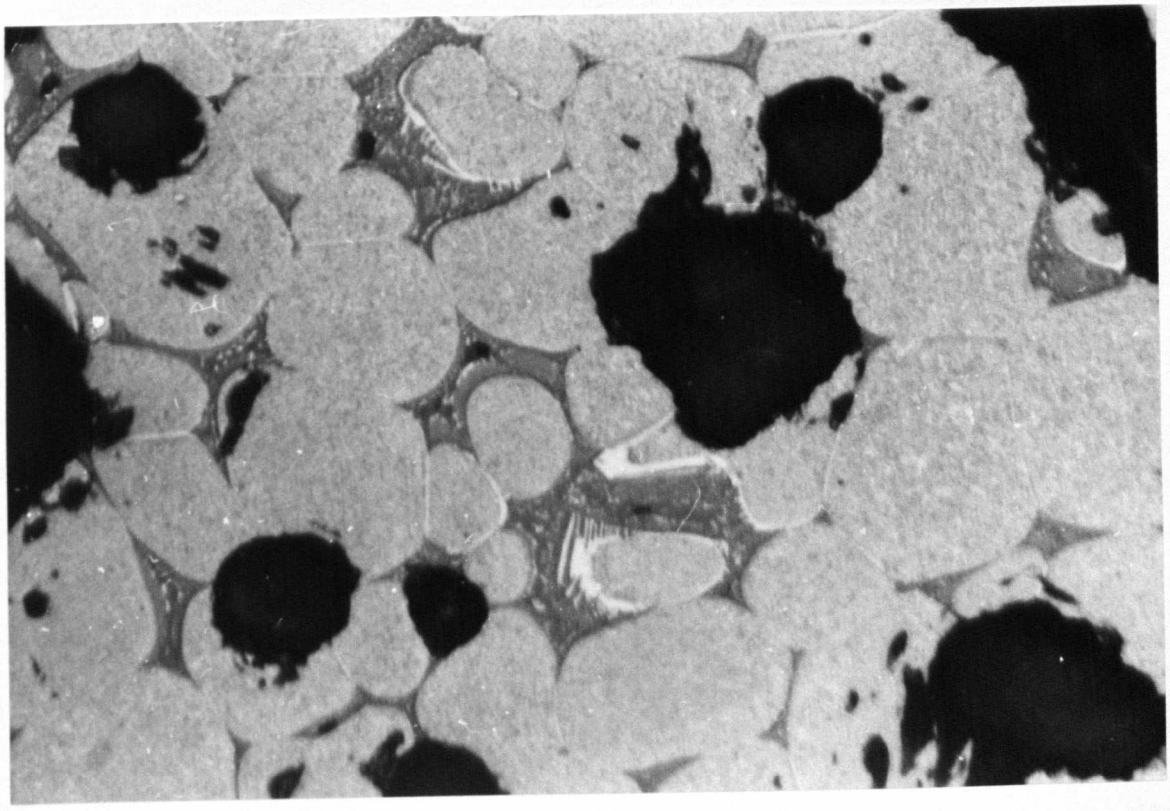

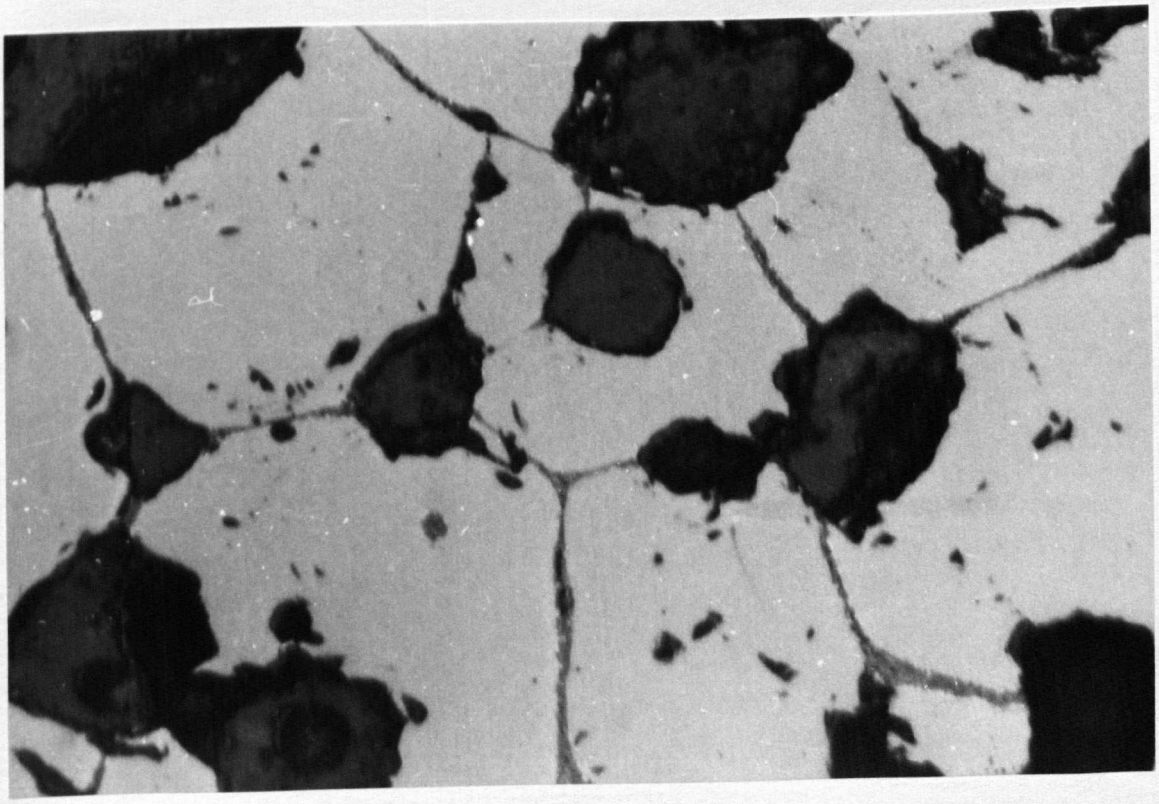

PLATE 12A

Micrograph of a specimen containing 19 wt.% MgO, 76 wt.% $Fe_2O_3$ and 5 wt.% $C_3MS_2$ after firing 2 hrs. at 1550°C and quenching in air. It shows magnesio-ferrite (angular white grains) and grey, rounded grains of magnesiowustite in a matrix that was liquid at 1550°C.
Black spots are pores.
(Magnification x 460.)

PLATE 12B

The same composition as Plate 12A but after firing 2 hrs. at 1550°C and quenching in water. It shows angular white grains of spinel (magnesioferrite) in a matrix that was liquid at 1550°C.
Black spots are pores.
(Magnification x 460.)

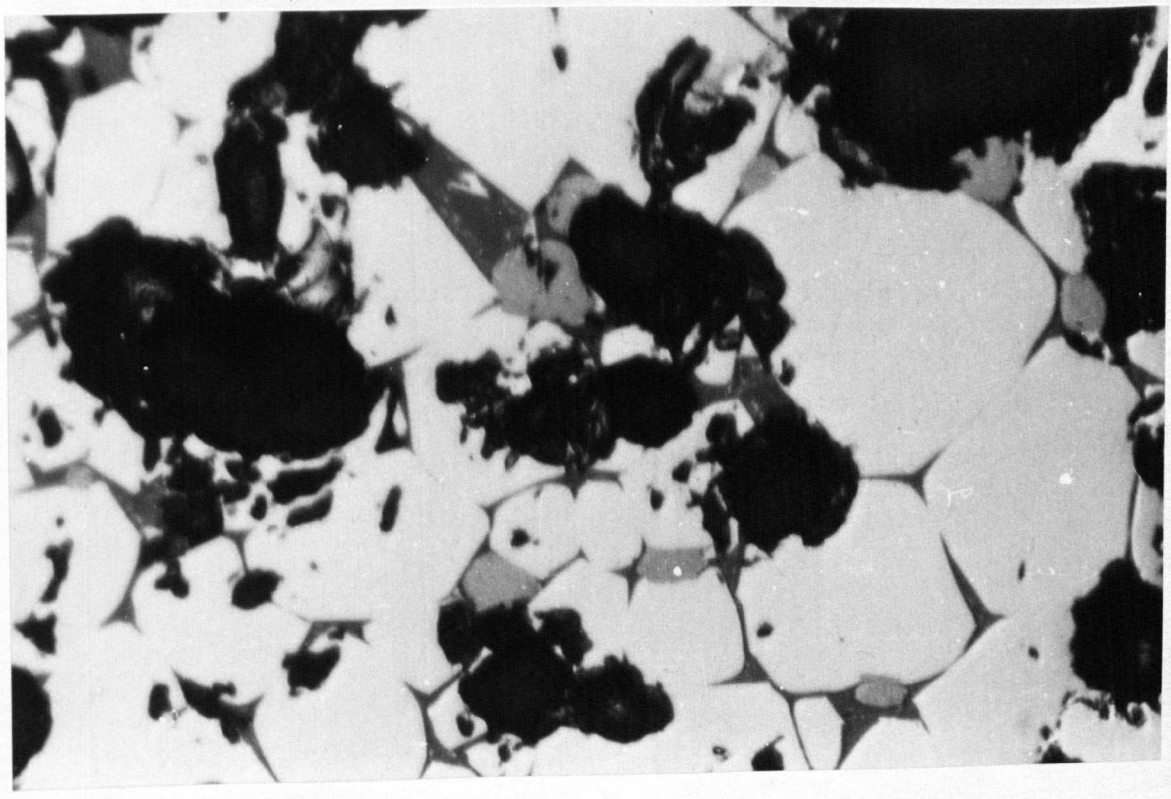

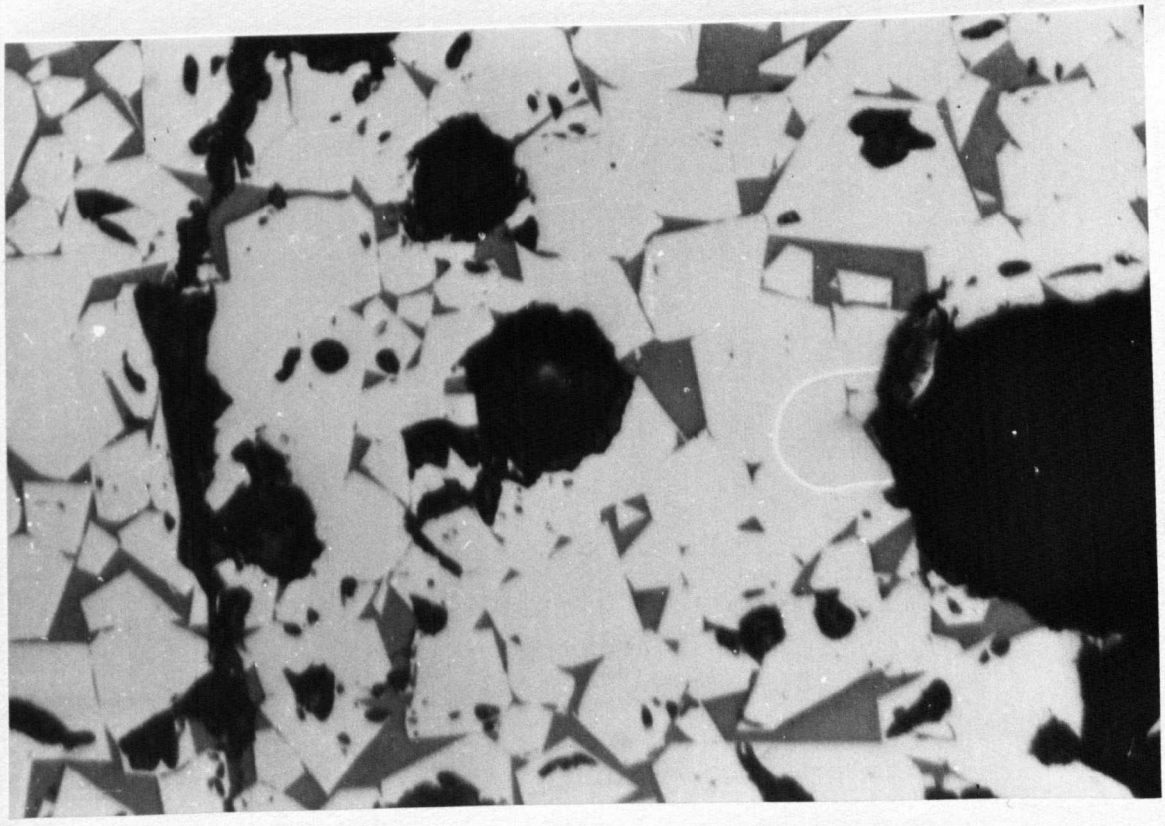

PLATE 13A

Micrograph of a specimen containing 5 wt.% MgO, 5 wt.% $Fe_2O_3$ and 90 wt.% $C_3MS_2$ after firing 2 hrs. at 1550°C and quenching in air. It shows rounded, light grains of magnesiowustite and large grey grains of merwinite (criss-crossed) in a matrix that was liquid at 1550°C.
Black spots are pores.
Sample etched with Ammonium Chloride Solution.
(Magnification x 460.)

PLATE 13B

The same composition as Plate 13A after 2 hrs. at 1550°C and quenching in water. It shows rounded dark twinned grains of $C_2S$ and rounded light grains of magnesiowustite in a matrix that was liquid at 1550°C.
Sample has been etched with Ammonium Chloride Solution.
The grey phase surrounding the $C_2S$ and MW grains and appearing in dendritic form is presumably merwinite precipitated from the liquid phase during cooling. The large grey rounded grains are resin and the black areas are pores.
(Magnification x 460.)

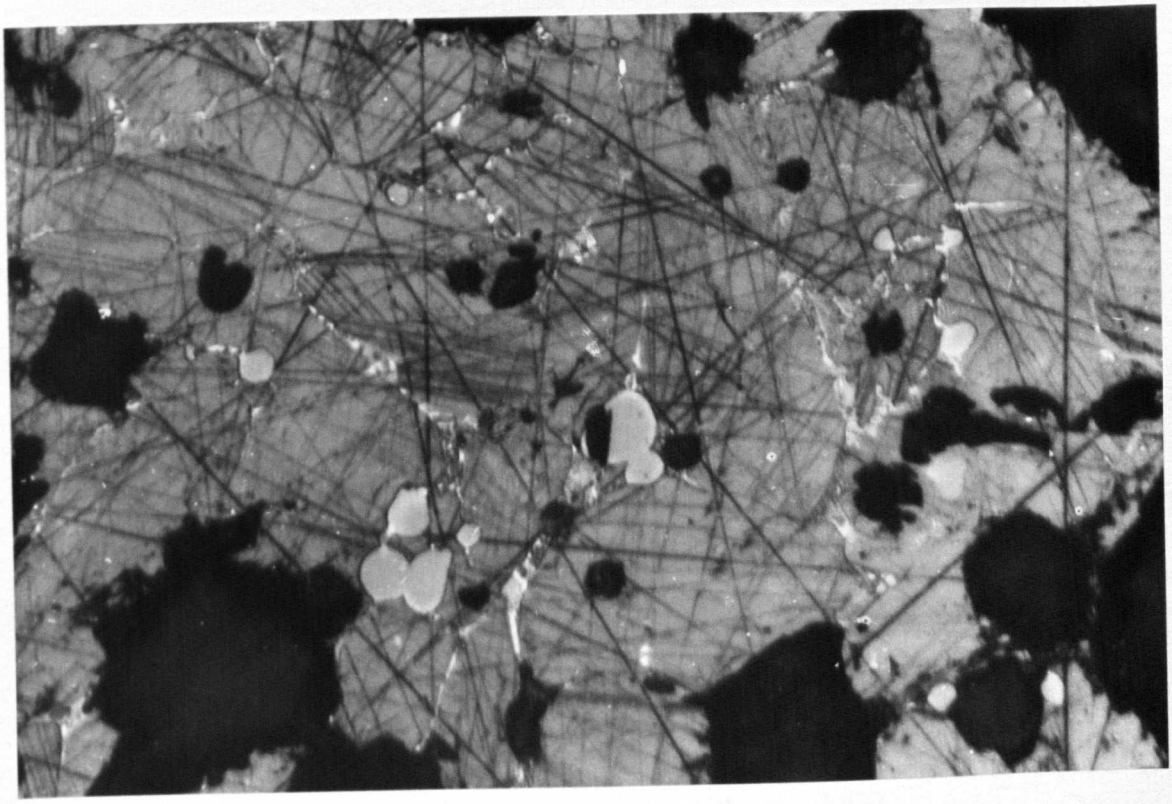

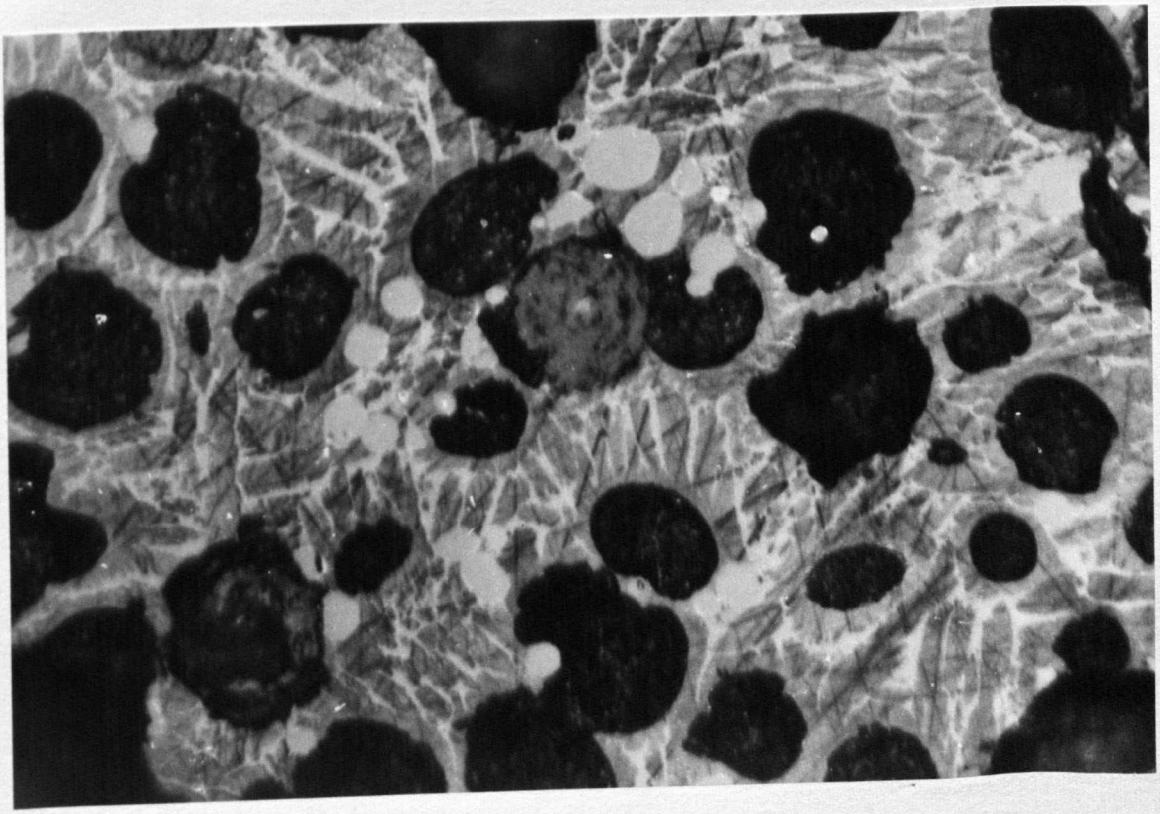

PLATE 14

Micrograph of a specimen containing 7.5 wt.% MF and 92.5 wt.% $C_3MS_2$ after firing 1 hr. at 1645°C in a magnesite crucible. It shows rounded dark twinned grains of $C_2S$ and rounded light grains of magnesiowustite in a matrix that was liquid at 1645°C. The grey phase surrounding the $C_2S$ and MW grains and appearing in dendritic form is presumably merwinite precipitated from the liquid phase during cooling. There was no appreciable penetration of the liquid phase into the magnesite crucibles.
Black spots are pores.
Sample etched in Ammonium Chloride Solution.
(Magnification x 460.)

PLATE 15

Micrograph of a specimen containing 7.5 wt.% $MgAl_{0.8}Cr_{1.2}O_4$ and 92.5 wt.% $C_3MS_2$ of the binary section $MgAl_{0.8}Cr_{1.2}O_4$-$C_3MS_2$ after firing 17 hrs. at 1520°C. It shows rounded, dark twinned grains of $C_2S$, white angular grains of spinel solid solution and light periclase grains (rounded and hexagonal shapes) in a matrix that was liquid at 1520°C. The grey phase surrounding the $C_2S$, the spinel solid solution and the periclase grains, and appearing in dendritic form is presumably merwinite precipitated from the liquid phase during cooling. Large grey grains are resin.
(Magnification x 460.)